Roles for Transcription Factors and Signaling Pathways in Hindbrain Segmentation and Ventricle Morphogenesis

by

Lyndsay Grace Selland

A thesis submitted in partial fulfillment of the requirements for the degree of

Doctor of Philosophy

in

Molecular Biology and Genetics

Department of Biological Sciences
University of Alberta

Abstract

During development, expression and localization of transcription factors and transcriptional co-regulators must be tightly controlled, and in turn they are required to regulate cellular identity and cellular processes. Often this involves complex interactions with signaling pathways. We are interested in the role of transcription factors and co-regulators in regulating hindbrain segmentation and ventricle morphogenesis.

Previous research has suggested that paralog group (PG) 1 *hox* genes may play a central role in establishing overall hindbrain identity, as the loss of *pbx* cofactors results in a loss of hindbrain identity. We find that *hoxb1a* regulates r4 identity, while *hoxb1b* is required for regulation of segmentation and rhombomere size. The loss of both *hoxb1b* and *pbx4* is required to revert the hindbrain to the r1 ground state identity. *Pbx* genes regulate RA signaling through regulation of RA synthesis, while *hoxb1b* is required for regulation of FGF signaling and together they establish overall hindbrain identity. This suggests a central role for *pbx*, as more than just a cofactor to PG1 *hox* genes.

Although previous research has identified processes involved in the development of the hindbrain ventricle, we wished to identify genes and signaling pathways involved in this process. The transcriptional co-regulator *taz* (*WW domain containing transcription regulator 1; wwtr1*) is localized to rhombomere boundaries, and *taz* mutants have disruptions in ventricle morphogenesis, causing midline separation defects and the mislocalization of apicobasal polarity components and mild reductions in cell proliferation. Previous work has shown that Taz is incorporated into the β-catenin destruction complex in the absence of Wnt ligands, where it recruits the E3 ubiquitin ligase β-TrCP (*beta-transducin repeat containing E3 ubiquitin protein ligase*), resulting in degradation of both β-catenin and Taz. Our results support roles for Wnt ligands at

rhombomere boundaries in regulating the stabilization of Taz protein at rhombomere boundaries. Furthermore both β–catenin and Taz are required transcriptional regulators for ventricle development. Taz also regulates the expression of *rfng* (*RFNG O-fucosylpeptide 3-beta-N-acetylglucosaminyltransferase)* and *wnt1 (wingless-type MMTV integration site family, member 1)* at rhombomere boundaries, suggesting roles for Taz in mediating Notch signalling in ventricle development. Although disruption of Notch signalling does affect the size of the hindbrain ventricle, loss of *taz* does not appear to affect Notch mediated patterning of neurogenesis. Together this supports roles for Taz as a component of the Wnt/β-catenin signaling pathway and in the regulation of Notch signaling at rhombomere boundaries, and we provide evidence that these interactions are involved in hindbrain ventricle morphogenesis.

Preface

This thesis is an original work by Lyndsay G. Selland. The study, of which this thesis is a part, has received research ethics approval from the University of Alberta Animal Policy and Welfare Committee. The author has met the Canadian Council on Animal Care (CCAC) mandatory training requirements for animal users on the Care and Use of Animals in Research, Teaching, and Testing.

A version of Chapter 3 was published:

Pillay, L.M., Selland, L.G., Fleisch, V.C., Leighton, P.L., Cheng, C.S., Famulski, J.K., Ritzel, R.G., March, L.D., Wang, H., Allison, W.T. and Waskiewicz, A.J., 2013. Evaluating the mutagenic activity of targeted endonucleases containing a Sharkey FokI cleavage domain variant in zebrafish. Zebrafish. 10, 353-64.

Lyndsay G. Selland performed experiments, analyzed data and edited the manuscript. Lyndsay G. Selland generated the *hoxb1b* and *wwtr1* TALENS, and performed zebrafish mutagenesis using TALENs. Valerie C. Fleisch generated the *prp2* ZFNs. R. Gary Ritzel generated the *crx* ZFNs. Figure 3.1 appears courtesy of Caroline S. Cheng. Figure 3.2 and Figure 3.3 result from experiments performed by Laura M. Pillay and Jakub K. Famulski. The data presented in Figure 3.4 results from experiments performed by Laura M. Pillay and Caroline S. Cheng. The data presented in Figure 3.5 results from experiments performed in collaboration with Laura M. Pillay. The data presented in Table 3.1 results from experiments performed by Laura M. Pillay, Valerie C. Fleisch and Lindsey D. March. The data presented in Table 3.2 was generated by Lyndsay G. Selland. Laura M. Pillay wrote the manuscript. Lyndsay G. Selland, Valerie C. Fleisch, Patricia L. A. Leighton, Caroline S. Cheng, and Jakub K. Famulski helped to analyze data, and edited the manuscript. Andrew J. Waskiewicz and W. Ted Allison were co-supervisory authors, analyzed data and edited the manuscript.

A version of Chapter 4 was published:

Selland, L.G., Koch, S., Laraque, M. and Waskiewicz, A.J., 2018. Coordinate regulation of retinoic acid synthesis by pbx genes and fibroblast growth factor signaling by

hoxb1b is required for hindbrain patterning and development. Mech Dev.

Lyndsay G. Selland performed experiments, analyzed data and wrote the manuscript. Sophie Koch and Malcolm Laraque performed *in situ* hybridization analysis of *hoxb1b;pbx4* compound mutants presented in Figure 4.6. Andrew J. Waskiewicz was the supervisory author, analyzed data and edited the manuscript.

Unless otherwise specified, data presented in this thesis is the author's original work.

Acknowledgements

I would like to thank my supervisor Dr. Andrew Waskiewicz for helping me to grow throughout my degree. You have always been available to discuss results and ideas, you have provided valuable feedback that has improved my presentation abilities and through your support I have become a better scientist.

Thank you to my committee members, Dr. Fred Berry and Dr. Kirst King-Jones for your mentorship and feedback.

To all of my lab mates, past and present, you always made working in the lab fun. You have always been valuable to bounce ideas off of, to help out with tough experiments, and you have always provided me with the best support through the good times and the bad.

I would never have reached this point without the support of my friends and family. You keep me grounded, give me chances to blow off some steam and make sure that I'm still having fun. To my Mom and Dad, you have always believed in me and encouraged me to dream big. You are always there to help me up when I fall down, and your love and support means the world to me.

Finally, thank you to my husband Louis. You have always been there for me, listening to my rants, driving me to the lab before the sun is up, bringing me snacks and keeping me company during late nights and your love and support is what keeps me going.

Table of Contents

List of Tables

List of Figures

List of Symbols, Nomenclature and Abbreviations

°C	degrees Celsius
aa	amino acid
aldh1a2 (raldh2)	*aldehyde dehydrogenase family 1, subfamily A2*
amot	*angiomotin*
amotl1	*angiomotin like 1*
amotl2a	*angiomotin like 2a*
amotl2b	*angiomotin like 2b*
AP	anteroposterior
apc	*adenomatous polyposis coli*
ascl1a	*achaete-scute family bHLH transcription factor 1a*
ascl1b	*achaete-scute family bHLH transcription factor 1b*
atl	*atlantis*
atoh1a	*atonal bHLH transcription factor 1a*
axin1 (mbl)	*axin 1 (masterblind)*
BCIP	5-bromo-4-chloro-3-indolyl-phosphate
BMN	branchiomotor neuron
BMP	bone morphogenetic protein
bp	basepair
BSA	bovine serum albumin
β-TrCP	*beta-transducin repeat containing E3 ubiquitin protein ligase*
cDNA	complementary deoxyribonucleic acid
cdx4	*caudal type homeobox 4*
Cpd E	Compound E; S,S)- 2-[2-(3,5-Difluorophenyl)-acetylamino]-N-(1-methyl-2-oxo-5-phenyl-2,3-dihydro-1H-benzo[e][1,4]diazepin-3-yl)-propionamide; Compound E
crb1	*crumbs family member 1*
crb2a (ome)	*crumbs family member 2a (oko meduzy)*
crb2b	*crumbs family member 2b*
CRISPR	clustered randomly interspersed short palindromic repeats
crx	*cone-rod homeobox*

CSF	cerebrospinal fluid
ct	cycle threshold
ctnnb2	*catenin, beta 2 (β-catenin)*
cyp1b1	*cytochrome P450, family 1, subfamily B, polypeptide 1*
cyp26a1	*cytochrome P450, family 26, subfamily a, polypeptide 1*
cyp26b1	*cytochrome P450, family 26, subfamily b, polypeptide 1*
cyp26c1	*cytochrome P450, family 26, subfamily C, polypeptide 1*
DAPT	N-[N-(3,5-Difluorophenacetyl)-L-alanyl]-S-phenylglycine t-butyl ester
DEAB	diethylaminobenzaldehyde
DEPC	diethylpyrocarbonate
DIG	digoxygenin
dla	*deltaA*
dlc	*deltaC*
dld	*deltaD*
dlx2a (dlx2)	*distal-less homeobox 2a*
DMSO	dimethylsulfoxide
DNA	deoxyribonucleic acid
DNase	deoxyribonuclease
dNTP	deoxyribonucleic triphosphate
dpf	days post fertilization
dusp6 (mkp3)	*dual specificity phosphatase 6*
DV	dorsoventral
ECL	Enhanced Chemiluminescence
ECM	extracellular matirx
eCSF	embryonic cerebrospinal fluid
EDTA	ethylenediaminetetraacetic acid
efnb2a	*ephrin B2a*
EM	embryo media
en2a (eng2)	*engrailed homeobox 2a*
epha4a	*eph receptor A4a*

EtOH	ethanol
FGF	fibroblast growth factor
fgf3	*fibroblast growth factor 3*
fgf8a (fgf8; ace)	*fibroblast growth factor 8a (acerebellar)*
FGFR	fibroblast growth factor receptor
fgfr1a	*fibroblast growth factor receptor 1a*
frmd6	*FERM domain containing 6*
g	gravity
gdf11	*growth differentiation factor 11*
GFP	green fluorescent protein
GO	gene ontology
GPCR	G-protein coupled receptor
gsk3aa	*glycogen synthase kinase 3 alpha a*
gsk3ab	*glycogen synthase kinase 3 alpha b*
gsk3b	*glycogen synthase kinase 3 beta*
h	hours
HDR	Homology directed repair
HEPES	4-(2-hydroxyethyl) piperazine-1-ethanesulfonic acid
her6	*hairy-related 6*
hmx4	*H6 family homeobox 4*
Hoxa1	*Homeobox A1*
hoxa2b	*homeobox A2b*
hoxa3a	*homeobox A3a*
Hoxb1	*Homeobox B1*
hoxb1a	*homeobox B1a*
hoxb1b	*homeobox B1b (homeobox a1)*
hoxb2	*homeobox b2*
hoxb2a	*homeobox B2a*
hoxb3	*homeobox b3*
hoxb3a	*homeobox B3a*
hoxd3a	*homeobox D3a*

hoxd4a	*homeobox D4a*
hpf	hours post fertilization
HRM	high resolution melt curve
HRP	Horseradish Peroxidase
Hyb	hybridization solution
ICG-001	(6S,9aS)-6-(4-hydroxybenzyl)-N-benzyl-8-(naphthalen-1-ylmethyl)-4,7-dioxo-hexahydro-2Hpyrazino[1,2-a]pyrimidine-1(6H)-carboxamide
In/Del	Insertion/Deletion
insm1a	*insulinoma-associated 1a*
IPTG	isopropyl β-D-1-thiogalactopyranoside
irx7	*iroquois homeobox 7*
isl1	*ISL LIM homeobox 1 (islet1)*
isl2b	*ISL LIM homeobox 2b (islet2b)*
kb	kilobase
krox20 (egr2b)	*early growth response 2b*
lats1	*large tumor suppressor kinase 1*
lats2	*large tumor suppressor kinase 2*
LB	Luria broth
lfng	*LFNG O-fucosylpeptide 3-beta-N-acetylglucosaminyltransferase*
lin7c	*lin-7 homolog C*
lmx1ba	*LIM homeobox transcription factor 1, beta a*
lmx1bb	*LIM homeobox transcription factor 1, beta b*
lrp5	*low density lipoprotein receptor-related protein 5*
lrp6	*low density lipoprotein receptor-related protein 6*
M	molar
mariposa (foxb1a)	*forkhead box B1a*
med12	*mediator complex subunit 12*
med14	*mediator complex subunit 14*
meis1a (meis4.1)	*meis homeobox 1a*

meis1b (meis1/meis1.1)	*meis homeobox 1b*
meis2a (meis2.2)	*meis homeobox 2a*
meis2b (meis2/meis2.1)	*meis homeobox 2b*
meis3 (mesi3.1)	*myeloid ecotropic viral integration site 3*
MeOH	methanol
mfng	*MFNG O-fucosylpeptide 3-beta-N-acetylglucosaminyltransferase*
mg	milligram
MHB	midbrain hindbrain boundary
mib (mib1)	*mind bomb E3 ubiquitin protein ligase 1 (mindbomb)*
min	minutes
mL	milliliter
mM	millimolar
MO	morpholino oligonucleotide
mob1a	*MOB kinase activator 1A*
mob1ba	*MOB kinase activator 1Ba*
mob1bb	*MOB kinase activator 1Bb*
mpp5a (nok)	*membrane protein, palmitoylated 5a (MAGUK p55 subfamily member 5; nagie oko)*
mRNA	messenger ribonucleic acid
MS222	tricaine methanesulfonate/ethyl 3-aminobenzoate methanesulfonate
MSC	mesenchymal stem cell
NBT	4-nitro blue tetrazolium chloride
neurod1	*neuronal differentiation 1*
neurod4	*neuronal differentiation 4*
nf2a	*neurofibromin 2a*
nf2b	*neurofibromin 2b*
ng	nanogram
ngn1	*neurogenin 1*
NHEJ	non-homologous end joining

NICD	notch intracellular domain
nlz2	*nocA-like zinc finger protein 2*
notch1a	*notch1a*
PBS	phosphate buffered saline
PBSDTT	PBST + 1% DMSO + 0.1% Triton X-100
PBST	PBS + 0.1% Tween-20
Pbx1	*Pre B cell leukemia homeobox 1*
Pbx2	*Pre B cell leukemia homeobox 2*
pbx2	*pre-B-cell leukemia homeobox 2*
pbx4 (lzr)	*pre-B-cell leukemia transcription factor 4 (lazarus)*
PCR	polymerase chain reaction
pea3 (etv4)	*ets variant 4*
PFA	paraformaldehyde
PG	paralog group
pg	pictogram
pknox1.1 (prep1/prep1.1)	*pbx/knotted 1 homeobox 1.1*
pknox1.2 (prep1.2)	*pbx/knotted 1 homeobox 1.2*
pou5f3 (oct4)	*POU domain, class 5, transcription factor 3*
ppp1r12a (mypt1)	*protein phosphatase 1, regulatory subunit 12A (myosin phosphatase targeting subunit 1)*
ppp1r14al (ppp1r14ab)	*protein phosphatase 1, regulatory (inhibitor) subunit 14Ab*
Prkci (has)	*protein kinase C, iota (heart and soul)*
ProK	proteinase K
prp1 (prnprs1)	*prion protein 1*
prp2 (prnprs2)	*prion protein 2*
PTU	1-phenyl-2-thiourea
PVDF	Polyvinylidene difluoride
qPCR	Real-time quantitative PCR

r	rhombomere
RA	retinoic acid
raraa	*retinoic acid receptor, alpha a*
rarab	*retinoic acid receptor, alpha b*
RARE	retinoic acid response element
rarga	*retinoic acid receptor gamma a*
rargb	*retinoic acid receptor, gamma b*
rfng	*RFNG O-fucosylpeptide 3-beta-N-acetylglucosaminyltransferase*
RMO44	Ab1-neurofilament-m
RNA	Ribonucleic acid
RNA-seq	RNA- sequencing
RNAse	ribonuclease
RPE	retinal pigmented epithelium
rpm	revolutions per minute
RT	room temperature
RT-PCR	reverse transcription polymerase chain reaction
RVD	repeat variable diresidue
rxraa	*retinoid X receptor, alpha a*
rxrab	*retinoid x receptor, alpha b*
rxrba	*retinoid x receptor, beta a*
rxrbb	*retinoid x receptor, beta b*
rxrga	*retinoid x receptor, gamma a*
rxrgb	*retinoid X receptor, gamma b*
s	seconds
sav1	*salvador family WW domain containing protein 1*
SB216763	3-(2,4-Dichlorophenyl)-4-(1-methyl-1H-indol-3-yl)-1H-pyrrole-2,5-dione
Scrib (llk)	*scribbled planar cell polarity protein (landlocked)*
SDS	sodium dodecyl sulfate
sema3gb	*sema domain, immunoglobulin domain (Ig), short basic domain, secreted, (semaphorin) 3Gb*

sfpq	*splicing factor proline/glutamine-rich*
sfrp5	*secreted frizzled-related protein 5*
SOC	super optimal broth
sox1b	*SRY (sex determining region Y)-box 1b*
sox2	*SRY (sex determining region Y)-box 2*
sox3	*SRY (sex determining region Y)-box 3*
spry1	*sprouty homolog 1*
spry2	*sprouty RTK signaling antagonist 2*
spry4	*sprouty homolog 4*
SSC	saline sodium citrate buffer
stk3 (mst2)	*serine/threonine kinase 3*
Su(H) (rbpj)	*recombination signal binding protein for immunoglobulin kappa J region a*; *suppressor of hairless*
TALE	Three amino acid loop extension
TALEN	transcription activator-like effector nucleases
taz (wwtr1)	*WW domain containing transcription regulator 1*
TBST	Tris-buffered saline + 0.1% Tween-20
tcf3a	*transcription factor 3a*
tcf3b	*transcription factor 3b*
tead1a	*TEA domain family member 1a*
tead1b	*TEA domain family member 1b*
tead3a	*TEA domain family member 3 a*
tead3b	*TEA domain family member 3 b*
tead4	*TEA domain transcription factor 4*
Tm	Melting temperature
tp53	*tumor protein p53*
UV	ultraviolet
val (mafba, kr)	*valentino (v-maf avian musculoaponeurotic fibrosarcoma oncogene homolog Ba; Kreisler)*
vhnf1 (hnf1ba)	*HNF1 homeobox Ba*
Windorphen	(Z)-3-Chloro-2,3-bis(4-methoxyphenyl)acrylaldehyde

Wnt	Wingless-type MMV integration site family
wnt1	*wingless-type MMTV integration site family, member 1*
wnt10b	*wingless-type MMTV integration site family, member 10b*
wnt3a	*wingless-type MMTV integration site family, member 3A*
wnt4a	*wingless-type MMTV integration site family, member 4a*
wnt8b	*wingless-type MMTV integration site family, member 8b*
X-gal	5-bromo-4-chloro-3-indolyl-β-D-galactopyranoside
XAV939	3,5,7,8-Tetrahydro-2-[4-(trifluoromethyl)phenyl]-4H-thiopyrano[4,3-d]pyrimidin-4-one
yap1 (yap)	*Yes-associated protein 1*
ZF	zinc finger
ZFN	zinc finger nuclease
zic1	*zic family member 1*
zic2a	*zic family member 2 a*
zic2b	*zic family member 2 b*
zic3	*zic family member 3 heterotaxy 1*
zic4	*zic family member 4*
Znp1	anti-synaptotagmin 2
Zn5	Activated leukocyte cell adhesion molecule a
zon	*zonderzen*
µg	microgram
µL	microliter
µM	micromolar

Chapter 1: Introduction

1.1 Zebrafish as a Model to Study the Role of Transcription Factors in Hindbrain Development

The hindbrain is the most posterior segment of the brain, located between the developing midbrain and spinal cord. In the adult, the hindbrain gives rise to the cerebellum, the pons, and the medulla oblongata (Gray and Clemente, 1985). The cerebellum receives and integrates signals from the spinal cord, sensory systems and other regions of the brain, and transmits that information to the motor cortex in order to coordinate sensory information with muscular responses and enable voluntary movements. The pons connects the brainstem with the cerebral cortex, while the medulla oblongata provides the transition from the brain to the spinal cord and contains nerve tracts required for autonomic functions including heart rate, breathing and blood pressure. Together, the medulla, the pons, and the fourth ventricle form the brainstem, in combination with the midbrain. The brainstem contains cells of the reticular formation, which regulate behaviors such as alertness, wakefulness and sleep. The reticulospinal neurons extend from the brainstem to the spinal cord, where they contact motor neurons responsible for postural control and locomotion. The hindbrain also contains 8 of the 12 pairs of cranial nerves, which are responsible for movements and detection of sensations in the face, head and neck. (Chandrasekhar et al., 1997; Hanneman et al., 1988; Hartenstein, 1993; Kimmel et al., 1982; Mendelson, 1986; Metcalfe et al., 1986; Moens and Prince). Neural crest cells also arise from the hindbrain and contribute to the connective tissues, bones and cartilage of the pharyngeal arches that form the face (Koentges and Matsuoka, 2002; Le Douarin and Kalcheim, 1999; Lumsden et al., 1991; Schilling and Kimmel, 1994). The hindbrain also gives rise to the cerebrospinal fluid (CSF) filled fourth ventricle. Cerebrospinal fluid provides protection from physical trauma (Hajdu, 2003; Segal, 2001) and also transports waste and nutrients in the adult brain (Cushing, 1914; Milhorat et al., 1971; Pollay and Curl, 1967; Segal, 2001). The adult hindbrain is incredibly complex, it must be able to send and receive a myriad of signals that are not only vital for our survival, but also can have a profound impact on our quality of life. Despite this complexity, the hindbrain develops from a relatively simple series of lineage-restricted compartments, that each expresses a unique constellation of genes. Investigation of the roles of transcription factors and signaling

pathways in the development of the hindbrain is important in expanding our understanding of the fundamental mechanisms underlying hindbrain development, but these studies may also further our understanding of human disorders affecting the hindbrain.

Transcription factors and co-regulators play vital roles in all developmental processes, including the proper specification and development of neural structures. They are indispensable in gene regulatory networks and often act as downstream effectors of signaling pathways. Transcription factors and co-regulators mediate complex gene expression patterns in development through activation or repression of transcription. They can specify tissue identity and regulate many diverse cellular processes. For many transcription factors however, relatively little is known about their direct transcriptional targets and the mechanisms by which they coordinate development. My work focuses on the role of transcription factors and co-regulators in the development of the vertebrate hindbrain.

Zebrafish are an attractive model organism in which to study hindbrain development, as they are amenable to genetic manipulation. Recent advances in the field have greatly enhanced the capacity for targeted mutagenesis through initial efforts made with Zinc Finger Nucleases (ZFNs) (Ben et al.; Doyon et al., 2008; Foley et al., 2009a; Foley et al., 2009b; Meng et al., 2008; Sander et al.), and subsequent work on Transcription Activator-like Effector Nucleases (TALENs) (Bedell et al., 2012; Cade et al., 2012; Cermak et al., 2011; Dahlem et al., 2012; Gupta et al., 2013; Huang et al., 2011; Moore et al., 2012; Sakuma et al., 2013; Sander et al., 2011a) and Clustered Regularly Interspersed Palindromic Repeats (CRISPRs) (Hwang et al., 2013). Additional mutants have been found through genetic screens (Lowery et al., 2009; Schier et al., 1996). Knockdown of gene function can be achieved using antisense morpholino oligonucleotides (Nasevicius and Ekker, 2000) and overexpression of genes of interest can be induced by mRNA microinjection. Additionally, as zebrafish develop external to the mother and are optically transparent, all stages of development are easily accessible, and this also allows for single cell resolution of mRNA and protein expression and localization though *in situ* hybridization and immunohistochemistry. Furthermore, transgenic strains allow for the visualization of structures within the

embryo (such as the cranial branchiomotor neurons in the *Tg(isl1:GFP)* strain) or outputs of signaling pathways (such as *Tg(top:GFP)* strain). Additionally, being vertebrates, the zebrafish hindbrain is similar to humans and there are clear mammalian orthologs for many genes examined. Therefore, defects in zebrafish development may be related to defects observed in other organisms and have implications for human health.

1.2 Overview of Hindbrain Development

Neural induction, occurring at the onset of gastrulation (5hpf) is required to specify the presumptive neurectoderm. Cell extrinsic factors (such as BMP (Bone morphogenetic protein), Wnt (Wingless-type MMV integration site) and FGF (Fibroblast growth factor) (Streit et al., 2000; Wilson et al., 2001)) from the presumptive mesoderm induce or inhibit neural induction, while the presence of intrinsic factors (such as members of the SRY-box containing genes B1 (Soxb1) family (Avilion et al., 2003; Sasai, 1998; Streit et al., 1997)) define a program in the cells which will go on to become the neurectoderm. Even at such early stages, the neurectoderm is composed of non-overlapping regions that will give rise to distinct anterior-posterior fates (Kimmel et al., 1990; Woo and Fraser, 1995) (Figure 1.1). First, neural tissue is specified with an anterior identity, by signals (Glinka et al., 1998; Heisenberg et al., 2001; Kim et al., 2000; Mukhopadhyay et al., 2001) from the embryonic organizer (reviewed by (De Robertis et al., 2000; Schier and Talbot, 2001)), and then signals (such as *wnt8* (Erter et al., 2001; Lekven et al., 2003; McGrew et al., 1997; Nasevicius and Ekker, 2000), FGF (Amaya et al., 1991; Griffin et al., 1995) and RA (Retinoic Acid) (reviewed in (Gavalas and Krumlauf, 2000)), from the lateral germ ring provide a "posteriorizing" signal (Erter et al., 2001; Feldman et al., 2000; Woo and Fraser, 1995; Woo and Fraser, 1997).

Following specification, the neurectoderm forms the neural plate (10hpf), which converges to form the neural keel (11.5-15hpf) (Figure 1.1). The neural keel then fuses at the dorsal midline, forming the neural rod (17hpf), which will undergo cavitation (Figure 1.1). Beginning anteriorly, cells spanning the neural tube accumulate apical markers (such as Pard3) at the cytokinetic furrow as they divide, resulting in daughter cells located on either side of the midline. The apical markers remain at the midline and

lead to cell polarization and the formation of the lumen and the neural tube (24hpf) (Figure 1.1) (Buckley et al., 2013; Clarke, 2009; Papan and Campos-Ortega, 1994; Tawk et al., 2007; Yang et al., 2009).

As morphogenesis of the brain is occurring to form the neural tube, signaling within distinct regions of the brain specifies distinct identities, such as the forebrain, midbrain and the hindbrain. The hindbrain is further subdivided into transient segments termed rhombomeres (r). Each rhombomere is a lineage-restricted compartment, in which distinct subsets of genes are expressed, imparting segmental identity. The segmental identity of each rhombomere then allows for the development of distinct neuronal populations and cell types from each compartment.

During early somite stages rhombomere boundaries begin to form (~11-12.5hpf), and subsequently can be identified by boundary specific gene expression. The r3/4 boundary is the first to be defined, followed by the r4/5 boundary, the r1/2 boundary, then the r2/3 boundary, the r6/7 boundary and finally the r5/6 boundary (Moens et al., 1998) (Figure 1.1). Rhombomere boundaries are refined through repulsive interactions between Eph receptors and their ligands in alternating rhombomeres (Bruckner et al., 1997; Cooke et al., 2001; Flenniken et al., 1996; Holland et al., 1996; Theil et al., 1998), and the ability of individual cells to change their anterior-posterior identity to match their neighboring cells (Schilling et al., 2001; Trainor and Krumlauf, 2000). This is vital for hindbrain development as the morphological segmentation of the hindbrain is essential for rhombomere-specific gene expression and organization of neurons born in the hindbrain (Figure 1.1 and 1.2) (Chandrasekhar et al., 1997; Hanneman et al., 1988; Lumsden and Keynes, 1989; Mendelson, 1986; Metcalfe et al., 1986; Trevarrow et al., 1990).

The subdivision of the brain into regions with specific identities (forebrain, midbrain and hindbrain) is also required for the development of the ventricular system. The brain ventricles secrete and are filled with cerebrospinal fluid (CSF) which provides a neural circulatory system for nutrients and waste, while also providing protection to the brain from physical trauma (Hajdu, 2003; Segal, 2001) (Cushing, 1914; Milhorat et al., 1971; Pollay and Curl, 1967; Segal, 2001). The correct dorsoventral (DV) and anteroposterior (AP) patterning of the neuroepithelium, enables the correct positioning

of the ventricles. (Britto et al., 2002; Elsen et al., 2008; Hjorth et al., 2002; Lumsden and Krumlauf, 1996; Rubenstein et al., 1998; Tannahill et al., 2005) The hindbrain ventricle begins to open at 18hpf in a stereotypic sequence, beginning with openings at rhombomere boundaries, and is fully open by 24pf where it will then continue to increase in size (Figure 1.1) (Gutzman and Sive, 2010).

1.3 Hindbrain Segmentation

Subdivision of the hindbrain into rhombomeres requires that each rhombomere forms a distinct lineage-restricted compartment with its own distinct profile of gene expression. Segmentation is required for neural organization as changes in rhombomere specification and segmentation are linked to neuroanatomical changes (Alexandre et al., 1996; Carpenter et al., 1993; Hill et al., 1995; Moens et al., 1996; Waskiewicz et al., 2001; Waskiewicz et al., 2002). Ephrins and Eph receptors are expressed in alternating rhombomeres, with receptors being expressed in r3/5 and ligands being expressed in r2/4/6 (Bovenkamp and Greer, 1997; Cooke et al., 2001; Mellitzer et al., 1999; Xu et al., 1995a); reviewed by (Cooke and Moens, 2002; Lumsden, 1999)). This pattern of two-segment periodicity sorts and segregates cells into the appropriate compartment where they can adopt segmental identity. Cells with distinct gene expression and cellular morphology form at the boundaries between rhombomeres, and act as signaling centers to pattern cell types within each rhombomere (Guthrie and Lumsden, 1991; Heyman et al., 1995; Heyman et al., 1993; Mahmood et al., 1995; Mahmood et al., 1996; Moens et al., 1996; Trevarrow et al., 1990; Yoshida and Colman, 2000). Even in the absence of inter-rhombomere boundaries, cells from adjacent segments do not intermix, likely due to the perseverance of Eph-Ephrin interactions (Nittenberg et al., 1997; White et al., 2000).

Establishment of lineage-restricted compartments each with its own distinct identity, through morphogen gradients and the specific expression of *hox* genes and other transcription factors is required to enable the development and organization of distinct neurons, and neural crest populations. A summary of the neurons and neural crest associated with specific rhombomeres is shown in Figure 1.2. Cells from r1 contribute to the cerebellum (Koster and Fraser, 2001; Wingate and Hatten, 1999; Zinyk

et al., 1998). Cranial neural crest cells arise in 3 distinct streams primarily from r2, r4 and r6. These streams contribute to the first, second and third branchial arches respectively and are vital for the development of craniofacial bones, cartilage and connective tissue (Koentges and Matsuoka, 2002; Le Douarin and Kalcheim, 1999; Schilling and Kimmel, 1994). A variety of neurons within the hindbrain exhibit segmental organization (Chandrasekhar et al., 1997; Hartenstein, 1993). Reticulospinal interneurons are organized in a reiterated pattern that is dependent on rhombomere identity (Hanneman et al., 1988; Kimmel et al., 1982; Mendelson, 1986; Metcalfe et al., 1986). The reticulospinal tracts extend from the brainstem to the spinal cord, where they contact motor neurons responsible for postural control and locomotion (Babalian and Chmykhova, 1987; Babalian and Shapovalov, 1984; Cruce, 1974; Shapovalov, 1972; Shapovalov, 1975; Ten Donkelaar, 1982). In zebrafish there are 27 different types of reticulospinal neurons within the hindbrain. The Rol2 neurons in r2, the Mauthner neurons in r4, and the Mid3cm neurons in r6 are readily identifiable by their size, cell shape and contralateral projections. Additional neurons can be identified in a stereotypic pattern, some of which project contralaterally, and others that project ipsilaterally (Kimmel et al., 1982; Lee and Eaton, 1991; Mendelson, 1986). Cranial motor neurons (CMN) are also dependent on hindbrain patterning for their development and organization (Chandrasekhar et al., 1997). The cranial motor neurons control the muscles of the face and head and are composed of clusters of neurons in the brainstem (Kandel et al., 2000). CMNs can be subdivided into 3 classes. The somatomotor neurons located in the midbrain and hindbrain, innervate the muscles of the tongue and eyes, the visceromotor neurons in the hindbrain innervate tear and sweat glands as well as smooth muscles and glands of the pulmonary, gastrointestinal and cardiovascular systems, while the branchiomotor neurons (BMN) in the hindbrain innervate the musculature arising from the branchial arches. The BMNs control the muscles responsible for facial expression, jaw movements and function of the larynx and the pharynx (reviewed in (Chandrasekhar, 2004)). The trigeminal (nV) branchiomotor neurons (BMNs) initially form in r2, before further subdividing into nVa and nVp clusters in r2 and r3 respectively, with their axons exiting the hindbrain from r2 (Chandrasekhar, 2004). The facial (nVII) BMNs are initially born in r4, after which they first migrate posteriorly to

r6/7 and then laterally to reach their final positions, leaving their axons behind to exit the neural tube from r4. The glossopharyngeal (nIX) BMNs are found in r7 and their axons exit the hindbrain from r6 while the vagal (nX) BMNs are found in the caudal hindbrain, and their axons exit the neural tube from r8 (Bally-Cuif et al., 1998; Chandrasekhar, 2004; Higashijima et al., 2000).

1.3.1 Genes Involved in Rhombomere Specification

Many genes and signaling pathway are required to specify rhombomere identity (Figure 1.2). FGF signaling and RA signaling play vital roles as morphogens to establish regional identity within the hindbrain. RA signals first from the embryonic margin during gastrulation stages, and later in the pre-somitic mesoderm and subsequently the somitic mesoderm promote posterior identity (Begemann et al., 2001; Drummond et al., 2013). Meanwhile FGF signals from the caudal mesoderm are first required during gastrulation (Roy and Sagerstrom, 2004; Walshe et al., 2002; Wiellette and Sive, 2004), and later FGF signals from the midbrain hindbrain boundary (MHB) oppose the RA gradient, while FGF signals from r4 also pattern r5/6 (Guo et al., 1999; Maves et al., 2002; Sleptsova-Friedrich et al., 2001). The specific contributions of these signaling pathways to hindbrain specification and development are discussed in sections 1.3.5 and 1.3.7. *Hox* genes are key in the specification of segmental identity, and misregulation or disruption leads to loss of or altered rhombomere identities (Alexandre et al., 1996; Bell et al., 1999; Chisaka et al., 1992; Jungbluth et al., 1999; Lufkin et al., 1991; Mark et al., 1993; McClintock et al., 2001; McClintock et al., 2002; Rossel and Capecchi, 1999; Studer et al., 1998; Waskiewicz et al., 2001; Waskiewicz et al., 2002; Weicksel et al., 2014; Zigman et al., 2014). The role of *hox* genes in hindbrain patterning is discussed in detail in section 1.3.3.

Vhnf1 (HNF1 homeobox Ba (hnf1ba)) is a homeodomain transcription factor expressed up to the boundary between r4/5 (Aragon et al., 2005). Both FGF and RA signaling have also been shown to lie upstream of *vhnf1* and regulate its expression (Hernandez et al., 2004; Pouilhe et al., 2007). Loss of *vhnf1* results in disrupted gene expression from r4-6, where *hoxb1a* expression that is normally restricted to r4 is expanded posteriorly, and the expression of r5/6 genes are reduced or lost (such as

krox20 (*early growth response 2a (egr2a)* and *val* (*valentino, v-maf avian musculoaponeurotic fibrosarcoma oncogene homolog Ba (mafba),* also known as *kreisler (kr)*) (Sun and Hopkins, 2001; Wiellette and Sive, 2004). Conversely, overexpression of *vhnf1* causes an expansion of *val* expression anteriorly (Sun and Hopkins, 2001; Wiellette and Sive, 2004). *Vhnf1* establishes a positive feedback loop with *val*, as *val* maintains *vhnf1* expression in r5/6 (Kim et al., 2005). Additionally, the TALE (three amino acid loop extension) homeodomain transcription factor *irx7 (iroquois homeobox 7)* represses *vhnf1* expression anterior to r5, while *vhnf1* in turn prevents *irx7* expression in r5 (Lecaudey et al., 2004). Together, this suggests a role for *vhnf1* in repressing r4 identity, while promoting r5/6 identity.

Val (*valentino, v-maf avian musculoaponeurotic fibrosarcoma oncogene homolog Ba (mafba),* also known as *kreisler (kr)*) is a bZip transcription factor that is expressed initially in a broad domain that is subsequently divided into r5/6 (Moens et al., 1996). In *val* mutants r5/6 fail to divide properly, instead acquiring an r4-like character (Cordes and Barsh, 1994; Giudicelli et al., 2003; Manzanares et al., 1997; Manzanares et al., 1999b; McKay et al., 1994; Moens et al., 1998; Moens et al., 1996; Prince et al., 1998). *Val* prevents *hoxb1a* from being expressed in r5/6, while promoting the expression of *hoxa3* and *hoxb3* in r5/6 (Manzanares et al., 1999a; Manzanares et al., 1997; Prince et al., 1998). This illustrates the requirement for *val* in the establishment of r5/6 identity.

Krox20 (*early growth response 2b (egr2b)*) is a zinc finger transcription factor that is expressed in r3 and r5 (Swiatek and Gridley, 1993). Expression of *krox20* in r3 is promoted by both Hox/Pbx and Irx7/Meis1b (Meis homeobox 1b (also known as meis1.1)) complexes, while r5 expression of *krox20* is regulated by *vhnf1* (Chomette et al., 2006; Stedman et al., 2009; Wassef et al., 2008). *Hoxb1* and *hoxb2* also regulate *krox20* expression (Helmbacher et al., 1998), while *krox20* itself also provides feedback to maintain its own expression in r3/5 (Chomette et al., 2006; Wassef et al., 2008). In *krox20* mutants, while cells with r3 and r5 identities form initially, but they are subsequently lost, resulting in a failure of r3/5 formation (Schneider-Maunoury et al., 1997; Swiatek and Gridley, 1993; Voiculescu et al., 2001). *Krox20* restricts *hoxb1* expression to r4 (Garcia-Dominguez et al., 2006), while promoting the expression of

hoxa2, *hoxb2* and *epha4a* in r3/5 (Maconochie et al., 1996; Nonchev et al., 1996a; Nonchev et al., 1996b). *Krox20* also cooperates with *val* to promote *hoxb3* expression in r5 (Manzanares et al., 2002) and with *hoxa1* to specify r3 identity (Helmbacher et al., 1998). Overall, *krox20* is essential for the development and establishment of segmental identity in rhombomeres 3 and 5.

1.3.2 Hox Proteins and Cofactors

W. Bateson (Bateson, 1894) first described homeotic transformations over a century ago. *Hox* genes were subsequently discovered in Drosophila as the HOM-C complex where they were observed to control the anteroposterior specification of the embryo (Lewis, 1978; McGinnis et al., 1984; Scott and Weiner, 1984). *Hox* genes are unique in that they form clusters within the genome where all *hox* genes are oriented in the same 5' to 3' direction of transcription (Duboule, 1992; Kessel and Gruss, 1990; Krumlauf, 1992a; Krumlauf, 1992b; McGinnis and Krumlauf, 1992). Additionally, the physical order of the genes on the chromosome is correlated with both their anteroposterior expression along the axis of the embryo (Dolle et al., 1991; Dolle et al., 1989; Duboule and Dolle, 1989; Gaunt, 1991; Graham et al., 1989; Hunt et al., 1991; Kessel and Gruss, 1991; Wilkinson et al., 1989) and the timing of their expression (Izpisua-Belmonte et al., 1991; Munke et al., 1986). Genes that are located at the 3' end of the cluster are expressed earlier and more anteriorly within the developing embryo, while those located further 5' are generally expressed later and more posteriorly (Dekker et al., 1993; Papalopulu et al., 1991; Simeone et al., 1990).

The *hox* complexes arose through duplication and divergence from a conserved common ancestral cluster (reviewed by (Akam, 1989; Duboule, 1992; Kessel and Gruss, 1990; Krumlauf, 1992b; McGinnis and Krumlauf, 1992; Scott et al., 1989)). During vertebrate evolution, a two-step duplication of this complex has resulted in at least 4 clusters (A to D) (Kappen et al., 1989), consisting of 13 paralogous groups of *hox* genes (McClintock et al., 2001). The teleost lineage has undergone an additional whole genome duplication resulting in a total of 48 *hox* genes (as opposed to the 39 present in other vertebrates). This has allowed for the loss of some genes in zebrafish, and the neo- or sub-functionalization of others (McClintock et al., 2001).

Hox proteins are characterized by a homeobox DNA binding domain, which is made up of 60 highly conserved amino acids and binds to a conserved TAAT motif in the regulatory regions of target genes (Knoepfler et al., 1996; Phelan et al., 1994). Hox factor binding and subsequent transcription of target genes is also dependent on interactions with cofactors such as Meis (Myeloid ecotropic integration site), Pbx (Pre-B cell leukemia homeobox) and Prep (Pbx/knotted 1 homeobox, Pknox) (Choe et al., 2002; Ebner et al., 2005; Ferretti et al., 2000; Jacobs et al., 1999; Mann, 1995; Mann and Affolter, 1998; Mann and Chan, 1996; Ryoo et al., 1999). These genes encode divergent homeodomain-containing proteins of the three amino acid loop extension (TALE) class and were originally identified in Drosophila where the mutants had disruptions in body pattern, similar to those seen in *hox* mutants (Peifer and Wieschaus, 1990; Rauskolb et al., 1993; Rauskolb et al., 1995). Hox-Pbx complexes can act to either repress or activate transcription, depending on the recruitment of other factors and extracellular signals (Gebelein et al., 2004; Kobayashi et al., 2003; Saleh et al., 2000). Regulatory regions within the DNA that are bound by Hox, include Pbx binding sites. Pbx/Exd (Extradenticle) bind to a paired recognition element on DNA cooperatively with Hox proteins (Chan et al., 1994; Chang et al., 1995). In vertebrates the paired Hox/Pbx regulatory elements were first identified in the promoters of *hox* genes, such as *Hoxb1*. *Hoxa1* activates expression of *Hoxb1*, which then maintains its own expression and mutation of the Hox or Pbx binding elements of the promoter abrogates reporter expression (Ferretti et al., 2000; Maconochie et al., 1997; Manzanares et al., 2001; Pöpperl et al., 2000; Samad et al., 2004). Additional support for interactions between Hox and Pbx comes from studies of the hexapeptide motif in Hox and the three amino acid loop in the Pbx homeodomain (Chang et al., 1995; Knoepfler and Kamps, 1995; Neuteboom et al., 1995; Passner et al., 1999; Phelan et al., 1995; Piper et al., 1999), although there is evidence that Pbx/Exd can bind to Hox proteins in the absence of the hexapeptide motif (Galant et al., 2002; Merabet et al., 2003). Indeed, mutation of the WM amino acids to AA in the *Hoxa1* hexapeptide motif prevents Pbx binding and target gene expression is transfected cells (Phelan et al., 1995; Remacle et al., 2002), and *in vivo*, resembles the *Hoxa1* loss of function phenotype where rhombomere 4 is reduced

and r5 is lost, albeit the overall phenotype is milder (Carpenter et al., 1993; Mark et al., 1993; Remacle et al., 2004).

Meis/Prep sites are often associated with Hox/Pbx binding sites, and cooperative binding of these targets by Hox/Pbx/Meis is observed *in vitro* (Berthelsen et al., 1998; Chang et al., 1997; Ebner et al., 2005). Knockdown of *prep1.1* or overexpression of dominant-negative forms of *meis* results in phenotypes similar to those found in *pbx4* mutants (Choe et al., 2002; Deflorian et al., 2004; Vlachakis et al., 2001; Waskiewicz et al., 2001). Additionally Meis/Prep and Pbx interact to regulate the stability (Jaw et al., 2000; Longobardi and Blasi, 2003; Waskiewicz et al., 2001) and subcellular localization and Pbx (Abu-Shaar et al., 1999; Berthelsen et al., 1999; Jaw et al., 2000; Mercader et al., 1999; Rieckhof et al., 1997).

While Hox proteins themselves are key regulatory transcription factors, they have also been shown to be subject to regulatory control by other factors. *Val (mafba/kr)* acts upstream of *hox* genes to pattern rhombomeres 5 and 6 (Frohman et al., 1993; McKay et al., 1994; Moens et al., 1998; Moens et al., 1996). RA has also been shown to regulate *hox* gene expression (Conlon and Rossant, 1992; Maden and Holder, 1992; Marshall et al., 1992; Morriss-Kay, 1993). RA response elements have been found in the promoter regions of various *hox* genes including *Hoxa7* (Langston and Gudas, 1992) and *hoxd4* (Popperl and Featherstone, 1993), and mutations of *RA receptor γ* (*rarγ*) result in homeotic phenotypes (Lohnes et al., 1993). Other morphogens such as Sonic Hedgehog (SHH) have also been shown to activate *hox* gene expression (Riddle et al., 1993). *Hox* genes also often regulate their own expression and the expression of other *hox* genes, through both direct and indirect mechanisms (Bienz and Tremml, 1988; Chouinard and Kaufman, 1991; McClintock et al., 2002; Thuringer et al., 1993). The TGFβ family member *Gdf11* (McPherron et al., 1999; Nakashima et al., 1999), and the pluripotency factor *Oct4* (Downs, 2008; Osorno et al., 2012) regulate the patterning of axial progenitors, while *hox* genes subsequently pattern the tissues derived from the progenitors (Aires et al., 2016; Jurberg et al., 2013), and changes in *gdf11* or *oct4* gene expression result in changes to *hox* gene expression (Aires et al., 2016; Jurberg et al., 2013; Liu, 2006; McPherron et al., 1999; Simandi et al., 2016; Szumska et al., 2008). Additionally, Polycomb group (PC-G) members have been shown to be negative

regulators of *hox* genes through promoting the formation of repressive heterochromatin (DeCamillis et al., 1992; Franke et al., 1992; Paro and Hogness, 1991), and the loss of PC-G genes results in ectopic *hox* gene expression and homeotic transformations (Paro, 1990; Paro and Zink, 1993; Struhl and Akam, 1985).

1.3.3 Roles for Hox Proteins in Rhombomere Specification

Paralog group (PG) 1-4 *hox* genes display nested domains of expression in which the AP boundaries map tightly to the junctions between rhombomeres (Hunt et al., 1991; Keynes and Krumlauf, 1994; Lumsden and Krumlauf, 1996; Maconochie et al., 1996; Wilkinson et al., 1989). A summary of *hox* gene expression in the hindbrain is shown in Figure 1.2. Generally, *hox* genes from the same PG have the same AP expression boundaries, such that members from *hox* PGs 2, 3, and 4 have anterior expression boundaries at the r2/3, r4/5 and r6/7 boundaries, respectively.

There are 3 PG 1 *hox* genes in mammals (*Hoxa1*, *Hoxb1* and *Hoxd1*), while zebrafish have 4 paralogs (*hoxa1a*, *hoxb1a*, *hoxb1b*, *hoxc1a*). The function of *hoxb1b* is equivalent to *Hoxa1*, while *hoxb1a* is homologous to *Hoxb1* (McClintock et al., 2001; McClintock et al., 2002). Zebrafish *hoxb1b* expression is first seen at 50% epiboly (5.25hpf) (Alexandre et al., 1996), and it is the first *hox* gene to be expressed in the zebrafish embryo. The anterior limit of *hoxb1b* expression is r4 and it eventually retreats leaving *hoxb1a* expression in r4 (Alexandre et al., 1996). *Hoxa1* and *Hoxb1* are expressed similarly in mouse (Studer et al., 1998). *Hoxd1*, *hoxa1a*, and *hoxc1a* are not expressed in the hindbrain rhombomeres during development. Expression of *hoxb1a (Hoxb1)* in r4 is activated by *hoxb1b (Hoxa1)*, and *hoxb1b* is required for segmentation and rhombomere size from r3-r6, which then impacts neural crest development, otic vesicle specification, and development of r4 associated neurons (Carpenter et al., 1993; Mark et al., 1993; McClintock et al., 2002; Weicksel et al., 2014; Zigman et al., 2014). Rhombomere 4-specific gene expression and neuron development requires r4 expression of *hoxb1a* (*Hoxb1*) (McClintock et al., 2002; Studer et al., 1998; Weicksel et al., 2014). Overexpression of either PG1 *hox* gene leads to homeotic transformations where r2 adopts an r4-like character (Alexandre et al., 1996; McClintock et al., 2002). Compound loss of *Hoxa1;Hoxb1* or *hoxb1a;hoxb1b* results in segmental defects in the hindbrain,

which are similar although somewhat exacerbated to those seen in *hoxb1b* (*Hoxa1*) loss of function (Gavalas et al., 1998; McClintock et al., 2002; Rossel and Capecchi, 1999; Studer et al., 1998; Weicksel et al., 2014; Zigman et al., 2014). In *Xenopus laevis*, knockdown of *hoxa1;hoxb1;hoxd1* results in a far more severe phenotype where there is a complete loss of segmental identity in the hindbrain (McNulty et al., 2005).

Hoxa2 (*hoxa2b*) is expressed from the r1/2 boundary and *Hoxb2* (*hoxb2a*) is expressed from the r2/3 boundary (Prince et al., 1998). *Hoxa2* is required for segmental identity in r2 as it is the only hox gene expressed in r2. Loss of *Hoxa2* reduces r2 while expanding r1, resulting in defects in cranial neural crest destined for the 2nd branchial arch (Gavalas et al., 1997; Rijli et al., 1998; Trainor and Krumlauf, 2000). *Hoxa2* also regulates r3 size, while r4 identity is partially dependent on *Hoxb2* (Davenne et al., 1999; Gavalas et al., 2003). Loss of both PG2 *Hox* genes illustrates roles for both *Hoxa2* and *Hoxb2* in generating the r2/3 boundary. Expression of *Hoxb2* in r3/5 is regulated by *Krox20* (Chavrier et al., 1988; Schneider-Maunoury et al., 1993; Sham et al., 1993; Swiatek and Gridley, 1993; Wilkinson et al., 1989). *Krox20* may also contribute to the expression of *Hoxa2*, *Hoxa3* and *Hoxb3* in r3/5 (Hunt et al., 1991; Krumlauf, 1993).

PG3 *hox* genes are expressed up to the r4/5 boundary, and loss of all 3 PG3 *hox* genes results in defects in r5/6 motor neurons and ectopic *Hoxb1* expression in r6 (Gaufo et al., 2003). The loss of one or two PG3 genes does not result in changes in hindbrain patterning, although there are defects in nIX cranial nerve development (Manley and Capecchi, 1997). Similarly, PG4 *hox* genes are expressed up to the r6/7 boundary, and their loss does not result in hindbrain defects (Horan et al., 1995).

Hox proteins also exhibit complex cross- and auto-regulatory loops. *Hoxb1*, *Hoxa3*, *Hoxb3* and *Hoxb4* all have known Hox/Pbx auto-regulatory elements. After RA has initiated *Hoxb1* and *Hoxb4* expression, they subsequently maintain their own expression in r4 and r7 respectively (Gould et al., 1997; Popperl et al., 1995). Similarly, *Hoxa3* and *Hoxb3* maintain their expression in r5 through autoregulation following the initiation of their expression by *Val* (Manzanares et al., 2001). *Hoxb1* expression is maintained in r4 through its auto-regulatory element, and *Hoxa1* and *Hoxb2* are also involved in the regulation *Hoxb1* expression (Manzanares et al., 2001). *Hoxb1* in turn regulates *Hoxa2* and *Hoxb2* expression in r4 (Maconochie et al., 1997; Tumpel et al.,

2007). Furthermore, *Hox3* members have been shown to regulate *Hoxa3* (Manzanares et al., 2001), while *Hox4* members regulate *Hoxb4* (Gould et al., 1997; Serpente et al., 2005).

1.3.4 Roles for Hox Cofactors in Rhombomere Specification

During hindbrain specification, two zebrafish *pbx* genes (*pbx2, pbx4*), five zebrafish *meis* genes (*meis1b, meis2b, meis1a, meis2a,* and *meis3*) and two zebrafish *prep/pknox* genes (*pknox1.1* and *pknox1.2*) are expressed (Pöpperl et al., 2000; Vlachakis et al., 2000; Waskiewicz et al., 2001; Waskiewicz et al., 2002; Zerucha and Prince, 2001), and differences in their expression are likely responsible for their functional differences (Pöpperl et al., 2000).

The phenotypes of *pbx* mutants are similar to those of *hox* mutants. Zebrafish *pbx4* mutants resemble *Hox* mutants in mouse and have a disruption of *Hox*-dependent patterning (Pöpperl et al., 2000; Waskiewicz et al., 2002). Facial branchiomotor neurons fail to migrate posteriorly in *pbx4* mutants, a phenotype which is also seen in *Hoxb1* mouse mutants, and loss of function of zebrafish *hoxb1a* (Arenkiel et al., 2004; Cooper et al., 2003; McClintock et al., 2002; Studer et al., 1998; Weicksel et al., 2014). Loss of *Pbx1* results in a phenotype similar to *Hoxa2* mutants in mouse, where second pharyngeal arch cartilage structures undergo a homeotic transformation to resemble first arch cartilage structures (Gendron-Maguire et al., 1993; Rijli et al., 1993; Selleri et al., 2001). Additionally, loss of maternal and zygotic *pbx4* in combination with knockdown of *pbx2* in zebrafish, transforms the hindbrain to an r1 identity, consistent with *pbx* genes having a role in *hox*-dependent patterning of the hindbrain (Waskiewicz et al., 2002). Although this phenotype is consistent with the knockdown of *hoxa1;hoxb1;hoxd1* in *Xenopus laevis* (McNulty et al., 2005), the zygotic loss of *hoxb1a* and *hoxb1b* in zebrafish does not recapitulate this phenotype (Weicksel et al., 2014). In addition, while overexpression of anterior *hox* genes leads to ectopic expression of hindbrain genes in anterior structures such as the eye and telencephalon, and homeotic transformations of segmental identity in the hindbrain, this effect requires Pbx function and is suppressed in *pbx4* mutants (Cooper et al., 2003; Pöpperl et al., 2000).

Meis genes are expressed in the hindbrain during rhombomere patterning, similar to *hox* genes (Sagerstrom et al., 2001; Waskiewicz et al., 2001). Overexpression of dominant negative forms of *meis* have similar phenotypes to *pbx4* mutants (Choe et al., 2002; Waskiewicz et al., 2001) indicating that Pbx-dependent regulation of hindbrain specification requires Meis. Co-expression of *meis3* in combination with *hoxb1b*, results in a far more severe homeotic transformation than the overexpression of *hoxb1b* alone, indicating that Hox function may be limited by Meis protein levels (Vlachakis et al., 2001). Meis and Pbx post-translationally regulate each other, and these interactions further serve to regulate Hox function. A dominant negative form of Pbx4 lacking a nuclear localization domain results in mislocalization of Meis to the cytoplasm (Choe et al., 2002). Meanwhile, Meis overexpression can stabilize Pbx proteins and partially rescue *pbx4* mutants through stabilization of maternally provided Pbx4 (Waskiewicz et al., 2001).

1.3.5 RA Signaling

Retinoids are typically provided by the diet and are not synthesized de novo. In the zebrafish embryo, Vitamin A is found in the egg yolk. Figure 1.3 provides an overview of RA signaling. Circulating retinol is bound by Retinol-binding protein 4 (Rbp4) and is taken up by target tissues via the transmembrane protein Stra6. Once retinol has been taken up by target tissues they are bound by cellular retinol-binding proteins (Crbp), which may control levels of intracellular retinol. Retinol is then oxidized to retinaldehyde by retinol dehydrogenases (Rdh). *Rdh10* is expressed in specific domains during development (Cammas et al., 2007; Romand et al., 2008) and the loss of *rdh10* results in characteristic defects associated with a loss of RA (Rhinn et al., 2011; Sandell et al., 2007). Retinaldehyde is then oxidized into Retinoic Acid by retinaldehyde dehydrogenases (Raldhs or Aldhs). RA is then bound by cellular retinoic acid-binding proteins (Crabp). *Aldhs* have distinct expression patterns correlated with areas of known RA activity (Niederreither et al., 1999; Niederreither et al., 2000). Cytochrome P450 1B1 (Cyp1b1) enzymes may also catalyze the oxidation of retinol into retinaldehyde and subsequently into RA (Chambers et al., 2007). In the nucleus, RA binds to Retinoic acid receptors (RARs) which heterodimerize with retinoid X receptors

(RXRs) (reviewed by (Rochette-Egly and Germain, 2009)). These complexes bind to Retinoic Acid response elements (RAREs). In the presence of RA, co-activators are recruited to induce chromatin re-modeling and assembly of the pre-initiation complex, while co-repressor complexes are recruited in the absence of RA.

In order for RA levels and distribution to be controlled during development, Cytochrome P450 subfamily 26 (Cyp26) enzymes hydroxylate RA into polar metabolites (Abu-Abed et al., 2001; Chithalen et al., 2002; de Roos et al., 1999; Hernandez et al., 2004; Niederreither et al., 2002; Sakai et al., 2001; Sirbu et al., 2005; Swindell and Eichele, 1999). The metabolism of RA mediated by Cyp26 enzymes is required to restrict RA mediated signaling to specific regions and cells within the embryo.

1.3.6 Roles for RA Signaling in Rhombomere Specification

Retinoic Acid is produced in the somatic mesoderm by *aldh1a2*, where it diffuses towards the hindbrain, creating a gradient across the anterior-posterior axis. Higher concentrations of RA are found posteriorly and activate progressively more posterior genes (Gavalas, 2002; Niederreither and Dolle, 2008). Retinoic acid synthesis, and the AP gradient are balanced by the rhombomere specific expression patterns of the *cyp26* genes (Abu-Abed et al., 2001; Sakai et al., 2001). The posterior limit of *cyp26* activity at the onset of RA-dependent gene expression helps to determine the boundaries of RA-responsive genes (Hernandez et al., 2007). *Pbx* genes have also been shown to play a role in regulation of *aldh1a2* expression (French et al., 2007; Maves et al., 2007; Vitobello et al., 2011). The RA gradient is also influenced and stabilized, both by feedback and feed forward mechanisms. RA induces the expression of *cyp26* enzymes, promoting the metabolism of RA itself. Meanwhile FGF signaling represses RA degradation (White et al., 2007; White and Schilling, 2008). Maintenance of the RA gradient across the hindbrain is essential for hindbrain development and patterning. Reductions in RA levels result in the loss of posterior hindbrain identity (Begemann et al., 2001; Dupe and Lumsden, 2001; Maden et al., 1996) while increases in RA disrupt the development of the anterior hindbrain (Gould et al., 1998; Hill et al., 1995; Morrison et al., 1997). These alterations are commonly associated with changes in *hox* gene

expression, and defects in segmental identity (Ferretti et al., 2000; Frasch et al., 1995; Gould et al., 1998; Morrison et al., 1997; Papalopulu et al., 1991; Yan et al., 1998). RA initiates the expression of *hox* genes, such as *Hoxa1*, *Hoxb1*, *Hoxa4*, *Hoxb4* and *Hoxd4* which all have RAREs in their promoters that control some aspect of their neural expression (Gavalas, 2002; Gavalas and Krumlauf, 2000; Gould et al., 1998; Maden, 2002; Marshall et al., 1994; Packer et al., 1998; Studer et al., 1998). Indeed, *Hoxa1* and *Hoxb1* require an intact RARE to initiate their expression in r4 (Dupe et al., 1997; Studer et al., 1998).

Exposure of pregnant mice or rats to exogenous RA has been shown to have a teratogenic effect on hindbrain development (Morriss, 1972). Depending on the time of exposure, it can have different effects on hindbrain development. Early exposure to RA during late gastrula or early neurula stages results in an increase in hindbrain size at the expense of other regions of the brain (Avantaggiato et al., 1996), while exposure to exogenous RA at later stages of development lead to a posteriorization of the hindbrain specifically, where anterior rhombomeres acquire a more posterior identity (Marshall et al., 1996). Similarly, loss of function of *cyp26* genes leads to posteriorization of the hindbrain, due to a loss of RA metabolism (Abu-Abed et al., 2001; Sakai et al., 2001). Compound loss of *cyp26a1* and *cyp26c1* results in a severe posteriorization and lack of segmentation from r1-4 (Maclean et al., 2009; Uehara et al., 2007).

Conversely, in vitamin A deficient quail, the anterior rhombomeres are expanded such that r4-8 are misspecified to an r3 identity (Gale et al., 1999). Similarly, treatment with a pan-RAR antagonist has phenotypes similar to *aldh1a2 (Raldh2)*, *Rarα;Rarβ* and *Rarα;Rarγ* mutants (Begemann et al., 2001; Dupe et al., 1999; Grandel et al., 2002; Niederreither et al., 2000; Wendling et al., 2001), where segmentation and patterning of the posterior hindbrain is disrupted. These alterations to the hindbrain lead defects in inner ear and branchial arch development, as well as alterations to cranial nerve differentiation. Zebrafish *aldh1a2* mutants have similar anteriorization of the hindbrain, where regions posterior to r6 are truncated (Begemann et al., 2001; Grandel et al., 2002). Together, this illustrates the integral role of RA in establishing regional identity in the hindbrain. More posterior rhombomeres require higher levels of RA for proper specification and disruption of the anterior-posterior RA gradient prevents proper

specification and segmentation of the rhombomeres.

1.3.7 FGF Signaling

FGF signaling transduces extracellular signals through transmembrane receptor tyrosine kinases, where they can subsequently activate multiple intracellular signal transduction pathways. FGF signaling through the Ras-MAPK pathway is shown in Figure 1.4. FGF ligands bind to Fgf receptors (FGFR), which are tyrosine kinases. Binding induces dimerization and trans-auto phosphorylation of specific tyrosine residues in the intracellular domain (Goetz and Mohammadi, 2013). Secreted FGFs are grouped based on biochemical function, sequence and evolutionary relationships. There are 5 subfamilies of paracrine FGFs, 1 subfamily of autocrine FGFs and 1 subfamily of intracellular FGFs. Most require heparin/heparin sulfate (HS)/Heparin sulfate proteoglycan (HSPG) as a cofactor to potentiate FGF ligand activity and enhance FGFR binding and activity (Ornitz and Leder, 1992; Ornitz et al., 1992; Rapraeger et al., 1991; Schreiber et al., 1985a; Schreiber et al., 1985b; Thomas et al., 1985; Yayon et al., 1991) although different families have different receptor specificities. The activated receptor then interacts with intracellular signaling pathways such as the Ras-MAPK (Mitogen activated protein kinase), PI3K/AKT (Phosphatidylinositol-3-kinase/protein kinase B), PLCγ (Phospholipase C, gamma) and STAT (Signal transducers and activators of transcription). We have focused on the Ras-MAPK pathway that is activated by the major FGFR kinase substrate Frs2α (FGFR substrate 2α). Frs2α is bound to the juxtamembrane region of the FGFR and anchored to the cell membrane (Kouhara et al., 1997; Ong et al., 2000) and interacts with Crkl (Crk-like). Activation of the FGFR results in phosphorylation of Frs2α, which subsequently recruits Grb2 (Growth factor receptor-bound 2). Grb2 then recruits Sos (Son of sevenless), which then activates the Ras GTPase. This then activates the MAPK pathway, which results in the activation of members of the Ets (E26 transformation-specific) transcription factor family, such as Etv4 (Ets variant 4/Pea3), Etv5 (Ets variant 5/Erm). These transcription factors then regulate expression of target genes such as *spry* (*sprouty*) and *dusp6* (*dual specificity phosphatase 6/mkp3*). Some of these proteins are also negative regulators of the FGF signaling pathway, such as Spry and Dusp6. There are 4 members in the Spry family (1-

4) and Spry interacts with Grb2 to inhibit Ras-MAPK signaling. Dusp6 is a MAPK phosphatase that specifically targets Erk (Extracellular signal-regulated kinase)/Mapk to provide negative feedback inhibition (Camps et al., 1998).

1.3.8 Roles for FGF Signaling in Rhombomere Specification

FGF has diverse roles in the development of the neural tube. FGF signals are required for neural induction (De Robertis and Kuroda, 2004; Delaune et al., 2005; Furthauer et al., 2004), and FGF has been shown to pattern posterior structures, as ectopic FGF shifts posterior genes anteriorly (Koshida et al., 2002; Kudoh et al., 2002; Pownall et al., 1998; Pownall et al., 1996). FGF signaling has also been shown to be required for the maintenance of neural progenitors (Akai et al., 2005), and for expression of genes in the spinal cord (Pownall et al., 1998; Pownall et al., 1996). Within the hindbrain, *fgf3* and *fgf8* are required for the formation of periphery structures associated with r5/6, such as the otic placode, the pharyngeal arch cartilages and cranial ganglia (Maroon et al., 2002; Maves et al., 2002; Phillips et al., 2001), Additionally, components of the FGF signaling pathway are expressed at rhombomere boundaries in chick, and *FGF3* play an organizing role at these boundaries by regulating the expression of boundary markers responsible for enriched ECM (extracellular matrix), axonal accumulation and neural differentiation (Weisinger et al., 2012). FGF signaling is also frequently associated with the development of the midbrain, cerebellum, and the midbrain-hindbrain boundary (Meyers et al., 1998; Reifers et al., 1998; Sleptsova-Friedrich et al., 2001).

FGF signaling is commonly associated with prominent developmental signaling centers. *Fgf3* and *fgf8* participate in patterning of the telencephalon from the anterior neural ridge (Rubenstein, 2000). *Fgf8* plays a prominent role at the MHB by patterning the midbrain and anterior hindbrain, and specifying the r0/1 boundary (Guo et al., 1999; Sleptsova-Friedrich et al., 2001; Wurst and Bally-Cuif, 2001). This is supported by the phenotype of *fgf8* mutants, which lack the MHB, and have a loss of r0 structures, while r1 is expanded anteriorly (Brand et al., 1996; Guo et al., 1999; Sleptsova-Friedrich et al., 2001).

There is additional evidence that FGF signaling is involved in establishing a

signaling centre in rhombomere 4. The loss of r4 associated genes, such as *Hoxa1* or *hoxb1a*, affects the development of adjacent rhombomeres (Helmbacher et al., 1998; Weicksel et al., 2014) while transplantation of r4 cells outside of the hindbrain is able to induce non-autonomous expression of the r5/6 markers, *val* and *krox20* (Maves et al., 2002). These results support r4 as a source of a signal, which is important in the patterning of its surrounding structures. FGF has been identified as the likely signal from r4. *Fgf3* expression is restricted to r4 in the hindbrain and *fgf8* expression is observed in r4, in addition to its expression domains in the MHB and r2. Loss of *fgf3* and *fgf8*, or pharmacological inhibition of FGF signaling in the hindbrain prevents specification of r5/6 specification (Marin and Charnay, 2000; Maves et al., 2002; Walshe et al., 2002; Wiellette and Sive, 2004). This suggests that the loss of FGF signals results in the loss of the r4 signaling centre and subsequent failure to pattern the adjacent rhombomeres. *Fgf3* expression in r4 is conserved in vertebrates (Lombardo et al., 1998; Mahmood et al., 1995; Mahmood et al., 1996; McKay et al., 1996; Tannahill et al., 1992), and it is commonly co-expressed in r4 with other Fgfs, such as *fgf8* in zebrafish (Maves et al., 2002) and *FGF4* in chick (Shamim and Mason, 1999) (which has similar receptor specificity to *fgf8* (Vlachakis et al., 2001)).

Other signaling pathways have been shown to be involved in regulation of the FGF signaling centre. RA is important for positioning of the signaling centre in r4, excess RA shifts the signaling centre anteriorly, while reductions in RA shift it posteriorly (Dupe and Lumsden, 2001; Hill et al., 1995; Walshe et al., 2002). Other genes including *follistatin, pbx2/4, hoxb1b, ppp1r14ab* (*protein phosphatase 1, regulatory (inhibitor) subunit 14Ab),* and *vhnf1* have been shown to be involved in regulating the expression of *fgf3/8* in the hindbrain (Aragon et al., 2005; Choe et al., 2011; Waskiewicz et al., 2002; Weisinger et al., 2008).

1.4 Hindbrain Ventricle Development

The forebrain, midbrain and hindbrain are delineated by characteristic morphological bends and constrictions. The lumen of these regions will form the ventricles when they are filled with cerebrospinal fluid (CSF). In adults the CSF protects the brain from physical trauma (Hajdu, 2003; Segal, 2001) and also functions as a neural

circulatory system to transport waste and nutrients (Cushing, 1914; Milhorat et al., 1971; Pollay and Curl, 1967; Segal, 2001). During embryogenesis, the ventricles and the embryonic CSF (eCSF) fulfill similar circulatory functions as they do in adults, and also may facilitate homeostatic, hormonal and morphogen signaling (Chodobski and Szmydynger-Chodobska, 2001; Emerich et al., 2005; Miyan et al., 2003; Sawamoto et al., 2006; Vigh and Vigh-Teichmann, 1998). The first phase of ventricle formation occurs between 17-24 hpf in zebrafish. This involves the initial shaping of the neural tube to open the brain ventricles, and is not dependent on circulation (Lowery and Sive, 2005). The second phase of ventricle morphogenesis occurs between 24-36 hpf, where coupled with the onset of circulation, the volume of the ventricle massively increases (Lowery and Sive, 2005; Wullimann et al., 2005). In vertebrates, the forebrain ventricle will divide to form the two lateral ventricles and the third ventricle, the hindbrain ventricle will become the fourth ventricle and the midbrain ventricle will become the cerebral aqueduct, connecting the third and fourth ventricles. (Gray and Clemente, 1985)

Development of the brain ventricular system relies first on the appropriate DV and AP patterning of the neuroepithelium, enabling the correct positioning of the ventricles (Britto et al., 2002; Elsen et al., 2008; Hjorth et al., 2002; Lumsden and Krumlauf, 1996; Rubenstein et al., 1998; Tannahill et al., 2005). In order for proper morphogenesis of the ventricles to occur the formation and maintenance of a continuous epithelium is required (Hong and Brewster, 2006; Lele et al., 2002). Subsequent changes in cell shape mediated by cytoskeletal dynamics (Eto et al., 2005; Fristrom, 1988; Lecuit and Lenne, 2007; Xia et al., 2005) and the anchoring and support of epithelium by the extracellular matrix (Ashkenas et al., 1996; Gato et al., 1993; Gullberg and Ekblom, 1995; Morriss-Kay and Crutch, 1982; Ojeda and Piedra, 2000; Schoenwolf and Fisher, 1983; Tuckett and Morriss-Kay, 1989; Yip et al., 2002) will shape the ventricles. Regulated cell death (Glucksmann, 1951; Kallen, 1955; Keino et al., 1994; Kuida et al., 1996), proliferation (Elsen et al., 2008; Kahane and Kalcheim, 1998; Nyholm et al., 2007; Sausedo et al., 1997; Schoenwolf and Alvarez, 1989; Tao and Lai, 1992; Tuckett and Morriss-Kay, 1989; Xuan et al., 1995), and transcriptional regulation of neuronal differentiation (Lowery and Sive, 2009) also contribute to ventricle morphogenesis. The initial secretion of eCSF by the neuroepithelium will subsequently inflate the ventricles

(reviewed in (Lowery and Sive, 2009)). Perturbations to any aspects of this developmental process can result in ventricle defects. Ventricular defects have been associated with developmental abnormalities including cranial neural tube closure defects, hydrocephalus and neurodevelopmental health disorders. Neural tube closure defects allow eCSF to escape as the ventricular system remains open and exposed instead of undergoing proper closure (Moore, 2006). This results in tissue degeneration, and in cases of anencephaly where the neural tube fails to close in the brain, infants are not viable (Moore, 2006). Hydrocephalus occurs in up to 1/300 births (Zhang et al., 2006) and can result from alterations in CSF production, absorption or flow (Ibanez-Tallon et al., 2004; Pourghasem et al., 2001; Zhang et al., 2006). This causes severe perturbations in brain development, including decreased neurogenesis (Mashayekhi et al., 2002). Numerous neurodevelopmental disorders including ADHD, Down's syndrome, Fragile X syndrome, schizophrenia and autism have been correlated with abnormalities with brain ventricle shape and size (Castellanos et al., 1996; Frangou et al., 1997; Gilmore et al., 2001; Hardan et al., 2001; Kurokawa et al., 2000; Nopoulos et al., 2007; Piven et al., 1995; Prassopoulos et al., 1996; Rehn and Rees, 2005; Reiss et al., 1995; Sanderson et al., 1999; Shenton et al., 2001; Wright et al., 2000).

1.4.1 Genes Involved in Ventricle Development

Multiple large-scale mutagenesis screens have identified mutants that have ventricle defects (Jiang et al., 1996; Malicki et al., 1996; Schier et al., 1996). Many of these mutations also result in defective circulation (such as mutants for *troponin T type 2a, cardiac (tnnt2a), neuronal PAS domain protein 4 like (npas4l), mix paired-like homeobox (mixl1), splicing factor proline/glutamine-rich (sfpq), mediator complex subunit 14 (med14), ATPase Na+/K+ transporting subunit alpha 1a, tandem duplicate 1 (atp1a1.1), fullbrain (ful), glaca (glc), landfill (lnf), turned down (twn), eraserhead (esa)* and *zonderzen (zon),* although circulation in *zon* mutants does recover) (Schier et al., 1996), and the defects in brain ventricle morphology may in fact be due to the lack of circulation. These screens, and other research have identified other genes and processes that are required for appropriate ventricle development.

Mutations in *mpp5a (membrane protein, palmitoylated 5a (MAGUK p55 subfamily member 5)* (Wei and Malicki, 2002)), *crb2a (crumbs family member 2a* (Omori and Malicki, 2006)) and *prkci (protein kinase C, iota* (Horne-Badovinac et al., 2001)) prevent the ventricles from opening uniformly, resulting in points along the ventricle where the midline fails to separate (Lowery et al., 2009). Mpp5a, Crb2a and Prkci can interact and form complexes that colocalizes to the apical neuroepithelial surface where it regulates junction formation and polarity (Horne-Badovinac et al., 2001; Hsu et al., 2006; Omori and Malicki, 2006). Apical localization of Mpp5a requires Crb2a, but not Prkci, and defects in apicobasal polarity may result in compromised neuroepithelial integrity, thereby preventing midline separation during ventricle morphogenesis (Lowery et al., 2009). A role for a polarized and organized neuroepithelium in ventricle morphogenesis is further supported by *cdh2 (cadherin 2, type 1, N-cadherin, neuronal)* mutants (Hong and Brewster, 2006; Lele et al., 2002). Cdh2 is required for polarized cell movements during neural tube morphogenesis, and loss of *cdh2* results in a disorganization of cells in the neural tube, with aberrant cell polarity, thereby causing defective ventricle formation (Hong and Brewster, 2006; Lele et al., 2002). Not only must the neuroepithelium be properly organized and polarized, and undergo stereotypic morphogenic movements, it must also undergo a process termed epithelial relaxation, in order for the ventricle to inflate (Gutzman and Sive, 2010). Ppp1r12a (Protein phosphatase 1, regulatory subunit 12a) regulates myosin contractility as a regulatory component of myosin phosphatase. In the absence of *ppp1r12a*, myosin phosphatase is not functional, and myosin regulatory light chain (MRLC) cannot be de-phosphorylated, resulting in over active myosin II (Hartshorne et al., 2004; Huang et al., 2008; Ito et al., 2004). Loss of this epithelial relaxation prevents the ventricle from inflating properly, as the epithelium remains too stiff (Gutzman and Sive, 2010).

Components of the ECM have also been shown to be important for ventricle morphogenesis. Mutations in *laminin, gamma 1 (lamc1)* and *laminin, beta 1a (lamb1a)* result in smaller ventricles and abnormalities in midbrain-hindbrain boundary (MHB) folding (Lowery et al., 2009). Loss of laminin in the basement membrane may affect shaping of the epithelium (Gutzman et al., 2008). Furthermore, loss of the ECM

component *fibronectin 1a (fn1a)* also results in smaller ventricles, however this phenotype is not evident until later stages on development (Lowery et al., 2009).

Neurogenesis has also been shown associated with ventricle development. The mediator complex is a multi-protein complex that bridges transcription factors and RNA polymerase II (Conaway et al., 2005). Mutations in components of this complex (*mediator complex subunit 12 (med12)* and *mediator complex subunit 14 (med14)*) have defects in select neuronal subtypes, and a reduction in ventricle size (Guo et al., 1999; Hong et al., 2005b; Lowery et al., 2009; Wang et al., 2006)). *Mind bomb (mind bomb E3 ubiquitin protein ligase 1 (mib1))* mutants which have increased numbers of early born neurons at the expense of later born neurons, disorganization of BMN and loss of rhombomere boundaries also have smaller ventricles (Bingham et al., 2003; Schier et al., 1996). Furthermore, *sfpq (splicing factor proline/glutamine-rich)*, and *neogenin* which are required for neuronal differentiation (Lowery et al., 2007; Mawdsley et al., 2004), and *her9*, *zic1* and *zic4*, which are involved in neural progenitor maintenance (Bae et al., 2005; Elsen et al., 2008), also result in defective ventricle morphogenesis when they are lost or knocked down (Bae et al., 2005; Elsen et al., 2008; Lowery et al., 2007; Mawdsley et al., 2004). Together, these finding suggest a correlation between neurogenesis and ventricle development.

Appropriate cell proliferation may also be required to facilitate ventricle morphogenesis. *Zic1 (zic family member 1)* and *zic4 (zic family member 4)* are required not only for roof plate development and expression of rhombomere boundary specific genes, but also for neural proliferation (Elsen et al., 2008). Knockdown of *zic1* and *zic4*, or knockdown of the genes which *zic1/4* regulate (*wnt1*, *rfng (RFNG O-fucosylpeptide 3-beta-N-acetylglucosaminyltransferase/radical fringe homolog)* and *lmx1b (LIM homeobox transcription factor 1, beta)*) result in midline separation defects (Elsen et al., 2008). *Zic2a* and *zic5*, which are regulated by Tcf (T-cell factor)/Lef (Lymphoid enhancer binding factor), have roles in promoting dorsal midbrain proliferation, and knockdown of *zic2a* results in reduced ventricles (Nyholm et al., 2007). The *curly fry (cfy)* mutant has reduced ventricles and abnormal cell proliferation, where cells in the neural keel either undergo increased mitosis, or mitotic cells are arrested (Song et al.,

2004). *Sfpq* also has roles in repressing apoptosis and promoting cell survival, which may contribute the ventricle defects observed (Lowery et al., 2007).

Finally, in order for the ventricle to inflate, CSF must be secreted into the lumen. *Atp1a1.1* (*ATPase Na+/K+ transporting subunit alpha 1a, tandem duplicate 1*) encodes a component of the Na+/K+ pump, which creates an ionic gradient across the membrane, allowing water to flow into the ventricle. Loss of *atp1a1.1* results in the almost complete loss of ventricle inflation (Lowery and Sive, 2005).

1.4.2 The Core Hippo Pathway

The Hippo signaling pathway was initially defined in *Drosophila* as tumor suppressor genes that when mutated, result in tissue overgrowth (*Warts* (Justice et al., 1995; Xu et al., 1995b), *Hippo* (Harvey et al., 2003; Jia et al., 2003; Pantalacci et al., 2003; Udan et al., 2003; Wu et al., 2003), *Salvador* (Kango-Singh et al., 2002; Tapon et al., 2002), *Mats* (Lai et al., 2005), *Yki* (Huang et al., 2005), *Sd* (Goulev et al., 2008; Wu et al., 2008; Zhang et al., 2008; Zhao et al., 2008a)). An overview of the core components of the Hippo signaling pathway is shown in Figure 1.5. The Stk3 kinase (also referred to as Mst kinase) phosphorylates and activates Lats1/2 (Chan et al., 2005). Stk3 also phosphorylates Sav1 (Callus et al., 2006) and Mob1a/1ba/1bb (Chan et al., 2005; Praskova et al., 2008) enabling these proteins to enhance the kinase activity of Stk3 and Lats1/2 respectively. Active Lats1/2 kinases phosphorylate Yap/Taz on HXRXXS consensus sites (Dong et al., 2007; Huang et al., 2005; Lei et al., 2008; Oh and Irvine, 2008; Zhao et al., 2007). The phosphorylated form of Yap/Taz is sequestered in the cytoplasm via interaction with 14-3-3 proteins (Zhao et al., 2007). The phosphorylation of Yap/Taz can also lead to them being targeted by the degradation machinery of the cell (Liu et al., 2010; Zhao et al., 2010). When Yap/Taz are not phosphorylated by the upstream kinase cascade, they are able to translocate to the nucleus where they bind to the promoters of target genes (Dong et al., 2007; Kanai et al., 2000; Lei et al., 2008; Oh and Irvine, 2008; Ren et al., 2010; Zhao et al., 2007) primarily through interactions with the TEAD (TEA domain) family of transcription factors (Goulev et al., 2008; Vassilev et al., 2001; Wu et al., 2008; Zhang et al., 2008; Zhao et al., 2008a) (however other transcription factors are also known to interact with Yap/Taz

(Alarcon et al., 2009; Ferrigno et al., 2002; Komuro et al., 2003; Omerovic et al., 2004; Strano et al., 2001; Varelas et al., 2008; Yagi et al., 1999). The core components of the *Drosophila* Hippo pathway are highly conserved.

1.4.3 Upstream Inputs to Hippo Signaling and Cross Talk

There are a myriad of inputs that regulate components of the core hippo pathway. This includes factors which regulate the Stk and Lats kinases, or sequester Yap/Taz in the cytoplasm, proteins and protein complexes associated with cell-cell junctions and cell polarity, G-protein-coupled receptor (GPCR) transduced signals, mechanotransduction, and metabolic signals, along with complex interactions with other signaling pathways such as Wnt, Tgf-B, Notch SHH and Mitogenic growth factor pathways. A summary of these interactions is shown in Figure 1.6.

One of the earliest described upstream regulators of the core Hippo pathway is the Merlin (Nf2)/Ex (Expanded)/Kibra complex, which has been shown to repress Yap/Taz activity through enhancing the kinase activity of Stk3 and recruitment of Yap/Taz to the plasma membrane (Angus et al., 2012; Baumgartner et al., 2010; Genevet et al., 2010; Hamaratoglu et al., 2006; McCartney et al., 2000; Moleirinho et al., 2013; Xiao et al., 2011; Yin et al., 2013; Yu et al., 2010; Zhang et al., 2010b). Nf2 also activates Lats1/2 kinases (Li et al., 2015b). Other kinases such as the Tao (Thousand and one amino acid) kinase family (Boggiano et al., 2011; Poon et al., 2011) and the MAP/microtubule affinity-regulating kinases (MARK1-4/Par1) 4 (Huang et al., 2013a; Mohseni et al., 2014) are known to directly phosphorylate Stk3 resulting in its activation. Rassf1a has been shown to activate Stk3 activity (Praskova et al., 2004), while conversely Rassf6 represses Stk3 activity (Ikeda et al., 2009). Stk3 can also be repressed by Salt inducible kinases (SIK1-3) (Wehr et al., 2013) and protein phosphatase 2A (PP2A) (Ribeiro et al., 2010), while the Ajuba protein family has been shown to inhibit Lats1/2 function (Das Thakur et al., 2010; Rauskolb et al., 2011).

While activation and repression of Stk3 and Lats1/2 will modulate Yap/Taz activity, there are also a variety of proteins that directly interact with Yap/Taz. This includes WW domain binding protein 2 (WBP2) (Chan et al., 2011b; Chen et al., 1997; Zhang et al., 2011b), multiple ankyrin repeats single KH domain-containing protein

(MASK) (Sansores-Garcia et al., 2013; Sidor et al., 2013), Zona occludens protein 1/2 (ZO1/2) (Oka et al., 2010; Remue et al., 2010), homeodomain-interacting protein kinase 2 (HIPK2) (Chen and Verheyen, 2012; Poon et al., 2012), protein tyrosine phosphatase non-receptor type 14 (PTPN14) (Huang et al., 2013b; Liu et al., 2013b; Poernbacher et al., 2012; Wang et al., 2012), casein kinase 1 (CSNK1) and β-TrCP (beta-transducin repeat containing E3 ubiquitin protein ligase) (Liu et al., 2010; Zhao et al., 2010).

Complexes associated with cell polarity and cell-cell junction have also been shown to regulate the hippo pathway. The Crumbs (Crb) complex has been shown to not only regulates the location and stability of Ex (Chen et al., 2010; Grzeschik et al., 2010; Ling et al., 2010; Robinson et al., 2010; Varelas et al., 2010)), but also to recruit Angiomotin (Amot) (Hirate et al., 2013; Paramasivam et al., 2011; Yi et al., 2011). Amot inhibits Yap/Taz by localizing them to the Crumbs complex, TJs and the actin cytoskeleton (Chan et al., 2011b; Hirate et al., 2013; Paramasivam et al., 2011; Varelas et al., 2010; Yi et al., 2011; Zhao et al., 2011), and through activation of Lats1/2 (Adler et al., 2013; Cordenonsi et al., 2011; Hirate et al., 2013; Mohseni et al., 2014; Paramasivam et al., 2011). Amot may also activate Yap/Taz through the formation of a DNA-bound complex with TEAD/Yap (Yi et al., 2013). Adherens junction associated E-cadherin can activate Skt3 (Kim et al., 2011) and form complexes with α/β-catenin, 14-3-3 proteins and phosphorylated Yap/Taz to prevent nuclear translocation (Schlegelmilch et al., 2011; Silvis et al., 2011). Other factors such as, Scribble (and its associated proteins Discs large (Dlg) and Lethal giant larvae (Lgl)) (Adler et al., 2013; Chen et al., 2012; Cordenonsi et al., 2011; Hirate et al., 2013; Menendez et al., 2010; Mohseni et al., 2014; Zhao et al., 2008b) and the Par3 polarity complex (Grzeschik et al., 2010; Menendez et al., 2010) have also been shown to regulate the Hippo pathway.

Signals transduced through GPCRs can modulate the Hippo pathway. Activation of $G\alpha_{12/13}$ or $G\alpha_{q/11}$ by ligands such as lysophosphatidic acid, sphingosine 1-phosphate, thrombin, angiotensin II and estrogen result in activation of Yap/Taz (Kim et al., 2013a; Miller et al., 2012; Mo et al., 2012; Wennmann et al., 2014; Yu et al., 2012; Zhou et al., 2015), while signals such as epinephrine and glucagon, which activate $G\alpha_s$ inhibit Yap/Taz through cAMP (cyclic adenosine monophosphate) and protein kinase A signaling (Kim et al., 2013a; Kim et al., 2013b; Miller et al., 2012; Mo et al., 2012;

Wennmann et al., 2014; Yu et al., 2013; Yu et al., 2012; Zhou et al., 2015). Signaling through GPCRs relies on signal transduction by Rho GTPases and regulation of the actin cytoskeleton, which in turn modulate Lats1/2 in a RhoA-dependent manner (Kim et al., 2013b; Wada et al., 2011; Yu et al., 2013; Yu et al., 2012; Zhao et al., 2012; Zhao et al., 2007). Not only are Rho GTPases and the actin cytoskeleton important for GPCR signaling, but they are also involved in relaying mechanical forces such as cell density, geometry and attachment so as to modulate Yap/Taz activity, through both Lats1/2 dependent and independent mechanisms (Aragona et al., 2013; Dupont et al., 2011Sansores-Garcia, 2013 #2037; Fernandez et al., 2011; Wada et al., 2011; Zhao et al., 2012).

Metabolic pathways are involved in the regulation of the Hippo pathway. The meyalonate pathway promotes Yap/Taz nuclear localization, while both glucose metabolism and aerobic glycolysis can promote Yap/Taz binding to TEAD (DeRan et al., 2014; Enzo et al., 2015; Mo et al., 2015; Sorrentino et al., 2014; Wang et al., 2015).

The Hippo pathway also interacts with other well-studied signaling pathways. Yap/Taz are bound by Axin and incorporated into the β-catenin destruction complex in the absence of Wnt ligand, where they recruit β-TrCP resulting in proteasomal degradation of both Yap/Taz and β-catenin. (Azzolin et al., 2014; Azzolin et al., 2012) (This interaction is described in more detail in section 1.4.5). Cytoplasmic Yap/Taz can restrict TGFβ signaling by sequestering Smad proteins in the cytoplasm, while nuclear Yap/Taz facilitate Smad mediated transcription (Alarcon et al., 2009; Ferrigno et al., 2002; Varelas et al., 2008). Yap/Taz can also induce expression of members of a variety of signaling pathways, such as *bmp4, jagged-1*, *gli2*, *amphiregulin*, and *insulin-like growth factor (IGF) binding proteins* and *receptors* (Camargo et al., 2007; Fernandez et al., 2009; Judson et al., 2012; Lai and Yang, 2013; Tschaharganeh et al., 2013; Xin et al., 2011; Zhang et al., 2009; Zhou et al., 2011).

Additionally, while nuclear Yap/Taz characteristically interact with TEAD transcription factors, they have also been shown to interact with other transcription factors, including Smads, T-box transcription factor 5 (Tbx5), RUNT-related transcription factors (Runx1/2) p73, ErbB4, Pax3 (Paired box 3) (Halder and Johnson, 2011; Wang et al., 2009). Traditionally, Yap/Taz have been thought to function as

transcriptional co-activators, recent work has also characterized roles for them as co-repressors through the recruitment of the nucleosome-remodeling and histone deacetylase (NuRD) complex at TEAD bound motifs (Kim et al., 2015). Yap/Taz also provide negative feedback signaling for the Hippo pathway itself through regulation of both negative pathway regulators and the Hippo pathway kinases themselves (Chen et al., 2015; Dai et al., 2015; Mohseni et al., 2014).

1.4.4 Roles for Yap/Taz in Development

Tissues which may require Yap/Taz activity have been identified by a Tead transgenic reporter (*Tg(4xGTIIC:d2EGFP))* (Miesfeld and Link, 2014). This transgenic line shows evidence of Tead activity in the epidermis, otic and lens vesicles, retinal pigmented epithelium (RPE), cardiac progenitor cells, presumptive sinus venosus, multiple cell types in the heart, striated muscles of the trunk and undifferentiated endoderm (Miesfeld and Link, 2014). Tead activity may be due to interactions with Yap/Taz, however it does not preclude interactions of Tead with other proteins, and Yap/Taz interactions with transcription factors other than Tead will also not be observed with this line.

Loss of function of *Yap* in mouse results in embryonic lethality at day 8.5 (Gee et al., 2011) while homozygous double mutants for *yap* and *taz* results in embryonic arrest during segmentation stages (~18hpf) (Kimelman et al., 2017; Miesfeld et al., 2015; Nakajima et al., 2017). This embryonic arrest is associated with severe body axis defects and faulty A-P axis elongation due to a loss of fibronectin deposition and cell adhesion in the epidermis, as well as a loss of germ layer and dorsoventral markers (Gee et al., 2011; Hu et al., 2013; Kimelman et al., 2017; Nakajima et al., 2017). Zebrafish mutants for *taz* do not have any reported overt morphological phenotypes (Miesfeld et al., 2015).

Yap and Taz are involved in the development of a variety of tissues and organs. Taz modulates mesenchymal stem cell (MSC) differentiation (Hong et al., 2005a), regulates thyroid gland size (Pappalardo et al., 2015) and interacts with the $SCF^{\beta\text{-}TrCP}$ E3 Ligase in the kidney (Tian et al., 2007). Yap regulates the size of the posterior lateral line primordium (Agarwala et al., 2015), and blastema growth following wounding (Mateus et al., 2015). Loss of function of *yap* and *taz* in zebrafish results in heart defects

and edema, and hemorrhages (Miesfeld et al., 2015) suggesting roles for Yap/Taz in cardiac development. Yap/Taz are required for migration of cardiac progenitor cells to the midline (Miesfeld and Link, 2014). Vascular regression (Nagasawa-Masuda and Terai, 2017), angiogenesis and vascular barrier maturation (Kim et al., 2017a) require Yap/Taz and blood flow induced shear stress reorganizes F-actin and results in nuclear localization of Yap, which is required for maintenance of blood vessels (Nakajima et al., 2017). Functional Yap and Taz are also required for transplanted cells to contribute to the retinal pigmented epithelium (Miesfeld et al., 2015), and loss of function of *yap* and *taz* results in defects in the development of the neural retina, retinal pigmented epithelium (RPE) and can result in coloboma (Miesfeld et al., 2015).

Yap activity often is associated with maintenance of neural progenitors. *Yap* knockdowns result in defects in the expression of proneural, and neuronal markers (Jiang et al., 2009). Yap has a role in maintaining the balance between expansion of the neural progenitor pool with differentiation of post-mitotic neurons and glia (Lavado et al., 2013). Yap is expressed by cells of the ventricular progenitor zone, and neural progenitors expressing *sox2* and *tead2* (Cao et al., 2008; Gee et al., 2011; Ramalho-Santos et al., 2002). Yap suppresses neural stem cell (NSC) differentiation through interactions with SMADs and mediates neural progenitor proliferation induced by SHH (Alarcon et al., 2009). Decreased Yap levels are correlated with neural cell cycle exit and terminal differentiation in the central nervous system (Zhang et al., 2012). In humans, *Drosophila*, *Xenopus* and chick, *yap/yki* maintain neural progenitors and suppress their differentiation (Cao et al., 2008; Hindley et al., 2016; Milewski et al., 2004; Zhang et al., 2011a). Other proteins and complexes such as Nf2, FatJ cadherin and FAT4/Dchs1 have also been shown to regulate neural progenitor maintenance and differentiation through modulating Yap activity (Cappello et al., 2013; Lavado et al., 2013; Van Hateren et al., 2011).

The Hippo pathway has also been associated with other developmental processes in the brain. *Yap* is expressed in a subpopulation of pre-migratory neural crest cells (Hindley et al., 2016), and Nf2/Yap are required for the development of the dorsal root ganglia and the corpus callosum (Lavado et al., 2014; Serinagaoglu et al., 2015). Additionally, the Hippo pathway restricts brain size by modulating larval neuroblasts

(Poon et al., 2016), while the microcephaly associated gene, Cyclin-dependent kinase 5 regulatory subunit 2 (CDK5RAP2) has been shown to interact with MST1, and regulate YAP/TAZ (Sukumaran et al., 2017). *Yap* has also been shown to be required for the generation of ependymal cells within the brain ventricles and maintaining apical junction integrity, as the loss of *Yap* results in hydrocephalus in mice (Park et al., 2016).

1.4.5 Interactions Between the Hippo Pathway and Apicobasal Polarity

Apicobasal polarity requires sorting of proteins to specific subcellular domains (Rodriguez-Boulan and Macara, 2014), where they form multi-protein complexes that establish cell-cell junctions. Formation of these junctions is the first step in polarization (Wang and Margolis, 2007). Adherens junction components (such as ZO-1 and actin) are localized apically, followed by localization of the Crumbs complex (Crb, Mpp5, Lin7c (Bachmann et al., 2001; Hong et al., 2001; Hsu et al., 2006; Kamberov et al., 2000; Yang et al., 2009)) which stabilizes the polarity and may also stabilize the actin cytoskeleton (Yang et al., 2009). Membrane association of Crb has been shown to be necessary and sufficient to confer apical character (Wodarz et al., 1995). Crb is required to target Mpp5a to the apical surface, as loss of Crb results in mis-localization of Mpp5a (Zou et al., 2013). Together Mpp5a, Crb2a and Prkci interact and localize to the apical neuroepithelial surface (Horne-Badovinac et al., 2001; Hsu et al., 2006; Omori and Malicki, 2006) and loss of any one of these genes results in ventricle midline separation defects (Lowery et al., 2009).

Components of the Crumbs complex have also been linked to actin organization. Lin7c and Mpp5a colocalizes with apically localized actin (Yang et al., 2009). Mpp5a has a FERM (Protein 4.1/Ezrin/Radixin/Moesin) binding domain, and FERM family members interact with trans-membrane proteins and stabilize actin (Bretscher et al., 2002). Merlin and Expanded are members of the FERM domain superfamily of proteins (Bretscher et al., 2002; Hamaratoglu et al., 2006; Pellock et al., 2007), and have been shown to associate with actin (Brault et al., 2001; Bretscher et al., 2002; James et al., 2001; Xu and Gutmann, 1998) and with each other (McCartney et al., 2000). They also interact with adherens junctions and tight junction associated proteins (such as α-catenin, Par3 (Gladden et al., 2010), and Angiomotin (Yi et al., 2011)) to promote assembly and

maturation (Gladden et al., 2010; Lallemand et al., 2003). Crb can bind to Ex through its FERM-binding motif (Grzeschik et al., 2010; Ling et al., 2010; Robinson et al., 2010), and regulate the localization of Ex, which results in down-regulation of Hpo, and subsequent up-regulation of nuclear Yki (Chen et al., 2010; Grzeschik et al., 2010; Ling et al., 2010; Robinson et al., 2010). Additionally, Yki can be regulated by Mer/Ex, but is also involved in regulating transcription of Mer/Ex (Hamaratoglu et al., 2006). Actin regulates and interacts with Yap/Taz as well. Actin tension prevents nuclear localization of Yap/Taz (Furukawa et al., 2017), and Yap acts through Arghap18 to modulate cortical actomyosin and mediate tissue tension in Medaka (Porazinski et al., 2015). Additionally, Yap can colocalize with the cytoskeleton through interactions with Amot (Chan et al., 2011a; Zhao et al., 2011).

The vertebrate homolog of *Merlin*, is *Nf2*, and there are two paralogs in zebrafish (*nf2a* and *nf2b*). The vertebrate homolog of *Expanded* has not been unambiguously identified. Sequence homology suggests that *frmd6* is homologous to *Ex*, and it may fulfill some of the functions of *Ex* in vertebrates, while other research has suggested that the *amot* family of genes may fulfill some of the functions of Ex as well (Angus et al., 2012; Bossuyt et al., 2014; Genevet and Tapon, 2011; Gunn-Moore et al., 2005; Moleirinho et al., 2013).

1.4.6 Canonical Wnt Signaling

The first member of the Wnt family was discovered in 1982 (Nusse and Varmus, 1982), and considerable work has characterized additional components of the canonical Wnt signaling pathway (summarized in Figure 1.7). Extracellular Wnt ligands bind to the cysteine-rich domain of the Frizzled receptor (Bhanot et al., 1996; Hsieh et al., 1999a; Hsieh et al., 1999b). Activation of the Wnt pathway can be modulated by extracellular Wnt antagonists which can either bind to the receptor (such as Dickkopf and Sclerostin/SOST families (Cruciat and Niehrs, 2013), or they can bind to the Wnt ligand itself (Such as secreted FZD-related proteins (Sfrps) (Holly et al., 2014) and Wnt Inhibitory Proteins (Niehrs, 2012)).

When Wnt ligands are not present Axin provides a scaffold for the formation of the β-catenin destruction complex. This complex is composed of Axin, APC

(Adenomatous polyposis coli complex), Gsk3 (serine/threonine glycogen synthase kinase 3), Ck1 (casein kinase 1) and Yap/Taz (Azzolin et al., 2014; Azzolin et al., 2012). Gsk3 and Ck1 phosphorylate β-catenin at N-terminal Ser/Thr residues (Liu et al., 2002). Yap/Taz recruit the E3 ubiquitin ligase β-TrCP which docks at the phosphorylated regions of β-catenin and induces ubiquitination of both β-catenin and Yap/Taz, resulting in their proteasomal degradation (Aberle et al., 1997; Azzolin et al., 2014; Azzolin et al., 2012; Kitagawa et al., 1999).

Binding of the Wnt ligand results in dimerization of Fzd (Frizzled) and Lrp5/6 (Low density lipoprotein receptor-related protein 5/6), leading to a conformational change (Janda et al., 2017), and phosphorylation of the cytoplasmic tail of Lrp by Gsk3 (Stamos et al., 2014). The cytoplasmic portion of Lrp recruits Axin, competing with Yap/Taz to bind Axin (Azzolin et al., 2014; Azzolin et al., 2012), while the cytoplasmic portion of Fzd binds to Dishevelled (Dvl) (Tauriello et al., 2012). Dvl and Axin then interact through their DIX domains (Fiedler et al., 2011; Schwarz-Romond et al., 2007a; Schwarz-Romond et al., 2007b). This interaction sequesters the β-catenin destruction complex at the cell membrane and Axin binding to Lrp6 releases both β-catenin and Yap/Taz, which allows nuclear translocation. β-catenin then interacts with the Tcf/Lef transcription factors to regulate gene expression (Behrens et al., 1996; Molenaar et al., 1996). In the absence of β-catenin Tcfs repress transcription through interaction with Groucho proteins (Cavallo et al., 1998; Roose et al., 1998), while β-catenin interacts with chromatin modifiers such as CBP (cyclic AMP response element-binding protein) and p300 histone acetyltransferase, to activate gene transcription (Emami et al., 2004; Hao et al., 2013; Mosimann et al., 2006; Stadeli et al., 2006; van de Wetering et al., 1997).

1.4.7 Wnt Signaling in Brain Development

Multiple *wnt* genes are expressed in the hindbrain during development. *Wnt1*, *wnt3, wnt7aa, wnt10b* and *wnt4b* all show tissue specific expression in the hindbrain, while others (*wnt2, wnt2ba, wnt2bb, wnt5a, wnt5b, wnt9a, wnt9b, wnt10a*, and *wnt11*) show more ubiquitous/non-specific expression (Duncan et al., 2015)..

The Wnt signaling pathway has also been shown to be involved in the formation of boundaries. Boundaries are essential to regulate segmental identity and coordinate patterns of growth and differentiation in adjacent compartments (Blair, 2003; Blair and Ralston, 1997; Clarke and Lumsden, 1993; Dahmann and Basler, 1999; Gaunt et al., 1997; Gaunt, 1997; Irvine, 1999; Irvine and Rauskolb, 2001; Lumsden and Krumlauf, 1996; Sanson, 2001; Trevarrow et al., 1990; Wingate and Lumsden, 1996). *Wingless (Wg*) is expressed at the dorsal-ventral boundary of the *Drosophila* wing margin, where it regulates outgrowth and differentiation (Couso et al., 1994; Couso et al., 1995; Couso and Martinez Arias, 1994; de Celis and Bray, 1997; de Celis et al., 1996; Kim et al., 1995; Kim et al., 1996; Micchelli et al., 1997; Rulifson and Blair, 1995; Rulifson et al., 1996). The Wnt signaling pathway has also been implicated in establishing boundaries between rhombomeres. The interface between rhombomeres is stabilized, and signaling between Ephrins and Eph receptors (Fraser et al., 1990; Mellitzer et al., 1999; Xu et al., 1999) prevents cell mixing. Interactions between adjacent rhombomeres induce the formation of boundary cells with distinct morphology that express unique molecular markers (Guthrie et al., 1991; Guthrie and Lumsden, 1991; Heyman et al., 1995; Heyman et al., 1993; Lumsden and Keynes, 1989; Xu et al., 1999). Boundary cells are a source of signals that function to organize neurons and glia within each rhombomere (Hanneman et al., 1988; Metcalfe et al., 1986; Trevarrow et al., 1990).

At least 4 *wnt* genes (*wnt1, wnt10b, wnt3a* and *wnt8b*) are upregulated at rhombomere boundaries (Lekven et al., 2003; Riley et al., 2004), and this upregulation of *wnt* expression at rhombomere boundaries is observed in other organisms, such as mouse (Manzanares et al., 2000; Rowitch et al., 1998). Elevated levels of *wnt* at rhombomere boundaries regulate patterning of the rhombomeres and Delta signals provide feedback to maintain the rhombomere boundaries as Wnt signaling centers (Riley et al., 2004). Segmentation mutants in which *wnt* gene expression at rhombomere boundaries is disrupted, are have a disorganization of cell types and they fail to form boundary associated cell types (Riley et al., 2004). Furthermore, *dla* and *mind bomb* mutants which have a disruption of Delta-Notch signaling (Appel et al., 1999; Itoh et al., 2003), initially form rhombomere boundaries, but these boundaries are not maintained and result in disorganization of the hindbrain (Riley et al., 2004). *Mind bomb* mutants

have also been shown to have defects in ventricle development (Schier et al., 1996).

Signaling from rhombomere boundaries, and an adjacent source of signaling molecules may be important for ventricle development. Signals from the roof plate regulate dorsal cell specification (Chizhikov and Millen, 2005), and may maintain rhombomere boundaries (Elsen et al., 2008). Roof plate markers such as *lmx1b* promote *wnt1* expression (Guo et al., 2007; O'Hara et al., 2005), and reductions in *wnt1* expression, as seen in *Limx1a* (*Dreher*) mouse mutants and in *wnt1* zebrafish morphants (Elsen et al., 2008) result in defects in ventricle development (Manzanares et al., 2000; Millonig et al., 2000). Knockdown of components upstream of *wnt1* such as *lmx1b*, *zic1*, *zic4*, and *rfng* similarly result in defects in ventricle morphogenesis (Amoyel et al., 2005; Cheng et al., 2004; Elsen et al., 2008). While morpholino mediated knockdown experiments suggest that disruptions to Wnt signaling lead to the loss of rhombomere boundary associated cell types (Riley et al., 2004), disruption of proneural gene expression and ectopic expression of hindbrain boundary markers (Amoyel et al., 2005), subsequent research has found that the decrease in proneural and neuronal marker expression and ectopic boundary marker expression is due to morpholino mediated activation of the Tp-53-mediated cell death pathway (Gerety and Wilkinson, 2011). Regardless, mis-expression of rhombomere boundary markers, such as *rfng* and *wnt1* may still be involved in disrupting ventricle morphogenesis (Elsen et al., 2008).

1.4.8 Notch Signaling

Notch signaling mediates cell-cell communication and is involved in establishing complex patterns within tissues and determining cell fate (Artavanis-Tsakonas et al., 1999; Irvine and Rauskolb, 2001; Lewis, 1998; Pourquie, 2001; Rida et al., 2004). Mutations in *Notch* were first described by Thomas Hunt Morgan (Morgan and Bridges, 1916), and subsequent work characterized other members of the Notch signaling pathway (Artavanis-Tsakonas et al., 1995; Artavanis-Tsakonas et al., 1999; Campos-Ortega, 1988; Vassin et al., 1987; Wharton et al., 1985) (Summarized in Figure 1.8). Notch receptors are inserted into the plasma membrane, where they encounter plasma membrane localized ligands on adjacent cells. Following their synthesis, Notch receptors undergo Furin mediated cleavage at site 1 (S1) in the Golgi (Blaumueller et al., 1997;

Gordon et al., 2009; Logeat et al., 1998) before being transported to the cell membrane. Binding of the Notch receptor to the ligands Delta/Serrate (Jagged) induces S2 cleavage of the Notch extracellular domain, mediated by the ADAM metalloprotease family (Pan and Rubin, 1997; Rooke et al., 1996). Subsequently S3 cleavage by the γ-secretase complex releases the Notch intracellular domain (NICD) (Donoviel et al., 1999; Levitan and Greenwald, 1995; Mumm et al., 2000; Schroeter et al., 1998; Struhl and Greenwald, 1999). The NICD translocates to the nucleus, where it regulates target gene transcription through binding to Rbpj (recombination signal binding protein for immunoglobulin kappa J region a; suppressor of hairless (Su(H))) (Fryer et al., 2002; Kao et al., 1998). Maml (Mastermind-like) and the p300 histone acetyltransferase are recruited along with the transcription machinery to activate target gene transcription (Kurooka and Honjo, 2000; Wu et al., 2000; Zhou et al., 2000).

Another component of the Notch signaling pathway are the *fringe* genes. These genes encode β-1,3 N-acetyl-glucosaminyltransferases and were first discovered in *Drosophila* (Irvine and Wieschaus, 1994), although vertebrate homologs have been identified (Qiu et al., 2004). Fringe glycosylates Notch in the Golgi, making Notch more susceptible to activation by the ligand Delta, instead of Serrate. In neighbouring cell populations, where one population is expressing Notch and Delta, and the other population is expressing Notch, Serrate and Fringe, the glycosylation of Notch enables a strong activation of Notch at the interface between the two cell populations, where glycosylated Notch encounters Delta (Panin et al., 1997).

1.4.9 Notch Signaling at Rhombomere Boundaries

Notch signaling is involved in the control of cell differentiation and cell intermingling across boundaries (Dominguez and de Celis, 1998; Micchelli and Blair, 1999; Papayannopoulos et al., 1998). Rhombomere boundaries have been associated with regulation of neurogenesis in the hindbrain. Differentiation of neurons first begins at rhombomere centers and neurons only form at rhombomere boundaries at late stages (Hanneman et al., 1988; Trevarrow et al., 1990). Delta is expressed in early neuroblasts, and is restricted from rhombomere boundaries (Cheng et al., 2004) while Notch receptors are expressed by neural progenitor cells (Del Amo et al., 1992; Higuchi et al.,

1995; Lardelli et al., 1994; Lindsell et al., 1996; Weinmaster et al., 1991; Weinmaster et al., 1992). Notch activation at rhombomere boundaries is responsible for the suppression of neuronal differentiation in boundary regions (Cheng et al., 2004). Notch activation also regulates cell affinity at rhombomere boundaries (Cheng et al., 2004), and induces boundary expression of F-actin and actin-binding molecules at adherens junctions (Major and Irvine, 2005; Major and Irvine, 2006).

Mutations in components of the Notch signaling pathway, such as *deltaA* (Appel et al., 1999; Riley et al., 1999), *deltaD* (*after eight*) (Holley et al., 2000; Holley et al., 2002; van Eeden et al., 1996), *notch1* (*deadly seven*) (Gray et al., 2001; van Eeden et al., 1996) and *mindbomb* (Bingham et al., 2003; Cheng et al., 2004; Itoh et al., 2003; Jiang et al., 1996; Park and Appel, 2003; Riley et al., 1999; Schier et al., 1996; van Eeden et al., 1996) have neurogenic phenotypes. Loss of function of *mindbomb* results in ectopic expression of neurogenic genes at early stages (Bingham et al., 2003; Itoh et al., 2003; Jiang et al., 1996; Park and Appel, 2003; Schier et al., 1996), resulting in an expansion of the pan-neuronal marker HuC/D throughout the hindbrain by 24 hpf (Cheng et al., 2004). This results in overproduction of rhombomere centre neurons such as reticulospinal neurons (Riley et al., 2004), increased numbers of rohon-beard neurons (Bingham et al., 2003), and a loss of commissural and later-born neurons (Itoh et al., 2003; Jiang et al., 1996; Park and Appel, 2003; Riley et al., 2004; Schier et al., 1996). Additionally, neurons in *mindbomb* mutants have defects in axonal pathfinding and fasciculation (Riley et al., 2004). Similar defects in neurogenesis are observed in *dlA* mutants (Riley et al., 2004). *Mindbomb* mutants have defective lateral inhibition, resulting in the premature differentiation of precursors, and depletion of neuroepithelial cells, leading to defects in hindbrain segmentation (Bingham et al., 2003). Rhombomere boundaries initially form in *mindbomb* mutants, but they fail to be maintained (Riley et al., 2004), and expression of rhombomere boundary associated genes is lost (Cheng et al., 2004).

Lfng and *Mfng* are expressed in the developing hindbrain in a segmental pattern in mice (Johnston et al., 1997) and in zebrafish, two *fringe* genes are expressed in the hindbrain. *Lunatic fringe* (*lfng; LFNG O-fucosylpeptide 3-beta-N-acetylglucosaminyltransferase*) is expressed primarily in even-numbered rhombomeres

and at lower levels in odd-numbered rhombomeres (Prince et al., 2001; Qiu et al., 2004). *Radical fringe* (*rfng; RFNG O-fucosylpeptide 3-beta-N-acetylglucosaminyltransferase*) is expressed specifically at rhombomere boundaries (Amoyel et al., 2005; Qiu et al., 2004). Zebrafish *lfng* is required cell autonomously to maintain neural progenitor cells and limit neuronal differentiation (Nikolaou et al., 2009). Knockdown of *rfng* results in a loss of boundary specific *wnt1* expression (Cheng et al., 2004), and has also been shown to cause midline separation defects in the hindbrain ventricle (Elsen et al., 2008). Loss of *rfng* expression and defects in ventricle formation have been associated with a number of mutants in which rhombomere boundaries or neurogenesis are disrupted, including mutants for *mindbomb, med12/14* and *sfpq* (Appel et al., 1999; Bingham et al., 2003; Cheng et al., 2004; Conaway et al., 2005; Guo et al., 1999; Hong et al., 2005b; Itoh et al., 2003; Lowery et al., 2009; Lowery et al., 2007; Mawdsley et al., 2004; Riley et al., 2004; Schier et al., 1996; Thomas-Jinu et al., 2017; Wang et al., 2006). Together, this may suggest a role for *rfng* in rhombomere boundary formation, neurogenesis and ventricle morphogenesis.

1.5 Summary

The embryonic vertebrate hindbrain gives rise to essential structures in the adult brain. Hindbrain associated neurons form vital circuits and neural crest populations arising from the embryonic hindbrain contribute to craniofacial and cardiac development. In the adult brain, the cerebellum coordinates movement by transmitting signals to the motor cortex, while the brainstem, which is made up of the medulla oblongata, the pons, the fourth ventricle and the midbrain is required for the coordination of higher order behaviors, including respiration and circulation (Gray and Clemente, 1985). Appropriate development of the hindbrain must be carefully controlled to ensure the proper development of adult tissues, and transcription factors and signaling pathways can have major effects on the development of the hindbrain.

My work has focused on two phases of hindbrain development, segmentation and specification of hindbrain rhombomeres, and morphogenesis of the hindbrain ventricle. Segmentation of the hindbrain into rhombomeres is a vital step in patterning the nascent hindbrain into distinct regions with unique identities. Division of the

hindbrain into rhombomeres and the appropriate expression of specific genes in each rhombomere is required for subsequent development and specification of neuroanatomy (Chandrasekhar et al., 1997; Hanneman et al., 1988; Hartenstein, 1993; Kimmel et al., 1982; Koentges and Matsuoka, 2002; Le Douarin and Kalcheim, 1999; Mendelson, 1986; Metcalfe et al., 1986; Schilling and Kimmel, 1994). Changes in rhombomere patterning affect neuronal differentiation, migration and overall organization, as well as affecting neural crest specification and migration. To establish rhombomere patterning, regionalization of the hindbrain through FGF and RA signaling is required (Gavalas, 2002; Maroon et al., 2002; Maves et al., 2002; Niederreither and Dolle, 2008; Phillips et al., 2001). Loss of RA signaling results in a loss of posterior hindbrain identity (Begemann et al., 2001; Dupe and Lumsden, 2001; Maden et al., 1996), while loss of FGF signaling results in disruption of the anterior hindbrain, and the r4 signaling centre, affecting the specification of the surrounding rhombomeres (r3-6) (Maroon et al., 2002; Maves et al., 2002; Phillips et al., 2001). A complex network of transcription factors is established in the hindbrain, with each transcription factor being expressed in a unique domain and performing a specific function. Paralog group 1-4 *hox* genes display nested expression domains, where PG 2 *hox* genes are expressed up to the r2/3 boundary, PG1 *hox* gene are expressed up to the r3/4 boundary, PG 3 *hox* genes are expressed up to the r4/5 boundary, and PG 4 *hox* genes are expressed up to the r6/7 boundary (with some exceptions) (Hunt et al., 1991; Keynes and Krumlauf, 1994; Lumsden and Krumlauf, 1996; Maconochie et al., 1996; Wilkinson et al., 1989). *Hox* gene expression is required for segmental identity, and loss of *hox* genes is associated with homeotic transformations and loss of segmental identity (Carpenter et al., 1993; Davenne et al., 1999; Gaufo et al., 2003; Gavalas et al., 1997; Gavalas et al., 2003; Gavalas et al., 1998; Mark et al., 1993; McClintock et al., 2002; McNulty et al., 2005; Rijli et al., 1998; Rossel and Capecchi, 1999; Studer et al., 1998; Trainor and Krumlauf, 2000; Weicksel et al., 2014; Zigman et al., 2014) Other transcription factors also play important roles in hindbrain development. *Vhnf1* is required for the development of r4-6 (Sun and Hopkins, 2001; Wiellette and Sive, 2004), *val* specifies and subdivides r5 and r6 (Cordes and Barsh, 1994; Giudicelli et al., 2003; Manzanares et al., 1997; Manzanares et al., 1999b; McKay et al., 1994; Moens et al., 1998; Moens et al., 1996; Prince et al., 1998), and *krox20* is required for

the formation of r3 and r5 (Schneider-Maunoury et al., 1997; Swiatek and Gridley, 1993; Voiculescu et al., 2001). Expression of Ephrins and Eph receptors in alternating segments is also an important step in sorting and segregating cells into the appropriate compartments (Bovenkamp and Greer, 1997; Cooke et al., 2001; Mellitzer et al., 1999; Xu et al., 1995a). Cells with distinct morphology and gene expression are established at the boundaries between rhombomeres, where they act as signaling centers to pattern cell types within each rhombomere (Guthrie and Lumsden, 1991; Heyman et al., 1995; Heyman et al., 1993; Mahmood et al., 1995; Mahmood et al., 1996; Moens et al., 1996; Trevarrow et al., 1990; Yoshida and Colman, 2000). Coordinate regulation of these genes and signaling pathways is required for the correct establishment of rhombomere identity, and the subsequent development of neural crest and neurons arising from the hindbrain.

Once the hindbrain has been specified and subdivided into rhombomeres, morphogenesis of the hindbrain ventricle can occur. Ventricle development requires a continuous epithelium (Hong and Brewster, 2006; Lele et al., 2002), which is anchored to the extracellular matrix (Ashkenas et al., 1996; Gato et al., 1993; Gullberg and Ekblom, 1995; Morriss-Kay and Crutch, 1982; Ojeda and Piedra, 2000; Schoenwolf and Fisher, 1983; Tuckett and Morriss-Kay, 1989; Yip et al., 2002). Together with changes in cell shape mediated by cytoskeletal dynamics (Eto et al., 2005; Fristrom, 1988; Lecuit and Lenne, 2007; Xia et al., 2005), this will shape the ventricles. Cell death (Glucksmann, 1951; Kallen, 1955; Keino et al., 1994; Kuida et al., 1996), proliferation (Elsen et al., 2008; Kahane and Kalcheim, 1998; Nyholm et al., 2007; Sausedo et al., 1997; Schoenwolf and Alvarez, 1989; Tao and Lai, 1992; Tuckett and Morriss-Kay, 1989; Xuan et al., 1995), and neuronal differentiation (Lowery and Sive, 2009) must also be properly regulated for ventricle morphogenesis. Finally, secretion of embryonic cerebrospinal fluid by the neuroepithelium will inflate the ventricles (Lowery and Sive, 2009). Defects in morphogenesis of the ventricles can affect CSF flow, neurogenesis and can result in hydrocephalus which has been associated with a variety of neurodevelopmental disorders (Moore, 2006).

In order to study the processes and genes involved in hindbrain development, it is important to be able to alter gene expression. This is commonly achieved in zebrafish

through either knockdown of genes via antisense morpholino oligonucleotides, or through the generation of mutants by targeted mutagenesis. There is evidence that morpholinos can cause off-target effects, which can confound phenotypic analyses (Amoyel et al., 2005; Ekker and Larson, 2001; Gerety and Wilkinson, 2011; Pickart et al., 2006; Robu et al., 2007), however the generation of mutant lines can also be time consuming and have variable effectiveness. In Chapter 3, we sought to improve the efficiency of ZFN and TALEN synthetic targeted endonucleases for use in zebrafish mutagenesis. We assayed for improved *in vitro* cleavage, and *in vivo* generation of mutations for ZFNs and TALENs containing a FokI nuclease variant termed *Sharkey* (Guo et al., 2010). While *Sharkey* ZFNs and *Sharkey* TALENs exhibit greater *in vitro* cleavage of target-site DNA than controls, only one of four *Sharkey* ZFNs displays produced a higher frequency of insertion/deletion mutations *in vivo*, and *Sharkey* TALENs fail to produce any insertion/deletion mutations *in vivo.* Our work provides evidence that the *Sharkey* variant of FokI may be useful in increasing the mutagenic activity of ZFNs, however it suggests that the *Sharkey* FokI variant should not be used in combination with TALENs as it ablates all mutagenic activity.

Hox genes are vital in the generation of hindbrain identity and previous work has suggested a central role for Paralog Group 1 *hox* genes in establishing hindbrain identity (Waskiewicz et al., 2002). We test this hypothesis in Chapter 4, by investigating the phenotypes of *hoxb1a*, *hoxb1b*, and *hoxb1a;hoxb1b* mutants to determine the respective and combined roles of PG1 *hox* genes in regulating hindbrain development. *Hoxb1a* is required for specification of r4 and r4-derived neurons. *Hoxb1b* more broadly affects rhombomere segmentation, size and neuronal development from r4-6. The combinatorial loss of both *hoxb1a* and *hoxb1b* largely resembles *hoxb1b* mutants, however we do uncover a novel role for *hoxb1a/b* in regulating *vhnf1*. *Hoxb1b* is required for appropriate FGF signaling in the hindbrain, while PG1 *hox* genes do not appear to overtly regulate RA signaling. Instead, *pbx* genes regulate *aldh1a2* expression. The loss of both *hoxb1b* and *pbx4* is required to revert the hindbrain to the r1 ground state, and this phenotype is plausibly explained by *pbx*-mediated changes to RA signaling in combination with the *hoxb1b* driven changes to FGF signaling. Our results suggest that

PG1 *hox* genes function together with *pbx* and other transcription factors to regulate FGF and RA signaling in the establishment of hindbrain identity.

The role of transcription factors and signaling pathways in ventricle development is poorly explored. We have identified a novel role for the transcriptional co-regulator *taz* in ventricle morphogenesis. Previous work has shown that in the absence of Wnt ligands, Taz is incorporated into the β-catenin destruction complex where it facilitates the degradation of both β-catenin and itself through recruitment of the E3 ubiquitin ligase β-TrCP (Azzolin et al., 2014; Azzolin et al., 2012). The interaction of Taz with β-catenin has been established in *in vitro* models, but it has only been shown *in vivo* in the murine intestine (Azzolin et al., 2014; Azzolin et al., 2012). We hypothesize that Taz interacts with the Wnt/β-catenin signaling pathway to regulate ventricle morphogenesis. We test this hypothesis in Chapter 5, by through examination of *taz* mutants and modulation of the Wnt signaling pathway with pharmacological inhibitors. We provide evidence that Taz interacts with the Wnt/β-catenin signaling pathway in zebrafish, and our research suggests that this interaction is required for ventricle morphogenesis. Taz protein localizes specifically to rhombomere boundaries, likely as a result of enriched Wnt expression at rhombomere boundaries, and loss of function of *taz* results in midline separation defects in the hindbrain ventricle. Furthermore, *taz* mutants have mislocalization and misregulation of apicobasal polarity components and the actin cytoskeleton. Stabilization of the β-catenin destruction complex results in the loss of Taz protein localization, and phenotypes similar to those observed in *taz* mutants, while inhibition of the β-catenin destruction complex stabilizes Taz protein throughout the hindbrain. This supports a role for the Wnt signaling pathway in stabilizing Taz at rhombomere boundaries thus facilitating ventricle morphogenesis. Finally, we determined that both β-catenin mediated transcription and Taz-mediated transcription are involved in morphogenesis of the hindbrain ventricle. Together this provides evidence for the involvement of Taz in Wnt signaling, and in regulating transcription and morphogenesis of the hindbrain ventricle.

Notch signaling has been previously been characterized to play important roles in mediating lateral inhibition at rhombomere boundaries (Bingham et al., 2003; Cheng et al., 2004; Itoh et al., 2003; Jiang et al., 1996; Park and Appel, 2003; Riley et al., 1999;

Schier et al., 1996; van Eeden et al., 1996), and loss of function, or knockdown of components of the Notch signaling pathway such as *mindbomb (mind bomb E3 ubiquitin protein ligase 1 (mib1))*, and *rfng (RFNG O-fucosylpeptide 3-beta-N-acetylglucosaminyltransferase)* have been shown to result in defects in ventricle morphogenesis (Elsen et al., 2008). We hypothesize that Taz may be involved in regulating Notch signals at rhombomere boundaries. We test this hypothesis in Chapter 6, through examination of components of the Notch signaling pathway. We find that loss of function of *taz* results in a loss of rhombomere boundary expression of *rfng*, but does not disrupt the expression of other components of the Notch signaling pathway. Alterations in cell proliferation and apoptosis have also been associated with both *taz* and *rfng* (Gerety and Wilkinson, 2011; Watt et al., 2017), and we find that *taz* mutants have mild reductions in cell proliferation, that may contribute to the ventricle defects observed in *taz* mutants. Additionally, while Notch has well established roles in regulating proneural gene expression and neurogenesis, we only find mild alterations in abducens neurons and rohon-beard neurons. This may indicate that Taz mediated regulation of *rfng* expression is disepnsible for neurogenesis. Pharmacological inhibiton of Notch signaling does however reduce ventricle size, but does not affect Taz localization, supporting a role for Notch signaling in the regulation of ventricle morphogenesis.

1.6 Figures

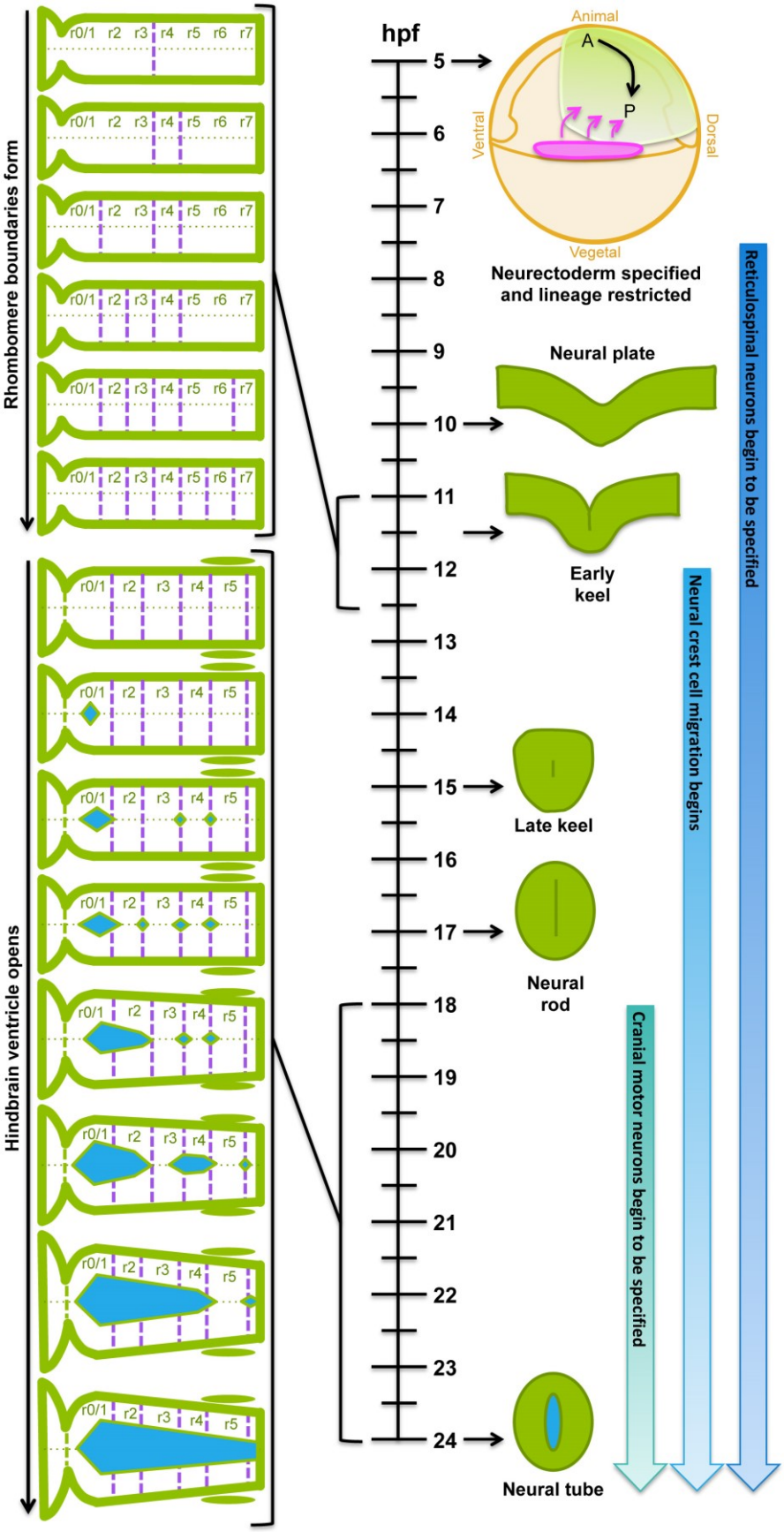
Rhombomere boundaries form
Hindbrain ventricle opens
r0/1 r2 r3 r4 r5 r6 r7
hpf
5
6
7
8
9
10
11
12
13
14
15
16
17
18
19
20
21
22
23
24
Animal
A
P
Ventral
Dorsal
Vegetal
Neurectoderm specified and lineage restricted
Neural plate
Early keel
Late keel
Neural rod
Neural tube
Reticulospinal neurons begin to be specified
Neural crest cell migration begins
Cranial motor neurons begin to be specified

Figure 1.1. Overview of Hindbrain Development

Hindbrain development begins with neural induction at approximately 5 hpf. The presumptive neural tissue is quickly regionalized into distinct anterior-posterior domains. Reticulospinal neurons are specified beginning as early as 7.5 hpf. By 10 hpf the neural plate forms, and has begun to form the neural keel by 11.5 hpf. During the early somite stages from approximately 11-12.5 hpf, rhombomere boundaries begin to form in a stereotypic sequence. Neural crest cell migration begins at approximately 12 hpf. The neural keel progresses to form the neural rod by 17 hpf, and the hindbrain ventricle begins to open at 18 hpf in a stereotypic sequence. Cranial motor neurons begin to be specified by 18hpf, and the neural tube lumen and hindbrain ventricle are completely open by 24 hpf. A, anterior; P, posterior; r, rhombomere.

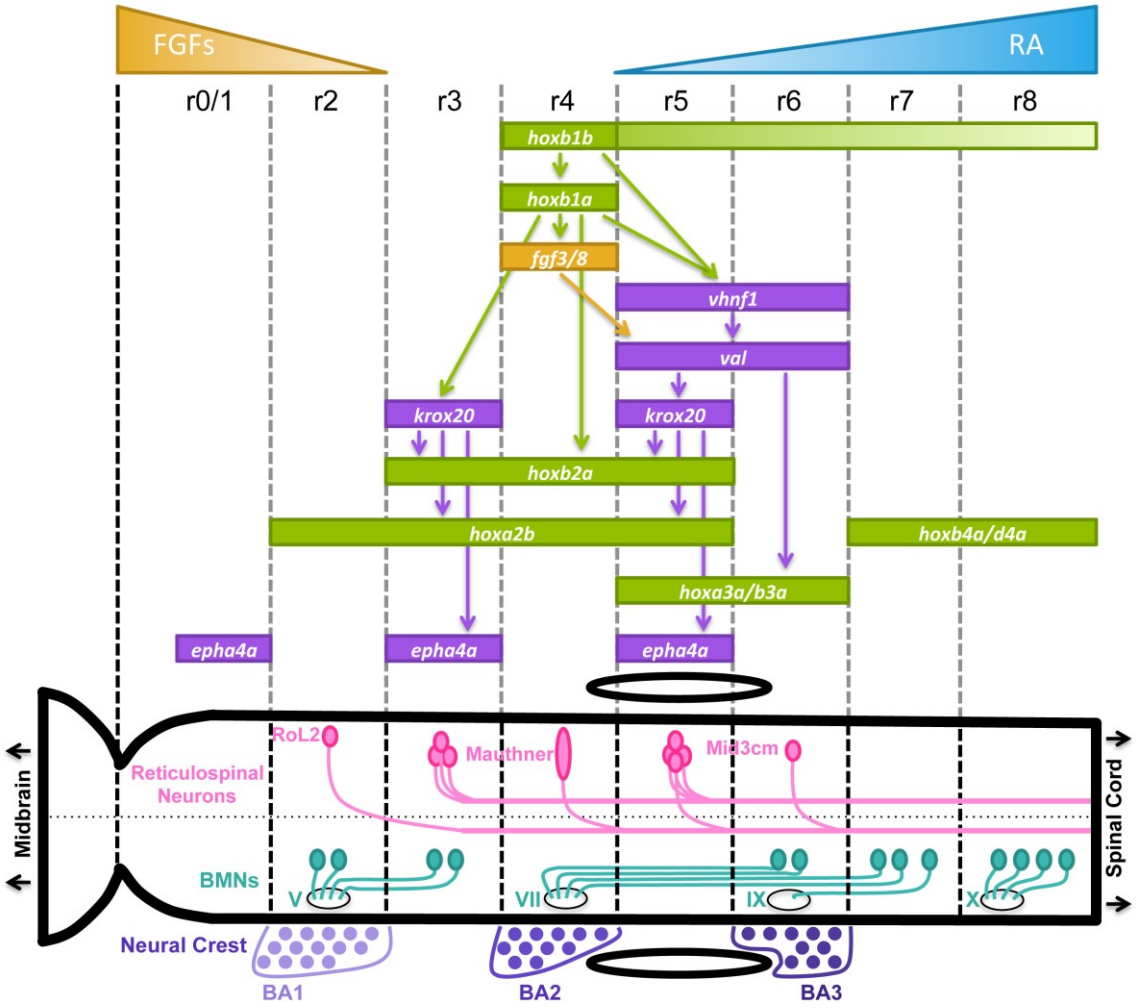

Figure 1.2. Factors Involved in Specification of Rhombomere Identity

The hindbrain is broadly regionalized by retinoic acid (RA) signals from the somites, and fibroblast growth factors (FGF) signals from the midbrain-hindbrain boundary and the r4 signaling centre. Interactions between *hox* genes, *fgfs*, transcription factors and *ephs* cooperate to establish the identity of each segment. An overview of the expression patterns and interactions between these factors is shown. Segmental identity serves to pattern the neuroanatomy of the hindbrain. Neural crest from r2, r4 and r6 will contribute to the first 3 branchial arches (BA) respectively. The reticulospinal neurons form a ladder-like pattern in the hindbrain, a subset of them are shown here. The Rol2 neurons in r2, the Mauthner neuron in r4 and the Mid3cm neurons in r6 all project contralaterally across the midline. There are additional reticulospinal neurons found in

each segment. The Branchiomotor neurons (BMNs) also show a rhombomere specific organization. The trigeminal (V) BMN cell bodies are found in both r2/3, and their axons exit the hindbrain from r2. The facial (VII) BMNs are born in r4, after which they migrate first posteriorly to r6/7 and then laterally, leaving their axons to exit the hindbrain from r4. The glossopharyngeal (IX) BMNs exit the hindbrain from r6, while their cell bodies are located in r7. The vagal (X) BMNs are located in the most posterior region of the hindbrain, with their axons exiting the hindbrain at the level of r8. r, rhombomere; FGFs, Fibroblast Growth Factors; RA, Retinoic Acid; BMNs, branchiomotor neurons; V, trigeminal; VII, facial; IX, glossopharyngeal; X, vagal; BA, branchial arch.

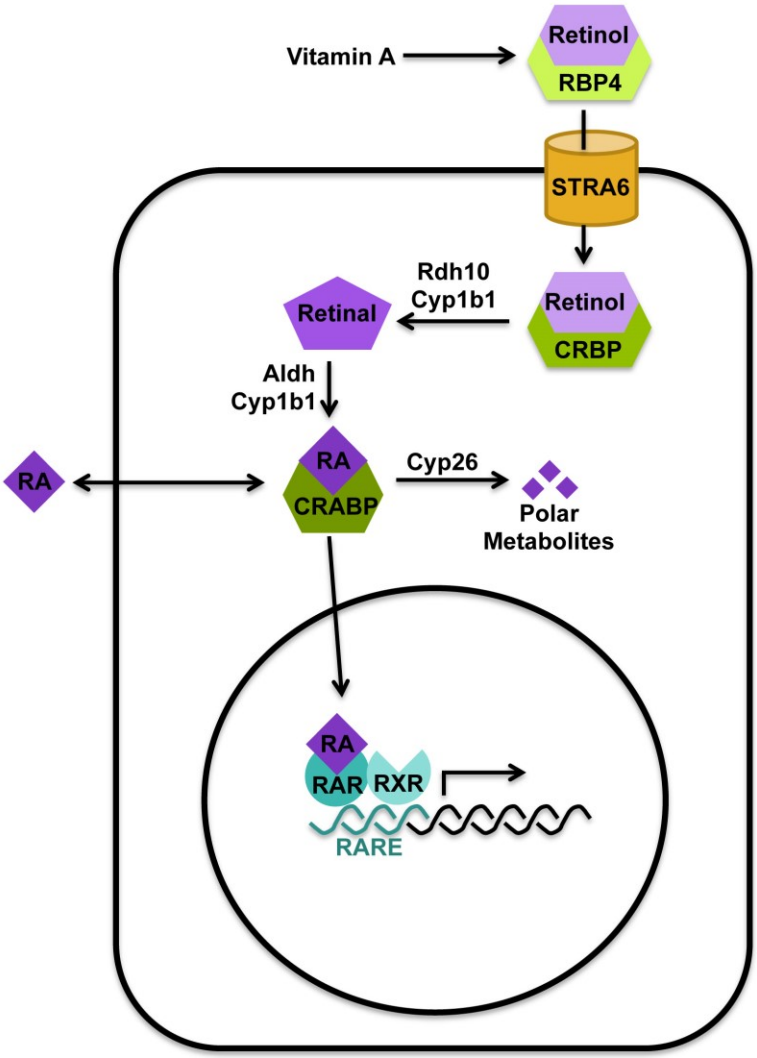

Figure 1.3. The Retinoic Acid Signaling Pathway

Vitamin A from dietary sources in mammals, and from the yolk in developing zebrafish is the source of retinol. Circulating retinol is bound by retinol-binding protein 4 (Rbp4), where it is then transported into the cytosol by Stra6. Once in the cytoplasm retinol is bound by cellular retinol-binding proteins (Crbp). Retinol is oxidized to retinaldehyde (Retinal) by Rdh10, and then further oxidized into Retinoic Acid (RA) by Retinaldehyde dehydrogenases (Aldhs or Raldhs). RA is bound by Cellular retinoic acid-binding proteins (Crabp). Cytochrome P450 1B1 (Cyp1b1) enzymes can also convert retinol into retinal and RA. Once synthesized, RA can be transported into the nucleus where it binds to RA receptor (Rar) and retinoid X receptor (Rxr) heterodimers that are bound to RA response elements (RARE) in the DNA. Binding of RA induces

the recruitment of co-activators to activate gene expression. RA is a diffusible morphogen and can regulate gene expression in adjacent tissues and cells, and it can be metabolized by the cytochrome P450 subfamily 26 (Cyp26) of enzymes into polar metabolites.

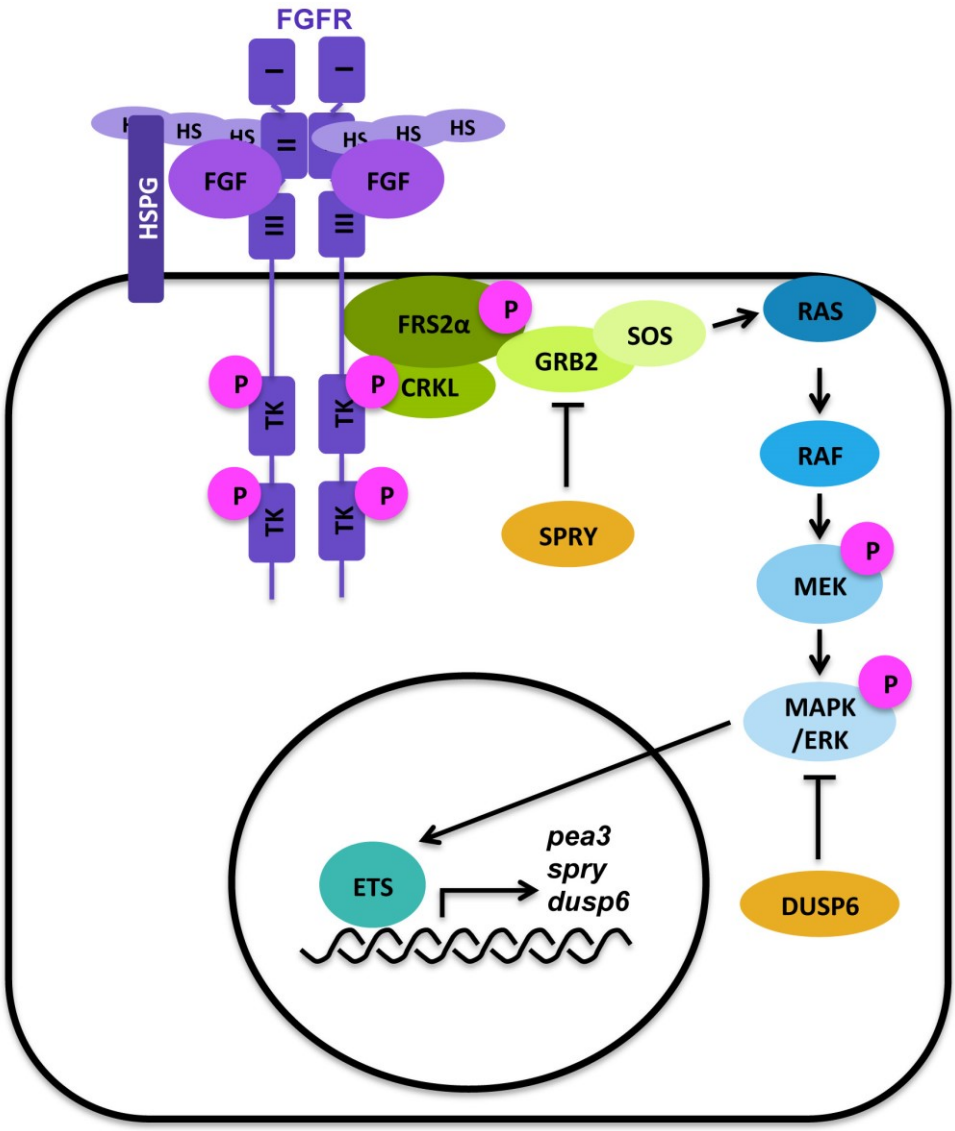

Figure 1.4. The Fibroblast Growth Factor Signaling Pathway

The Fibroblast growth factor (Fgf) receptor contains 3 extracellular immunoglobulin domains (I, II and III) and two intracellular tyrosine kinase domains. Binding of Fgfs to the FGF receptor (Fgfr) with heparin sulfate (HS) or heparin sulfate proteoglycan (HSPG) cofactors activates the tyrosine kinase domains of the Fgfr and induces phosphorylation. The activated receptor can then induce intracellular signaling pathways. Frs2α (FGFR substrate 2α) interacts with Crkl (CRK-like) and is phosphorylated by the active Fgfr. This recruits Grb2 (growth factor receptor-bound 2), which then recruits the guanine nucleotide exchange factor Sos (son of sevenless). Sos subsequently activates the Ras GTPase, which then signals through the MAPK (mitogen

activated protein kinase) pathway. Raf phosphorylates Mek (Mitogen-activated protein kinase kinase), which then phosphorylates Mapk/Erk (extracellular signal-regulated kinase). Mapk/Erk activates Ets (E26 transformation-specific) family transcription factors and induces the expression of target genes. Some of these target genes are negative regulators of FGF signaling and provide feedback inhibition. Spry (sprouty) inhibits the Ras-MAPK pathway through interactions with Grb2, while Dusp6 (dual-specificity phosphatase 6) specifically dephosphorylates Mapk/Erk.

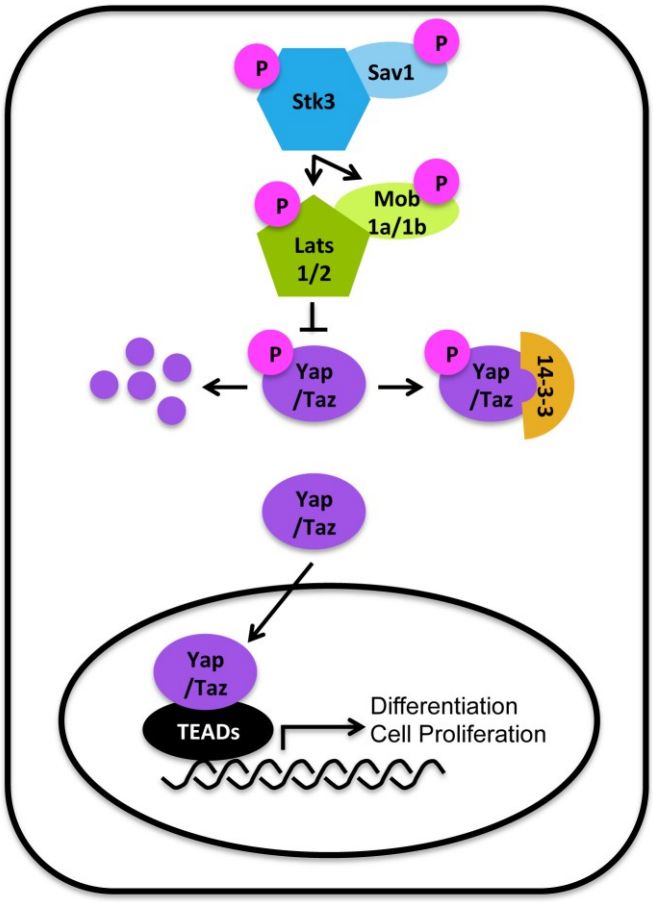

Figure 1.5. Components of the Core Hippo Signaling Pathway

The Stk3 (serine/threonine-protein kinase 3) kinase phosphorylates Sav1 (salvador family WW domain containing protein 1), Lats1/2 (large tumor suppressor kinase 1/2) and Mob1a/1ba/1bb (MOB kinase activator 1A/1Ba/1Bb). Phosphorylation activates Lats1/2, while Sav1 and Mob1a/1b phosphorylation help to enhance the kinase activity of both Stk3 and Lats1/2 respectively. Phosphorylated Lats1/2 then phosphorylate Yap (yes-associated protein 1)/Taz (WW domain containing transcription regulator 1; wwtr1), resulting in either degradation, or the sequestration of Yap/Taz in the cytoplasm by 14-3-3 proteins. When Yap/Taz are not phosphorylated they can translocate into the nucleus where they regulate target gene expression through interacting with TEAD (TEA domain) transcription factors.

Figure 1.6. Upstream Inputs and Cross-talk with the Hippo Signaling Pathway

There are numerous inputs that modulate the activity of the Core Hippo pathway. Stk3 (serine/threonine-protein kinase 3) and Sav1 (salvador family WW domain containing protein 1) can be activated by proteins such as RASSF1a (Ras association domain family member), TAOK (Thousand and one amino acid kinase) and MARK (MAP/microtubule affinity-regulating kinases). Interactions between FRMD6 (FERM domain containing 6), NF2 (neurofibromin 2), Kibra and the apical actin network also activate Stk3/Sav1. Conversely, Stk3/Sav1 can be inhibited by proteins such as RASSF6, SIK (Salt inducible kinases) and PP2A (protein phosphatase 2A). Tight junction (TJ) associated proteins (Par3/6 (partitioning defective homolog) and αPKC (alpha-protein kinase C) can also inhibit Stk3/Sav1. Lats1/2 (large tumor suppressor

kinase 1/2) and Mob1a/1ba/1bb (MOB kinase activator 1A/1Ba/1Bb) can be activated by FAT, NF2 and GPCR (G-protein coupled receptor) signaling through $G\alpha_s$, while GPCR signaling through $G\alpha_{q/11}$, $G\alpha_{12/13}$ and Rho, inhibit Lats1/2 and Mob1a/1b. Mob1a/1b are also inhibited by ZYX (zyxin) and Ajub (ajuba). Yap (yes-associated protein 1)/Taz (WW domain containing transcription regulator 1; wwtr1) can be sequestered in the cytoplasm through interactions with the membrane associated Crumbs complex (composed of Crumbs, LIN7C (Lin-7 homolog c), PALS, PATJ (Pals1-Associated Tight Junction) and AMOT (angiomotin)). The Crumbs complex can also be regulated by TJ associated proteins. Yap/Taz can also be sequestered by E-cadherin associated proteins, α-catenin, β-catenin and 14-3-3, which are regulated by Dlg (Discs large) and Scrib (Scribble). AMOT, ZO-1 (Zona occludens 1) and PTPN14 (Protein tyrosine phosphatase non-receptor type 14) have also been shown to sequester Yap/Taz in the cytoplasm. In the nucleus, Yap/Taz are able to interact not only with TEAD (TEA domain family member) transcription factors, but also with other transcription factors such as p73, RUNX (RUNT-related transcription factors), TBX5 (T-box transcription factor 5), SMAD (Mothers against DPP homolog) and PAX3 (paired box 3).

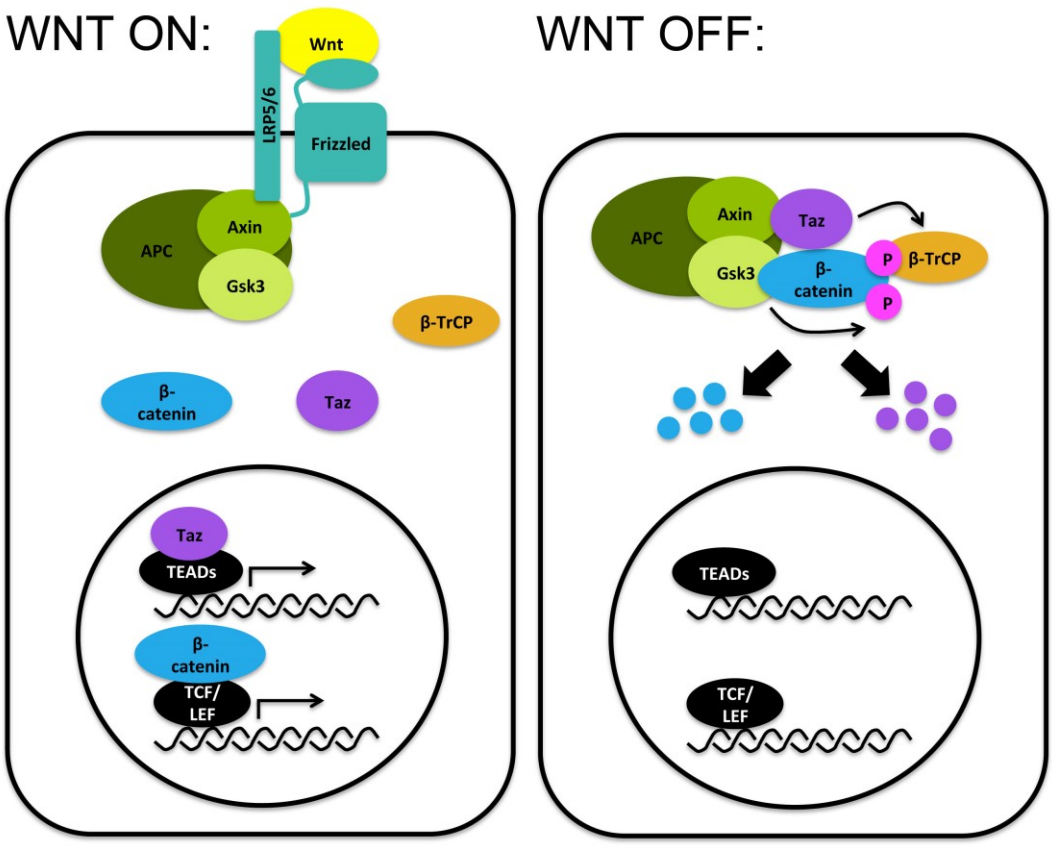

Figure 1.7. The Canonical Wnt Signaling Pathway

Binding of extracellular Wnts (Wingless-type MMV integration site family) to the Frizzled (Fzd) receptor induces dimerization of Lrp5/6 (Low density lipoprotein receptor-related protein 5/6) and Frizzed and intracellular recruitment of the β-catenin destruction complex through interactions between Axin (Axis inhibition protein) and Lrp5/6. Sequestration of the β-catenin destruction complex allows for nuclear localization of Yap (yes-associated protein 1, not shown)/Taz (WW domain containing transcription regulator 1; wwtr1) and β-catenin where they interact with TEAD (TEA domain family member) and Tcf (T-cell factor)/Lef (Lymphoid enhancer binding factor) transcription factors respectively to regulate target gene transcription. In the absence of Wnt ligands, the β-catenin destruction complex formed from Axin, APC (adenomatous polyposis coli complex), Gsk3 (serine/threonine glycogen synthase kinase 3), and Yap/Taz is able to bind β-catenin. Gsk3 phosphorylates β-catenin and Yap/Taz recruits the E3 ubiquitin ligase β-TrCP (beta-transducin repeat containing E3 ubiquitin protein ligase). β-TrCP induces ubiquitination and proteasomal degradation of β-catenin and Yap/Taz.

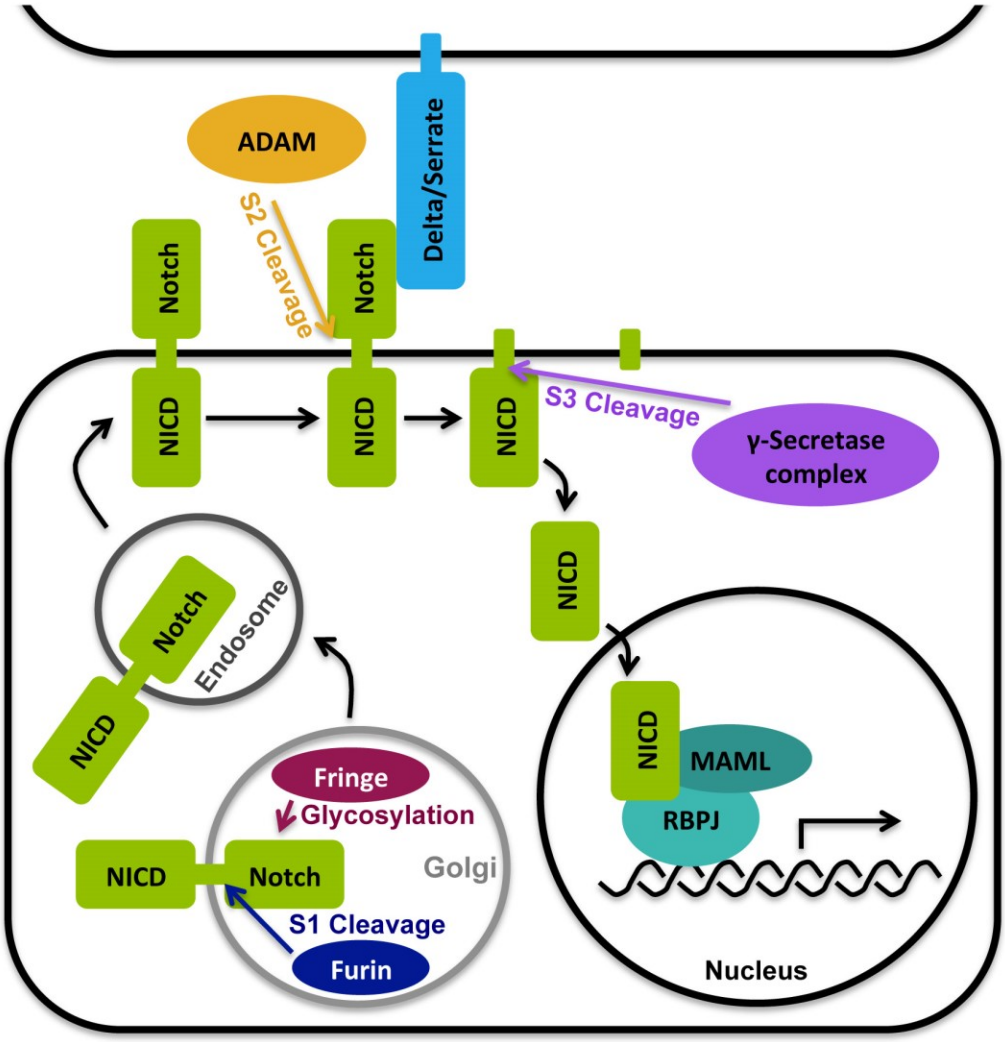

Figure 1.8. The Notch Signaling Pathway

The notch receptor undergoes Furin-mediated S1 (site 1) cleavage, and may undergo glycosylation in the golgi before being transported to the cell membrane via endosome. Glycosylation by Fringe proteins make Notch more susceptible to activation by the ligand Delta, as opposed to Serrate. When the Notch receptor encounters Delta or Serrate ligands ADAM metalloproteases cleave the extracellular portion of the Notch receptor, which is subsequently endocytosed by the cell presenting the ligand. The y-secretase complex then cleaves the intracellular portion of notch, releasing the Notch intracellular domain (NICD). The NICD then translocates to the nucleus where it binds to the DNA-binding Rbpj (recombination signal binding protein for immunoglobulin kappa J region a; suppressor of hairless (Su(H))) and Maml (Mastermind-like) to regulate target gene expression.

Chapter 2: Materials and Methods

2.1 Ethics statement

Larval and adult zebrafish were cared for in accordance with Canadian Council for Animal Care (CCAC) guidelines and this study was approved by the University of Alberta Animal Care and Use Committee for Biosciences (protocol 427).

2.2 General Zebrafish Care

2.2.1 Animal Care, Fish Lines and Maintenance

Care of embryonic and adult zebrafish was performed as outlined in Westerfield (2007) (Westerfield, 2007). Embryos were grown at 25.5°C, 28.5°C or 33°C, in embryo media (EM, 15 mM NaCl, 500 nM KCl, 1 mM $CaCl_2$ •$2H_20$, 150 nM KH_2PO_4, 1 mM Na_2HPO_4 anhydrous, 1 mM $MgSO_4$ •$7H_2O$, 715 nM $NaHCO_3$, 10,000 units penicillin, 10 mg/ml streptomycin (Sigma)) and stages of development were determined using standardized morphological criteria (Kimmel et al., 1995). Embryos older than 24 hours post fertilization (hpf) were treated with 0.006% 1-phenyl-2-thiourea (PTU) (SIGMA) to prevent pigment formation. Unless otherwise noted, AB strain zebrafish were used. Transgenic fish lines used include *Tg(isl1:GFP)* (Higashijima et al., 2000). Mutant fish lines used include *lazarus* (*lzr/pbx4*^{b557}), *hoxb1a*^{sa1191}, *hoxb1b*^{ua1006}, *taz* (*wwtr1/taz*^{ua1015}).

The *hoxb1a*^{sa1191} allele obtained from the Sanger Institute (Kettleborough et al., 2013), contains a G to A transition resulting in a stop codon at amino acid 269 (W269X). This allele is predicted to cause a truncation within the homeodomain and lack amino acids critical for homeodomain DNA binding activity (McClintock et al., 2001; Scott et al., 1989). Genotyping for *hoxb1a* is performed using a dCAPs assay (Haliassos et al., 1989) involving PCR followed by a digest with EcoRV. The wildtype allele produces a 173 bp band while the mutant allele produces a 149 bp band (Primer sequences listed in Table 2.1).

The *lzr/pbx4*^{b557} mutation was originally identified by Pöpperl (Pöpperl et al., 2000) based on the altered expression of *krox20*. Genotyping for the *lzr* mutation is performed using a dCAPs assay involving PCR followed by digest with XbaI. The

wildtype allele produces a 289 bp band while the mutant allele produces a 259 bp band (Primer sequences listed in Table 2.1).

The *hoxb1b*^{ua1006} and *taz*^{ua1015} mutant alleles were generated using Transcription Activator-Like Effector Nucleases (TALENs) (described in Section 2.9.2). The *hoxb1b*^{ua1006} mutant contains a 13 bp insertion 63 bp downstream of the start codon. This mutation is predicted to generate a 43 amino acid long protein where the first 21 amino acids correspond to the correct wildtype Hoxb1b protein (G22FfsX23). This truncated protein completely lacks the DNA-binding homeodomain and is predicted to lack all transcriptional activity. *Hoxb1b* mutants are genotyped based on PCR product size where the wildtype allele produces a 112 bp band and the mutant allele produces a 125 bp band (Primer sequences listed in Table 2.1). The *taz*^{ua1015} mutant contains a 29bp deletion 25bp downstream of the start codon. This mutation is predicted to generate a 19 amino acid long protein where the first 8 amino acids correspond to the wildtype Taz protein (I9KfsX12). This truncated protein lacks all functional domains. *Taz* mutants are genotyped based on PCR product size where the wildtype allele produces a 119 bp band and the mutant allele produces a 90 bp band (Primer sequences listed in Table 2.1).

Pbx-depleted embryos were generated by injecting *pbx4* heterozygous incrosses with a cocktail of 4 previously described *pbx2/4* translation blocking morpholinos (MO; Table 2.2) (Erickson et al., 2007).

Embryos were either dechorionated manually using Dumont #5 fine-pointed forceps (Fine Science Tools) or enzymatically. To enzymatically dechorionate embryos, embryos were immersed in a solution of 1 mg/mL pronase E (SIGMA) and swirled until the first few chorions begin to deflate. Embryos were then repeatedly washed in EM in a glass beaker until the majority of embryos have come out of their chorions.

Prior to mRNA in situ hybridization analysis or immunohistochemical analyses, (unless otherwise stated) embryos were fixed in 4% paraformaldehyde (PFA) in phosphate buffered saline (PBS: 137 mM NaCl, 2.7 mM KCl, 10 mM Na_2HPO_4, 1.8 mM KN_2PO_4 pH 7.4) (SIGMA) at 4°C overnight, or for 5 hours at RT.

2.2.2 Fin Clipping

To identify adult fish that were carriers for mutant alleles, tail fin clips were performed. Individual adult fish were anesthetized in 0.642 mM tricaine methanesulfonate (MS222) and placed on a clean paper towel where a small portion of the caudal tail fin was amputated with a scalpel. The fish were rinsed in fresh water and placed in individual tanks for recovery. The amputated fin was transferred to a PCR tube on ice, and subsequently the genomic DNA was extracted (See Section 2.4.1).

2.3 Embryo Manipulation

2.3.1 Morpholino Antisense Oligonucleotide Injections

Translation-blocking morpholino antisense oligonucleotides (MO; GeneTools) sequences and injection doses can be found in Table 2.2. Lyophilized MO stock were diluted in sterile water to a concentration of 10 mg/ml. Stock MO were heated to 65°C, and diluted to the desired concentration in Danieau Buffer (17.4 mM NaCl, 0.21 mM KCl, 0.12 mM $MgSO_4 \bullet 7H_2O$, 0.18 mM $Ca(NO_3)_2 \bullet 4H_20$, 1.5 mM HEPES) and stored at 4°C. Prior to injection, working MO stocks were heated to 65°C for 10 min, and allowed to cool to RT. MOs are injected into the yolk of 1-2 cell embryos. Dose was estimated based on bolus size and known concentration. Injections were performed using an ASI MPPI-2 Pressure Injector (Applied Scientific Instruments).

2.3.2 mRNA Injections

Prior to injection, mRNA was thawed on ice and diluted to the working concentration in DEPC- treated water (0.1% diethyl pyrocarbonate in H_20) and then injected into the cell of 1-cell stage embryos. Dose was estimated based on bolus size and known concentration. Injections were performed using an ASI MPPI-2 Pressure Injector (Applied Scientific Instruments).

2.3.3 Pharmacological Treatments

All compounds were dissolved in Dimethyl sulfoxide (DMSO; SIGMA) and diluted in EM to a working concentration. Equivalent solutions of DMSO/EM were used as solvent controls. A 5nM solution of all-trans Retinoic Acid (RA) (SIGMA) was used to activate retinoic acid signaling and was applied to live embryos at 50% epiboly (5.25 hpf). Embryos were allowed to develop to 4 somites (11 hpf) and then fixed in 4% PFA. A 0.1-20 μM solution of XAV939 (SIGMA) was used to inhibit Wnt signaling and was applied at tailbud. A 1-20 μM solution of SB216763 (SIGMA) was used as a Wnt signaling agonist and was applied at tailbud or 2 hpf. A solution of 10-200 μM ICG-001 (Tocris Bioscience) + 10-100 μM Windorphen (SIGMA) was used to prevent nuclear B-catenin transcription regulation and was applied at tailbud or 2hpf. A 50-200 μM solution of DAPT (SIGMA) or a 25-100 μM solution of Compound E (Cpd E; Calbiochem) in EM + 1% DMSO were used to prevent Notch intracellular domain cleavage and was applied at tailbud. Embryos treated with XAV939, SB216763, ICG-001+Windorphen, DAPT or Compound E were grown to 22-28 hpf and then were assessed for phenotypes, fixed in 4% PFA or anaesthetized and dissected for qPCR analysis.

2.3.4 Dextran Injections

Dextran injections were performed as described by Gutzman and Sive (2009) (Gutzman and Sive, 2009). Texas Red Dextran (10,000 MW) (Life Technologies) was dissolved 10 mg/ml in Danieau Buffer (17.4 mM NaCl, 0.21 mM KCl, 0.12 mM $MgSO_4$ $\bullet 7H_2O$, 0.18 mM $Ca(NO_3)_2$ $\bullet 4H_20$, 1.5 mM HEPES). Staged and dechorionated embryos were anesthetized in MS222. Embryos were then oriented in an agar-coated dish, and the Texas Red dextran solution was injected into the hindbrain ventricle, until the solution can be observed throughout the ventricle. Embryos were then mounted and oriented on a glass slide with low-melting point agarose.

2.4 Molecular Methods

2.4.1 Isolation of Genomic DNA

Genomic DNA was extracted based on the protocol described by Meeker et al. (2007) (Meeker et al., 2007). For fin clips or pooled embryos, embryos/tissue was immersed in 100 µL of 50 mM NaOH. For single embryos, embryos were immersed in 20 µL of 50 mM NaOH. Samples were boiled at 95 °C for 20 minutes, with intermittent vortexing, and then cooled on ice. The solution was neutralized using $1/10^{th}$ volume of 1 M Tris-HCl pH 8. For genotyping, genomic DNA is diluted 1 in 2, for HRM analysis genomic DNA is diluted 1 in 10.

2.4.2 mRNA Extraction

Total mRNA was extracted from embryos using the RNAqueous-4PCR Total RNA Isolation kit (Invitrogen/Ambion). Embryos were grown to the desired stage and dechorionated. For hindbrain specific RNA isolation, embryos were anesthetized with MS-222 and the hindbrain was dissected and stored on ice until all dissections were complete. Embryos were vortexed to homogenize tissue in 350 µL lysis/binding solution then, 350 µL 64% EtOH was added and the solution was vortexed for 30s. The solution was transferred to a filter cartridge in a collection tube and centrifuged at maximum speed for 1 min. The flow-through was discarded and 700 µL of wash solution #1 was added and centrifuged for 1 min at maximum speed. The flow-through was discarded and 500 µL of wash solution #2/3 was added and centrifuged for 1 min at maximum speed. The last step was repeated once. The filter cartridge was transferred to a new collection tube and 40 µL of elution buffer pre-heated to 70°C was applied to the filter cartridge and centrifuged for 30 s at maximum speed. 30 µL of pre-heated elution buffer was applied to the filter cartridge and centrifuged for 30 s at maximum speed. RNA was stored at -80°C.

2.4.3 One-Step Reverse Transcriptase PCR (RT-PCR)

One-step RT-PCR was performed using the SuperScript III One-Step RT-PCR System with Platinum Taq DNA Polymerase (Invitrogen). Each reaction was composed of 12.5 µL of 2x Reaction mix, 1 µL of RNA template, 1 µL of Superscript III Platinum Taq, 1 µL of 5 µM forward primer, 1 µL of 5 µM reverse primer and 8.5 µL of DEPC-treated water. The PCR cycle conditions were 54°C for 30 min (cDNA synthesis), 94°C for 2 min (denaturation), followed by 30 cycles of 94°C for 15 s (denaturation), 55-65°C for 30 s (primer annealing), and 68°C for 1 min/kb (extension), followed by a final extension at 68°C for 5 min. RT-PCR products were analyzed by gel electrophoresis.

2.4.4 Polymerase Chain Reaction (PCR)

For PCR reactions performed using Phusion Hot Start II DNA Polymerase (Thermo Scientific), reactions were set up containing 10 µL 5x HF buffer, 1 µL of 10 mM dNTPs, 5 µL of 5 µM Forward Primer, 5 µL of 5 µM Reverse Primer, 1 µL template, 0.5 µL Hot-Start Phusion and 27.5 µL of nuclease-free water. The PCR cycle conditions were 98°C for 1 min (initial denaturation), followed by 30-40 cycles of 98°C for 20 s (denaturation), primer specific Tm for 15 s (primer annealing), 72°C for 30 s/kb (extension), followed by a final extension at 72°C for 10 min.

For PCR reactions performed using TaKaRa Ex Taq DNA polymerase (TaKaRa), reactions were set up containing 2.5 µL of 10x ExTaq Buffer (Mg^{2+} plus), 2 µL dNTP mixture (2.5 mM each), 1 µL of 5 µM forward primer, 1 µL of 5 µM Reverse primer, 2-3 µL template, 0.2 µL Ex Taq and nuclease-free water to 25 µL total. The PCR cycle conditions were 94°C for 2 min (initial denaturation) followed by 30-40 cycles of 94°C for 15 s (denaturation), primer specific Tm for 15 s (primer annealing), 72°C for 1 min/kb (extension) followed by a final extension at 72°C for 3 min.

For PCR reactions performed using *Taq* DNA polymerase (recombinant) (Thermo Scientific), reactions were set up containing 2.5 µL of 10x Taq Buffer, 2.5 µL of dNTP mixture (2.5 mM each), 2 µL of 25 mM $MgCl_2$, 1 µL of 5 µM forward primer, 1 µL of 5 µM reverse primer, 2-3 µL of template, 0.2 µL *Taq* DNA polymerase and nuclease-free water to 25 µL total. The PCR cycle conditions were 95°C for 3 min (initial denaturation), followed by 30-40 cycles of 95°C for 30 s (denaturation), primer

specific Tm for 30 s (primer annealing), 72°C for 1 min/kb (extension), followed by a final extension at 72°C for 5 min.

2.4.5 Gel Extraction

Gel extractions were performed using the QIAquick Gel Extraction kit (Qiagen). The band to be extracted is excised from gel with a clean blade and placed in a 1.7 mL tube. 300 µL of QG buffer was added to the gel slice and incubated at 50-60°C for 10 mins, with periodic vortexing until the gel piece was melted. 100 µL of 100% Isopropanol was added and mixed, then the solution was transferred to a column in a collection tube. Column was centrifuged for 1 min at maximum speed and flow-through was discarded. 500 µL of QG buffer was added to the column and centrifuged for 1 min at maximum speed. Flow-through was discarded and 750 µL of PE buffer was added to the column, and allowed to stand for 5 min. The column was then centrifuged for 1 min at maximum speed and flow-through was discarded. The column was centrifuged for 1 min at maximum speed and transferred to a new 1.7 mL tube. DNA was eluted by adding 30 µL of Elution Buffer, leaving it to stand for 1 min, then centrifuging column for 1 min at maximum speed. DNA was stored at -20°C.

2.4.6 TOPO TA Cloning

Ligation of blunt end PCR products was performed using the TOPO-TA cloning kit (Life Technologies) For PCR products not generated with 3' adenine overhangs, reactions were set up containing 15 µL of gel purified PCR product (Section 2.4.5) with 2 µL of 10x Ex Taq Buffer, 1 µL of 10 mM dNTPs, 1 µL of TaKaRa Ex Taq and 1 µL of nuclease-free water. The reaction was then incubated for 10 min at 72°C. To clone PCR product into either pCR4-TOPO (for riboprobe synthesis) or pCR2.1-TOPO (for other applications) reactions were set up containing 2 µL PCR product (gel extracted, with A's), 0.5 µL of Salt solution, and 0.5 µL of TOPO vector. The reaction was incubated at RT for 5-30 mins. Following incubation, the TA ligation reaction was transformed into One Shot TOP10 Chemically Competent *E. coli* (Invitrogen) (as described in section 2.4.8) and spread on LB plates (1% Bacto-tryptone, 0.5% Bacto-yeast extract, 0.17 M NaCl, 1.5% Bacto-agar, pH 7) containing carbenicillin or kanamycin.

2.4.7 Ligation

Insert and vector plasmids were digested with the appropriate restriction endonucleases (RE), analyzed by gel electrophoresis and gel extracted (Section 2.4.5). The concentration of the digested gel extracted insert and vector was determined using a NanoDrop ND-1000 Spectrophotometer. Using the NEBioCalculator (http://nebiocalculator.neb.com/#!/ligation), the mass of insert and vector DNA to be used in the ligation reaction was determined. The required volumes of vector and insert DNA were combined with 2 µL of 10x T4 DNA ligase buffer, 1 µL of T4 DNA ligase (NEB) and nuclease-free water to a final volume of 20 µL. Reactions were incubated at RT for 10 mins or O/N at 16°C and 5 µL of the reaction was transformed (Section 2.4.8) into 50 µL of competent cells. Ligation reactions were performed in combination with a vector alone control.

2.4.8 Transformation

10-50 µL of One Shot TOP10 Chemically Competent *E. coli* (Invitrogen) were added to reaction/plasmid and incubated on ice for 20 mins. The transformation reaction was heat shocked at 42°C for 45 s and incubated on ice for 5 min. 100-200 µL of Super optimal broth with catabolite repression (SOC, 2% Bacto-tryptone, 0.5% Bacto-yeast extract, 10 mM NaCl, 2.5 mM KCl, 10 mM $MgCl_2$, 10 mM $MgSO_4$, 20 mM glucose) was added and reaction was incubated at 37°C for 30-60 min. Transformations were plated on LB containing the antibiotic required for selection of transformants. Plates were incubated inverted at 37°C O/N.

2.4.9 Miniprep

3 mL of LB (1% Bacto-tryptone, 0.5% Bacto-yeast extract, 0.17 M NaCl, pH 7) containing the antibiotic required for selection was inoculated and grown at 37°C O/N with shaking. Minipreps were performed using the QIAprep spin Miniprep kit (Qiagen). 1.5 mL of the culture was transferred to a 1.7 mL tube, the remaining culture was be stored at 4°C. Cells were pelleted by centrifugation at maximum speed for 5 min, and the supernatant was discarded. Cells were resuspended in 250 µL of chilled P1 buffer, and 250 µL of P2 buffer was added, then tube was inverted 5 times. 350 µL of N3 buffer

was then added and tubes were inverted 5 times before being centrifuged at maximum speed for 10 min. The supernatant was the transferred to a column in a collection tube and centrifuged for 1 min at maximum speed. The flow-through was discarded and 750 µL of PE buffer was added and columns were centrifuged for 1 min at maximum speed. The flow-through was discarded and the column was centrifuged for 1 min at maximum speed. The column was then placed in a new 1.7 mL tube, and 50 µL of Elution Buffer was added and column was centrifuged for 1 min at maximum speed. DNA was stored at -20°C.

2.4.10 Maxiprep

Maxipreps were performed using the QIAGEN Plasmid Maxi Kit (QIAGEN). Cells were pelleted in 50 mL conical tubes by centrifuging at 4°C at maximum speed for 15 min. Cells were resuspended in 10 mL of chilled P1 buffer, 10 mL of P2 buffer was added and the solution was inverted 5 times. The solution was incubated for 5 min at RT and 10 mL of chilled P3 was added. The solution was inverted 5 times and incubated on ice for 20 min. The solution was then centrifuged for 30 min at 4°C at maximum speed. During the centrifugation, the Qiagen columns were equilibrated with 10 mL QBT. Following centrifugation, the supernatant was carefully added to the column and allowed to flow-through by gravity. The column was washed twice with 30 mL of QC buffer and the DNA was eluted into a new 50 mL conical tube with 15 mL of QF buffer. 10.5 mL of 100% isopropanol was added to the eluted DNA, vortexed and incubated at -20°C for 15-30 min to precipitate the DNA. DNA was pelleted by centrifugation at 4°C at maximum speed for 30 min. The supernatant was removed and the DNA was resuspended in 1 mL of 70% EtOH in a 1.7 mL tube. DNA is pelleted again by centrifugation at 4°C at maximum speed for 10 min. The supernatant was removed; the pellet allowed to dry and then the pellet was resuspended in 100-400 µL of 1xTE pH 8.0. DNA was stored at -20°C.

2.4.11 Sequencing

Sequencing reactions were either submitted as aliquots containing 3-6 µL of template, 0.5 µL of 5 µM sequencing primer plus water to a total volume of 10 µL to the

Molecular Biology Service Unit for in-house sequencing, or samples were prepared as follows, before submission to the Molecular Biology Service Unit for capillary electrophoresis analysis. Sequencing reactions were performed by combining 2 µL of BigDye premix, 6 µL of 2.5x buffer (200 mM Tris-HCl pH 9, 50 mM $MgCl_2$), 1 µL of 5 µM primer, 50-400 ng of template and nuclease-free water to a total volume of 20 µL. The PCR cycle conditions were 25 cycles of 96°C for 30 s, 50°C for 15 s, 60°C for 2 min. To clean up the sample, the reaction was transferred to a 1.7 mL tube and 2 µL of 1.5 M NaOAc / 250 mM EDTA was added. 80 µL of 95% EtOH was added and the solution was vortexed and incubated at -20°C for 15 min. The solution was then centrifuged at 4°C for 15 min at maximum speed. The supernatant was removed, and 500 µL of 70% EtOH was added, then the solution was centrifuged for 5 min at 4°C at maximum speed. The supernatant was then removed, and the pellet dried.

Sequencing results were analyzed using MacVector or 4 Peaks, pairwise and multiple sequence alignments were performed using Clustal Omega, and translation of DNA sequences into protein sequences was performed using ExPASy.

2.4.12 RNA Riboprobe Synthesis

RNA riboprobes were either transcribed from purified, linearized plasmid DNA (Table 2.3) or from PCR products with an integrated T7 RNA polymerase site (Thisse and Thisse, 2008) (Table 2.4).

Plasmids were linearized by restriction digest with the appropriate enzyme. Linearized plasmids were purified by adding 160 µL DEPC- treated water and 200 µL Phenol/Chloroform/Isoamyl Alcohol and vortexing for 20 s. The solution was centrifuged for 5 min at maximum speed, the top layer was transferred to a new tube, where an equal volume of chloroform was added. The solution was vortexed for 20 s, centrifuged for 5 min at maximum speed and the top layer was transferred to a new tube. 1/10 volume of NaAc and 3 volumes of 100% RNAse free EtOH were added and the solution was placed on ice for 15 min, then centrifuged for 20 min at 4°C at maximum speed. The pellet was washed with 100 µL 70% EtOH, dried, and resuspended in 7 µL of DEPC- treated water. Alternatively, gene specific PCR products were amplified from

RNA using the SuperScript III One-Step RT-PCR System (Section 2.4.3), and the appropriate band was purified by gel extraction (Section 2.4.5).

Antisense fluorescein or digoxigenin (DIG)-labeled probes were transcribed by combining 7 µL of linearized purified DNA/PCR product, with 2 µL of 10x transcription buffer, 2 µL of DIG RNA labeling mix, 1 µL of appropriate RNA polymerase, 1 µL RNase inhibitor and 7 µL of DEPC- treated water. The reaction was incubated at 37°C for 2 hrs. After 1 hour, 1 µL of the appropriate RNA polymerase was added. To remove DNA, 1 µL RNase-free DNAse was added and the reaction was incubated for 5 min at 37°C. 2 µL of 0.25 M EDTA pH 8 was added to stop the reaction and the probe RNA was purified using SigmaSpin post-reaction Sequencing Reaction Clean-Up columns (SIGMA). The column was centrifuged in a collection tube for 15 s at 750 xg, then the base of the column is broken off and the lid removed, before being centrifuged 2 min at 750 xg. The column was placed in a new collection tube, and the probe synthesis reaction was applied to the centre of column and centrifuged for 4 min at 750 xg. 2 µL of 0.25 M EDTA pH 8, 1 µL of RNAseOUT and 25 µL of DEPC- treated water were added to the final product to inhibit degradation. RNA was stored at -80°C. Probes diluted in pre-hybridization solution to a working concentration were stored at -20°C.

2.4.13 mRNA Synthesis

All constructs used for mRNA expression are listed in Table 2.5. Plasmid DNA was linearized with the appropriate enzyme. Following digestion, 10 µL of DEPC-treated water, 2.5 µL of 10% SDS, and 2 µL of 10 mg/mL ProK were added and incubated for 1 hr at 50°C to remove RNases. To purify the linear plasmid, 50 µL of DEPC-treated water, 10 µL of NaOAc pH 5.3, 85.5 µL of DEPC-treated water and 200 µL of phenol chloroform isoamyl alcohol were added to the reaction. The solution was vortexed for 20 s, centrifuged for 5 min at maximum speed and the upper layer was transferred to new tube. An equal volume of chloroform was added to the solution, and the solution was vortexed for 20 s, then centrifuged for 5 min at maximum speed. The upper layer was transferred to a new tube, and 1/10 volume of 3 M NaAc pH 5.2, and 3 volumes of 100% EtOH were added to precipitate the DNA. The solution was then vortexed and incubated at -20°C for 15 min followed by centrifugation for 20 min at 4°C

at maximum speed. The pellet was washed with 100 µL of 70% EtOH/DEPC-treated water and resuspended in 10 µL of DEPC- treated water.

mRNA synthesis was performed using either SP6 or T7 mMessage mMachine Kits (Ambion) by combining 10 µL of 2x NTP/CAP, with 2 µL of 10x Reaction Buffer, 2 µL of linear purified DNA, 2 µL of enzyme mix and 4 µL of nuclease-free water. Reactions were incubated for 2 hrs at 37°C. DNA was removed by adding 1 µL DNase I and incubating the reaction at 37°C for 15 min. If construct did not contain a poly (A) tail, one was added using the Poly (A) Tailing Kit (Ambion). 36 µL of nuclease-free water, 20 µL of 5x *E*-PAP buffer, 10 µL of 25 mM MnCl2 and 10 µL of 10 mM ATP were added to the 20 µL mMessage mMachine reaction. 0.5 µL of this solution was removed and saved to verify addition of the poly(A) tail by gel electrophoresis. 4 µL of *E*-PAP was added to the remaining reaction mixture and incubated for 1 hr at 37°C.

RNA was recovered using Amicon Ultra Centrifugal Filters (Millipore). Samples were topped up to 500 µL with DEPC-treated water and placed in a column in a collection tube. The column was centrifuged for 4 min at 14000 xg. The flow-through was discarded and the column was inverted in a new collection tube. The column was centrifuged for 3 min at 1000 xg. The RNA was then topped up to 500 µL with DEPC-treated water and placed in a new column in a collection tube. The column was centrifuged for 4 min at 14,000 xg. The flow-through was discarded and the column was inverted in a new collection tube. The column was centrifuged for 3 min at 1000 xg. RNA concentration was measured using a NanoDrop ND-1000 Spectrophotometer and stored at -80°C.

2.4.14 Site-directed Mutagenesis

Site-directed mutagenesis primers are listed in Table 2.6. Un-phosphorylated primers were phosphorylated by combining 1 µL of 10x T4 PNK buffer, 0.25 µL of T4 PNK, 0.5 µL of 100 µM primer and 8.25 µL of nuclease-free water. The reaction was incubated at 37°C for 45 min.

The site directed mutagenesis PCR reaction contained 17 µL of PT1.1xMM (3.125 mM KCl, 12.5 mM Tris-HCl pH 8.5, 0.09375 mM $MgCl_2$ $6H_20$, 0.125% BSA, 0.25 mM of each dNTP), 1 µL of 20x NAD (10 mM), 1 µL of 5 µM phosphorylated

forward primer, 1 µL of 5 µM phosphorylated reverse primer, 0.5 µL of DMSO, 0.3 µL of Taq DNA ligase, 1 µL of Pfu Ultra DNA polymerase (Agilent), and either 0.1, 0.5 or 1 µL of maxiprepped plasmid DNA (Section 2.4.10). Nuclease-free water was added to a final reaction volume of 22.8 µL. The PCR cycle conditions were 95°C for 2 min (initial denaturation), then 30 cycles of 95°C for 1 min (denaturation), 55°C for 1 min (annealing), 65°C for 90 s/kb (extension), followed by 72°C for 10 min. PCR products were then incubated with 1 µL of DpnI for 30 min at 37°C to digest the original plasmid. The reaction was then transformed and verified by Sanger sequencing (Section 2.4.11). Reactions were performed in combination with a no primer control.

2.4.15 Real-time quantitative PCR (qPCR)

Following RNA extraction (Section 2.4.2) DNA was removed by combining 70 µL of eluted RNA with 19 µL of DEPC- treated water, 10 µL of DNAseI buffer and 1 µL of DNAseI. The reaction was incubated for 30 min at 37°C. RNA was purified using RNeasy Mini Kit (Qiagen). 350 µL of RLT Buffer + 1% β-mercaptoethanol was added to DNAse I-treated RNA and vortexed. 250 µL of 100% EtOH was added to the solution and mixed by pipetting. The solution was transferred to a column in a collection tube and centrifuged for 15 s at 10,000 rpm. The flow-through was discarded and in a new collection tube, 500 µL of RPE was added and the column was centrifuged for 15 s at 10000 rpm. The flow-through was discarded and 500 µL of RPE was added to the column and centrifuged for 2 min at 10000 rpm. The column was transferred to a new collection tube and centrifuged for 1 min at maximum speed. The column was transferred to a new collection tube and 10 µL of DEPC-treated water was added and the column was centrifuged for 1 min at 10000 rpm to elute RNA.

cDNA was synthesized using the AffinityScript QPCR cDNA Synthesis Kit (Agilent) by combining 15 µL of 2x MM, 4.5 µL of random hexamers, 1.5 µL of RT/RNAse block enzyme mix and 9 µL of purified RNA. The PCR cycle conditions were 25°C for 5 min (primer annealing), 42°C for 30 min (cDNA synthesis), 95°C for 5 min (reaction termination). cDNA was stored at -20°C.

qPCR analysis of cDNA was performed using the Brilliant II SYBR Green QPCR Master Mix (Agilent). 7.5 µL of 2x SYBR Master mix, was combined with 0.45

µL of 5 µM Forward primer, 0.45 µL of 5 µM Reverse primer, 4.6 µL of nuclease-free water, and 2 µL of cDNA template. All cDNA samples were run in replicates of 4-6, and each experiment was repeated 3 times. The PCR cycle conditions were 95°C for 10 min (initial denaturation), followed by 45 cycles of 95°C for 20 s (denaturation) 55°C for 1 min (annealing and extensions). Fluorescence readings were taken after the 55°C annealing step. The Ct value data were analyzed using the comparative Ct method (2-ΔΔCt method) (Livak and Schmittgen, 2001) All qPCR primers sequences are listed in Table 2.7. All primers were validated with a 2/4-fold dilution series. Valid primers produced a coefficient of determination (R^2) of 0.98 or higher.

2.4.16 RNA-seq

RNA sequencing was performed on *taz*$^{-/-}$ mutant embryos and AB control embryos at 24hpf. *Taz*$^{-/-}$ mutants were identified based on presence of midline separation defects. Whole embryos were stored in 100 µL RNAlater to stabilize cellular RNA, and sent to Otogenetics Co (Norcross GA, USA) for RNA extraction, library prep, next-generation sequencing and bioinformatics analysis. The Database for Annotation, Visualization and Integrated Discovery (DAVID; https://david.ncifcrf.gov/; v6.8) was used to perform Gene Ontology (GO) analysis.

2.5 Whole Mount *in situ* Hybridization

2.5.1 Single Color

Whole mount *in situ* hybridization was performed essentially as previously described (Thisse and Thisse, 2008). Fixed embryos were washed 4 times for 5 min in PBST (PBS + 0.1% Tween-20) and permeabilized with 10 µg/ml Proteinase K. Embryos were permeabilized as follows: 30 s for 4 somites (11 hpf), 90 s for 10 somites (12 hpf), 3 min for 18 somites (18 hpf) to 24 hpf, 5-7 min for 28 hpf, 30 min for 36 hpf, 40 min for 48 hpf, 60 min for 60 hpf, and 90 min for 72 hpf. Embryos were re-fixed in 4% PFA for 20 min and washed 4 times for 5 min in PBST. Embryos were then incubated in hybridization solution (50% formamide, 5x sodium saline citrate (SSC), 50 µg/mL heparin, 0.1% Tween-20, 92 mM citric acid) with 500 µg/mL tRNA for at least 2 hours

at 65°C. Embryos were then incubated in hybridization solution containing fluorescein and/or DIG-labeled overnight at 65°C. Following hybridization, the following stringency washes were performed at 65°C: 5 min in 66% hybridization solution/33% 2X SSC, 5 min in 33% hybridization solution/66% 2x SSC, 5 min in 2x SSC, 20 min in 0.2x SSC + 0.1% Tween-20, and twice for 20 min in 0.1x SSC + 0.1% Tween-20. The following washes were then performed at RT: 5 min in 66% 0.2x SSC / 33% PBST, 5 min in 33% 0.2x SSC/ 66% PBST and 5 min in PBST. Embryos were then blocked in PBST containing 2% sheep serum and 2 mg/ml Bovine Serum Albumin for at least 1 hour at RT. Embryos were incubated in a 1:5000 dilution of sheep anti-DIG-AP FAB fragments (Roche) in blocking solution for at least 2 hours at RT. Embryos were washed 5 times for 15 min in PBST and then either stored at 4°C O/N, or colored immediately. For coloration, embryos were first washed 4 times for 5 min in coloration buffer (100 mM Tris-HCl pH 9.5, 50 mM $MgCl_2$, 100 mM NaCl, 0.1% Tween-20), and then incubated in a solution containing 10mL of coloration buffer with 45 µL of 4-nitro-blue tetrazolium (NBT; Roche) and 35 µL of 5-bromo-4-chloro-3-indolyl phosphate, toluidine salt (BCIP; Roche) until visible coloured precipitate formed. The coloration reaction was stopped by 4 quick washes followed by two 15 min washes in either 100% MeOH or Stop Solution (PBST + 1 mM EDTA, pH 5.5).

2.5.2 Two Color

For two color *in situs*, DIG-labeled probes were colored first with NBT/BCIP, and coloration was stopped with 4 washes for 5 min in water followed by 10 min incubation in 0.1 M Glycine pH 2.2. Embryos were washed 4 times for 5 min in PBST and re-blocked for at least 1 hr. Embryos were then incubated in a 1:10000 dilution of sheep anti-FL-AP FAB fragments (Roche) in blocking solution for at least 2 hours. Embryos were washed 4 times for 5 min in 0.1 M Tris-HCl pH 8.2 + 0.1% Tween-20. FastRed Tablets (Sigma) were dissolved and syringe filtered in 2 mL of 0.1 M Tris-HCl pH 8.2 + 0.1% Tween-20 per tablet, and embryos were allowed to colour in this solution until visible coloured precipitate formed. Coloration was stopped with 4 washes for 5 min in PBST.

2.6 Immunohistochemistry

2.6.1 Acetylated Tubulin

Embryos were fixed in Dents (80% MeOH / 20% DMSO) overnight. Embryos were rehydrated into PBST (5 min – 50% MeOH / 50% PBST, 5 min – 25% MeOH / 75% PBST, 5min – PBST), and then washed in PBSDTT (PBST + 1% DMSO + 0.1% Triton X-100) for 5 min before being blocked for 90 min at RT in PBSDTT + 10% GS + 0.1% BSA. Anti-Acetylated Tubulin (SIGMA) was diluted 1:500 in block and incubated O/N at 4°C. Embryos were washed 5 times for 5 min in PBSDTT, and Goat anti-Mouse IgG Alexa Fluor 488 (Invitrogen) was diluted 1:500 in block and embryos were incubated O/N at 4°C in the dark. Embryos were then washed in PBSDTT once for 5 min and 4 times for 10 min.

2.6.2 Active Caspase

Embryos were fixed in 4% PFA and washed 3 times for 20 min in PBST. Embryos were then washed once for 5 min in MilliQ + 0.1% Tween-20 and permeabilized for 7 min in ice-cold acetone. Embryos were then washed for 5 min in MilliQ + 0.1% Tween-20 and then blocked for 30-90 min in PBSDTT + 5% GS. Anti-Active Caspase 3 (BD Biosciences) was diluted 1:400 in block and incubated either O/N at 4°C or for 2hrs at RT. Embryos were then rinsed twice in PBSDTT and washed twice for 20 min in PBSDTT. Goat anti-Rabbit IgG Alexa Fluor 555/568 (Invitrogen) and TO-PRO-3 (Invitrogen) were each diluted 1:1000 in block, and embryos were incubated O/N at 4°C or for 2 hrs at RT. Embryos were then rinsed twice in PBSDTT, and then washed 4 times for 15 min in PBSDTT.

2.6.3 Crb2a

Embryos were fixed in 4% PFA then washed in PBST 4 times for 5 min. Embryos were then blocked in PBST + 10% GS + 1% Triton X-100 for 1 hr. Zs4 (ZIRC) was diluted 1:10 in block and embryos were incubated O/N at 4°C. Embryos were then washed 5 times for 15 min in PBST. Goat anti-Mouse IgG Alexa Fluor 488

(Invitrogen) was diluted 1:800 in block, along with TO-PRO-3 (Invitrogen), diluted 1:1000 and incubated O/N at 4°C. Embryos were then washed 3 times for 60 min in PBST.

2.6.4 Phalloidin

Embryos were fixed in 4% PFA. (Embryos cannot be stored in MeOH) Embryos were then washed 4 times for 5 min in PBST and 2 times for 5 min in TBST (50 mM Tris, 150 mM NaCl, 0.1% Tween-20, pH 7.6). Embryos were permeabilized in 4% Triton X-100 in TBST (45 min for 3 dpf, 75 min for 4 dpf, 10 min for 19-24 hpf) and then washed twice for 5 min in TBST. Alexa Fluor 488 Phalloidin (Invitrogen) was diluted 1:100 in TBST + 50 mg/ml BSA (SIGMA) and embryos were incubated O/N at 4°C in the dark. Embryos were then washed 6 times for 5 min in TBST.

2.6.5 Phospho-Erk

P-Erk antibody staining was performed based on the protocol used by Liu *et al.* (2013) (Liu et al., 2013a). Embryos were fixed in 4% PFA at the 4 somite stage (11 hpf). Embryos were then washed 5 times for 5 minutes in PBST, then washed in MilliQ + 0.1% Tween for 5 minutes. Embryos were permeabilized with ice-cold acetone for 7 min, and washed again in MilliQ + 0.1% Tween for 5 minutes, and PBST 5 times for 5 minutes. Antigen repair was performed by boiling the embryos for 10 minutes in 10 mM EDTA (pH 8). After cooling to room temperature and washing 2 times for 5 minutes in PBS, embryos were blocked for 1 hour (3% BSA, 5% GS, 1% DMSO in PBS) and incubated in antibody (Phospho-p44/42 MAPK (Erk1/2) (Thr202/Tyr204) Rabbit mAb (Cell Signaling, 4370) diluted 1:200 in block) overnight at 4°C. Embryos were then washed in PBS + 3% BSA + 1% DMSO 5 times for 30 s followed by one 30 minute wash in PBS + 3% BSA + 1% DMSO. Embryos were re-blocked for 1 hour and incubated in Goat anti-Rabbit IgG Alexa-Fluor 488 (Invitrogen) and TO-PRO-3 (Invitrogen) each diluted 1:1000 in block overnight at 4 °C. Embryos were then washed 5 times for 15 minutes in PBST.

2.6.6 Phospho-Histone H3

Embryos were fixed in 4% PFA and washed 5 times for 5 minutes in PBST. Embryos were then permeabilized with Proteinase K and re-fixed in 4% PFA for 20 min. Embryos were washed again 5 times for 5 minutes. Antigen retrieval was performed by incubating embryos for 10 min at 95°C in 10 mM Citric acid. Embryos were then blocked in PBS + 3% BSA + 0.5% Triton for 1 hour. Anti-phospho histone H3 (BD Biosciences) was diluted 1:1000 in block for 2 hr at RT and then washed 5 times for 15 min in PBST. Goat anti-Rabbit IgG Alexa Fluor 488 (Invitrogen) and TO-PRO-3 (Invitrogen) were diluted 1:1000 in block and embryos were incubated 2 hrs at RT and then washed in PBST 5 times for 15 min.

2.6.7 RMO44

Reticulospinal neurons were examined using the RMO44 antibody (SIGMA). Embryos were allowed to develop to 48 hpf and then dechorionated and fixed in 2% trichloroacetic acid in PBS for 3 hrs. Embryos were washed twice with PB (0.1 M phosphate buffer pH 7.4) and then washed 3 times in PB-Triton (81 mM Na_2HPO_4, 19 mM NaH_2PO_4, 0.5% Triton X-100). Embryos were blocked with 1 mL PB-Triton + 10% goat serum + 0.1% BSA for 1 hr. Embryos were then incubated with antibody diluted 1:100 in blocking solution for 48 hrs. Antibody can be removed and reused 5-10 times. Embryos were washed in PB-Triton 6 times for 15 minutes and then incubated in Goat anti-mouse IgG Alexa-Fluor 488 (Invitrogen) diluted 1:500 in blocking solution. Embryos were then washed 6 times for 15 minutes in PB-Triton.

2.6.8 Taz/Yap

Taz/Yap immunohistochemistry was performed as described in Clark et al. (2011), and Miesfeld et al. (2015) (Clark et al., 2011; Miesfeld et al., 2015). Embryos were fixed in 4% PFA then washed 3 times for 5 min in PBS and blocked for 1 hr in PBS + 10% GS +1% Triton X-100 + 1% Tween-20. Yap (Cell Signaling 4912) or Taz (Cell Signaling 8418) were diluted 1:200 in block and embryos were incubated O/N at RT. Embryos were rinsed twice in PBS + 1% Tween-20 and washed 3 times for 60 min in PBS + 1% Tween-20. Goat anti-Rabbit IgG Alexa Fluor 488 (Invitrogen) was diluted

1:800 in block with TO-PRO-3 (Invitrogen) diluted 1:1000 and embryos were incubated O/N at RT. Embryos were then rinsed 4 times in PBS + 1% Tween-20 and washed 5 times for 20 min in PBS + 1% Tween-20.

2.6.9 Zn-5/Zn-12/Znp-1

Embryos were fixed in 4% PFA, O/N at 4°C or at RT for 5 hrs. Embryos were then washed 5 times for 5 min in PBST. Embryos were permeabilized for 10 min in 10 µg/mL Proteinase K (SIGMA) in PBST, re-fixed in 4% PFA for 20 min and washed in PBST 5 times for 5 min. Embryos were then blocked in PBST + 2% GS + 2 mg/ml BSA + 0.1% Triton for 1 hr. Antibodies were diluted in block (zn-5 – 1:250, zn-12 – 1:500, znp-1 – 1:100; ZIRC) and incubated O/N at 4°C. Embryos were then washed 5 times for 30 min in PBSDTT, and blocked in PBSDTT + 1% GS for 1 hour. Goat anti-Mouse IgG Alexa Fluor 488 (Invitrogen) was diluted 1:750 in block and incubated O/N at 4°C in the dark. Embryos were then washed in PBSDTT 6 times for 15 min in the dark.

2.7 Photography and Image Analysis

2.7.1 Mounting and Photography

For images obtained on the compound and confocal microscope, embryos were manually deyolked with insect pins, passed through 30% glycerol, 50% glycerol and 70% glycerol, then mounted on glass slides an imaged using either a Zeiss AxioImager Z1 compound scope using and AxioCam HR camera and Axiovision SE64 Rel.4.8 software (Zeiss) or a Zeiss LSM 510 confocal microscope using Zeiss Zen software. Whole embryos were suspended in 2.5-3% Methyl cellulose and imaged using an Olympus SZX12 stereomicroscope (Olympus) with a Micropublisher 5.0 RTC camera and QCapture Suite PLUS Software v3.3.1.10 (QImaging). Figures were assembled in Photoshop. (Adobe Photoshop CS4)

2.7.2 Measurements of Area

To quantify ventricle area, dorsal mounts of *atoh1a in situ* hybridizations were imaged (Sections 2.5.1 and 2.7.1). The focal plane was determined such that the inside edge of *atoh1a* expression was in focus for each image and the hindbrain ventricle was outlined manually and measured using ImageJ software (National Institutes of Health).

To quantify the area of *aldh1a2* expression*, aldh1a2 in situ* hybridizations were imaged (Section 2.5.1 and 2.7.1), and the region of aldh1a2 staining was outlined manually and measured using ImageJ software (National Institutes of Health).

Measurements were averaged for each genotype/treatment group and data was analyzed using Analyses of Variance (ANOVA) followed by a post-hoc Tukey's Honest Significant Difference test.

2.7.3 Measurements of Fluorescence Intensity

To quantify P-Erk fluorescence intensity, P-Erk immunohistochemistry was performed and imaged (Sections 2.6.5 and 2.7.1), and the region of P-Erk fluorescence in the hindbrain was outlined manually and integrated density and area were measured using ImageJ software (National Institutes of Health). Background mean grey value was also measured in an area adjacent to the embryo. Measurements for each genotype were then averaged.

To quantify Taz fluorescence intensity, Taz immunohistochemistry was performed and imaged (Sections 2.6.8 and 2.7.1), and 4-5 regions at either rhombomere boundaries, or between rhombomere boundaries were selected for each image and integrated density and area were measured using ImageJ software (National Institutes of Health). Background mean grey value was also measured in 4 regions adjacent to the embryo. These measurements were then averaged for each image, and an average for each treatment was calculated.

For all fluorescence intensity measurements, corrected fluoresce was calculated (Burgess et al., 2010) (Corrected fluorescence = Integrated Density – [Area selected x mean grey value of background]) and data was analyzed using Analyses of Variance (ANOVA) followed by a post-hoc Tukey's Honest Significant Difference test.

2.8 Protein Analysis

2.8.1 Deyolking Embryos

Embryos were deyolked based on the protocol developed by Link et al. (2006) (Link et al., 2006). 1 mL of deyolking buffer (55 mM NaCl, 1.8 mM KCl, 1.25 mM $NaHCO_3$, cOmplete mini EDTA-free protease inhibitor tablets (Roche)) was added to dechorionated embryos and pipetted up and down to disrupt yolk. The solution was vortexed for 30 s at 1100 rpm and centrifuged for 1 min at 3000 rpm. The supernatant was removed and 1 mL of deyolking wash buffer (110 mM NaCl, 3.5 mM KCl, 10 mM Tris-HCl pH 8.5, 2.7 mM $CaCl_2$, cOmplete mini EDTA-free protease inhibitor tablets (Roche)) was added. The solution was vortexed at 1100 rpm for 30 s and centrifuged for 1 min at 3000 rpm, then the supernatant was removed.

2.8.2 Western Analysis

Westerns were performed on 10-25 embryos per sample, at 70% epiboly (8 hpf). After embryos were dechorionated with pronase E (Section 2.2.1) and deyolked (Section 2.8.1), 3 µL of 1x sample loading buffer + 2.5% B-mercaptoethanol was added per embryo, vortexed to lyse cells. NuPAGE 4-12% Bis-Tris Protein Gels (Invitrogen) were run in the X-Cell Sure Lock Mini-Cell system (Invitrogen). Cell lysates were boiled, centrifuged at 4°C and placed on ice. In each well 10 µL of sample, ladder or 1x sample loading buffer was loaded and the gel was run at 200 V for 1 hour. Protein was transferred to PVDF membrane using the TE 77 ECL Semi-dry transfer apparatus (Amersham), as per apparatus instructions with 4 pieces of Whatman paper on either side and run at 30 V for 1 hour. Following transfer, the PVDF was re-wet in 100% MeOH, and rinsed 3-4x in water. The membrane was blocked O/N at 4°C or for 1 hour at RT (5% skim milk in TBST – anti-Flag antibody, 1% ovalbumin / 1% Sheep serum / 1% BSA in TBST – anti-Myc antibody, 5% skim milk / 2% BSA / 2% Goat serum – anti-HA antibody. The primary antibody was diluted 1:1000-1:10000 (anti-Flag antibody 1:2000, anti-Myc antibody 1:7500, anti-HA antibody 1:1000 to 1:2000) in block and incubated at RT for at least 1 hour or O/N at 4°C. The membrane was then washed 4 times for 5 min in TBST, and then incubated in goat anti-mouse HRP-linked

F(ab') fragments (GE Healthcare Life Sciences) diluted 1:5000-1:15000 in TBST for 1 hour at RT. The membrane was then washed 4 times for 5 min in TBST. Chemiluminescent detection was performed using the Pierce Super Signal West Pico Chemiluminescent Substrate Kit (Thermo Scientific). A 1:1 dilution of the solutions was prepared and the membrane was incubated for 3-5 min. The membrane was then exposed to autoradiography film (Kodiak) and developed.

* Western Analysis for data presented in Chapter 3 was performed by Laura M. Pillay, and Jakub Famulski.

2.8.3 Targeted Endonuclease Protein Synthesis and *in vitro* DNA Cleavage Assay

The *in vitro* DNA cleavage assay was adapted from the *in vitro* transcription-translation assay for rapid screening of ZFNs for sequence-specific cleavage activity (Mani et al., 2005). ZFN or TALEN constructs were transcribed and translated using the TNT SP6 Coupled Rabbit Reticulocyte Lysate System (Promega). Each reaction was composed of 100 to 500 ng of pCS2-FokI ZFN (RR or DD; control or *Sharkey*) or pCS2TAL3 TALEN (RR or DD; control or *Sharkey*) plasmid DNA, 25 µL of TNT Rabbit Reticulocyte Lysate, 2 µL of TNT Reaction buffer, 1 µL of TNT RNA Polymerase, 1 µL of 1 mM Amino Acid Mixture Minus Leucine, 1 µL of 1 mM Amino Acid Mixture Minus Methionine, 1 µL of RNase OUT (Life Technologies), and DEPC-treated water (total volume 50 µL). The reaction was incubated at 30°C for 90 minutes, then 1µL of RNase H was added and the reaction was incubated at 37°C for 15 min.

After synthesis, 0.1–2 µL of 5′ ZFN or TALEN (RR; control or *Sharkey*) and 3′ ZFN or TALEN (DD; control or *Sharkey*) protein lysates were combined with 500 ng of target-site-containing plasmid DNA, 2 µL 10x Restriction Buffer 4 (NEB) or 10x FastDigest Buffer (Fermentas), and 0.5 µL of plasmid-linearizing restriction enzyme (20 µL total volume). This reaction was incubated at 37°C for 2 to 3.5 hours. Digested plasmid DNA was purified by gel extraction (Section 2.4.5), and digested DNA fragments were analysed by agarose gel electrophoresis. Anecdotal evidence suggests that the plasmid purification step improves the resolution and separation of DNA fragments.

* Targeted Endonuclease Protein Synthesis and *in vitro* DNA Cleavage Assays for data presented in Chapter 3 were performed by Laura M. Pillay, and Jakub Famulski.

2.9 Zebrafish Mutagenesis

2.9.1 Zinc Finger Nuclease (ZFN) Construction

Algorithm-based (http://pgfe.umassmed.edu/ZFPsearch.html) detection of suitable ZFN target sequences was performed as previously described (Meng et al., 2008) with preference given to purine-rich sequences, guanine-rich sequences, and sequences containing a six-nucleotide spacer region between ZFN recognition sites. ZFN target sequences can be found in Table 2.8.

To identify and construct suitable ZFN arrays for *prp2*, *hmx4*, and *crx*, zinc finger library construction and two-stage omega-based bacterial one-hybrid selection of zinc finger arrays was performed as previously described, (Meng et al., 2008), except for hmx4 ZFNs, in which the bacterial one-hybrid selection target-site plasmids were modified so that the fourth base pair on the opposite strand always corresponded to the hmx4 zinc finger domain's recognition site (as opposed to the Zif268 scaffold zinc finger domain's recognition site. The *prp1*, *nlz2*, *gdf11*, and *sfrp5* ZFN arrays were designed through context-dependent assembly (CoDA) as previously described, (Sander et al., 2011b) using the ZiFiT Targeter Version 3.3 algorithm (zifit.partners.org/ZiFiT) to select the ZFN target-sites (Sander et al., 2010; Sander et al., 2007).

All selected zinc finger arrays were cloned into the previously described pCS2-HA-GAAZFP-FokI-RR (5′ arrays) or pCS2-Flag-TTGZFP-FokI-DD (3′ arrays) ZFN expression vectors (Addgene) (Meng et al., 2008). The DD (R487D, N496D) and RR (D483R, H537R) cleavage domain mutations favor heterodimeric cleavage activity, and, therefore, reduce ZFN toxicity (Miller et al., 2007; Szczepek et al., 2007).

ZFNs containing the Sharkey FokI cleavage domain have previously been shown to exhibit greater in vitro activity than those containing the wild type FokI cleavage domain (Guo et al., 2010). Sharkey variants of the ZFN expression vectors (pCS2-Flag-TTGZFP-SharkeyFokI-DD; pCS2-HA-GAAZFP-SharkeyFokI-RR) were synthesized

through site-directed mutagenesis (2.4.14) of the original expression vectors using primers listed in Table 2.6.

The following amounts of 5' and 3' control or Sharkey ZFN mRNAs were injected into single-cell zebrafish embryos: prp2 ZFN mRNA, 20 pg; hmx4 ZFN mRNA, 200 pg; and crx ZFN mRNA, 100 pg.

* Zinc Finger Nuclease Construction for data presented in Chapter 3 was performed by Laura M. Pillay, Valerie C. Fleisch, and Gary Ritzel.

2.9.2 Transcription Activator-like Effector Nuclease (TALEN) Construction

Our protocol for constructing TALENs was largely based on the published work of Cermak *et al*. (2011). TALEN target sites can be found in Table 2.9. pFUSA and pFUSB7 plasmids were linearized with BsaI and gel purified (Section 2.4.5). To assemble each half TAL construct, plasmids for RVDs 1-10 were digested with BsaI and ligated into the linearized pFUSA. Plasmids for RVDs 11-17 were digested with BsaI and ligated into the linearized pFUSB7. Digestion and linearization was performed under the following conditions: 10 cycles: 37°C ^{for} 5 min, 16°C for 10 min; 1 cycle: 50°C for 5 min, 80°C for 5 min. Reactions were then incubated at 37°C for 1 hour with a plasmid safe DNase before transformation. Correct colonies were identified by colony PCR with pCR8_F1: ttgatgcctggcagttccct and pCR8_R1: cgaaccgaacaggcttatgt, and subsequently confirmed by presence of appropriate band in Esp3I restriction digest. To assemble to final full length TAL construct each ½ TAL was combined with the appropriate pLR vector and was digested with Esp3I and ligated into the destination vector (pCS2-DD for TAL1, and pCS2-RR for TAL2). Digestion and linearization was performed under the following conditions: 10 cycles: 37°C for 5 min, 16°C for 10 min; 1 cycle: 37°C for 15 min, 80°C for 5 min. The reaction was then transformed and correct colonies were identified by colony PCR with TAL_F1: TTGGCGTCGGCAAACAGTGG and TAL_R2: GGCGACGAGGTGGTCGTTGG and subsequently confirmed by presence of appropriate band in SphI/BamHI double digest. TAL constructs were linearized with SalI, and mRNA was synthesized using SP6

mMessage mMachine kit (Ambion; Section 2.4.13). mRNA injections were performed at the one cell stage with 200-400 pg of each TAL mRNA (Section 2.3.2).

2.9.3 Clustered Regularly Interspaced Short Palindromic Repeats (CRISPR) guide RNA Construction

Gene specific oligos were designed using the CHOPCHOP (http://chopchop.cbu.uib.no/) or CrisprScan (http://www.crisprscan.org/) online tools, to target either the beginning of the gene, or to target specific protein domains. Each target site is 20 nucleotides long, plus a PAM sequence. The 20-nucleotide long target site was inserted into the SP6 oligo, and in combination with a constant oligo, the sgRNA can be synthesized (Varshney et al., 2015). Crispr target sites and oligo sequences can be found in Table 2.10.

Oligos were annealed in a reaction consisting of 7 µL of 100 µM SP6 gene specific oligo, 7 µL of 100 µM constant oligo, and 2 µL of 10x NEB Buffer 3 and 4 µL of MilliQ. The reaction was placed in 800 mL of boiled water, and left to cool to room temperature. Annealed oligos were filled in with T4 DNA polymerase by combining 2.5 µL of 10 mM dNTPs with 4 µL of 5x Buffer, 0.2 µL of 100x BSA, 0.5 µL of T4 DNA polymerase, 2.8 µL of MilliQ, 10 µL of annealed oligos. The reaction was incubated at 12°C for 1 hour and purified using the GeneJet PCR Purification kit (Fermentas). A 1:1 volume of binding buffer was added to the filled in oligos and mixed, then a 1:2 volume of 100% isopropanol was added and mixed. The solution was transferred to a column and centrifuged for 1 min at maximum speed. The flow-through was discarded and 700 µL of wash buffer was added. The column was centrifuged for 1 min at maximum speed and the flow-through was discarded. The column was centrifuged again for 1 min at maximum speed, and transferred to a new collection tube. 30 µL nuclease-free water was added to the column and centrifuged for 1 min at maximum speed.

SgRNA is transcribed using the SP6 MEGAScript Kit (Ambion). Each reaction consisted of 0.5 µL of ATP, 0.5 µL of GTP, 0.5 µL of CTP, 0.5 µL of UTP, 0.5 µL of 10x Buffer, 0.5 µL of SP6 enzyme mix, 1 µL of nuclease-free water and 1 µL of sgRNA template. The reaction was incubated for 4 hours at 37°C., then 14 µL of DEPC-treated water and 1 µL of DNase were added and incubated for 15 min at 37°C to remove DNA.

To cleanup the sgRNA transcription reaction, 10 µL of 5 M ammonium acetate and 60 µL of 100% RNase-free EtOH were added, and the solution was incubated at -80°C until frozen. The solution was then centrifuged at 4°C for 15 min at maximum speed, the supernatant was removed, and 1 mL 70% RNase-free EtOH was added. The solution was then centrifuged at 4°C for 5 min at maximum speed, the supernatant was removed and the pellet was dried at RT before being and resuspended in 20-50 µL of RNase-free water.

SgRNA was injected either with Cas9 mRNA, or Cas9 protein (PNA Bio) To generate Cas9 mRNA, the plasmid was linearized with NotI and purified using the GeneJet PCR Purification kit (Fermentas) (as described above). Capped Cas9 mRNA is transcribed using SP6 mMessage mMachine Kit (Ambion), (Section 2.4.13). Cas9 mRNA is injected at a dose of 600 ng, and sgRNA are injected at the highest concentration possible (Section 2.3.2).

2.9.4 High Resolution Melt (HRM) Curve Analysis

High resolution melt (HRM) curve analysis primers were designed using the following parameters, with the ideal conditions in parentheses: GC content 50-65% (55%), Melting temperature 55-67°C (62°C), primer length 20-27 nucleotides (22 nucleotides) and amplicon length 70-200 base pairs (90 base pairs). HRM primer sequences can be found in Table 2.11. Primers had melting temperatures within 1°C of each other, and amplicons were designed surrounding target site and within an exon. HRM primers were tested on genomic DNA diluted 1/10, and run in triplicate. HRM reactions were performed using either the Type-it HRM PCR Kit (Qiagen) or the MeltDoctor HRM Master Mix (Applied Biosystems).

For reactions performed with the Type-it HRM PCR kit, each reaction consisted of 5 µL of Master mix, 1.4 µL of 5 µM Forward Primer, 1.4 µL of 5 µM Reverse Primer, 0.2 µL of Nuclease-free water and 2 µL template. Each reaction was run using the Rotor Gene Q qPCR machine (Qiagen) with the following PCR cycle conditions, 95°C for 5 min (initial activation), then 45 cycles of 95°C for 10 s, and 55°C for 30 s, followed by the temperature increasing from 65°C to 95°C in 0.1°C steps, with a 1 second wait

between steps. Melting profiles were analyzed using the Rotor Gene Software 2.0 (Qiagen).

For reactions performed with the MeltDoctor HRM Master Mix, each reaction consisted of 2 μL of diluted DNA, 5 μL of MeltDoctor HRM Master Mix (Applied Biosystems), 0.6 μL each of 5 μM forward and reverse primer, and 1.8 μL of water. Each reaction was run using the 7500 Fast Real-Time PCR System (Applied Biosystems), with the following PCR cycle conditions: 95°C for 10 min (initial denaturation), then 40 cycles of 95°C for 15 s and 60°C for 20 s followed by disassociation curve at 95°C for 15 s, 60°C for 1 min, 95°C for 15 s and 60°C for 15 s. Melting profiles were analyzed using HRM v.2.0 software (Life Technologies)

2.9.5 P0 and F1 Identification

Injected embryos were grown to 24 hpf, then 20 injected and 20 uninjected embryos were dechorionated (Section 2.2.1) and pooled genomic DNA was extracted (Section 2.4.1)

The region surrounding the target site was amplified by PCR, gel extracted and TOPO cloned (Sections 2.4.4, 2.4.5 and 2.4.6). HRM was performed on individual colonies, to identify potential variants (Section 2.9.4), which were then miniprepped (Section 2.4.9) and sequenced (Section 2.4.11). If injected embryos show reasonable levels of insertion/deletion generation the remaining injected embryos were grown up to adulthood.

To identify founders with germline mutations, injected adults were crossed and embryos collected. HRM was performed in triplicate on either pools of genomic DNA (5 pools of 10 embryos), or genomic DNA from individual embryos (24 embryos) (Sections 2.4.1 and 2.9.4). Samples identified as variant were then amplified by PCR, gel extracted, TOPO cloned and sequenced (Sections 2.4.4, 2.4.5, 2.4.6 and 2.4.11). F1 generations for P0's carrying desirable mutations are grown to adulthood and fin clipped (Section 2.2.2). Genomic DNA is extracted and HRM is performed on each sample in triplicate (Section 2.4.1 and 2.9.4). Variants are PCR amplified gel extracted, TOPO cloned and sequenced (Sections 2.4.4, 2.4.5, 2.4.6 and 2.4.11) to identify mutations.

2.10 Tables

Table 2.1. Genotyping primers

Gene	Forward Primer (5'-3')	Reverse Primer (5'-3')	Tm (°C)	RE	WT size (bp)	Mutant size (bp)
hoxb1a	GCCGCAAAACACTATTCGGACAA	TCTGTTTCATTCGGCGGTTTTGATA	58	EcoRV	173	149
hoxb1b	CGATTTATAACCGTGGTTCTAACAC	CCCTCGGGAATGTAACTATTTGT	58	N/A	112	125
taz	CCATCGGCCATTTTAATCGAAG	AAAGAGCCTCCAGATCCGTGTC	63	N/A	119	90
pbx4	GTGGCTCGTTCGGCTCCGCGTTTGTATC	CTCTCGTCGGTGATGGCCATGATCTTCT	55	XbaI	289	259

Table 2.2. Morpholino antisense oligonucleotides

Gene	Morpholino Sequence (5'-3')	Dose
pbx2	CCGTTGCCTGTGATGGGCTGCTGCG	1 ng
pbx2	GCTGCAACATCCTGAGCACTACATT	2 ng
pbx4	AATACTTTTGAGCCGAATCTCTCCG	3 ng
pbx4	CGCCGCAAACCAATGAAAGCGTGTT	3 ng

Table 2.3. Plasmid Based Probes

Gene	Vector	Antibiotic	Transcribe	Linearize
alas2	pCR4-TOPO	Carbenicillin	T3	NotI
aldh1a2	pSport	Carbenicillin	SP6	EcoRI
ascl1a	pCR4-TOPO	Carbenicillin	T7	PmeI
ascl1b	pCR4-TOPO	Carbenicillin	T7	PmeI
atoh1a	pCR4-TOPO	Carbenicillin	T7	PmeI
atoh1b	pCR4-TOPO	Carbenicillin	T3	NotI
atoh1c	pCR4-TOPO	Carbenicillin	T7	PmeI
ctgfa	pCR4-TOPO	Carbenicillin	T3	NotI
ctgfb	pCR4-TOPO	Carbenicillin	T3	NotI
cyp26b1	pCR4-TOPO	Carbenicillin	T7	PmeI
cyp26c1	pCR4-TOPO	Carbenicillin	T3	NotI
deltaA	pCR4-TOPO	Carbenicillin	T3	NotI
dlx2			T7	XbaI
dusp6	pCR4-TOPO	Carbenicillin	T7	PmeI
efnb2a	pCR4-TOPO	Carbenicillin	T3	NotI
epha4a		Carbenicillin	T3	EcoRI
etv5b	pCR4-TOPO	Carbenicillin	T7	PmeI
fech	pCR4-TOPO	Carbenicillin	T7	PmeI
fgf3		Carbenicillin	T7	BamHI
fgf8	pCR4-TOPO	Carbenicillin	T3	NotI
her11	pCR4-TOPO	Carbenicillin	T7	PmeI
her3	pCR4-TOPO	Carbenicillin	T7	PmeI
her5	pCR4-TOPO	Carbenicillin	T3	NotI
her6	pCR4-TOPO	Carbenicillin	T3	NotI
her9	pCR4-TOPO	Carbenicillin	T7	PmeI
hoxa2b		Carbenicillin	T3	Asp718
hoxa3a	pCR2.1-TOPO	Carbenicillin	T7	BamHI
hoxb1a 3'UTR	pCR4-TOPO	Carbenicillin	T7	PmeI
hoxb1b	pCR4-TOPO	Carbenicillin	T3	NotI
hoxb2a		Carbenicillin	T7	XbaI
hoxb3a		Carbenicillin	T7	PstI
hoxd3a	pCR4-TOPO	Carbenicillin	T7	PmeI
hoxd4a		Carbenicillin	T7	EcoRI
islet1	pCR4-TOPO	Carbenicillin	T3	NotI
krox20			T3	PstI
lfng	pCR4-TOPO	Carbenicillin	T3	NotI
mariposa		Carbenicillin	T7	BamHI
neuroD1	pCR4-TOPO	Carbenicillin	T3	NotI
neuroD4	pCR4-TOPO	Carbenicillin	T7	PmeI
neuroD6a	pCR4-TOPO	Carbenicillin	T7	PmeI

neuroD6b	pCR4-TOPO	Carbenicillin	T3	NotI
neurogenin1	pCR4-TOPO	Carbenicillin	T7	PmeI
nr1d1	pCR4-TOPO	Carbenicillin	T7	PmeI
nr1d2a	pCR4-TOPO	Carbenicillin	T7	PmeI
nr2f2	pCR4-TOPO	Carbenicillin	T7	PmeI
nr6a1b	pCR4-TOPO	Carbenicillin	T7	PmeI
pea3	pCR4-TOPO	Carbenicillin	T7	PmeI
ppox	pCR4-TOPO	Carbenicillin	T3	NotI
sox19a	pCR4-TOPO	Carbenicillin	T3	NotI
sox19b	pCR4-TOPO	Carbenicillin	T3	NotI
sox1a	pCR4-TOPO	Carbenicillin	T3	NotI
sox1b	pCR4-TOPO	Carbenicillin	T3	NotI
sox2	pCR4-TOPO	Carbenicillin	T3	NotI
sox3	pCR4-TOPO	Carbenicillin	T3	NotI
spry2	pCR4-TOPO	Carbenicillin	T3	NotI
spry4	pCR4-TOPO	Carbenicillin	T3	NotI
tif1y	pCR4-TOPO	Carbenicillin	T3	NotI
val			SP6	XhoI
wwtr1/taz	pCR4-TOPO	Carbenicillin	T7	PstI
yap1	pCR4-TOPO	Carbenicillin	T3	NotI

Table 2.4. PCR based probes

Gene	Forward Primer (5'-3')	Reverse Primer (5'-3')	Promoter	Size (bp)	Tm (°C)
arpc5b	GTCAAGGATCGAGCTGAAGG	TAATACGACTCACTATAGGGTTCAACATGATTGGCTTCCA	T7	1068	60
ccnd1	GTTGCAGCTTTTAGGAGCAACT	TAATACGACTCACTATAGGGAGATGAATAGCGATCCCTTCAA	T7	601	60.1
ccne1	ATGCCAAGCAAGAAAGTGCT	TAATACGACTCACTATAGGGATCGCTCTCATTTTGGGTTG	T7	446	60/ 60.1
ccne2	CCAGACCAGAGCTGAAGGAC	TAATACGACTCACTATAGGGATATGCCTTTGGCATTGAGG	T7	881	60/ 59.9
crb1	TGATGTTGCCTCAGGTTGTATC	TAATACGACTCACTATAGGGCTGAATGGAAACAGGTTGAACA	T7	776	60
crb2a	GGGATCTCTACTTGACCCAGTG	TAATACGACTCACTATAGGGCAGACACGATCCACCATTTAGA	T7	1000	60
crb2b	TGCTTGAGTTAATTGCTGGAGA	TAATACGACTCACTATAGGGAAGTCAGAGGCTCTTCTGATGG	T7	706	60
cyr61	ACACCACACACGATTGTTTAGC	TAATACGACTCACTATAGGGAACTGGAACACACACACACACA	T7	663	60
diap1	GCTTCTCACTGAAAACATGGTG	TAATACGACTCACTATAGGGCCCATCTGATCGAGACTCTTCT	T7	537	59.8
dlg1	TGGAACAGAAGCTGATTACGAA	TAATACGACTCACTATAGGGCGGAGCCTGAACTAATACTGCT	T7	1085	59.9
dlg2	GGATTATGAAGTGGATGGGAGA	TAATACGACTCACTATAGGGTCTTTTGAGGGAATCCAGATGT	T7	453	60.2/ 59.9
dlg3	CGACAGGAGATCCATTACACAA	TAATACGACTCACTATAGGGACAGCATCCTCCAATGTCTTTT	T7	949	60
llgl1	TGACGCCTAACGGAATTCTTAT	TAATACGACTCACTATAGGGTGATCTCGTCCTGAAACAGAGA	T7	600	60
llgl2	CTAAGCCTAAAGCAGGCAATGT	TAATACGACTCACTATAGGGCCTTAGTCATCCAACCCTTGTC	T7	442	59.9
lmx1ba	CACCATGAGCTG	TAATACGACTCACTAT	T7	944	60

	CTACTCCA	AGGGGCTTCAGGGTTTGCTTTCAG			
lmx1bb	ATGCCTGGAGAAAATTGCAC	TAATACGACTCACTATAGGGAAGTGTCGCTGTCAATGTCG	T7	728	60.1/59.9
mfng	ATTCGAGCTCATTGAACCAGAT	TAATACGACTCACTATAGGGACTTTTTGTAGGAGGCCATGAA	T7	706	60.1/60
mpp5a	ACACCCAGTCTTTGAAGGTGTT	TAATACGACTCACTATAGGGCCCATTTAGTGTCCTGGAAGAG	T7	788	59.9/60
myo9b	TCTGGCCTAGAAAGGCTCAA	TAATACGACTCACTATAGGGGACACTAGGCGGCATTTCTC	T7	712	60.1/59.8
pard3	CCACGGATTATAAGAGGACGAG	TAATACGACTCACTATAGGGTCCGTTCTGCTTCTGTGTGTAT	T7	639	60/59.8
pard6a	TCTTTGGGTTGCTCCTATGTCT	TAATACGACTCACTATAGGGGTGATTATTTTCACTGGCACGA	T7	972	60.1/60
pard6b	GCAGAATTCAGACCGGTTCTCTT	TAATACGACTCACTATAGGGTAGCGATCATCATGTCCGTTAC	T7	649	59.9/60
ppp1r12a	CAGGGAAGCTGTCTCCTAAAGA	TAATACGACTCACTATAGGGGCTGATAGCTGGAGGTTCTGTT	T7	411	60/59.9
prkci	CACTTTCTGCCATTTGTAACCA	TAATACGACTCACTATAGGGCGGTGACTGTATCGAAAAACAA	T7	820	60
rfng	ACTATGTGATCCTGCCCAGTCT	TAATACGACTCACTATAGGGAGCCACCCTGTTTCTTCATTTA	T7	980	60
scrib	CATACAGCTGTTGAAGCTTTGC	TAATACGACTCACTATAGGGACAAGCATACGGATCTCCTGTT	T7	881	60.1/60
wnt1	GCCATTACAAGTGCTGGTGTTA	TAATACGACTCACTATAGGGCTGAAGCATGCGTTTCAGATAG	T7	875	60.1/60
zic4	CGTACAACTGCAAAGTCAGAGG	TAATACGACTCACTATAGGGAGCACAAAACGAGGAAAGAGTC	T7	890	60/59.9

Table 2.5. mRNA expression plasmids

Construct	Vector	Linearize	Transcribe
drTCF3	pCS2+MT	NotI	SP6
eGFP	pT7TS	BamHI	T7
Hoxb1a	pCS2	NotI	SP6
Hoxb1a^{sa1191}	pCS2	NotI	SP6
Hoxb1b	pCS2	NotI	SP6
Hoxb1b *sharkey*FokI TALEN-DD	pCS2TAL3-*sharkey*FokI-DD	NotI	SP6
Hoxb1b *sharkey*FokI TALEN-RR	pCS2TAL3-*sharkey*FokI-RR	NotI	SP6
Hoxb1b TALEN-DD	pCS2TAL3-DD	NotI	SP6
Hoxb1b TALEN-RR	pCS2TAL3-RR	NotI	SP6
Hoxb1b^{ua1006}	pCS2	NotI	SP6
Taz	pCS2	NotI	SP6
Taz *sharkey*FokI TALEN-DD	pCS2TAL3-*sharkey*FokI-DD	NotI	SP6
Taz *sharkey*FokI TALEN-RR	pCS2TAL3-*sharkey*FokI-RR	NotI	SP6
Taz TALEN-DD	pCS2TAL3-DD	NotI	SP6
Taz TALEN-RR	pCS2TAL3-RR	NotI	SP6
Taz ΔCC	pCS2	NotI	SP6
Taz ΔPDZ	pCS2	NotI	SP6
Taz ΔTA	pCS2	NotI	SP6
Taz ΔWW	pCS2	NotI	SP6

Table 2.6. Site-directed mutagenesis primers

Gene	Mutation	Forward Primer (5'-3')	Reverse Primer (5'-3')
SharkeyFokI-DD	S418P	ATTGAATTAATTGAAATTGCCAGAAATCCCACTCAGGATAGAATTCTTG	CAAGAATTCTATCCTGAGTGGGATTTCTGGCAATTTCAATTAATTCAAT
SharkeyFokI-RR	K441E	GAAAGTTTATGGATATAGAGGTGAACATTTGGGTGGATCAAGGAA	TTCCTTGATCCACCCAAATGTTCACCTCTATATCCATAAACTTTC

Altered nucleotide sequences are underlined

Table 2.7. qPCR primers

Gene	Forward Primer (5'-3')	Reverse Primer (5'-3')
amot	GATGGTGGATATGCTGTCTGAA	CCCTCTTTGTGGATGATTTAGC
amotl1	GCGTCATTATTATCCTTACCCAAC	AGAGAGAGTGATAAAGGAGGCAGA
amotl2a	GAACGGCAGAGGAATCATCA	CTGCTGGATGGCTAACAGAGTAG
amotl2b	CTCCTTATACCGAATACCCCTTTT	GTCTCTTGTTCTCGTTCATAAGCA
ef1a	CCTTCGTCCCAATTTCAGG	CCTTGAACCAGCCCATGT
frmd6	ACTCTTGTACGATTTTCCTTGGAC	GAGGACAGCCTGTGTAGTAGATCA
nf2a	CTTAAGCAAGAGCTGGAGGTGT	CCCTCTTTGTGGATGATTTAGC
nf2b	GCTGAAATGGAGTTTAGTTGTGAG	CCAGGCATATGTGTCTTTTACTGT

Table 2.8. ZFN target sequences

Gene	ZFN Target Site (5'-3')
crx	AGCCCCATTATGCTGTGAACGGGTTA
gdf11	ACCCAACATCAGCAGAGAGGTGGTTA
hmx4	TAAACTCAACAGAGAGGGGGATGCGA
nlz2	GCACTTCTGCTTCCCCGATGCCGTCA
prp1	GGCAGGCAGCTATCCAGCTGGAGGCA
prp2	CCACCTCCCTACCCTGGTGCTGGAGG
sfrp5	TCACTTCAGCCTCTTCGGCAGAGGAGT

ZFN recognition sites are underlined

Table 2.9. TALEN target sequences

Gene	Target Site (5'-3')
hoxb1b	GGTTCTAACACTTATAGTTCGAAAGTTGGGTGTTTTCCTGTAGAG CAAGAATACTTGCC
wwtr1/taz	TGAGCGGTAATCCTCTCCAGCCGATACCGGGCCACCAGGTGATC CATGTCGCCA

TALEN Recognition sites are underlined

Table 2.10. CRISPR target sequences/oligos

Gene	Target Site (5'-3')	Oligo sequence (5'-3')
Constant oligo	N/A	AAAAGCACCGACTCGGTGCCACTTTTTCAAGT TGATAACGGACTAGCCTTATTTTAACTTGCTA TTTCTAGCTCTAAAAC
meis1b	GGAGCTGGGGCC CGTGATTC**AGG**	ATTTAGGTGACACTATAGGAGCTGGGGCCCG TGATTCGTTTTAGAGCTAGAAATAGCAAG
meis1b	GGTACTGGTGGG AGTGGAGC**TGG**	ATTTAGGTGACACTATAGGTACTGGTGGGAG TGGAGCGTTTTAGAGCTAGAAATAGCAAG
meis1b	GGGCTGTGTGCG GGTACTGG**TGG**	ATTTAGGTGACACTATAGGGCTGTGTGCGGG TACTGGGTTTTAGAGCTAGAAATAGCAAG
meis1b	GGGCGGCATGGC GTTGGTGT**GGG**	ATTTAGGTGACACTATAGGGCGGCATGGCGT TGGTGTGTTTTAGAGCTAGAAATAGCAAG
rfng	AGATCCGCCTGA CGCTGTGG**AGG**	ATTTAGGTGACACTATAAGATCCGCCTGACG CTGTGGGTTTTAGAGCTAGAAATAGCAAG
rfng	AGGCGGATCTGC CTCAGCCG**CGG**	ATTTAGGTGACACTATAAGGCGGATCTGCCTC AGCCGGTTTTAGAGCTAGAAATAGCAAG
rfng	GGCAGATCCGCC TGACGCTG**TGG**	ATTTAGGTGACACTATAGGCAGATCCGCCTG ACGCTGGTTTTAGAGCTAGAAATAGCAAG
rfng	GGTTTTGTTGGA GCCGACAT**GGG**	ATTTAGGTGACACTATAGGTTTTGTTGGAGCC GACATGTTTTAGAGCTAGAAATAGCAAG
rfng	GGGAATAAGCA GCACCAGCA**GG G**	ATTTAGGTGACACTATAGGGAATAAGCAGCA CCAGCAGTTTTAGAGCTAGAAATAGCAAG
rfng	TGCGAGGGAAA GCAGAAAGC**AG G**	ATTTAGGTGACACTATATGCGAGGGAAAGCA GAAAGCGTTTTAGAGCTAGAAATAGCAAG
stk3	GGATGTATGTCT GCATACGG**AGG**	ATTTAGGTGACACTATAGGATGTATGTCTGCA TACGGGTTTTAGAGCTAGAAATAGCAAG
yap1	GACTGGCGGAGG TGCTGAGG**TGG**	ATTTAGGTGACACTATAGACTGGCGGAGGTG CTGAGGGTTTTAGAGCTAGAAATAGCAAG

Pam is bolded, and target site in oligo is underlined.

Table 2.11. HRM primers

Gene	Forward Primer (5'-3')	Reverse Primer (5'-3')	Tm (°C)	Size (bp)
hoxb1b	CGATTTATAACCGTGGTTCTAACAC	CCCTCGGGAATGTAACTATTTGT	58.3/58.2	125
meis1b	TATACCCCACTATGGGATGGAC	CTTTATCTCTTTTTAGAGCGTCATTG	59.8/59,1	200
rfng	GCTCTGCAGCAGTGAGTCAGG	ACTACCACCCCTGGTGTCTTCAT	63.8/63.1	264
stk3	ATGGCGCCTGAAGTAATCC	GACTCCTCTCAGTGTCCTCCAC	60.1/60.3	149
taz	CCATCGGCCATTTTAATCGAAG	AAAGAGCCTCCAGATCCGTGTC	64.6/64.1	119
yap	CAGTTTCTCCTGGTGCACTGA	GGCATGTCATCAGGTATCTCGT	61.4/61.3	94

Chapter 3: Evaluating the mutagenic activity of targeted endonucleases containing a *Sharkey* FokI cleavage domain variant in zebrafish

A version of this chapter was published. Pillay, L.M., Selland, L.G., Fleisch, V.C., Leighton, P.L., Cheng, C.S., Famulski, J.K., Ritzel, R.G., March, L.D., Wang, H., Allison, W.T. and Waskiewicz, A.J., 2013. Evaluating the mutagenic activity of targeted endonucleases containing a Sharkey FokI cleavage domain variant in zebrafish. Zebrafish. 10, 353-64. Lyndsay G. Selland generated the *hoxb1b* and *wwtr1* TALENS, and performed zebrafish mutagenesis using TALENs. The data presented in Table 3.2 was generated by Lyndsay G. Selland. The data presented in Figure 3.5 results from experiments performed by Lyndsay G. Selland in collaboration with Laura M. Pillay.
Final publication is available from Mary Ann Liebert, Inc., publishers http://dx.doi.org/10.1089/zeb.2012.0832

3.1 Introduction

Zinc finger nucleases (ZFNs) selectively target and cleave specific gene sequences, making them a powerful tool for genome manipulation. These synthetic restriction endonucleases are composed of chimeric fusions tandemly linking three or more Cys_2His_2 zinc fingers to the non-specific FokI endonuclease domain (Cathomen and Joung, 2008; Durai et al., 2005; Kim and Berg, 1996; Porteus and Carroll, 2005). Each zinc finger recognizes and binds to a specific DNA sequence. When two independent ZFNs bind DNA in a tail-to-tail orientation, with proper spacing (Figure 3.1 A), their FokI endonuclease domains dimerize and generate double-strand DNA breaks (Bibikova et al., 2001; Gupta et al., 2013; Mani et al., 2005). These breaks are subsequently repaired through homologous recombination (Bibikova et al., 2003; Bibikova et al., 2001; Kandavelou et al., 2005; Porteus and Baltimore, 2003; Urnov et al., 2005) or non-homologous end joining (NHEJ) (Beumer et al., 2006; Bibikova et al., 2002). NHEJ is an error-prone process that generates point mutations, insertions and deletions (Brennan and Schiestl, 1998; Hagmann et al., 1998; Hefferin and Tomkinson, 2005; Kovalchuk et al., 2004; Roth and Wilson, 1986). Repair of ZFN-induced lesions produces frameshift, nonsense or missense mutations, thereby abrogating gene function. ZFNs are especially useful for performing targeted mutagenesis in organisms that are not amenable to the generation of embryonic stem cell lines. To date, ZFNs have been successfully used to mutagenize mammalian cell lines (Lee et al., 2010; Lombardo et al., 2007; Maeder et al., 2008; Miller et al., 2007; Moehle et al., 2007; Perez et al., 2008; Porteus, 2006; Urnov et al., 2005; Zou et al., 2011), plants (Lloyd et al., 2005; Sander et al., 2011b; Shukla et al., 2009; Townsend et al., 2009; Wright et al., 2005; Yuen et al., 2013), *Drosophila melanogaster* (Beumer et al., 2006; Bibikova et al., 2002; Bozas et al., 2009), *Caenorhabditis elegans* (Morton et al., 2006), silkworm (Takasu et al., 2010), sea urchin (Ochiai et al., 2010), *Xenopus laevis* (Bibikova et al., 2001), mice (Carbery et al., 2010), rats (Geurts et al., 2009; Moreno et al., 2011), swine (Whyte and Prather, 2012; Yang et al., 2011) catfish (Dong et al., 2011), and zebrafish (Ben et al., 2011; Doyon et al., 2008; Foley et al., 2009a; Foley et al., 2009b; Meng et al., 2008; Sander et al., 2011c).

Individual zinc fingers use a seven-amino acid motif to recognize and bind a specific DNA triplet sequence, with possible additional contact to the fourth base on the opposite strand (Figure 3.1 B) (Kim and Berg, 1996; Pavletich and Pabo, 1991). This motif can be modified to generate custom zinc finger domains with novel DNA sequence specificities (Beerli and Barbas, 2002). Precise recognition of ZFN target sequences is achieved by arranging zinc fingers with desirable DNA-binding specificities in tandem arrays. The mutagenesis activity of a ZFN is primarily dependent on the DNA-binding affinity and specificity of its zinc finger array (Cornu et al., 2008; Urnov et al., 2005). Consequently, multiple approaches have been used to generate custom zinc finger arrays. The modular assembly approach makes use of individual, pre-selected zinc finger domains that are assembled into arrays (Bae et al., 2003; Beerli and Barbas, 2002; Gonzalez et al., 2010; Kim et al., 2010; Liu et al., 1997; Mandell and Barbas, 2006; Segal et al., 2003). Although rapid and facile, this strategy does not take context-dependent effects between neighboring zinc fingers into consideration (Isalan et al., 1997; Isalan et al., 1998), and exhibits a high rate of failure in mutagenesis applications (Kim et al., 2009; Ramirez et al., 2008; Sander et al., 2011b). Cell-based library screening methods have successfully been used to construct and identify zinc finger arrays with desirable sequence specificities (Cornu et al., 2008; Foley et al., 2009b; Greisman and Pabo, 1997; Hurt et al., 2003; Isalan and Choo, 2001; Maeder et al., 2008; Meng et al., 2008; Pruett-Miller et al., 2008). However, library construction and validation is time- and labor-intensive. Furthermore, the success rate for obtaining mutations using arrays identified through cell-based screening methods is still somewhat low (~50-67%) (Foley et al., 2009b; Maeder et al., 2008; Townsend et al., 2009; Zhang et al., 2010a; Zou et al., 2009).

Transcription activator-like effector nucleases (TALENs) are a second technology used for targeted mutagenesis applications. To date, TALENs have been successfully used to mutagenize mammalian cell lines (Cermak et al., 2011; Ding et al., 2013; Hockemeyer et al., 2011; Mussolino et al., 2011; Sakuma et al., 2013; Sanjana et al., 2012; Stroud et al., 2013; Sun et al., 2012), plants (Cermak et al., 2011; Li et al., 2012; Mahfouz et al., 2011; Zhang et al., 2013), yeast (Li et al., 2011b), *Drosophila melanogaster* (Liu et al., 2012; Sakuma et al., 2013), nematodes (Wood et al., 2011),

silkworm (Ma et al., 2012; Sajwan et al., 2013), *Xenopus laevis* (Ishibashi et al., 2012; Lei et al., 2012; Sakuma et al., 2013), mice (Menoret et al., 2013; Sung et al., 2013; Wefers et al., 2013), rats (Mashimo et al., 2013; Menoret et al., 2013; Tesson et al., 2011), swine (Carlson et al., 2012), medaka (Ansai et al., 2013), and zebrafish (Bedell et al., 2012; Cade et al., 2012; Dahlem et al., 2012; Gupta et al., 2013; Huang et al., 2011; Moore et al., 2012; Sakuma et al., 2013; Sander et al., 2011a). Like ZFNs, TALENs also induce double-strand breaks that are repaired through homologous recombination, or NHEJ to generate insertions and deletions that alter gene function. A TALEN consists of a TAL effector array fused to the FokI endonuclease domain (Christian et al., 2010; Li et al., 2011a). TAL effectors recognize and bind to specific DNA sequences through series of repeated modules (Boch and Bonas, 2010; Bogdanove and Voytas, 2011; Deng et al., 2012; Mak et al., 2012). Each module contains a repeat variable di-residue that preferentially recognizes and binds to a specific nucleotide (C, T, A, or G/A) (Boch and Bonas, 2010; Deng et al., 2012; Mak et al., 2012). Consequently, TALENs can be engineered to recognize nearly any DNA sequence, without the requirement for selection assays. Notably, TALENs have been shown to elicit a greater mutation rate than ZFNs in zebrafish (Chen et al., 2013b). However, the somatic mutation rate obtained by using TALENs is still quite variable (<1% to 100%), and depends upon the selected TALEN scaffold, as well as the targeted locus (Bedell et al., 2012).

We sought to improve the efficiency of ZFN and TALEN synthetic targeted endonucleases for use in zebrafish mutagenesis. Towards this aim, we examined the activity of both ZFNs and TALENs containing a FokI nuclease variant termed *Sharkey* (Guo et al., 2010). We demonstrate that all tested *Sharkey* ZFNs exhibit greater *in vitro* cleavage of target-site DNA than controls. However, only one of four *Sharkey* ZFNs displays significantly greater activity *in vivo* in zebrafish, producing a higher frequency of insertion/deletion mutations than control ZFNs. As with ZFNs, we demonstrate that *Sharkey* TALENs exhibit greater *in vitro* cleavage of target-site DNA than controls. However, all *Sharkey* TALENs examined fail to produce any insertion/deletion mutations in zebrafish, displaying absent or significantly reduced *in vivo* mutagenic activity in comparison to control TALENs. Notably, embryos injected with *Sharkey* ZFNs and TALENs do not exhibit an increase in toxicity-related defects or mortality.

3.2 Results

3.2.1 Rapid *in vitro* verification of ZFN target-sequence cleavage

We used two distinct methods to engineer zinc finger nuclease proteins (ZFNs) that selectively bind target-sequences within seven chosen zebrafish genes: *prion protein 2* (*prp2*/*prnprs3*), *H6 family homeobox 4* (*hmx4*), *cone-rod homeobox* (*crx*), *prion protein 1* (*prp1*/*prnprs1*), *secreted frizzled-related protein 5* (*sfrp5*), *growth differentiation factor 11* (*gdf11*), and *nocA-like zinc finger protein 2* (*nlz2*/*znf503*). For *prp2*, *hmx4*, and *crx,* we used a previously described bacterial one-hybrid system to screen a diverse library of zinc finger domains for their ability to bind the selected target-sequence (Meng et al., 2008). For *prp1*, *sfrp5*, *gdf11*, and *nlz2*, we used a context-dependent modular assembly (CoDA) method that makes use of pre-selected zinc finger arrays(Sander et al., 2011b). All zinc finger arrays were cloned into pCS2-FokI ZFN (DD and RR) expression vectors (Meng et al., 2008). The DD and RR cleavage domain mutations prevent homodimeric cleavage activity, thereby reducing ZFN off-target activity and toxicity (Miller et al., 2007; Pruett-Miller et al., 2008; Szczepek et al., 2007).

Previous studies used restriction, PCR, or sequencing-based genotyping assays to analyze somatic mutations in ZFN-injected zebrafish embryos (Foley et al., 2009a; Meng et al., 2008; Sander et al., 2011b). Such studies demonstrate that mutagenesis success rates are variable, and are highly dependent on target-site sequence and ZFN array construction methodology. Our bacterial one-hybrid screens for *prp2*, *hmx4*, and *crx* yielded a large variety of prospective 5' and 3' ZFN arrays (data not shown). However, the laborious nature of identifying *in vivo* somatic mutations precludes the analysis of multiple potential ZFN arrays. Consequently, before testing individual pairs of ZFNs *in vivo*, we assayed their ability to cleave their respective gene's target sequence *in vitro*. To do this, we used a modified *in vitro* transcription-translation assay. We synthesized 5' and 3' ZFN crude protein lysates by coupled *in vitro* transcription/translation, and incubated them along with plasmid containing the ZFN target-sequence, buffer, and plasmid-linearizing restriction enzyme. Analysis of purified,

digested plasmid DNA by gel electrophoresis demonstrates whether or not ZFN arrays possess appropriate DNA cleavage activity. For *prp2, hmx4*, *crx*, and *prp1*, we selected those ZFNs with the greatest *in vitro* cleavage activity for subsequent analyses (data not shown). Notably, the *sfrp5*, *gdf11*, and *nlz2* CoDA 5' and 3' ZFNs failed to cleave their respective targets (data not shown), and were excluded from further analyses.

3.2.2 Increased efficiency of *Sharkey* FokI nuclease-containing ZFNs *in vitro*

ZFN efficiency is dependent on the affinity and specificity of individual ZFN arrays (Cornu et al., 2008; Urnov et al., 2005), length and identity of the spacer region between ZFN recognition sites (Bibikova et al., 2001; Handel et al., 2009), interaction between FokI nuclease domains (Miller et al., 2007; Szczepek et al., 2007), and catalytic activity of the FokI nuclease domain (Guo et al., 2010). In an attempt to improve the efficiency of our ZFN arrays, we made use of a FokI nuclease variant termed *Sharkey*. This variant was initially developed and identified through a directed-evolution strategy, and demonstrates greater than fifteen-fold more catalytic activity than wild type FokI nuclease (Guo et al., 2010).

We first wanted to determine if incorporating the *Sharkey* FokI nuclease into our ZFN arrays enhanced their function *in vitro*. To do this, we used our *in vitro* DNA cleavage assay to evaluate the abilities of control versus *Sharkey* FokI nuclease-containing ZFNs to cleave target-site-containing plasmid DNA (Figure 3.2). To compare ZFN cleavage activities, we diluted protein lysates (0.5X or 0.1X). As shown for *prp2* ZFN pairs (Figure 3.2 A), samples containing *Sharkey prp2* ZFN protein lysate demonstrate more cleavage of *prp2* ZFN target-site-containing plasmid DNA than samples containing control *prp2* ZFN protein lysate. We observe similar results for *hmx4* (Figure 3.2 B), *prp1* (Figure 3.2 C), and *crx* ZFNs (Figure 3.2 D). Western analysis confirmed that comparable amounts of control and *Sharkey* 5' and 3' ZFN proteins were present in the lysates used for these analyses (Figure 3.3). Our results demonstrate that *Sharkey* ZFNs exhibit increased *in vitro* cutting efficiency over control ZFNs. Combined, these data suggest that *Sharkey* FokI nuclease-containing ZFNs cleave DNA more efficiently than control FokI-nuclease containing ZFNs *in vitro*.

3.2.3 *In vivo* mutagenesis by *Sharkey* FokI nuclease-containing ZFNs

Given that *Sharkey* ZFNs function more efficiently than control ZFNs to cleave target-site DNA *in vitro*, we next wanted to determine if *Sharkey* ZFNs possess more *in vivo* mutagenic activity than control ZFNs. To do this, we injected single-cell zebrafish embryos with mRNAs encoding control or *Sharkey* ZFNs, and determined the sequence of target-site genomic DNA. Sequencing results from control versus *Sharkey* ZFN mRNA-injected embryos are summarized in Table 3.1. For *crx*, embryos injected with *Sharkey* ZFN mRNA exhibit a twenty-six times greater frequency of target-site specific insertion and deletion (indel) mutations than embryos injected with control ZFN mRNA (*Sharkey*, 31.2%, control, 1.2%; Table 3.1). This difference in *crx* indel frequency is statistically significant ($p<0.0001$). For *prp2*, *prp1*, and *hmx4* the difference in indel frequency between embryos injected with *Sharkey* ZFN mRNA and embryos injected with control ZFN mRNA is not statistically significant (Table 3.1; p-values: *prp2*, 0.738; *prp1*, 0.621; *hmx4*, 0.669). Combined, these data suggest that *Sharkey* FokI nuclease-containing ZFNs have the capacity to exhibit greater *in vivo* mutagenic activity than control FokI nuclease-containing ZFNs.

3.2.4 Toxicity of *Sharkey* FokI nuclease-containing ZFNs

One concern with using *Sharkey* ZFNs is that increased activity of the FokI nuclease might result in additional off-target effects, thereby increasing the morbidity, and decreasing the survival of injected embryos. We therefore quantified the proportion of embryos that exhibit non-specific developmental defects (referred to as 'monster'-like), and the mortality rates of embryos injected with mRNAs encoding control or *Sharkey* ZFNs (Figure 3.4). In all cases examined, we failed to observe a significant difference (corrected p-value=1.000 for each) in the mortality rates of embryos injected with control versus *Sharkey* ZFN mRNAs (Figure 3.4). Furthermore, we note that embryos injected with control and *Sharkey* ZFN mRNAs exhibit a comparable proportion of monster-like phenotypes (Figure 3.4; corrected p-values: *prp2,* 0.202; *hmx4,* 1.000*; crx,* 1.000). Combined, these data suggest that, in comparison to control ZFNs, *Sharkey* ZFNs do not significantly alter the morbidity and survival of zebrafish embryos.

3.2.5 Decreased *in vivo* mutagenesis by *Sharkey* FokI nuclease-containing TALENs

Given that some *Sharkey* ZFNs may exhibit increased *in vivo* mutagenesis activity in zebrafish when compared to control ZFNs, we next wanted to determine if applying the *Sharkey* FokI nuclease variant to our *WW domain containing transcription regulator* 1 (*wwtr1/taz*) and *homeo box B1b* (*hoxb1b*) TALENs would also increase their activity. To do this, we injected single-cell zebrafish embryos with mRNAs encoding control or *Sharkey* TALENs, and determined the frequency of indel mutations present in target-site genomic DNA using a combination of high-resolution melt curve analysis and sequencing. Results from control versus *Sharkey* TALEN mRNA-injected embryos are summarized in 3.2. Embryos injected with control TALENs demonstrate a modest target-site specific indel frequency (Table 3.2; *wwtr1*, 17.2%; *hoxb1b*, 5.9%). Conversely, in each case examined, embryos injected with *Sharkey* TALENs fail to exhibit any target-site specific indel mutations (Table 3.2; *wwtr1*, 0.0%; *hoxb1b*, 0.0%). The difference in *wwtr1* indel formation is statistically significant ($p<0.0001$). Notably, we fail to observe a significant difference in the mortality rates or monster-like phenotypes of embryos injected with control versus *Sharkey* TALEN mRNAs (Figure 3.5 A, corrected p-value=1.000 for each).

We next wanted to determine if incorporating the *Sharkey* FokI nuclease into our TALENs somehow reduced or destroyed their capacity to cleave target-site DNA. We therefore used our *in vitro* DNA cleavage assay to evaluate the abilities of control versus *Sharkey* FokI nuclease-containing TALENs to cleave target-site-containing plasmid DNA (Figure 3.5 B). Notably, protein lysate samples containing *Sharkey wwtr1* TALENs demonstrate more cleavage of *wwtr1* TALEN target-site-containing plasmid DNA than samples containing control *wwtr1* TALENs (Figure 3.5 B). Western analysis confirmed that comparable amounts of control and *Sharkey* 5' and 3' TALEN proteins were synthesized and present in the lysates used for these analyses (Figure 3.5 C). Combined, these results suggest that *Sharkey* FokI nuclease-containing TALENs cleave DNA more efficiently than control FokI-nuclease containing TALENs *in vitro*, but possess absent or reduced *in vivo* mutagenic activity in zebrafish.

3.3 Discussion

Zinc finger nucleases (ZFNs) have been used to generate mutations in organisms that are not amenable to homologous recombination-based genetic modifications (Ben et al., 2011; Doyon et al., 2008; Foley et al., 2009a; Geurts et al., 2009; Meng et al., 2008; Moreno et al., 2011; Sander et al., 2011b), and are being evaluated for usage in gene therapies (Alper, 2009; Cannon and June, 2011; Perez et al., 2008). Improving these molecular tools is therefore relevant to both biological and clinical applications. In this study, we have described techniques that may enhance the efficiency and success of constructing ZFNs for use in mutagenesis applications.

The practical application of ZFNs relies on their ability to generate double-strand breaks in specific DNA sequences. Previous research suggests that both target-site affinity/specificity, and cleavage activity are critical determinants of ZFN function (Bibikova et al., 2003; Bibikova et al., 2002; Porteus and Baltimore, 2003; Urnov et al., 2005). Without DNA-binding specificity, engineered ZFNs demonstrate low or off-target cleavage activity (Alwin et al., 2005; Miller et al., 2007; Porteus, 2006; Porteus and Baltimore, 2003; Szczepek et al., 2007). Off-target ZFN activity results in increased cytotoxicity and non-specific morphological defects (Cornu et al., 2008). Context-dependent array selection strategies account for cooperativity among zinc finger domains, and permit recognition of the fourth base pair on the opposite strand of the ZFN target-sequence (Desjarlais and Berg, 1993; Dreier et al., 2000; Elrod-Erickson et al., 1996; Isalan et al., 1998; Kim and Berg, 1996; Pavletich and Pabo, 1991). These features allow for the selection of ZFNs with greater target-site affinity and specificity than those obtained through modular assembly approaches (Kim et al., 2009; Ramirez et al., 2008). Multiple context-dependent array construction methods have been used with varying degrees of success to construct ZFN arrays for use in mutagenesis applications.

We successfully used two distinct context-dependent array selection methodologies for constructing ZFNs with desirable target-site specificities. The first method was initially used to generate the Wolfe and Lawson *kdrl* ZFNs, and uses a two-phase bacterial one-hybrid assay to construct suitable ZFN arrays (Meng et al., 2008). We used this bacterial one-hybrid approach to construct ZFN arrays for *prp2*, *hmx4*, and *crx*. For *prp2* and *crx*, we performed target-site selections and constructed ZFN arrays

essentially as previously described (Meng et al., 2008). For *hmx4*, however, we increased context-dependent selection of individual zinc finger domains by modifying the initial screening phase to account for recognition of the fourth base on the opposite strand. We also altered the *hmx4* libraries to include OPEN-method zinc finger domain motifs that were previously shown to recognize triplets in the *hmx4* target-site (Maeder et al., 2008). Our *prp2*, *hmx4*, and *crx* ZFNs each function effectively *in vivo* in zebrafish, generating insertion/deletion (indel) mutations at a detectable frequency in injected embryos (*prp2*: 4.6%; *hmx4*: 1.2%; *crx*: 1.2%).

The second method that we used to construct ZFN arrays is context-dependent modular assembly (CoDA). The CoDA approach to ZFN array construction combines pre-selected zinc finger pairs into three-finger arrays using standard cloning techniques (Sander et al., 2011b). CoDA takes context-dependent effects between adjacent zinc fingers into consideration, and has been used successfully to mutagenize both plants and zebrafish (Sander et al., 2011b). CoDA target-site identity is quite stringent, owing primarily to the existence of only 18 fixed middle zinc finger units (Sander et al., 2011b). Nonetheless, we identified an ideal CoDA-compatible target-site in the *prp1* gene, and used this method to construct *prp1* ZFNs. Such an approach is rapid, and with commercial minigene technology, is not labor-intensive. Our *prp1* CoDA ZFNs function effectively *in vivo* in zebrafish, generating indel mutations at a detectable frequency (1.1%) in injected embryos. Notably, we have achieved variable success with CoDA ZFN array construction, as only one (*prp1*) out of the four (*nlz2*, *sfrp5, gdf11*) CoDA ZFNs that we tested successfully cleaves target-site DNA *in vitro* (data not shown).

Not all ZFNs constructed through context-dependent selection strategies function effectively to generate somatic mutations. Testing ZFNs *in vivo* can be time-consuming and expensive, especially in instances where mutation frequencies are quite low. We therefore elaborated on published work (Mani et al., 2005) and established a system to rapidly gauge the target-site-specific cleavage activity of ZFNs *in vitro*. We demonstrate that this system can be used to evaluate the target-site-specific cleavage activity of ZFN pairs. In all cases examined, those ZFNs that functioned to cleave target-site DNA in our *in vitro* assay also generated somatic mutations *in vivo* in zebrafish. Our results therefore establish our *in vitro* cleavage assay as a good predictor of ZFN fitness in *in vivo*

mutagenesis applications. Notably, in addition to evaluating ZFN function, we demonstrate that our *in vitro* cleavage assay can also be used to evaluate the target-site-specific cleavage activity of other synthetic restriction endonucleases, such as transcription activator-like effector nucleases (TALENs).

The mutagenesis efficiency of a ZFN is partially dependent on the catalytic activity of its endonuclease domain (Guo et al., 2010). We enhanced the catalytic activity of our ZFNs using the *Sharkey* FokI endonuclease domain variant. We demonstrate that *Sharkey* ZFNs exhibit increased *in vitro* cleavage of target-site DNA over control ZFNs. Our results also suggest that less *Sharkey* ZFN protein is required to elicit site-specific DNA cleavage *in vitro*. More importantly, we demonstrate that, in limited instances, *Sharkey* ZFNs have the capacity to exhibit greater *in vivo* mutagenic activity than control ZFNs, producing up to a twenty-six-fold increase in the indel mutation frequency of injected zebrafish embryos (Table 3.1). This expands upon previous research in cell culture, which has shown that *Sharkey* ZFNs demonstrate three- to six-fold more mutagenic activity in HEK 293 cells when compared to wild type ZFNs (Guo et al., 2010). Notably, ours is the first study to assess the relative mutagenic activity of control and *Sharkey* ZFNs *in vivo* in embryos. We did not systematically evaluate the off-target cleavage activity of *Sharkey* ZFNs in zebrafish. However, in comparison to control ZFNs, we find that *Sharkey* ZFNs do not increase the frequency of morphological defects, or the mortality of injected embryos. Our overall results suggest that incorporating the *Sharkey* FokI endonuclease domain into ZFNs may be a simple method of enhancing their mutagenic activity *in vivo*. Notably, introducing double-strand DNA breaks near a desired recombination site can dramatically increase the frequency of homologous recombination in mammalian cells(Choulika et al., 1995; Smith et al., 1995). ZFNs have previously been used in this capacity (Bibikova et al., 2003; Porteus and Baltimore, 2003). Consequently, the enhanced catalytic activity of *Sharkey* ZFNs may also be extremely beneficial for homologous recombination-mediated genome engineering applications.

TALENs have recently been shown to be up to ten times more mutagenic than ZFNs in zebrafish (Chen et al., 2013b). Furthermore, TALENs can be targeted to nearly any DNA sequence, and their modular nature makes them easy to design and assemble.

For these reasons, TALENs are quickly becoming the technology of choice for targeted mutagenesis in animal models. Notably, TALENs have recently been used to elicit genome modification by homologous recombination, albeit at low frequency (Bedell et al., 2012; Zu et al., 2013).

Given the partial success that we achieved in increasing the mutagenic activity of our ZFNs using the *Sharkey* FokI endonuclease variant, we sought to determine if this variant could also be applied to TALENs to enhance their catalytic activity. We demonstrate that *Sharkey* TALENs exhibit increased *in vitro* cleavage of target-site specific DNA over control TALENs. However, unlike with ZFNs, we demonstrate that *Sharkey* TALENs exhibit significantly reduced *in vivo* mutagenic activity in injected zebrafish embryos when compared to control TALENs (Table 3.2). Our overall results suggest that incorporating the *Sharkey* FokI endonuclease domain into TALENs may severely abrogate their *in vivo* mutagenesis function in zebrafish.

3.4 Figures

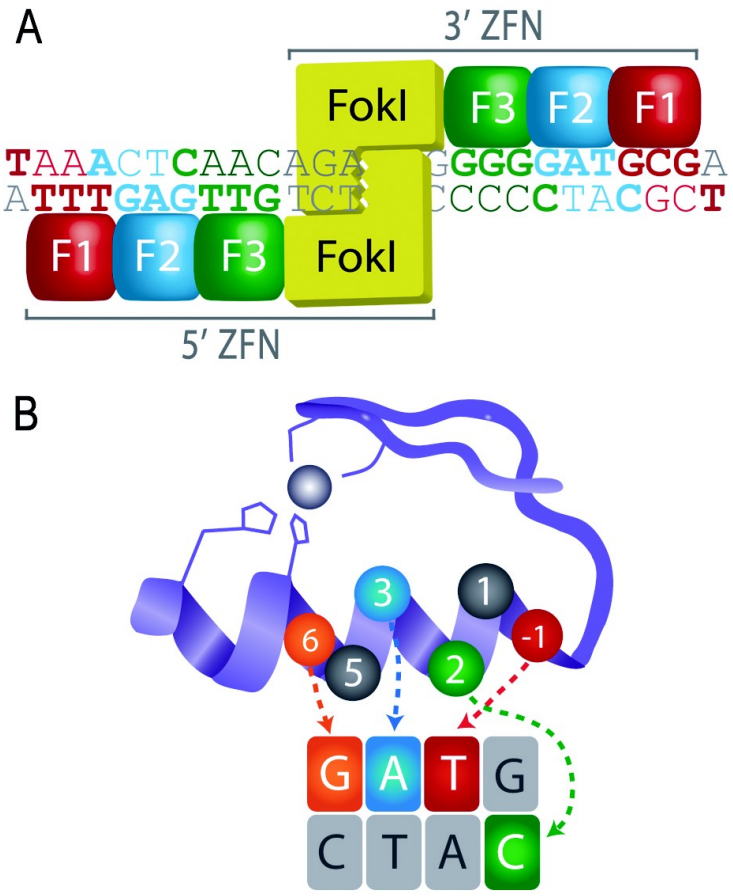

Figure 3.1. Zinc finger nuclease (ZFN) structure and target-site recognition.

(**A**) Schematic diagram of two ZFN arrays bound to *hmx4* ZFN target-site DNA. Each ZFN consists of three zinc finger domains (F1, F2, F3) fused to the non-specific FokI endonuclease domain (FokI). Individual zinc finger recognition of DNA sequence is indicated by matched colors. Upon sequence-specific binding of two ZFNs, dimerized FokI endonuclease domains generate double-strand DNA breaks. (**B**) Schematic diagram of an individual zinc finger motif bound to target-site DNA. DNA-binding affinity and specificity is achieved by a seven amino-acid recognition motif. The amino acid side chains -1, 3, and 6 contact a triplet of DNA on the top strand, while the amino acid side chain at position 2 contacts a fourth base on the bottom strand.

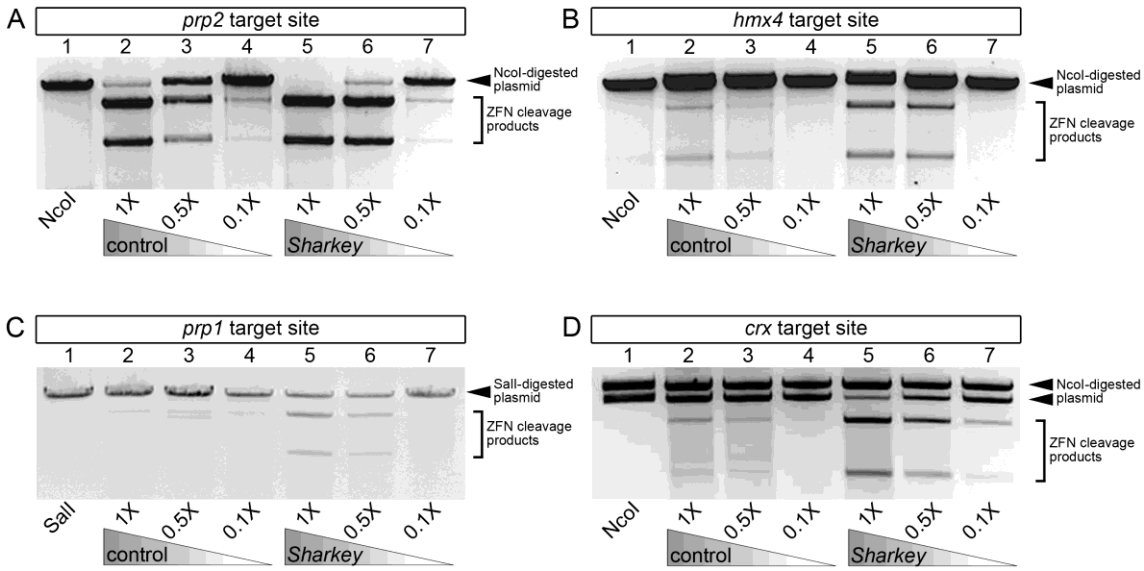

Figure 3.2. *In vitro* comparison of target-site specific DNA cleavage activity between control and *Sharkey* zinc finger nucleases (ZFNs).

ZFN crude protein lysates were used at normal concentration (1X), or were diluted to one-half (0.5X) or one-tenth (0.1X) the amount. Gel-electrophoretic analyses of *prp2* (**A**), *hmx4* (**B**), *prp1* (**C**), and *crx* (**D**) target-site cleavage products. Incubation with NcoI (**A**,**B**,**D**) or SalI (**C**) alone produces a specific cleavage profile (lane 1; arrowheads). Incubation with NcoI (**A**,**B**,**D**) or SalI (**C**) and ZFN crude protein lysates produces two additional cleavage products (brackets), indicating ZFN-mediated cleavage of target-site plasmid. In all cases, *Sharkey* ZFN crude protein lysates (lanes 5-7) exhibit more cleavage of target-site plasmid than control ZFN crude protein lysates (lanes 2-4).

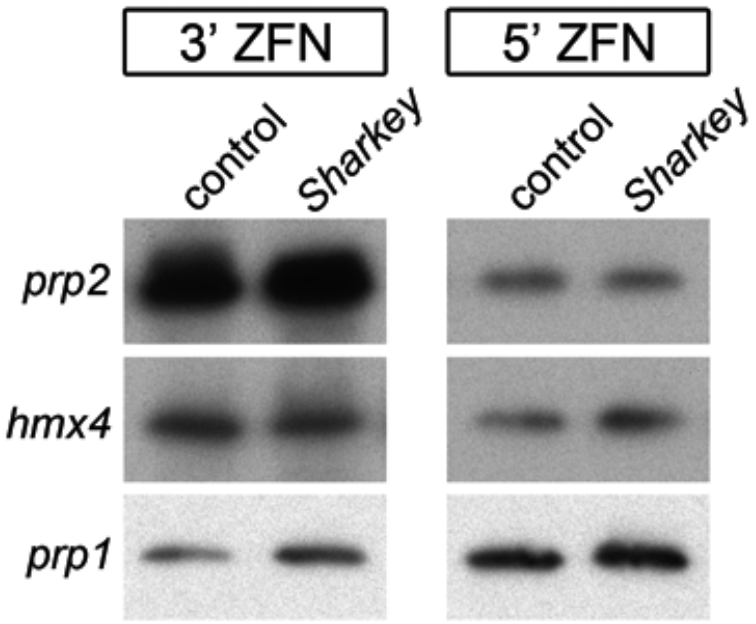

Figure 3.3. Western immunoblot analyses of control and *Sharkey* 5' and 3' ZFN crude protein lysates used in *in vitro* target-site cleavage assay.

3' ZFNs are detected with anti-Flag antibody, while 5' ZFNs are detected with anti-HA antibody.

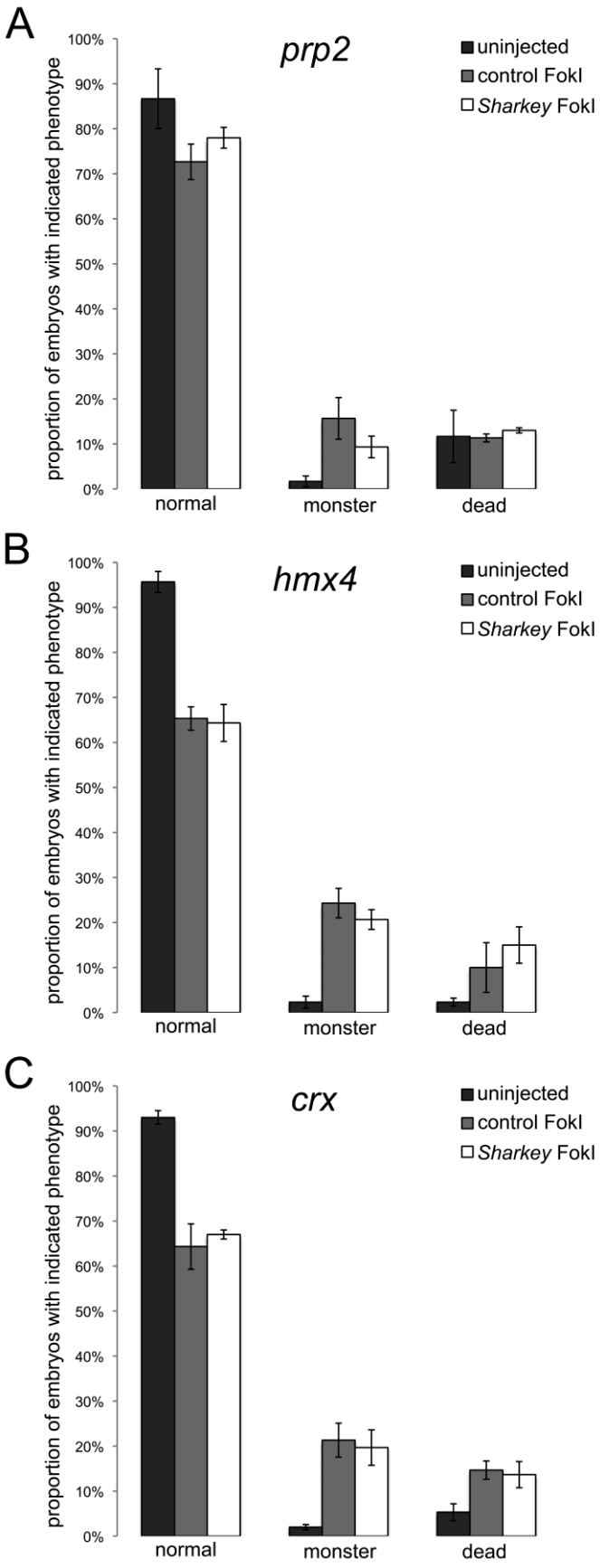
A
prp2
uninjected
control FokI
Sharkey FokI
proportion of embryos with indicated phenotype
100%
90%
80%
70%
60%
50%
40%
30%
20%
10%
0%
normal
monster
dead
B
hmx4
uninjected
control FokI
Sharkey FokI
proportion of embryos with indicated phenotype
normal
monster
dead
C
crx
uninjected
control FokI
Sharkey FokI
proportion of embryos with indicated phenotype
normal
monster
dead

Figure 3.4. Effects of injecting control and *Sharkey* zinc finger nuclease (ZFN) mRNAs on embryonic morphology and mortality.

Graphs demonstrating the mean proportion of embryos with indicated phenotype at ~ 24 hours post fertilization, following injection of mRNAs encoding control FokI or *Sharkey* FokI *prp2* (**A**), *hmx4* (**B**), or *crx* (**C**) ZFNs. Mean proportion of uninjected embryos with indicated phenotype are also given. Error bars represent standard error. In no category are proportions of control FokI and *Sharkey* FokI mRNA-injected embryos statistically different from each other (corrected p-values > 0.05 for each). See text for statistical tests.

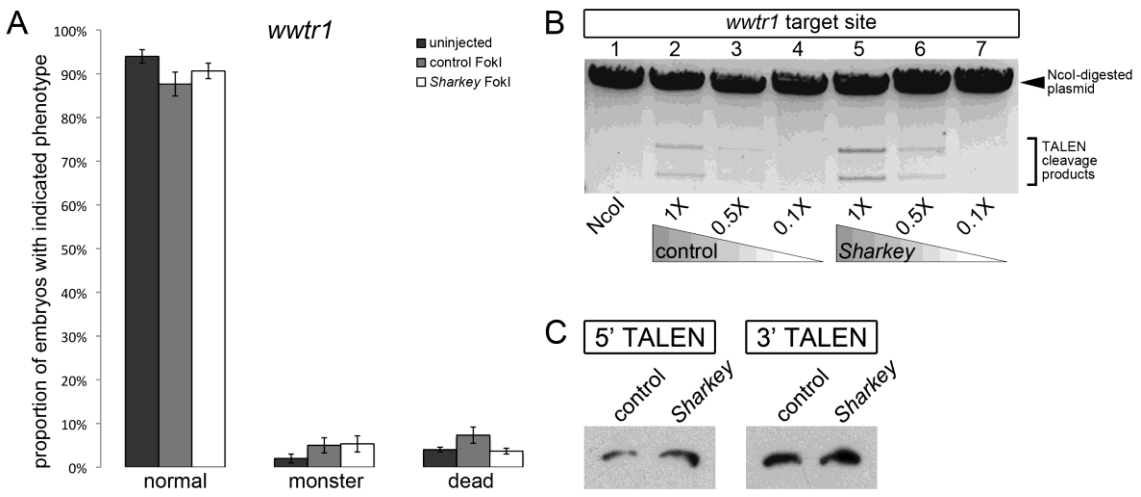

Figure 3.5. Comparison of control and *Sharkey wwtr1* transcription activator-like effector nuclease (TALEN)s.

(**A**) Graph demonstrating the mean proportion of embryos with indicated phenotype at ~ 24 hours post fertilization, following injection of mRNAs encoding control FokI or *Sharkey* FokI *wwtr1* TALENs. Mean proportion of uninjected embryos with indicated phenotype are also given. Error bars represent standard error. In no category are proportions of control FokI and *Sharkey* FokI mRNA-injected embryos statistically different from each other (corrected p-value > 0.05 for each). See text for statistical tests. (**B**) *In vitro* comparison of target-site specific DNA cleavage activity between control and *Sharkey wwtr1* TALENs. TALEN crude protein lysates were used at normal concentration (1X), or were diluted to one-half (0.5X) or one-tenth (0.1X) the amount. Gel-electrophoretic analyses of target-site cleavage products. Incubation with NcoI alone produces a specific cleavage profile (lane 1; arrowhead). Incubation with NcoI and TALEN crude protein lysates produces two additional cleavage products (brackets), indicating TALEN-mediated cleavage of target-site plasmid. *Sharkey* TALEN crude protein lysates (lanes 5-7) exhibit more cleavage of target-site plasmid than control TALEN crude protein lysates (lanes 2-4). (**C**) Western immunoblot analyses of control and *Sharkey* 5' and 3' TALEN crude protein lysates used in *in vitro* target-site cleavage assay. 5' ZFNs are detected with anti-Flag antibody, while 3' ZFNs are detected with anti-HA antibody.

3.5 Tables

Table 3.1. Analyses of target-site specific mutations present in zebrafish embryos injected with control or *Sharkey* zinc finger nuclease (ZFN) mRNAs.

ZFN	***Number of Clones Screened***	***Number of Indel Mutations***	***Indel Frequency (%)***
prp2	130	6	4.6
prp2 (*Sharkey*)	93	3	3.2
hmx4	82	1	1.2
hmx4 (*Sharkey*)	182	5	2.7
prp1	87	1	1.1
prp1 (*Sharkey*)	90	3	3.3
crx	83	1	1.2
crx (*Sharkey*)	157	49	31.2[a]

PCR fragments containing the ZFN target-site were amplified, cloned, and sequenced. Data indicates combined frequency of insertions and deletions (indel frequency). [a]Indicates significant difference in indel mutation frequency between embryos injected with *Sharkey* and control ZFNs, as determined by two-tailed Fisher's exact test ($p<0.0001$).

Table 3.2. Analyses of target-site specific mutations present in zebrafish embryos injected with control or Sharkey transcription activator-like effector nuclease (TALEN) mRNAs.

TALEN	***Number of Clones Screened***	***Number of Indel Mutations***	***Indel Frequency (%)***
wwtr1	81	14	17.2
wwtr1 (*Sharkey*)	82	0	0.0 [a]
hoxb1b	85	5	5.9
hoxb1b (*Sharkey*)	44	0	0

PCR fragments containing the TALEN target-site were amplified, cloned, and analyzed through a combination of high-resolution melt curve analysis followed by sequencing. Data indicates combined frequency of insertions and deletions (indel frequency). [a]Indicates significant difference in indel mutation frequency between embryos injected with Sharkey and control TALENs, as determined by two-tailed Fisher's exact test ($p<0.0001$).

Chapter 4: Coordinate regulation of retinoic acid synthesis by *pbx* genes and fibroblast growth factor signaling by *hoxb1b* is required for hindbrain patterning and development

A version of this chapter has been published. Selland, L.G., Koch, S., Laraque, M. and Waskiewicz, A.J., 2018. Coordinate regulation of retinoic acid synthesis by pbx genes and fibroblast growth factor signaling by hoxb1b is required for hindbrain patterning and development. Mech Dev.
http://dx.doi.org/10.1016/j.mod.2018.02.005

4.1 Introduction

The vertebrate hindbrain is transiently divided into a series of lineage-restricted segments, known as rhombomeres. Segmental gene expression generates distinct populations of neurons (Moens and Prince, 2002) including both reticulospinal interneurons (Kimmel et al., 1982) and cranial branchiomotor neurons (BMN) (Chandrasekhar et al., 1997). Two key signaling pathways – Fibroblast Growth Factor (FGF) and Retinoic Acid (RA) – regulate early gene expression within the vertebrate hindbrain. Global loss of either FGF or RA signaling results in profound changes to reticulospinal and BMN differentiation (Alexandre et al., 1996; Holder and Hill, 1991; Maden and Holder, 1991; Maves et al., 2002; Maves and Kimmel, 2005; Papalopulu et al., 1991; van der Wees et al., 1998). Yet, the regulation of hindbrain FGF and RA signaling remains incompletely understood.

Hox (*homeobox transcription factor*) genes are evolutionarily conserved transcription factors that regulate anterior-posterior (A-P) patterning of hindbrain rhombomeres (McGinnis and Krumlauf, 1992). Hox factor binding and subsequent transcription of target genes is dependent on interactions with cofactors such as Meis (Myeloid ecotropic integration site) and Pbx (Pre-B cell leukemia homeobox) (Mann, 1995). Paralog Group 1 (PG1) *hox* genes are expressed early in hindbrain specification and development, with *hoxb1b* expression beginning at 50% epiboly (5.25hpf) in the presumptive hindbrain and *hoxb1a* expression beginning at tailbud, restricted to rhombomere 4 (r4), the first compartment of the hindbrain to form a distinct segment (Alexandre et al., 1996). Due to their early expression in the hindbrain, and their role as transcriptional regulators, PG1 Hox proteins are hypothesized to play an important role in establishing pattering and segmentation in the hindbrain. Loss of Hox cofactors Pbx2/4 in zebrafish abrogates expression of *hoxa2b*, *hoxb2a*, *hoxb1a*, *hoxb3a*, and *hoxa3* (defining a loss of segmental identity that spans r2-r6). Taken together with an expansion of r1 markers (*epha4a* and *fgfr1*), this implies that Pbx is necessary to define the identity of r2-r6 (Waskiewicz et al., 2002). The expression of *hoxb1b*, however, is normal in Pbx depleted embryos, and Pbx is known to act as a cofactor for all anterior Hox proteins tested (Cooper et al., 2003; Pöpperl et al., 2000; Waskiewicz et al., 2002). As such, researchers proposed a model in which Pbx-Hox-1 complexes lie at the top of a

hierarchy to regulate and initiate hindbrain patterning and segmental gene expression. Consistent with this model, knockdown of *hoxa1/b1/d1* in *Xenopus laevis* causes a loss of segmental identity similar to that observed in Pbx-depleted zebrafish embryos (McNulty et al., 2005). However, murine *Hoxa1*;*Hoxb1* compound mutants have milder defects in hindbrain development, exhibiting a loss of r4 accompanied by alterations to the surrounding r3-6 regions (Gavalas et al., 1998; Rossel and Capecchi, 1999; Studer et al., 1998). Similar phenotypes are observed in zebrafish mutants for *hoxb1b* and *hoxb1a*. *Hoxb1a* regulates r4 specific gene expression and associated neurons (Weicksel et al., 2014) whereas *Hoxb1b* is required for segmentation and rhombomere size, with additional phenotypes observed in neural crest, ear, and r4 associated neurons (Weicksel et al., 2014; Zigman et al., 2014). Compound loss of both *hoxb1a* and *hoxb1b* results in hindbrain segmentation defects similar to those observed in *hoxb1b* mutants (Weicksel et al., 2014; Zigman et al., 2014).

While the studies of Pbx-depleted embryos (Waskiewicz et al., 2002) and Hox-1 *Xenopus* morphants (McNulty et al., 2005) both show a loss of segmental identity, the loss of PG1 *Hox* genes in zebrafish and murine model have a much more subtle phenotype (Weicksel et al., 2014; Zigman et al., 2014). This paradox likely reflects a more complex role for Pbx in regulating hindbrain patterning than originally proposed, and this argues that other Pbx-dependent factors are required for hindbrain patterning. Therefore, we hypothesize that hindbrain segmentation requires not only Hox-Pbx complexes, but also Pbx complexes with other cofactors than Hox, and the loss of both may be sufficient to prevent hindbrain segmentation.

The effectors of Pbx and Hox PG1 genes remain incompletely characterized. Given their broad effects on segmental patterning, it is logical to assume they have roles in regulating core signaling pathways, such as RA and FGF. RA synthesis is catalyzed by the rate-limiting Aldh1a2 (Aldehyde dehydrogenase 1 family, member A2; and also known as Retinaldehyde dehydrogenase or Raldh2) enzyme, which provides a source of RA posterior to the hindbrain (Niederreither et al., 1999; Niederreither et al., 2000). Cyp26 (Cytochrome P450 family 26) enzymes act to inhibit RA signaling by hydroxylating RA (Abu-Abed et al., 2001; Niederreither et al., 2002) in the forebrain, midbrain, and anterior hindbrain (de Roos et al., 1999; Hernandez et al., 2004; Sakai et

al., 2001; Sirbu et al., 2005; Swindell and Eichele, 1999). This creates a gradient of RA across the A-P axis of the hindbrain where higher concentrations of RA activate progressively more posterior genes (Gavalas, 2002). Reduced RA levels result in the loss of posterior hindbrain identity (Begemann et al., 2001; Dupe and Lumsden, 2001; Maden et al., 1996) while increased levels of RA disrupt the development of the anterior hindbrain (Gould et al., 1998; Hill et al., 1995; Morrison et al., 1997), with such alterations commonly ascribed to changes in *hox* gene expression (Ferretti et al., 2000; Frasch et al., 1995; Gould et al., 1998; Morrison et al., 1997; Papalopulu et al., 1991; Yan et al., 1998). Additionally, there is evidence that *hox* and *pbx* genes act upstream of retinoic acid signaling. In mouse, loss of *Hoxa1/Pbx1* or *Pbx1/2* causes a reduction in *Aldh1a2* expression (Vitobello et al., 2011), and *pbx2/4* depleted zebrafish embryos also exhibit reduced *aldh1a2* expression in the trunk and retina (French et al., 2007; Maves et al., 2007).

FGF signaling is frequently associated with the development of the midbrain, cerebellum, and the midbrain-hindbrain boundary (Meyers et al., 1998; Reifers et al., 1998; Sleptsova-Friedrich et al., 2001), however it is also required for inter-rhombomere signaling within the hindbrain. The FGF ligands, *fgf3* and *fgf8 (fgf8a),* are expressed in the r4 signaling center and loss of these genes, or pharmacological inhibition thereof, disrupts the development of the surrounding rhombomeres, in particular r5/6 (Marin and Charnay, 2000; Maves et al., 2002; Walshe et al., 2002; Wiellette and Sive, 2004). *Hox* genes have been linked to regulation of the expression of FGFs in the hindbrain. The loss of *pbx2/4* results in a failure of *fgf3* and *fgf8* to be expressed in r4, and *hoxb1b* has been shown to indirectly regulate *fgf3* through the protein phosphatase *ppp1r14al* (Choe et al., 2011).

In this manuscript, we investigate the phenotypes of *hoxb1a*, *hoxb1b*, and *hoxb1a;hoxb1b* mutants to determine the respective and combinatorial roles of PG1 *hox* genes in regulating hindbrain RA and FGF signaling. Our work illustrates that *hoxb1b* is required for appropriate FGF signaling in the hindbrain, while PG1 *hox* genes do not appear to overtly regulate RA signaling. We uncover a novel role for *Hoxb1a/b* in regulating *vhnf1*. The loss of both *hoxb1b* and *pbx4* is required to revert the hindbrain to the r1 ground state, and this phenotype is plausibly explained by changes to RA

signaling in combination with the *hoxb1b* driven changes to FGF signaling. Taken together, our results do not support a simple linear pathway in which PG1 Hox proteins function alone at the top of a hierarchy of hindbrain pattern formation. Instead, PG1 *hox* genes function in concert with *pbx* and other transcription factors to regulate FGF and RA signaling to establish hindbrain identity.

4.2 Results

4.2.1 *Hoxb1a* is required for r4 specification and *hoxb1b* regulates hindbrain segmentation and rhombomere size

To determine the role of zebrafish PG1 *hox* genes in regulating hindbrain signaling pathways, we created a *hoxb1b*^{ua1006} mutant through TALEN (TAL effector nuclease) mediated mutagenesis (Cermak et al., 2011). An allele containing a 13 bp insertion 63 bp downstream of the start codon was identified (Fig 4.1 A). This mutation is predicted to generate a 43 amino acid long protein where the first 21 amino acids correspond to the correct wildtype Hoxb1b protein (G22FfsX23). This truncated protein completely lacks the DNA-binding homeodomain and is predicted to be a hypomorph or a null and lack transcriptional activity. We obtained from the Sanger institute (Kettleborough et al., 2013), a *hoxb1a*^{sa1191} mutant containing a G to A transition resulting in a stop codon at amino acid 269 (W269X) (Fig 4.1 B). This allele is predicted to cause a truncation within the homeodomain and lack amino acids critical for homeodomain DNA binding activity (McClintock et al., 2001; Scott et al., 1989), likely resulting in a hypomorph. To determine if the *hoxb1b*^{ua1006} and the *hoxb1a*^{sa1191} mutations retain biological activity, we assayed for the ability of the mutant *hoxb1b or hoxb1a* mRNA to cause homeotic transformations (Fig 4.1 C-H). Overexpression of wildtype *hoxb1b* causes an anterior duplication of r4, resulting in ectopic expression of *hoxb1a* transcript in presumptive r2 (McClintock et al., 2001) (Fig 4.1 D; 66/88 embryos affected). In contrast, overexpression of the mutant *hoxb1b*^{ua1006} mRNA failed to produce an anterior duplication of r4 (Fig 4.1 E; 0/82 embryos affected) providing evidence that the mutant Hoxb1b protein has strongly reduced biological activity. Similarly, overexpression of wildtype *hoxb1a* causes ectopic expression of *hoxb1a*

transcript in presumptive r2 (McClintock et al., 2001) (Fig 4.1 G; 30/34 embryos affected). Overexpression of the mutant *hoxb1a*^{sa1191} mRNA failed to produce an anterior duplication of r4 (Fig 4.1 H; 0/38 embryos affected) providing evidence that the mutant Hoxb1a protein also has strongly reduced biological activity.

Previous work has shown that knockdown of paralog group 1 *hox* genes in zebrafish results in mild morphological phenotypes (McClintock et al., 2002). We examined zebrafish homozygous for *hoxb1a*$^{sa1191/sa1191}$ (hereafter referred to as *hoxb1a*$^{-/-}$; embryos genotyped for the *sa1191* allele via dCaps PCR, see section 4.4 for details) and homozygous for *hoxb1b*$^{ua1006/ua1006}$ (hereafter referred to as *hoxb1b*$^{-/-}$; embryos genotyped for the *ua1006* allele via PCR, see section 4.4 for details) for morphological defects (Fig 4.2 A-L). *Hoxb1a*$^{-/-}$ mutants lack any major morphological defects, and *hoxb1b*$^{-/-}$ mutants have a small otic vesicle (Fig 4.2 A-C, E-G, I-K). *Hoxb1a*$^{-/-}$*;hoxb1b*$^{-/-}$ double mutants display a small otic vesicle accompanied by cardiac edema and die between 3 dpf and 4 dpf (Fig 4.2 A,D,E,H,I,L). These phenotypes are consistent with a role for PG1 *hox* genes in hindbrain development, as indicated by changes in otic vesicle size, and additionally provide evidence that the concurrent loss of both *hoxb1a* and *hoxb1b* results in more severe defects in embryonic development.

Researchers have previously examined rhombomere boundary specification in zebrafish *hoxb1b*$^{-/-}$ mutants (expression of *sema3gb* (Zigman et al., 2014)). We wished to extend this analysis to *hoxb1a*$^{-/-}$ and embryos doubly homozygous for mutations in *hoxb1a* and *hoxb1b*. We find that embryos lacking *hoxb1a*$^{-/-}$ are overtly normal (*mariposa (forkhead box B1a; foxb1a*; Fig 4.3 A, B), whereas embryos lacking *hoxb1b* display defects to r2/3, r3/4 and r6/7 boundaries (Fig 4.3 A,C, 15/15 embryos). Compound loss of *hoxb1b* in addition to *hoxb1a* results in a more severe phenotype, with no rhombomere boundaries detected (Fig 4.3 A, D; 3/3 embryos). Prior research on compound *hox* PG1 mutants examined segmental gene expression in r3-r6 and concluded that Hoxb1a regulates r4 gene expression and that Hoxb1b plays an essential role in regulating rhombomere size (Weicksel et al., 2014). Our analyses of *hoxb1a*$^{-/-}$, *hoxb1b*$^{-/-}$ and *hoxb1a*$^{-/-}$*;hoxb1b*$^{-/-}$ mutants (*krox20*, Fig 4.3 E-H, *hoxb1b*$^{-/-}$: 29/29 embryos, *hoxb1a*$^{-/-}$*;hoxb1b*$^{-/-}$: 5/5 embryos; *hoxb1a*, Fig 4.3 I-L, *hoxb1a*$^{-/-}$: 10/10 embryos, *hoxb1b*$^{-/-}$: 14/14 embryos, *hoxb1a*$^{-/-}$*;hoxb1b*$^{-/-}$: 4/4 embryos; *hoxb2a*, Fig 4.3

M-P, *hoxb1a*$^{-/-}$: 16/16 embryos, *hoxb1b*$^{-/-}$: 7/7 embryos, *hoxb1a*$^{-/-}$*;hoxb1b*$^{-/-}$: 3/3 embryos; *hoxa2b,* Fig 4.3 Q-T, *hoxb1a*$^{-/-}$: 10/10 embryos, *hoxb1b*$^{-/-}$: 8/8 embryos, *hoxb1a*$^{-/-}$*;hoxb1b*$^{-/-}$: 3/3 embryos) confirmed such prior results. Examination of additional markers also shows that rhombomere size is further altered (*krox20*, Fig 4.3 E,H, 5/5 embryos; *epha4a*, Fig 4.4 A,D, 5/5 embryos; *val,* Fig 4.4 E,H, 4/4 embryos; *hoxa3a,* Fig 4.4 I,L 3/3 embryos; *hoxb3a* Fig 4.4 M,P, 4/4 embryos) and rhombomere specific gene expression in r4 and r5 is lost or reduced in *hoxb1a*$^{-/-}$*;hoxb1b*$^{-/-}$ mutants (*hoxb1a*, Fig 4.3 I,L, 4/4 embryos; *hoxb2a*; Fig 4.3 M,P, 3/3 embryos; *hoxa2b*, Fig 4.3 Q,T, 3/3 embryos; *hoxa3a,* Fig 4.4 I,L, 3/3 embryos). Taken together, our results support a model in which zebrafish PG1 genes have distinct and overlapping functions.

Neural crest migration has solely been analyzed in *hoxb1b* single mutants (Zigman et al., 2014). Therefore, we performed an analysis of *dlx2* expression in *hoxb1a*$^{-/-}$, *hoxb1b*$^{-/-}$ and compound *hoxb1a*$^{-/-}$*;hoxb1b*$^{-/-}$ mutants. Consistent with prior results, the loss of *hoxb1b* causes fusion of the r2 and r4 neural crest streams (Fig 4.5 A,C, 9/9 embryos), whereas loss of *hoxb1a* causes no discernable effect (Fig 4.5 A,B). Compound loss of PG1 *hox* genes results in a reduction in *dlx2* expression within the second arch and disruption of the neural crest streams (Fig 4.5 A,D, 8/9 embryos).

Prior research on compound PG1 *hox* mutants has demonstrated alterations to branchiomotor and Mauthner neurons (Weicksel et al., 2014). We sought to extend such results to include an analysis of reticulospinal neurons. Consistent with the defects in r4 gene expression, *hoxb1a*$^{-/-}$ mutants fail to develop the stereotypical r4 born Mauthner neurons (Fig 4.5 E, F; bilateral loss of Mauthner: 8/10 embryos, unilateral loss of Mauthner: 2/10 embryos), whereas other neurons are overtly normal. An analysis of *hoxb1b*$^{-/-}$ mutants shows a similar loss of Mauthner neurons with a partial loss of r6-specific Mid3cm (Fig 4.5 E, G; bilateral loss of Mauthner: 9/12 embryos, unilateral loss of Mauthner: 3/12; bilateral loss of Mid3cm: 7/12 embryos, unilateral loss of Mid3cm: 4/12). Compound loss of *hoxb1a* and *hoxb1b* showed a comparable phenotype to loss of *hoxb1b* including loss of the r3-specific reticulospinal neuron (Fig 4.5 E; bilateral loss of Mauthner: 3/3 embryos; bilateral loss of Mid3cm: 2/3 embryos, unilateral loss of Mid3cm: 1/3; bilateral loss of r3 reticulospinal: 3/3 embryos). To expand this analysis to other hindbrain neurons with segment-specific identity, we next analyzed branchiomotor

neuron (BMN) specification with the use of *Tg(isl1:gfp)*. Loss of Hoxb1a results in a loss of facial BMN migration posteriorly out of r4 (Fig 4.5 I, J, 11/11 embryos), whereas loss of Hoxb1b results in normal migration to r6/7, with fewer neurons present (Fig 4.5 I,K, 12/12 embryos). In contrast to our results, Weicksel et al. (2014) detected a partial loss of facial motor neuron migration in *hoxb1b*$^{-/-}$ mutants, although it is possible this is explained by differences in protocol (immunofluorescence vs. transgene) or strain background. Compound loss of *hoxb1a* and *hoxb1b* results in a reduced number of facial BMNs, which fail to migrate posteriorly out of r4 (Fig 4.5 I, L, 5/5 embryos).

Taken together with the results from gene expression and neuronal differentiation, we conclude that PG1 *Hox* genes have distinct and overlapping roles. Hoxb1b regulates rhombomere size whereas Hoxb1a regulates r4-specific gene expression. Our detailed analyses of *hoxb1a;hoxb1b* double mutants have pinpointed additional phenotypes that indicate PG1 functions in rhombomeres outside of r4, such as the mis-specification of neurons in r3 and r6.

4.2.2 Loss of both Hoxb1b and Pbx4 is required to revert the hindbrain to an r1-like groundstate

Our analysis of rhombomere boundaries in *hoxb1a*$^{-/-}$;*hoxb1b*$^{-/-}$ double mutants reveals that they are disrupted throughout the hindbrain while the three neural crest streams are less distinct than observed in wildtype embryos, a phenotype which bears a striking resemblance to embryos lacking the Hox cofactor Pbx4 (Pöpperl et al., 2000). The Mauthner neuron and Mid3cm phenotypes in *hoxb1a*$^{-/-}$;*hoxb1b*$^{-/-}$ double mutants also accord with loss of Pbx. However, segmental gene expression in the anterior hindbrain (r1 and r2) of *hoxb1a*$^{-/-}$;*hoxb1b*$^{-/-}$ double mutants is overtly normal demonstrating that loss of PG1 *hox* genes is not sufficient to cause the hindbrain to revert to an r1-like ground state. This provides support for an alternative model of Pbx function in which it functions (at least partly) independently of PG1 *hox* genes to pattern the hindbrain. Therefore, we wished to determine if compound loss of zygotic *hoxb1b* and *pbx4* is sufficient to generate a loss of hindbrain patterning. To study the genetic interaction between Hoxb1b and Pbx, we created *hoxb1b*$^{-/-}$*; pbx4*$^{b557/b557}$ double mutants (hereafter referred to as *hoxb1b*$^{-/-}$*;pbx4*$^{-/-}$; embryos genotyped for the *b557* allele via

dCaps PCR, see section 4.4 for details). We assayed for hindbrain segmentation and patterning first using *eng2 (engrailed homeobox 2a; eng2a)* as a marker for the midbrain-hindbrain boundary and *krox20* to label r3/5 (Fig 4.6 A). While *hoxb1b*$^{-/-}$ mutants show a characteristic r3 domain expansion and r4 reduction (Fig 4.6 A,B, 6/6 embryos), in *pbx4*$^{-/-}$ mutants r3 is severely reduced (Fig 4.6 A,C, 12/12 embryos). The *hoxb1b*$^{-/-}$;*pbx4*$^{-/-}$ double mutants display a complete loss of *krox20* expression in r3/5 (Fig 4.6 A,D, 3/3 embryos). To determine if this loss of expression is due to the conversion of the hindbrain to an r1-like ground state, expression of *epha4a,* a marker of r1/3/5, was examined. In the *hoxb1b*$^{-/-}$;*pbx4*$^{-/-}$ double mutants, r1 territory is expanded posteriorly throughout the hindbrain (Fig 4.6 E,H, 3/3 embryos) whereas expression is normal in *hoxb1b*$^{-/-}$ mutants (Fig 4.6 F; 4/4 embryos). This indicates that while the combined loss of *hoxb1a* and *hoxb1b* is insufficient to cause a loss of hindbrain identity, the loss of *hoxb1b* and *pbx4* reverts the hindbrain to an r1-like ground state. Taken together with prior analyses of Pbx2/4-depleted embryos, this supports a model in which Pbx4 interacts with factors aside from Hoxb1b to pattern the nascent hindbrain.

4.2.3 PG1 *hox* genes share redundant functions in regulation of *vhnf1*

In most cases, *hoxb1a* and *hoxb1b* appear to have separate functions and do not show synergy upon compound loss. To determine if *hoxb1a* and *hoxb1b* share any redundant functions, we searched for genes that were affected solely by the loss of both *hoxb1a* and *hoxb1b* and found one such target, *vhnf1 (HNF1 homeobox Ba; hnf1ba).* We find that the expression of *vhnf1* is reduced in *hoxb1a*$^{-/-}$;*hoxb1b*$^{-/-}$ double mutants whereas expression is unaffected in single mutants (Fig 4.7 A-D, 5/5 embryos). *Vhnf1* is also known to be responsive to retinoic acid (RA) levels (Hernandez et al., 2004; Maves and Kimmel, 2005; Pouilhe et al., 2007), so we wished to determine if *hoxb1a* and *hoxb1b* regulate *vhnf1* expression through RA signaling. Embryos were treated with 5 nM exogenous RA to see if this would rescue *vhnf1* expression. 5nM RA treatment resulted in a discernable increase of *vhnf1* levels in both wildtype and mutant embryos (Fig 4.8 A-D), confirming that *vhnf1* is responsive to RA. However, treatment with exogenous RA was only partially able to rescue *vhnf1* expression in the *hoxb1a*$^{-/-}$;*hoxb1b*$^{-/-}$ double mutants (Fig 4.8 B, 3/3 embryos). *Vhnf1* expression was increased to a

similar expression level as seen in the DMSO-treated wildtype controls (Fig 4.8 C), however it fails to increase *vhnf1* expression to the same degree as see in the RA treated wildtype controls (Fig 4.8 A). This suggests that there may be both RA dependent and RA independent roles for *hoxb1a* and *hoxb1b* in the regulation of *vhnf1*.

4.2.4 Paralog group 1 *hox* genes are not crucial regulators of retinoic acid signaling

Retinoic acid signaling is necessary for specification of hindbrain fates posterior to r3 (Hernandez et al., 2004). Zebrafish *aldh1a2 (aldehyde dehydrogenase 1 family member A2)* mutants, and those treated with an antagonist to block RA receptor activity have a shortened hindbrain accompanied by otic vesicle defects. Loss of RA also causes defects in BMN migration (Linville et al., 2004). To determine if PG1 *hox* genes regulate RA signaling in the hindbrain, we first assayed for the synthesis of RA, by examining the expression of the RA synthesis enzyme *aldh1a2.* At 70% epiboly (8hpf), the presumptive hindbrain, and domain of *hoxb1b* expression, partially overlap with *aldh1a2* expression (Maves and Kimmel, 2005) and at this stage, changes in RA synthesis could have profound effects on the initiation of rhombomere-specific gene expression. However, examination of PG1 *hox* mutants shows that the loss of *hoxb1a* and/or *hoxb1b* does not have an effect on the levels of *aldh1a2* transcript (Fig 4.9 A-D). As RA synthesis does not appear to be altered, we next examined the *cyp26* family of genes, which are activated by RA signaling, and hydroxylate RA into non-signaling polar derivatives (Hernandez et al., 2007) (Fig 4.9 E-L). *Hoxb1a*$^{-/-}$ mutants have no alterations in the expression of *cyp26b1 (cytochrome P450, family 26, subfamily b, polypeptide 1)* and *cyp26c1(cytochrome P450, family 26, subfamily c, polypeptide 1)* (Fig 4.9 E, F, I, J). In both the *hoxb1b*$^{-/-}$ mutants and the *hoxb1a*$^{-/-}$;*hoxb1b*$^{-/-}$ double mutants, r4 expression of *cyp26c1* is disrupted (Fig 4.9 E, G, H, 16/17 *hoxb1b*$^{-/-}$ embryos, 7/7 *hoxb1a*$^{-/-}$;*hoxb1b*$^{-/-}$ embryos; two-color *in situ* hybridization for *cyp26c1/krox20* was performed to confirm rhombomere identity, Fig 4.10 A-D) and *cyp26b1* expression does not show distinct r3 and r4 domains (Fig 4.9 I, K, L, 20/20 *hoxb1b*$^{-/-}$ embryos, 8/8 *hoxb1a*$^{-/-}$;*hoxb1b*$^{-/-}$ embryos) indicating a role for *hoxb1b* in regulating the expression of these enzymes, likely in r4.

The decrease of *cyp26b1/c1* expression in r4 may result in a localized increase in RA levels, as there is less of the Cyp26b1/c1 enzyme present to metabolize RA. Conversely, since RA regulates *cyp26b1/c1* transcription, the decrease in *cyp26b1/c1* expression in r4 may be a result of an r4-specific decrease in RA levels. In order to determine if levels of RA signaling have been altered in the hindbrain, we examined the expression of known RA-regulated genes (*hoxd4a* and *meis3*). Expression of both RA target genes is unaffected in all mutants (Fig 4.9 M-T), indicating that RA signaling within r4 is overtly unchanged despite the alterations in *cyp26b1*/*c1* expression.

4.2.5 *Pbx* genes regulate Retinoic Acid synthesis during early hindbrain specification

The loss of hindbrain identity that is observed in the *hoxb1b*$^{-/-}$;*pbx4*$^{-/-}$ double mutants, is not observed in *hoxb1a*$^{-/-}$;*hoxb1b*$^{-/-}$ double mutants. These data suggest that *pbx4* is not solely dependent on *hoxb1b* to generate hindbrain identity, and alterations to signaling pathways may underlie the loss of hindbrain identity observed in *hoxb1b*$^{-/-}$;*pbx4*$^{-/-}$ double mutants. RA signaling is not significantly altered by the loss of PG1 *hox* genes, and represents a possible mechanism for the loss of hindbrain identity observed in *hoxb1b*$^{-/-}$*;pbx4*$^{-/-}$ double mutants. Further supporting this hypothesis is work in mouse that shows that *Raldh2* (orthologous to zebrafish *aldh1a2*) expression in *Hoxa1/Pbx1* nulls is reduced (Vitobello et al., 2011). Similarly, loss of murine *Pbx1/2* also causes a decrease *Raldh2* expression (Vitobello et al., 2011). In zebrafish, *pbx2/4* depleted embryos also exhibit reduced *aldh1a2* expression in the trunk and retina during later stages of development (French et al., 2007; Maves et al., 2007).

To determine whether *pbx* is involved in early regulation of RA signaling, we examined expression of *aldh1a2* in *pbx4*$^{-/-}$ mutants, which have had *pbx* levels further reduced using *pbx2/4* morpholinos. Pbx2/4 depleted embryos display a decrease in the *aldh1a2* expression domain at 90% epiboly (9hpf) (Fig 4.11 A-E, 22/22 *pbx4*$^{-/-}$;*pbx2/4* MO injected embryos). The area of *aldh1a2* expression was measured and Pbx2/4 depleted embryos have a 21% decrease in the area of *aldh1a2* expression compared to uninjected wildtype embryos (Fig 4.11 E; Uninjected wildtype: 135890 μm^2, Uninjected *pbx4*$^{-/-}$*:* 130628 μm^2, *pbx2/4*MO injected wildtype: 110737 μm^2, *pbx2/4*MO injected

pbx4$^{-/-}$*:* 107364 μm^2; ANOVA, post-hoc Tukey's: uninjected wildtype vs *pbx2/4*MO injected wildtype, p-value 0.003; uninjected wildtype vs *pbx2/4*MO injected *pbx4*$^{-/-}$, p-value 0.001) indicating that *pbx* genes are required for appropriate RA synthesis.

4.2.6 Hoxb1b regulates Fibroblast Growth Factor Signaling

To determine the mechanism by which PG1 *hox* genes regulate hindbrain patterning, we examined components of FGF signaling within the hindbrain. The expression of *fgf3* and *fgf8* in r4 is required to establish the hindbrain signaling center that facilitates the development of r5/6 (Maves et al., 2002). Inhibition of FGF signaling, and the consequent loss of the r4 signaling center results in neuronal defects including a failure of facial BMNs to migrate (Roy and Sagerstrom, 2004). While no reticulospinal defects are observed when FGF signaling is inhibited, the BMN phenotype is similar to that observed in the PG1 *hox* mutants. Furthermore, *hoxb1b* regulates *ppp1r14al*, a protein phosphatase that controls expression of *fgf3* in the r4 signaling center (Choe et al., 2011).

To determine if the r4 FGF-signaling center is established in PG1 *hox* mutants we assayed for the expression of the FGF ligands, *fgf3* and *fgf8*. At early stages of hindbrain development *fgf3* expression in r4 is lost in both *hoxb1b*$^{-/-}$ mutants and in *hoxb1a*$^{-/-}$;*hoxb1b*$^{-/-}$ double mutants, but not in *hoxb1a*$^{-/-}$ single mutants (Fig 4.12 A,B,C,D, 16/16 *hoxb1b*$^{-/-}$ embryos, 4/4 *hoxb1a*$^{-/-}$*;hoxb1b*$^{-/-}$ embryos). Consistent with previous research (Weicksel et al., 2014), at later stages of hindbrain development, *hoxb1a*$^{-/-}$ single mutants have decreased *fgf3* expression (Fig 4.13 A-B, 5/6 embryos), indicating that while the loss of *hoxb1a* does not affect initiation of *fgf3* expression, it may affect the maintenance of *fgf3* expression at later stages. *Fgf8* is normally expressed in the MHB, r4 and the medial region of r2 (Fig 4.12 E; two-color *in situ* hybridization for *fgf8/krox20* was performed to confirm rhombomere identity, Fig 4.14 A-D). We do not see a loss of *fgf8* in any mutants, however the spatial domains are demonstrably altered. In *hoxb1a*$^{-/-}$ mutants *fgf8* expression within the presumptive r2 region is closer to the r4 region and the MHB displays an 'arrowhead' shape (Fig 4.12 E,F, 14/19 embryos). In *hoxb1b*$^{-/-}$ mutants, *fgf8* is ectopically expressed in r3 and the lateral portions of expression in r4 are disrupted (Fig 4.12 E,G, 19/19 embryos). In the *hoxb1a*$^{-/-}$;*hoxb1b*$^{-}$

$^{-/-}$ double mutants we also see ectopic expression of *fgf8* in r3 and a further disruption in the expression of *fgf8* in the lateral portions of r4 (Fig 4.12 E,H, 8/8 embryos). While *fgf8* is mildly altered in *hoxb1a*$^{-/-}$ mutants, initiation of *fgf3* expression is normal (although the maintenance of *fgf3* expression at later stages is affected). These results support a role for Hoxb1b in regulating *fgf3* initiation and a complex role for PG1 genes in establishing the appropriate spatial domain of *fgf8* expression within the anterior hindbrain.

To determine if the alterations to *fgf3* and *fgf8* alter overall FGF signaling in the hindbrain, we examined both FGF-dependent gene expression (*pea3 (ets variant 4; etv4), dusp6 (dual specificity phosphatase 6),* and the *spry* (*sprouty*) family) (Fig 4.12 I-B'; two-color *in situ* hybridization for *dusp6/krox20* and *spry2/krox20* was performed to confirm rhombomere identity, Fig 4.14 E-L)) and localization of P-Erk within the hindbrain (Fig 4.15 A-E) (Casci et al., 1999; Furthauer et al., 2004; Kawakami et al., 2003; Komisarczuk et al., 2008; Raible and Brand, 2001; Reich et al., 1999; Roehl and Nusslein-Volhard, 2001; Tsang and Dawid, 2004). *Hoxb1a*$^{-/-}$ mutants do not have significant alterations to the expression of *pea3*, (Fig 4.12 I,J) *dusp6* (Fig 4.12 M,N) or *spry1/2/4* (Fig 4.12 Q,R,U,V,Y,Z). In *hoxb1b*$^{-/-}$ mutants and in *hoxb1a*$^{-/-}$;*hoxb1b*$^{-/-}$ mutants we observe a change in the posterior expression domains of *pea3* (Fig 4.12 I,K,L, 6/7 *hoxb1b*$^{-/-}$ embryos, 6/6 *hoxb1a*$^{-/-}$;*hoxb1b*$^{-/-}$ embryos) and *dusp6* (Fig 4.12 M,O,P, 10/11 *hoxb1b*$^{-/-}$ embryos, 5/5 *hoxb1a*$^{-/-}$;*hoxb1b*$^{-/-}$ embryos) along with ectopic expression of *spry1/2* in r3 (Fig 4.12 Q,S,T,U,W,X, *spry1:* 25/25 *hoxb1b*$^{-/-}$ embryos, 9/9 *hoxb1a*$^{-/-}$;*hoxb1b*$^{-/-}$ embryos, *spry2:* 19/19 *hoxb1b*$^{-/-}$ embryos, 5/5 *hoxb1a*$^{-/-}$;*hoxb1b*$^{-/-}$ embryos), and ectopic expression of *spry4* in r4 (Fig 4.12 Y,A',B', 23/23 *hoxb1b*$^{-/-}$ embryos, 4/4 *hoxb1a*$^{-/-}$;*hoxb1b*$^{-/-}$ embryos). Given the complexity of the feedback loops established in this pathway, we wanted to determine if the increase in *pea3* represented an increase in overall FGF signaling, or if the concurrent increase in *dusp6* and *spry1*/2/*4* would result in an overall decrease in FGF signaling. To measure FGF activity, we assayed levels of phosphorylated ERK (P-Erk) in the hindbrain. In wildtype embryos, P-Erk can be seen in a stripe across presumptive r4, and in lateral wings adjacent to the hindbrain (Fig 4.15 A). *Hoxb1a*$^{-/-}$ mutants show localization of P-Erk similar to wildtype embryos (Fig 4.15 A,B,E), while *hoxb1b*$^{-/-}$ and *hoxb1a*$^{-/-}$;*hoxb1b*$^{-/-}$ double mutants have

decreased P-Erk within presumptive r4 (Fig 4.15 A,C,D,E, 20/25 *hoxb1b*$^{-/-}$ embryos, 9/9 *hoxb1a*$^{-/-}$;*hoxb1b*$^{-/-}$ embryos). Fluorescence intensity of P-Erk staining within the hindbrain was measured and *hoxb1b*$^{-/-}$ mutants have a 45% decrease in intensity while *hoxb1a*$^{-/-}$;*hoxb1b*$^{-/-}$ double mutants have a 68% decrease in intensity. (Fig 4.15 E; Wildtype: 86490590 AU, *hoxb1a*$^{-/-}$*:* 78175326 AU, *hoxb1b*$^{-/-}$: 47583826 AU, *hoxb1a*$^{-/-}$*;hoxb1b*$^{-/-}$*:* 27314030 AU; ANOVA, post-hoc Tukey's: Wildtype vs *hoxb1b*$^{-/-}$, p-value 0.007; Wildtype vs *hoxb1a*$^{-/-}$*;hoxb1b*$^{-/-}$*,* p-value 0.001) Taken together, such results argue that increases in *dusp6* and/or *spry* gene expression correlate with decreased FGF signaling. As such, we propose that Hoxb1b has two functions in regulating FGF signaling – generating the correct spatial domain of FGF ligands and restricting the expression of FGF signaling modulators such as *dusp6* and *spry1/2/4.*

4.3 Discussion

4.3.1 Loss of PG1 *hox* genes is not sufficient to cause a loss of hindbrain patterning

Hoxb1a is required for the expression of r4-associated genes and these defects in gene expression underlie the loss of the r4 Mauthner reticulospinal neuron and the failure of the facial BMNs to migrate out of r4. *Hoxb1b* regulates hindbrain segmentation, rhombomere size, and rhombomere specific gene expression in r4/5, which are required for specification of the r2/4 neural crest streams, and the development of the Mauthner and Mid3cm reticulospinal neurons and specification of the number of facial BMNs. The phenotypes we observe are consistent with those observed for other alleles of *hoxb1a* and *hoxb1b* (Weicksel et al., 2014; Zigman et al., 2014). Overall, zebrafish PG1 *hox* mutants closely resemble murine PG1 *hox* mutants (Carpenter et al., 1993; Chisaka et al., 1992; Erickson et al., 2007; Goddard et al., 1996; Mark et al., 1993), indicating a conservation of function for PG1 *hox* genes between species.

Overall*,* *hoxb1a*$^{-/-}$;*hoxb1b*$^{-/-}$ double mutants closely resemble *hoxb1b*$^{-/-}$ single mutants. They have similar defects in rhombomere segmentation, size and gene expression as well as defects in neural crest specification, r3/4/6 reticulospinal neuron

development, and facial BMN development and migration. However, there are a few cases where the phenotype of the *hoxb1a*$^{-/-}$;*hoxb1b*$^{-/-}$ double mutants is more severe than the *hoxb1b*$^{-/-}$ single mutant. *Hoxb1a* expression is completely lost in the *hoxb1a*$^{-/-}$;*hoxb1b*$^{-/-}$ double mutants and r5 expression of *hoxb2a* and *hoxa2b* is reduced. Additionally, the specification of all 3 neural crest streams is disrupted. Interestingly, we found one case where *hoxb1a* and *hoxb1b* share redundant functions, as only *hoxb1a*$^{-/-}$;*hoxb1b*$^{-/-}$ double mutants have reduced *vhnf1* expression. While previous research has shown that *pbx*-depleted embryos have reduced *vhnf1* expression (Waskiewicz et al., 2002), our research not only supports this conclusion, and clarifies that specifically *hoxb1a* and *hoxb1b* are involved in the regulation of *vhnf1* expression. Furthermore, this phenotype is partially rescued by treatment with exogenous RA, suggesting both RA dependent and RA independent roles for *hoxb1a* and *hoxb1b* in the regulation of *vhnf1* expression.

The main role of Pbx cofactors is to facilitate *hox* binding to transcriptional targets, and Pbx is known to act as a cofactor for anterior Hox proteins such as Hoxb1b and Hoxb1a (Cooper et al., 2003; Pöpperl et al., 2000). Previous work has shown that the loss or knockdown of maternal and zygotic *pbx2* and *pbx4,* causes the hindbrain to revert to an r1-like groundstate which lacks r2-6 identity (Waskiewicz et al., 2002). From this it was proposed that Pbx-Hox-1 complexes lie at the top of a hierarchy to regulate and initiate hindbrain segmental identity. However, despite results in *Xenopus* showing that a knockdown of *hox-1* paralogs results in a loss of hindbrain segmental identity (McNulty et al., 2005), zebrafish have a phenotype similar to murine models (Gavalas et al., 1998; Rossel and Capecchi, 1999; Studer et al., 1998), where the loss of PG1 *hox* genes in zebrafish is not sufficient to revert the hindbrain to a r1-like ground state. In order to determine if PG1 *hox* genes are involved in the generation of the r1 ground state we examined zygotic *hoxb1b*$^{-/-}$;*pbx4*$^{-/-}$ double mutants. Under these conditions, we observe that the hindbrain reverts to an r1-like groundstate, lacking r2-6 identity, and this provides evidence that the zygotic loss of only *hoxb1b* and *pbx4* is sufficient to prevent hindbrain segmentation. This is consistent with a role for PG1 *hox* genes in regulating some aspects of hindbrain patterning, however it also argues for an

even more central role for Pbx, not solely as a Hoxb1b cofactor in the establishment of hindbrain identity.

4.3.2 RA signaling is regulated by *pbx* genes, but not PG1 *hox* genes

Retinoic acid signaling is known to regulate A-P patterning in the hindbrain, and is thought to function by establishing *hox* gene expression (Ferretti et al., 2000; Frasch et al., 1995; Gould et al., 1998; Morrison et al., 1997; Papalopulu et al., 1991; Yan et al., 1998), which in turn can regulate RA synthesis (Maves et al., 2007; Vitobello et al., 2011). In mouse, *Hoxa1* regulates *Raldh2* expression in conjunction with *Pbx* genes (Vitobello et al., 2011), and in zebrafish *pbx2/4* regulate *aldh1a2* in the trunk and retina (French et al., 2007; Maves et al., 2007). In light of this, altered RA signaling is a potential mechanism through which PG1 *hox* genes may regulate development of the hindbrain. Surprisingly, the loss of PG1 *hox* genes in any combination is insufficient to cause a reduction in *aldh1a2* expression. We do see alterations in the expression of the RA metabolizing enzymes *cyp26b1*/*c1* in r4 in *hoxb1b*$^{-/-}$ single and *hoxb1a*$^{-/-}$*;hoxb1b*$^{-/-}$ double mutants. As RA regulates *cyp26b1*/*c1*, the change in their expression domain may be due to localized decreases in RA levels. Conversely, loss of *cyp26b1/c1* expression domains may cause localized increases in RA levels. Examination of the RA responsive genes *hoxd4a* and *meis3* do not reveal any observable changes in RA levels in the *hoxb1b*$^{-/-}$ or *hoxb1a*$^{-/-}$*;hoxb1b*$^{-/-}$ mutants. Depletion of *cyp26b1*/*c1* does not result in hindbrain patterning defects (Hernandez et al., 2007), which is consistent with our results showing that *hoxb1b*$^{-/-}$ single and *hoxb1a*$^{-/-}$*;hoxb1b*$^{-/-}$ double mutants do not have a complete loss of hindbrain patterning. Additionally, the loss of RA signaling affects facial BMN migration (Linville et al., 2004), which is not observed in *hoxb1b*$^{-/-}$ mutants.

As RA signaling does not underlie the relatively mild defects in hindbrain development caused by the loss of *hoxb1b,* we wished to determine if instead, alterations to RA signaling are caused by a loss of *pbx* genes. This would be consistent with previous research showing that *Hoxa1* and *Pbx1* regulate *Raldh2* expression in mouse (Vitobello et al., 2011), and that *pbx*-depleted embryos have reduced *aldh1a2* expression at later stages of development in zebrafish (French et al., 2007; Maves et al., 2007). As we are investigating the establishment of hindbrain identity and segmentation, we have

investigated earlier stages of development than previously investigated, and our results show that at 90% epiboly (9hpf), during early stages of hindbrain development and specification, the expression domain of *aldh1a2* is reduced in *pbx* depleted embryos. Although alterations to RA signaling are not responsible for the hindbrain defects observed in *hoxb1b* mutants, the phenotype of the *hoxb1b*$^{-/-}$;*pbx4*$^{-/-}$ double mutants, is similar to the loss of hindbrain patterning seen in *pbx* depleted embryos (Waskiewicz et al., 2002). In light of the lack of changes observed in PG1-*hox* mutants to RA signaling, this argues that alterations to RA synthesis resulting from the loss of *pbx* genes may be required in combination with the loss of *hoxb1b* in order to revert the hindbrain to an r1-like groundstate.

4.3.3 PG1 *hox* genes regulate FGF signaling

FGF signals from the r4 signaling center are essential for development of adjacent rhombomeres in the hindbrain. Loss or depletion of these signals leads to loss of r5/6 patterning and development (Maves et al., 2002). Misregulation of this signaling pathway and the r4 signaling center contributes to the hindbrain patterning defects observed in PG1 *hox* mutants. Although FGF signaling is largely unchanged in *hoxb1a*$^{-/-}$ mutants at early stages of hindbrain specification, our work has shown that the loss of *hoxb1b* results in a loss of *fgf3* expression in r4. *Hoxb1b* is likely regulating *fgf3* through the protein phosphatase 1 regulatory subunit *ppp1r14al,* which has been previously implicated in *hoxb1b*-mediated regulation of *fgf3* (Choe et al., 2011). While previous research has examined the effect of the loss of PG1-*hox* genes on *fgf3* expression (Choe et al., 2011; Waskiewicz et al., 2002; Weicksel et al., 2014), we have expanded this analysis to include *fgf8,* which has also been shown to be required for establishment of the r4 FGF signaling centre (Maves et al., 2002). Upon examination of *fgf8* expression, a novel alteration in the expression pattern was observed where *fgf8* is ectopically expressed in r3 and the lateral regions of r4 expression are disrupted. This suggests that one role for Hoxb1b in modulating FGF signaling is generating the correct spatial domains of FGF ligands.

While previous research has examined the regulation of *fgf3* expression by PG1 *hox* genes (Choe et al., 2011; Waskiewicz et al., 2002; Weicksel et al., 2014), we wished

to expand our analysis to include downstream FGF signaling effectors, especially since the expression domains of *fgf8* do not show a straightforward loss of FGF ligand in *hoxb1b* mutants. Therefore, we examined P-Erk localization to determine the overall effect on FGF signaling. In *hoxb1b*$^{-/-}$ mutants, there is a significant decrease in P-Erk localization in the hindbrain at 4 somites (11hpf). This is consistent with changes in the posterior expression domains of *dusp6* and *spry1/2/4*. Although these genes are known to be activated by FGF signaling, *dusp6* inhibits FGF signaling through dephosphorylation of activated Erk proteins (Tsang and Dawid, 2004), and *spry* has been shown to sequester proteins upstream of the Erk cascade such as Grb2 (Casci et al., 1999) and Raf (Reich et al., 1999). Increased expression in the posterior domains of *dusp6* and *spry1/2/4* may be responsible for the decrease in P-Erk localization. This provides evidence for a plausible role for Hoxb1b in restricting the expression domains of FGF signaling modulators including *dusp6* and *spry1/2/4*.

Our results support a novel model, in which *hoxb1b* is required at two stages of FGF signaling, first in generating the correct spatial domains of FGF ligands, and secondly in restricting the expression domains of FGF signaling modulators. Appropriate signals from the r4 FGF signaling centre are required for patterning and development of adjacent rhombomeres, and misregulation of FGF signaling is a key contributor to the hindbrain patterning defects observed in *hoxb1b*$^{-/-}$ and *hoxb1a*$^{-/-}$;*hoxb1b*$^{-/-}$ double mutants.

4.3.4 Conclusions

We have shown that PG1 *hox* genes play important roles in zebrafish hindbrain patterning and specification, including coordinate regulation of *vhnf1*. However, the loss of *pbx4* in combination with *hoxb1b* is required to generate an r1-like ground state. This indicates that *pbx* plays a central role in hindbrain specification, as more than just a cofactor to PG1 *hox* genes. Additionally, we have shown that although PG1 *hox* genes do not overtly regulate RA signaling, *pbx* genes regulate RA synthesis at early stages of hindbrain development, and this is a contributing factor in the loss of hindbrain identity observed in *hoxb1b*$^{-/-}$;*pbx4*$^{-/-}$ double mutants. While the defects in hindbrain pattern in *hoxb1a*$^{-/-}$ mutants are restricted to r4, and may be explained by alterations in r4 gene

expression driven by *hoxb1a*, the broader alterations to hindbrain patterning observed in *hoxb1b*$^{-/-}$ mutants may be explained by the striking changes in both FGF ligand expression and the misregulation of FGF signaling modulators.

4.4 Figures

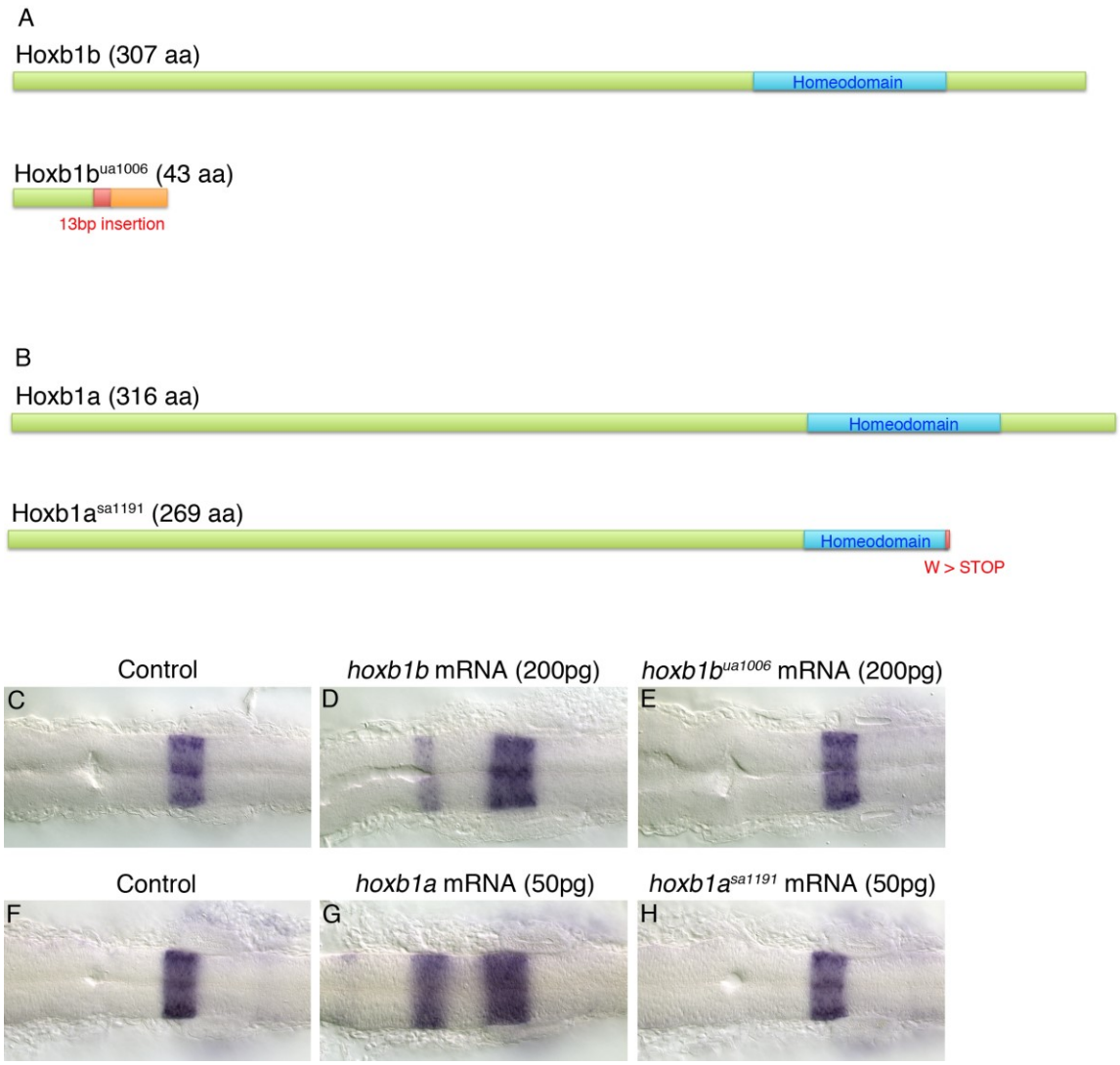

Figure 4.1. *Hoxb1b*^{ua1006} and *hoxb1a*^{sa1191} mutations.

(A) The *hoxb1b*^{ua1006} mutation was generated via TALEN-mediated mutagenesis and contains a 13 bp insertion 63 bp downstream of the start codon. This mutation results in a truncated 43 aa protein. (B) The *hoxb1a*^{sa1191} mutation contains a G to A resulting in a truncation part way through the homeodomain at amino acid 269. To determine if the protein produced by the *hoxb1b*^{ua1006} allele retains any function, 200 pg of wildtype *hoxb1b* RNA (D) and 200 pg of mutant *hoxb1b* RNA containing the ua1006 mutation (E) were over expressed. In situ hybridization for the 3'UTR of *hoxb1a* in uninjected controls (C, F) shows normal expression in rhombomere 4. Overexpression of wildtype *hoxb1b* RNA results in a homeotic transformation where a duplicated region *hoxb1a*

expression is observed in r2 (66/88 embryos affected) (D). Overexpression of *hoxb1b*^{ua1006} RNA fails to cause a homeotic transformation, indicating a lack of biological activity (0/82 embryos affected) (E). Similarly, to determine if the protein produced by the *hoxb1a*^{sa1191} allele retains any function, 50 pg of wildtype *hoxb1a* RNA (G) and 50 pg of mutant *hoxb1b* RNA containing the sa1191 mutation (H) were over expressed. Overexpression of wildtype *hoxb1a* RNA results in a homeotic transformation where a duplicated region *hoxb1a* expression is observed in r2 (30/34 embryos affected) (G). Overexpression of *hoxb1a*^{sa1191} RNA fails to cause a homeotic transformation, indicating a lack of biological activity (0/38 embryos affected)(H). All embryos are dorsal views, anterior to the left, 18hpf.

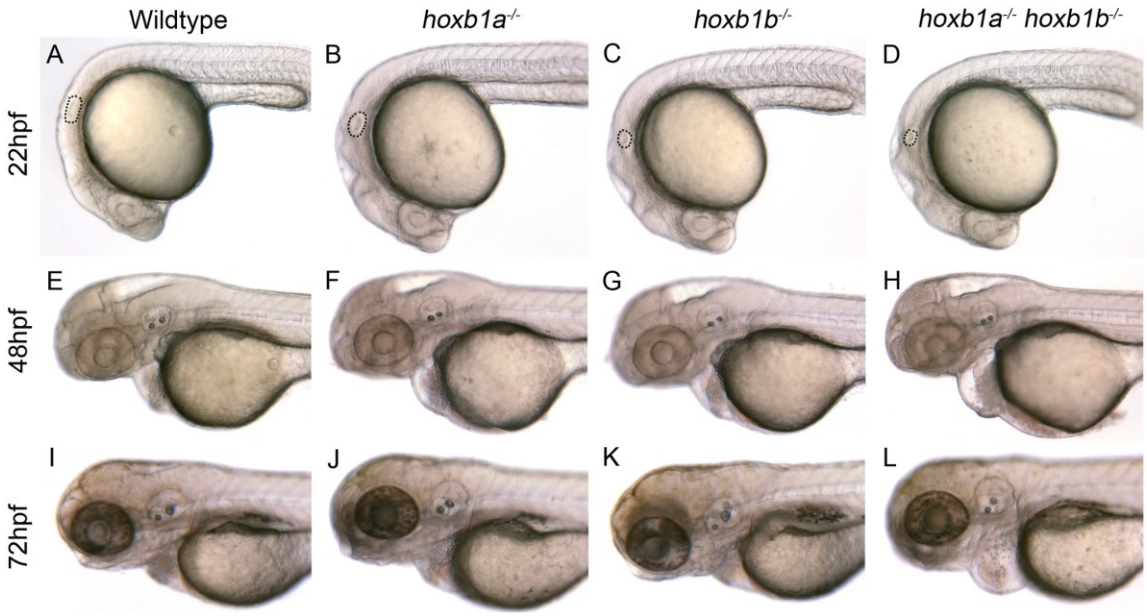

Figure 4.2. Morphology of paralog group 1 hox mutants.

Embryos were imaged consecutively at 22 hpf (A-D), 48 hpf (E-H) and 72 hpf (I-L) to examine gross morphological defects. *Hoxb1a*$^{-/-}$ mutants (B, F, J) do not have any major morphological defects as compared to wildtype embryos. (A, E, I) *Hoxb1b*$^{-/-}$ mutants have a small otic vesicle at 22 hpf (C) which does not persist at later stages (G, K). *Hoxb1a*$^{-/-}$;*hoxb1b*$^{-/-}$ mutants have a small otic vesicle at 22 hpf (D) and develop cardiac edema at later stages (H, L). All embryos have been genotyped for *hoxb1a*^{sa1191} and *hoxb1b*^{ua1006}. All embryos are lateral views, anterior to the left. hpf, hours post fertilization.

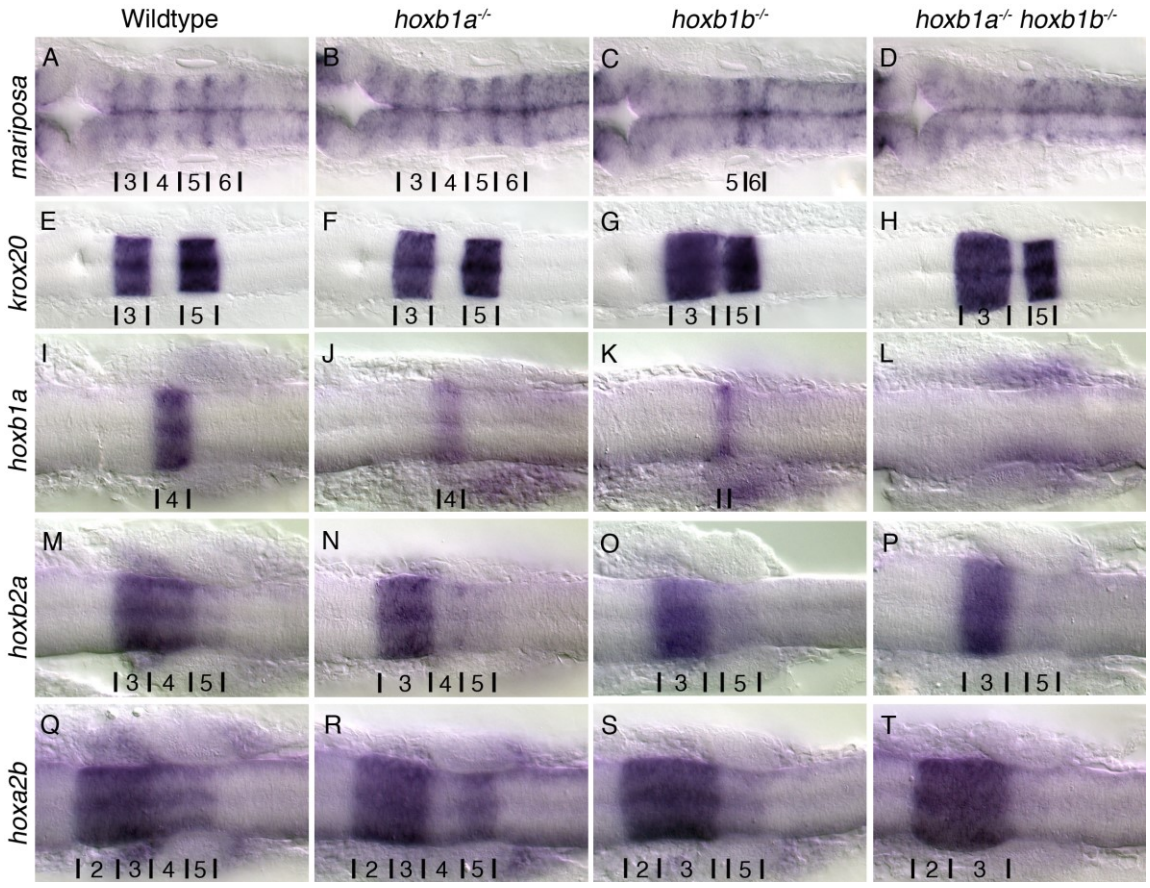

Figure 4.3. PG1 *hox* mutants have defects in hindbrain patterning.

Rhombomere boundaries are delineated by the expression of *mariposa* (A-D). Wildtype (A) and *hoxb1a*$^{-/-}$ mutants (B) have normal rhombomere boundaries while *hoxb1b*$^{-/-}$ mutants (15/15 embryos; C) have disrupted boundaries anterior to r5/6, and the boundaries in *hoxb1a*$^{-/-}$*;hoxb1b*$^{-/-}$ mutants (3/3 embryos) (D) are not visible. *Krox20* (E-H) expression in rhombomeres 3 and 5 are maintained in all embryos, however rhombomere 3 is expanded and r4 is reduced in *hoxb1b*$^{-/-}$ (29/29 embryos)(G) and *hoxb1a*$^{-/-}$*hoxb1b*$^{-/-}$ (5/5 embryos) (H) mutants. *Hoxb1a* is expressed in r4 (I), *hoxb2a* in r3-5 (M), *hoxa2b* in r2-5 (Q). Expression of *hoxb1a* is reduced in *hoxb1a*$^{-/-}$ mutants (7/7 embryos) (J), and *hoxb2a* and *hoxa2b* expression in r4 is lost (16/16 embryos and 10/10 embryos respectively) (N, R). *Hoxb1b*$^{-/-}$ mutants have reduced expression of *hoxb1a* (14/14 embryos) (K), and expression of *hoxb2a* (7/7 embryos) (O) and *hoxa2b* (8/8 embryos) (S) in r4 is lost. In *hoxb1a*$^{-/-}$*;hoxb1b*$^{-/-}$ mutants expression of *hoxb1a* (4/4 embryos) (L), *hoxb2a* (3/3 embryos) (P) and *hoxa2b* (3/3 embryos) (T) in r4 is lost and r5 expression of *hoxb2a* (3/3 embryos) (P) and *hoxa2b* (3/3 embryos) (T) is reduced. All

embryos have been genotyped for *hoxb1a*^{sa1191} and *hoxb1b*^{ua1006}. All images are dorsal views, anterior to the left, (A-D) 22 hpf, (E-T) 18 hpf.

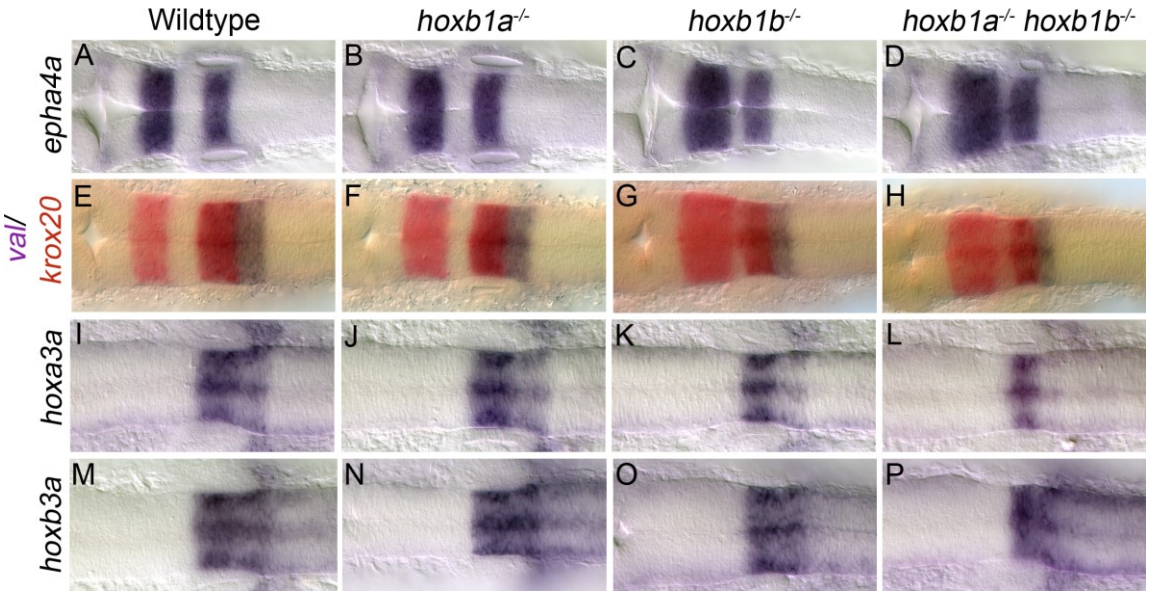

Figure 4.4. Alterations to rhombomere size in paralog group 1 hox mutants.

Wildtype embryos show the normal expression patterns for *epha4a* in r3/5 (A), *krox20* in red in r3/5 and *val* in purple in r5/6 (E), and *hoxa3a* (I) and *hoxb3a* (M) in r5/6. Expression of all markers are unaffected in *hoxb1a*$^{-/-}$ mutants (B,F,J,N). *Hoxb1b*$^{-/-}$ mutants have an increase in the A-P extent of r3 as observed in *epha4a* (C) and *krox20* (G) expression. The A-P extent of r4 is reduced in *hoxb1b*$^{-/-}$ mutants as seen in the space between r3/5 staining of *epha4a* (C) and *krox20* (G). The A-P extent of r5/6 is also slightly reduced in *hoxb1b*$^{-/-}$ mutants as seen by *val* (G), *hoxa3a* (K) and *hoxb3a* (O) expression. *Hoxb1a*$^{-/-}$;*hoxb1b*$^{-/-}$ mutants have a similar expansion or r3 and reduction in the A-P extent of r4 as evidenced by *epha4a* (D) and *krox20* (H) expression. The A-P extent of r5/6 is also reduced in *hoxb1a*$^{-/-}$;*hoxb1b*$^{-/-}$ mutants as seen by *val* (H), and *hoxb3a* (P) expression. *Hoxb1a*$^{-/-}$;*hoxb1b*$^{-/-}$ mutants also have a decrease in the expression of *hoxa3a* in r6 (L). All embryos have been genotyped for *hoxb1a*^{sa1191} and *hoxb1b*^{ua1006}. All embryos are dorsal views, anterior to the left, (A-D) 22 hpf, (E-P) 18 hpf. hpf, hours post fertilization.

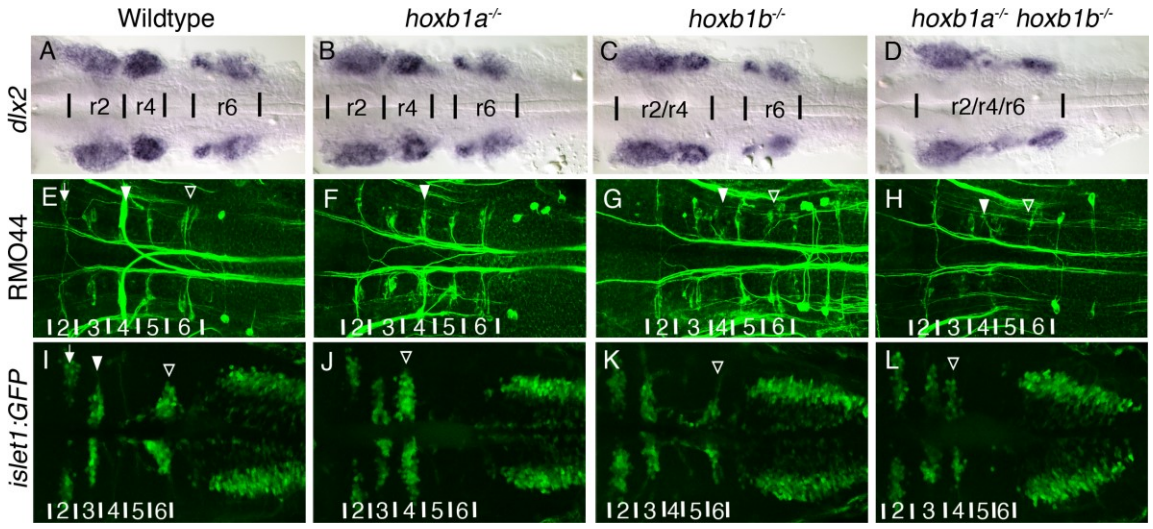

Figure 4.5. The loss of PG1 *hox* genes causes defects in both neural crest, and hindbrain associated neuronal populations.

In *hoxb1a*$^{-/-}$ mutants three neural crest streams exit the hindbrain (B), similar to wildtype (A). The r2 and r4 streams are fused in *hoxb1b*$^{-/-}$ mutants (9/9 embryos; C) and all three neural crest streams are less distinct in *hoxb1a*$^{-/-}$*;hoxb1b*$^{-/-}$ mutants, with the r4 stream being reduced (8/9 embryos; D). The Rol2 neurons (r2) (arrow), Mauthner neurons (r4) (filled arrowhead), and Mid3cm neurons (r6) (empty arrowhead) are reticulospinal neurons (labeled by RMO44) that project contralaterally across the midline (E). In *hoxb1a*$^{-/-}$ mutants the Mauthner neuron (r4) is lost (filled arrowhead), however there is a neuron resembling Rol2 in its position (10/10 embryos; F). In *hoxb1b*$^{-/-}$ (12/12 embryos; G) and *hoxb1a*$^{-/-}$*;hoxb1b*$^{-/-}$ (3/3 embryos; H) mutants, the Mauthner (filled arrowhead) and the Mid3cm (empty arrowhead) neurons are absent. Visualized with the transgenic *islet1:GFP* line, trigeminal BMNs differentiate to form two clusters in r2 (arrow) and r3 (filled arrowhead), the facial BMNs are born in r4 and subsequently their cell bodies migrate posteriorly to r6/7 and then laterally to their final positions (empty arrowhead; I). The facial BMNs fail to migrate posteriorly in *hoxb1a*$^{-/-}$ mutants (11/11 embryos; J), empty arrowhead). *Hoxb1b*$^{-/-}$ mutants specify fewer facial BMNs, however they migrate appropriately (12/12 embryos; K, empty arrowhead). In *hoxb1a*$^{-/-}$*;hoxb1b*$^{-/-}$ mutants there are fewer facial BMNs which fail to migrate posteriorly (5/5 embryos; L, empty arrowhead). All embryos have been genotyped for *hoxb1a*^{sa1191} and *hoxb1b*^{ua1006}. All images are dorsal views, anterior, to the left, (A-D) 22 hpf, (E-L) 48 hpf.

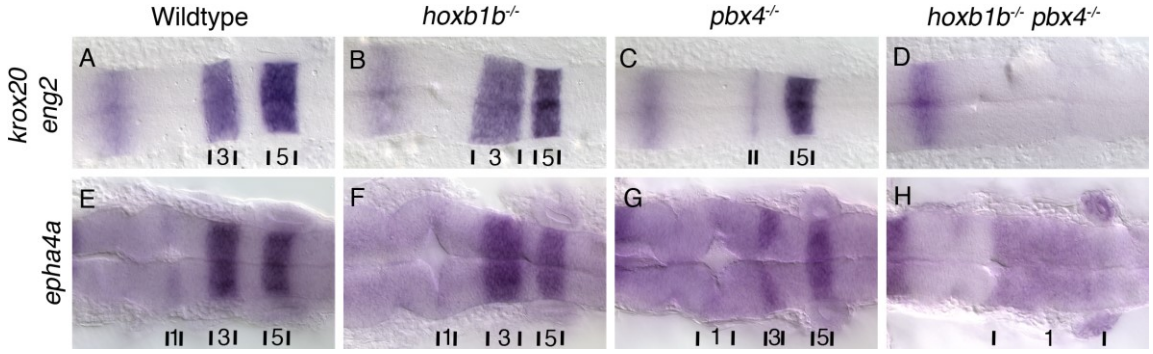

Figure 4.6. *Hoxb1b*$^{-/-}$;*pbx4*$^{-/-}$ double mutants revert to the r1-like ground state.

Eng2 expression in the midbrain-hindbrain boundary is observed in all embryos (A-D), however *krox20* and *epha4a* expression are altered. As previously observed, *hoxb1b*$^{-/-}$ mutants have an expanded r3 domain and a reduced r4 domain (6/6 embryos; B, F). In *pbx4*$^{-/-}$ mutants r3 is drastically reduced (12/12 embryos; C,G), and in *hoxb1b*$^{-/-}$;*pbx4*$^{-/-}$ double mutants all *krox20* expression in r3 and r5 is lost (3/3 embryos) (D), while the r1 domain of *epha4a* expression is expanded posteriorly throughout the hindbrain (3/3 embryos) (H). All embryos have been genotyped for *pbx4*^{b557} and *hoxb1b*^{ua1006}. All images are dorsal views, anterior to the left, 22 hpf.

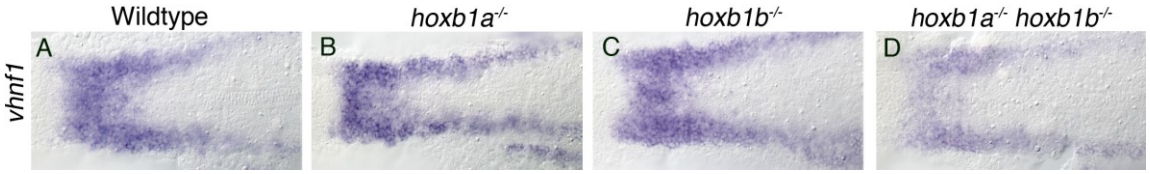

Figure 4.7. *Vhnf1* requires PG1 *hox* genes.

Vhnf1 shows reduced expression when both *hoxb1b* and *hoxb1a* are lost (5/5 embryos; D) compared to wildtype (A). This reduction is not observed when either *hoxb1a* (B) of *hoxb1b* (C) are lost alone. All embryos have been genotyped for *hoxb1a*^{sa1191} and *hoxb1b*^{ua1006}. All images are dorsal views, anterior to the left, 4 somite stage (11 hpf).

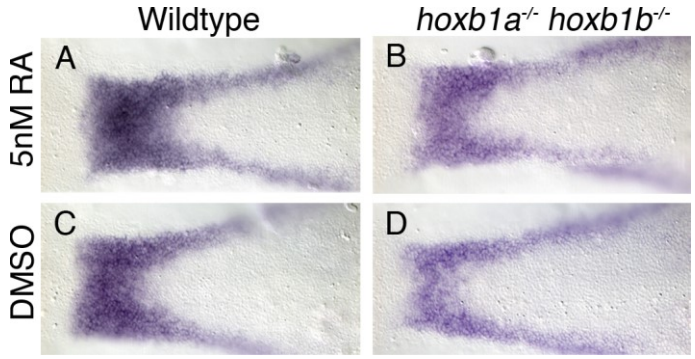

Figure 4.8. PG1 *hox* genes regulate *vhnf1* in a retinoic acid independent mechanism.

In order to determine if the decrease in *vhnf1* expression observed in *hoxb1a*$^{-/-}$ *hoxb1b*$^{-/-}$ mutants is due to defects in RA, embryos were treated with 5nM RA (A,B) or DMSO (C,D) and then *vhnf1* expression was analyzed. Wildtype embryos treated with 5nM RA (A) showed an increase in *vhnf1* expression as compared to those treated with DMSO (C). In *hoxb1a*$^{-/-}$;*hoxb1b*$^{-/-}$ mutants, there is an increase in expression of *vhnf1* in embryos treated with RA (3/3 embryos) (B), as compared to controls (D), however *vhnf1* expression has not recovered to wildtype levels (A). All embryos have been genotyped for *hoxb1a*^{sa1191} and *hoxb1b*^{ua1006}. All images are dorsal views, anterior to the left, 4 somite stage (11 hpf).

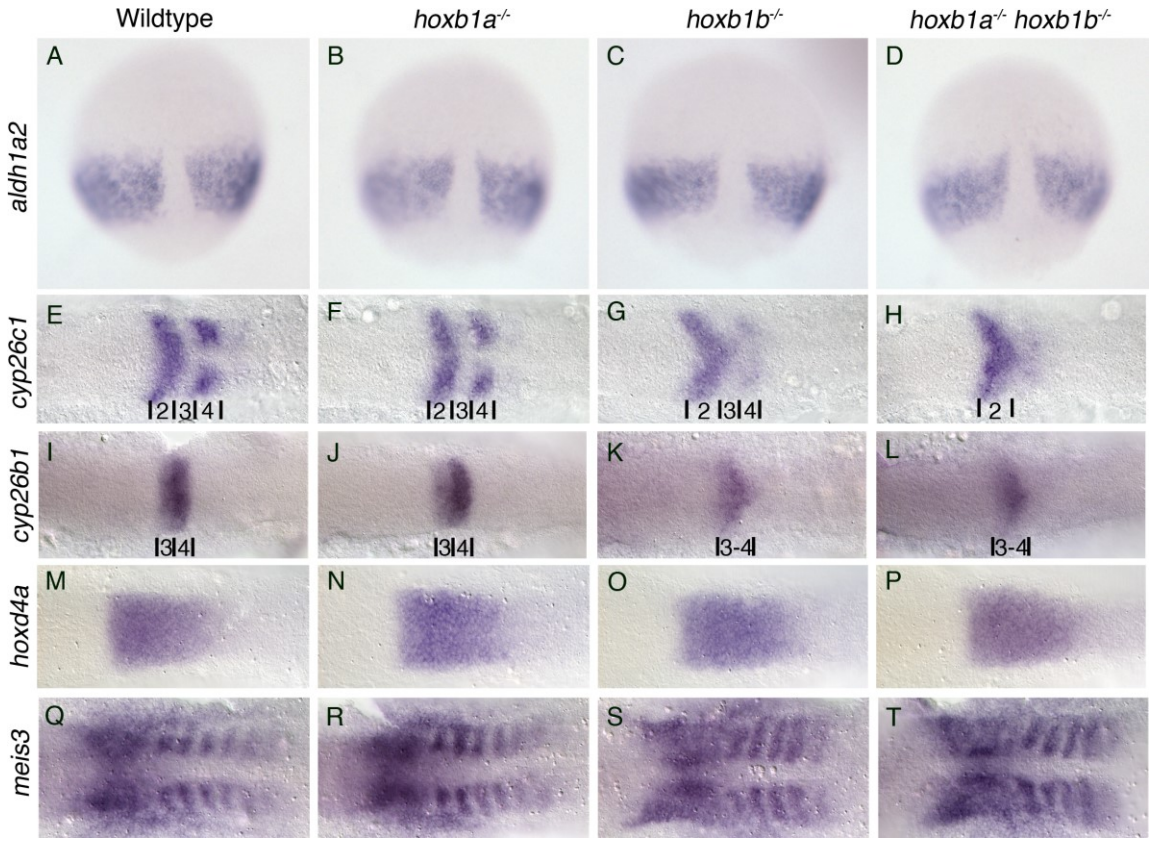

Figure 4.9. RA signaling is unaffected by the loss of PG1 *hox* genes.

The expression of *aldh1a2* at 70% epiboly (8hpf) is unchanged in paralog group 1 mutants (B, C, D) as compared to wildtype (A). The loss of *hoxb1b* causes a downregulation of *cyp26c1* (*hoxb1b*$^{-/-}$*:* 16/17 embryos, *hoxb1a*$^{-/-}$*;hoxb1b*$^{-/-}$*:* 7/7 embryos) (G, H) and *cyp26b1* (*hoxb1b*$^{-/-}$*:* 20/20 embryos, *hoxb1a*$^{-/-}$*;hoxb1b*$^{-/-}$*:* 8/8 embryos) (K, L) in r4. *hoxb1a*$^{-/-}$ mutants show no reduction in the expression of *cyp26c1* (F) or *cyp26b1* (J) in r4. The expression of RA dependent genes, *hoxd4a* (M-P) and *meis3* (Q-T) are unaffected by the loss of paralog group 1 *hox* genes. All embryos have been genotyped for *hoxb1a*^{sa1191} and *hoxb1b*^{ua1006}. All images are dorsal views, (A-D) anterior to the top, 70% epiboly (8 hpf), (E-T) anterior to the left, 4 somite stage (11 hpf).

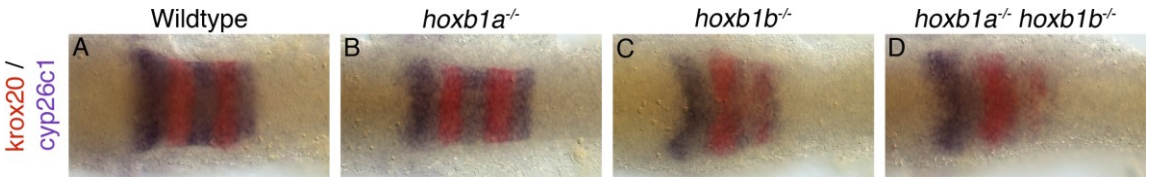

Figure 4.10. Two-color analysis of rhombomere identity with *cyp26c1*

The expression of *cyp26c1* is examined in combination with *krox20*. *Cyp26c1* is shown in purple, while *krox20* is shown in red. *Krox20* expression labels r3 and r5. *Cyp26c1* expression is observed in r2/4/6 in wildtype (A) and *hoxb1a*$^{-/-}$ mutants (B). The loss of *hoxb1b* causes a downregulation of *cyp26c1* in r4 (C, D). All embryos have been genotyped for *hoxb1a*^{sa1191} and *hoxb1b*^{ua1006}. All images are dorsal views, anterior to the left, 4-5 somite stage (11 hpf).

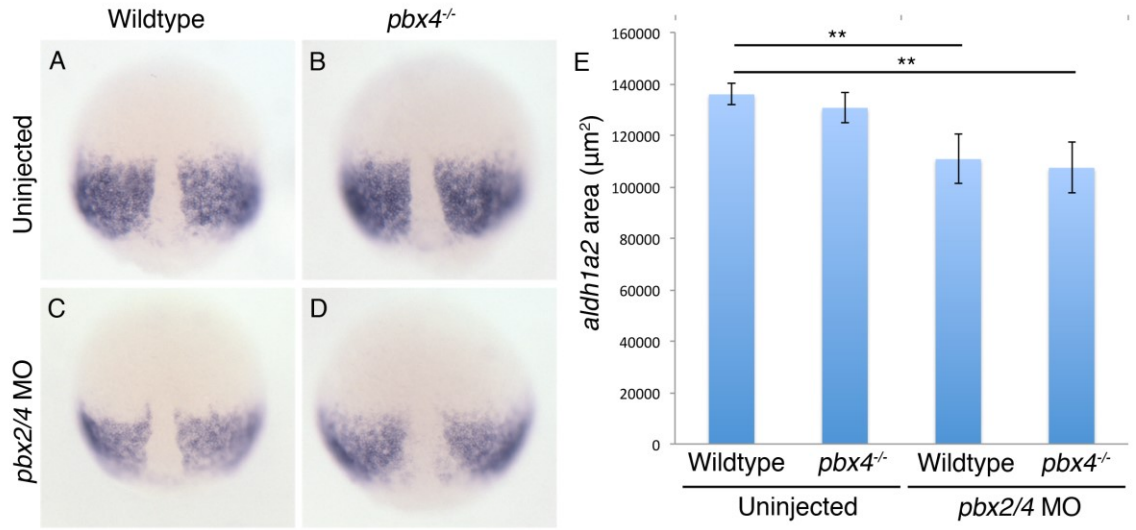

Figure 4.11. RA signaling is altered in *pbx* depleted embryos.

To determine if the loss of hindbrain identity is due to defects in RA signaling, *aldh1a2* expression was examined. *Pbx4*$^{-/-}$ mutants that are treated with *pbx2/4* morpholinos have a near complete knockdown of both maternal and zygotic Pbx. At early stages of hindbrain specification there is a decrease in *aldh1a2* expression in wildtype embryos treated with *pbx2/4* morpholinos (C) as compared to uninjected wildtype (A) or *pbx4*$^{-/-}$ mutants (B). There is a decrease in both *aldh1a2* expression level and domain in *pbx4*$^{-/-}$ mutants injected with *pbx2/4* morpholinos (22/22 embryos) (D). The area of *aldh1a2* expression was measured using Image J, and the average was calculated (E). Zygotic *pbx4*$^{-/-}$ mutants treated with *pbx2/4* morpholinos have a 21% decrease in the area of aldh1a2 expression compared to uninjected wildtype embryos. Error bars indicate standard deviation. Uninjected wildtype: 135890 µm^2, uninjected *pbx4*$^{-/-}$*:* 130628 µm^2, *pbx2/4*MO injected wildtype: 110737 µm^2, *pbx2/4*MO injected *pbx4*$^{-/-}$*:* 107364 µm^2. (ANOVA, post-hoc Tukey's: uninjected wildtype vs *pbx2/4*MO injected wildtype, p-value 0.003; uninjected wildtype vs *pbx2/4*MO injected *pbx4*$^{-/-}$, p-value 0.001) All embryos have been genotyped for *pbx4*^{b557}. All images are dorsal views, anterior to the top, 90% epiboly (9 hpf).

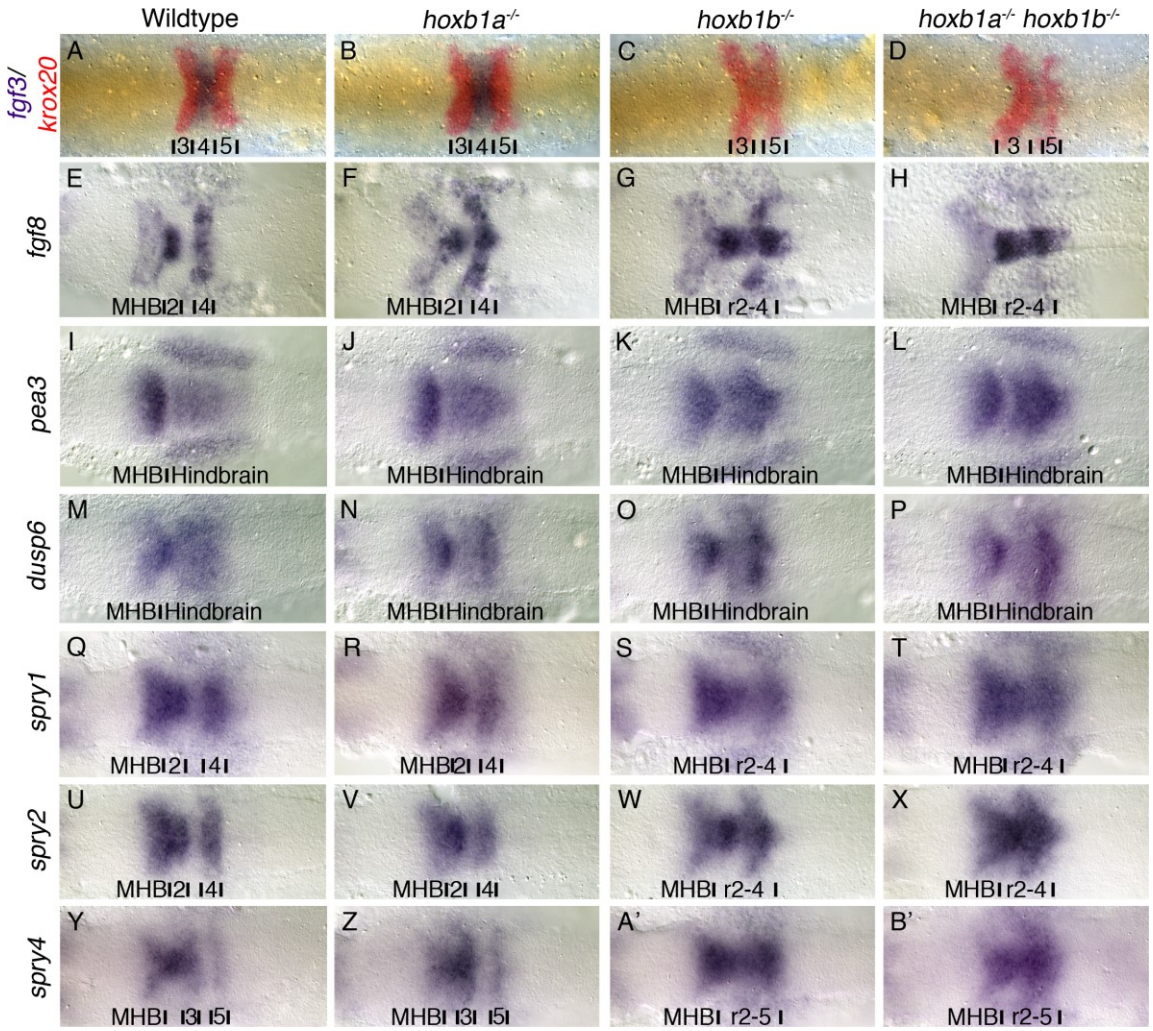

Figure 4.12. *Hoxb1b* regulates FGF signaling

Fgf3 is expressed in r4 in wildtype embryos (A) and *hoxb1a*$^{-/-}$ mutants (B). *Fgf3* expression is lost in *hoxb1b*$^{-/-}$ mutants (16/16 embryos; C) and *hoxb1a*$^{-/-}$;*hoxb1b*$^{-/-}$ mutants (4/4 embryos) (D). *Fgf8* is expressed in r4, medial r2 and the MHB (E). The loss of *hoxb1a* reduces the space between r2 and r4 and the MHB becomes arrowhead shaped (14/19 embryos; F). In *hoxb1b*$^{-/-}$ mutants (19/19 embryos; G) and *hoxb1a*$^{-/-}$ *hoxb1b*$^{-/-}$ mutants (8/8 embryos; H) there is ectopic expression of *fgf8* in r3 and reduced expression in the lateral portions of r4. The expression of FGF responsive genes, *pea3* (I-L), *dusp6* (M-P), *spry1* (Q-T), *spry2* (U-X), and *spry4* (Y-B') are unaltered from wildtype (I, M, Q, U, Y) in *hoxb1a*$^{-/-}$ mutants (J, N, R, V, Z). In both *hoxb1b*$^{-/-}$ mutants (*pea3:* 6/7 embryos, *dusp6:* 10/11 embryos, *spry1:* 25/25 embryos, *spry2:* 19/19 embryos, *spry4:* 23/23 embryos; K, O, S, W, A') and *hoxb1a*$^{-/-}$;*hoxb1b*$^{-/-}$ mutants (*pea3:*

6/6 embryos, *dusp6:* 5/5 embryos, *spry1:* 9/9 embryos, *spry2:* 5/5 embryos, *spry4:* 4/4 embryos; L, P, T, X, B') there is an increase in expression levels. *Spry1* and *spry2* show ectopic expression in r3 (S, T, W, X), while *spry4* is ectopically expressed in r4 (A', B'). All embryos have been genotyped for *hoxb1a*^{sa1191} and *hoxb1b*^{ua1006}. All images are dorsal views, anterior to the left, 4 somite stage (11 hpf).

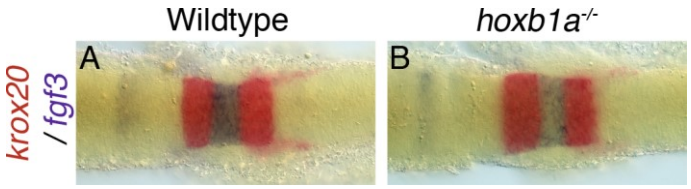

Figure 4.13. *Fgf3* is reduced in *hoxb1a* mutants by 10 somites

Fgf3 is expressed in r4 in wildtype embryos (A) and by 10 somite stage (12 hpf), *fgf3* expression is reduced in *hoxb1a*$^{-/-}$ mutants (B). All embryos have been genotyped for *hoxb1a*^{sa1191}. All images are dorsal views, anterior to the left, 10 somite stage (12 hpf).

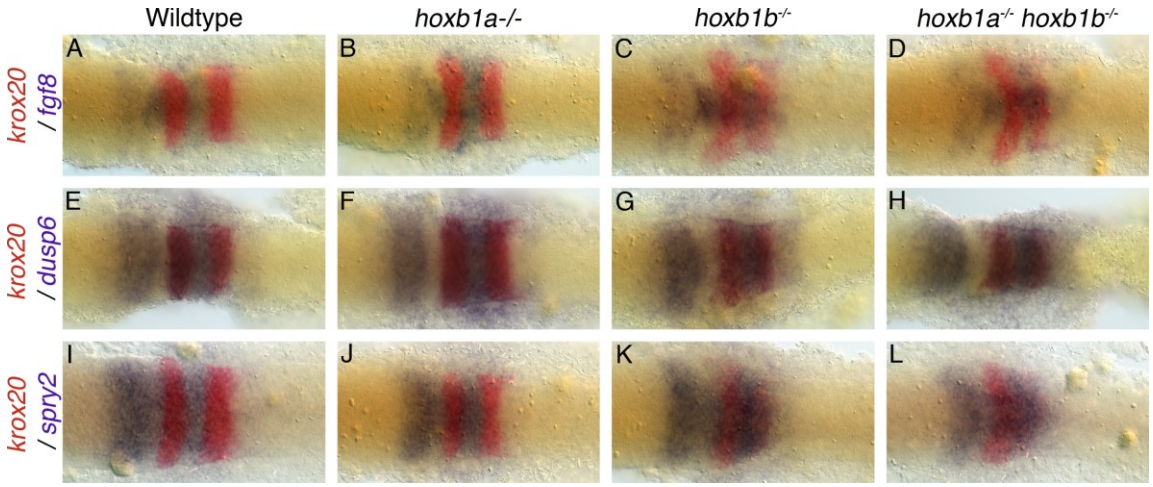

Figure 4.14. Two-color analysis of rhombomere identity with *fgf8, dusp6* and *spry2*

The expression of representative markers is examined in combination with *krox20*. *Fgf8, dusp6* and *spry2* are shown in purple, while *krox20* is shown in red. *Krox20* expression labels r3 and r5. *Fgf8* is expressed in r4, medial r2 and the MHB (A). The loss of *hoxb1a* reduces the space between r2 and r4 and the MHB becomes arrowhead shaped (B). In *hoxb1b*$^{-/-}$ mutants (C) and *hoxb1a*$^{-/-}$ *hoxb1b*$^{-/-}$ mutants (D) there is ectopic expression of *fgf8* in r3 and reduced expression in the lateral portions of r4. The expression of FGF responsive genes, *dusp6* (E-H), and *spry2* (I-L), are unaltered from wildtype (E, I) in *hoxb1a*$^{-/-}$ mutants (F,J). In both *hoxb1b*$^{-/-}$ mutants (G, K) and *hoxb1a*$^{-/-}$;*hoxb1b*$^{-/-}$ mutants (H, L) there is an increase in expression levels. *Spry2* shows ectopic expression in r3 (K, L). All embryos have been genotyped for *hoxb1a*^{sa1191} and *hoxb1b*^{ua1006}. All embryos are dorsal views, anterior to the left, 4-5 somite stage (11 hpf).

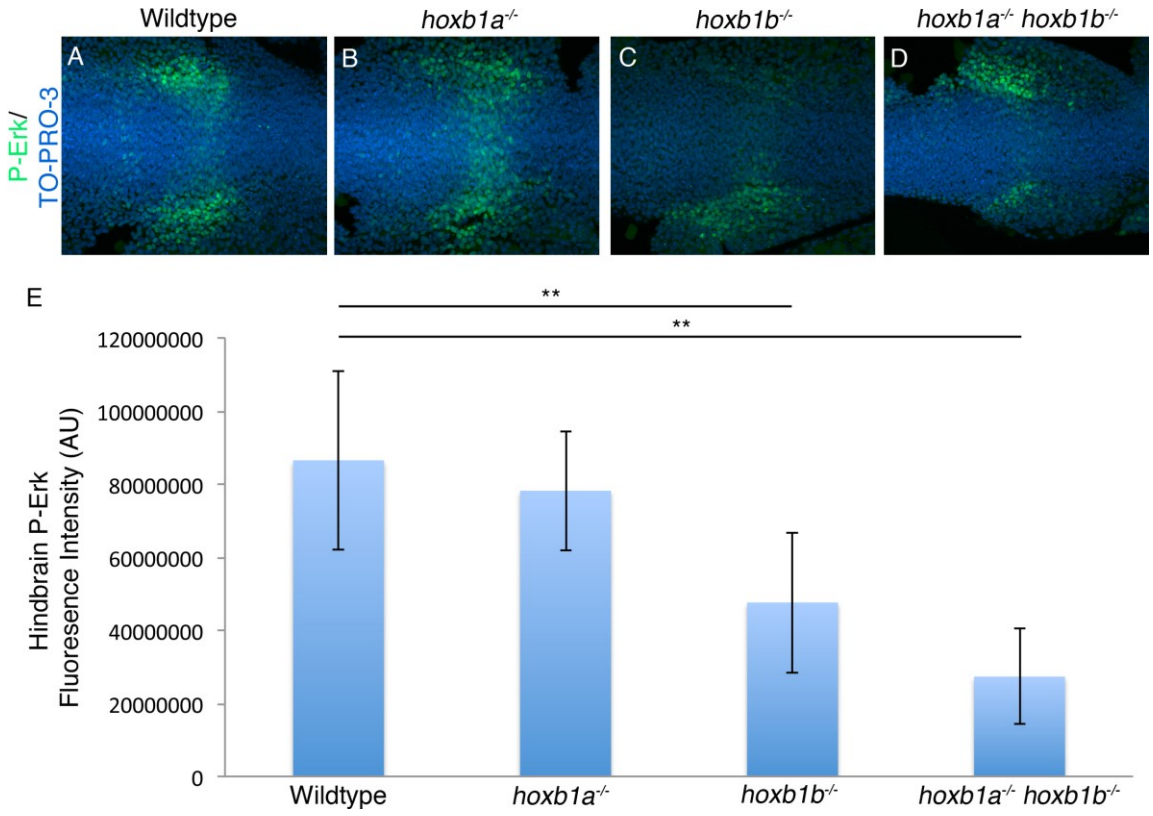

Figure 4.15. *Hoxb1b* regulation of FGF signaling results in decreased P-Erk localization

P-Erk is localized across the hindbrain in presumptive r4 and in lateral wings adjacent to the hindbrain in wildtype and *hoxb1a*$^{-/-}$ mutants (A-B). In *hoxb1b*$^{-/-}$ mutants (20/25 embryos; C) and *hoxb1a*$^{-/-}$ *hoxb1b*$^{-/-}$ mutants (9/9 embryos; D) P-Erk localization in the r4 domain across the hindbrain is reduced. Fluorescence intensity in the hindbrain was quantified using Image J, and the average fluorescence intensity was calculated (E). *Hoxb1b*$^{-/-}$ mutants have a 45% decrease in intensity while *hoxb1a*$^{-/-}$;*hoxb1b*$^{-/-}$ double mutants have a 68% decrease in intensity. Error bars indicate standard deviation. Wildtype: 86490590 AU, *hoxb1a*$^{-/-}$*:* 78175326 AU, *hoxb1b*$^{-/-}$: 47583826 AU, *hoxb1a*$^{-/-}$*;hoxb1b*$^{-/-}$*:* 27314030 AU (ANOVA, post-hoc Tukey's: Wildtype vs *hoxb1b*$^{-/-}$, p-value 0.007; Wildtype vs *hoxb1a*$^{-/-}$*;hoxb1b*$^{-/-}$, p-value 0.001) All embryos have been genotyped for *hoxb1a*^{sa1191} and *hoxb1b*^{ua1006}. All images are dorsal views, anterior to the left, 4 somite stage (11 hpf).

Chapter 5: Taz and Wnt/β-catenin signaling at rhombomere boundaries is required for ventricle morphogenesis

5.1 Introduction

Following neurulation in vertebrates, the brain is subdivided into the forebrain, midbrain and hindbrain. The lumen of the neural tube will form the cerebrospinal fluid (CSF) filled ventricles. During embryogenesis, the ventricles and the embryonic CSF (eCSF) provide similar circulatory functions as they do in adults, while also facilitating homeostatic, hormonal and morphogen signaling (Chodobski and Szmydynger-Chodobska, 2001; Emerich et al., 2005; Miyan et al., 2003; Sawamoto et al., 2006; Vigh and Vigh-Teichmann, 1998). Ventricle defects can result in hydrocephalus due to alterations in CSF production, absorption or flow (Ibanez-Tallon et al., 2004; Pourghasem et al., 2001; Zhang et al., 2006). Hydrocephalus occurs in up to 1/300 births (Zhang et al., 2006) and can cause severe perturbations in brain morphology and decreased neurogenesis (Mashayekhi et al., 2002). Numerous neurodevelopmental disorders including ADHD, Down's syndrome, Fragile X syndrome, schizophrenia and autism have been correlated with abnormalities with brain ventricle shape and size (Castellanos et al., 1996; Frangou et al., 1997; Gilmore et al., 2001; Hardan et al., 2001; Kurokawa et al., 2000; Nopoulos et al., 2007; Piven et al., 1995; Prassopoulos et al., 1996; Rehn and Rees, 2005; Reiss et al., 1995; Sanderson et al., 1999; Shenton et al., 2001; Wright et al., 2000). Thus, an understanding of the mechanisms required for proper ventricular development is vital to determine the causes underlying these disorders and may facilitate the development of potential treatments.

Several genes have been shown to be involved in the development of the ventricles. Defects in apicobasal polarity may result in compromised neuroepithelial integrity, thereby preventing midline separation during ventricle morphogenesis (Lowery et al., 2009). Mutations in apicobasal polarity components *mpp5a (membrane protein, palmitoylated 5a (MAGUK p55 subfamily member 5))* (Wei and Malicki, 2002), *crb2a (crumbs family member 2a)* (Omori and Malicki, 2006) and *prkci (protein kinase C, iota)* (Horne-Badovinac et al., 2001) results in ventricle defects (Lowery et al., 2009). Together, Mpp5a, Crb2a and Prkci interact and form a complex that colocalizes to the apical neuroepithelial surface where it regulates junction formation and polarity (Horne-Badovinac et al., 2001; Hsu et al., 2006; Omori and Malicki, 2006). Regulation of

cytoskeletal components is also important for ventricle development. Ppp1r12a (Protein phosphatase 1, regulatory subunit 12a) facilitates ventricle inflation through mediating epithelial relaxation via regulation of myosin contractility (Gutzman and Sive, 2010). Additionally, knockdown of hindbrain expressed transcription factors and morphogens results in ventricle defects. Knockdown of *zic1 (zic family member 1)* and *zic4 (zic family member 4)* results in loss of roof plate, and rhombomere boundary markers and midline separation defects in the hindbrain ventricle (Elsen et al., 2008). Furthermore, knockdown of roof plate and rhombomere boundary markers regulated by *zic1/4*, such as *wnt1*, *rfng (RFNG O-fucosylpeptide 3-beta-N-acetylglucosaminyltransferase/radical fringe homolog)* and *lmx1b (LIM homeobox transcription factor 1, beta)* result in midline separation defects (Elsen et al., 2008). Together, this suggests roles for distinct transcription factors and signaling pathways at rhombomere boundaries in ventricle development.

We wished to investigate roles for the transcriptional co-activator Taz, in ventricle development. Taz is most commonly associated with the canonical Hippo signaling pathway, where phosphorylation of the upstream kinases (Stk3, Sav1, Lats1/2, and Mob1a/1ba/1bb) results in the phosphorylation and inactivation of Taz/Yap. (Callus et al., 2006; Chan et al., 2005; Dong et al., 2007; Huang et al., 2005; Lei et al., 2008; Liu et al., 2010; Oh and Irvine, 2008; Praskova et al., 2008; Zhao et al., 2010; Zhao et al., 2007). When Taz/Yap are not phosphorylated, they can translocate to the nucleus where they bind to the promoters of target genes (Dong et al., 2007; Kanai et al., 2000; Lei et al., 2008; Oh and Irvine, 2008; Ren et al., 2010; Zhao et al., 2007) primarily through interactions with the TEAD (TEA domain) family of transcription factors (Goulev et al., 2008; Vassilev et al., 2001; Wu et al., 2008; Zhang et al., 2008; Zhao et al., 2008a).

The roles of Yap and Taz have most commonly been studied in relation to their role in cancer, however they have also been implicated in diverse tissues and processes. Tead transgenic reporters (*Tg(4xGTIIC:d2EGFP))* have suggested roles for Taz/Yap in epidermis, otic and lens vesicles, retinal pigmented epithelium (RPE), cardiac progenitor cells, presumptive sinus venosus, multiple cell types in the heart, striated muscles of the trunk and undifferentiated endoderm (Miesfeld and Link, 2014). Although *taz* mutants in zebrafish have been reported to have no overt morphological phenotypes (Miesfeld et

al., 2015), studies using knockdown techniques and work in other model systems, support roles for Taz and Yap in body axis specification, posterior body elongation, development of the thyroid, kidney, lateral line, heart, vascular system, and retina (Agarwala et al., 2015; Gee et al., 2011; Hu et al., 2013; Kim et al., 2017a; Kimelman et al., 2017; Miesfeld et al., 2015; Miesfeld and Link, 2014; Nagasawa-Masuda and Terai, 2017; Nakajima et al., 2017; Pappalardo et al., 2015; Tian et al., 2007). Yap/Taz activity is often associated with the maintenance of neural progenitors (Cao et al., 2008; Gee et al., 2011; Han et al., 2015; Hindley et al., 2016; Lavado et al., 2013; Milewski et al., 2004; Ramalho-Santos et al., 2002; Zhang et al., 2011a) and *Yap* is required for the generation of ependymal cells within the brain ventricles (Park et al., 2016). Yap/Taz frequently regulate cytoskeletal and extracellular matrix components in a variety of developmental contexts, including the deposition of fibronectin in the epidermis and notochord (Kimelman et al., 2017), and regulation of actomyosin contractility and extracellular matrix proteins in the vascular system (Kim et al., 2017a; Nagasawa-Masuda and Terai, 2017).

Recent work has characterized an additional role for Taz in Wnt/β-catenin signaling (Azzolin et al., 2014; Azzolin et al., 2012) (Summarized in Fig 5.1 A). When no Wnt ligands are present, Yap/Taz bind to Axin1, and are incorporated into the β-catenin destruction complex. Subsequently Gsk3 phosphorylates β-catenin. Yap/Taz then recruits the E3-ubiquitin ligase, β-TrCP, which then targets both Yap/Taz and β-catenin for degradation. In this way the β-catenin destruction complex acts as a cytoplasmic sink for Yap/Taz, preventing nuclear translocation, while also triggering the eventual degradation of the protein. Conversely when Wnt ligand is present, it induces the clustering of the Lrp5/6 receptors, which then compete with Yap/Taz for binding to Axin1. Axin1 binding to Lrp5/6 releases both β-catenin and Yap/Taz, which allows nuclear translocation. Once in the nucleus β-catenin binds TCF/Lef and activates target gene expression, while Yap/Taz will activate target gene expression through interactions with other transcription factors, such as TEAD. This interaction supports a model in which some outputs of Wnt signaling previously attributed to β-catenin mediated transcription, are in fact due to Yap/Taz mediated transcription. This interaction has been shown in *in vitro* systems as well as in *in vivo* models, such as the adult murine

small intestine (Azzolin et al., 2014; Azzolin et al., 2012). Further support for these interactions comes from previous research that has shown that Taz phosphorylation mediates interaction between itself and the $SCF^{\beta\text{-}TrCP}$ E3 Ligase complex (Tian et al., 2007).

Multiple *wnt* genes are expressed in the hindbrain during development, and at least 4 *wnt* genes (*wnt1, wnt10b, wnt3a* and *wnt8b*) are upregulated at rhombomere boundaries (Lekven et al., 2003; Riley et al., 2004). Elevated levels of *wnt* at rhombomere boundaries regulate patterning of the rhombomeres and Delta signals from boundary adjacent regions provide feedback to maintain the rhombomere boundaries as Wnt signaling centers (Riley et al., 2004). Segmentation mutants such as *mindbomb,* in which *wnt* gene expression at rhombomere boundaries is disrupted, have a disorganization of cell types and they fail to form boundary associated cell types (Riley et al., 2004). *Mindbomb* mutants have also been shown to have defects in ventricle development (Schier et al., 1996). Similarly, loss of *wnt1* via morpholino mediated knockdown, or as is seen in *Limx1a* (*Dreher*) mouse mutants result in defects in ventricle development (Elsen et al., 2008; Manzanares et al., 2000; Millonig et al., 2000). The interaction of Taz with the β-catenin destruction complex (Azzolin et al., 2014; Azzolin et al., 2012), suggests that tissues and processes that Wnt signaling has been found to be involved in may also be experiencing Taz-mediated regulation of target gene expression.

In this chapter, we investigated a developmental context for interactions between Taz and Wnt signaling. We demonstrate that Taz protein localizes to rhombomere boundaries, and loss of function of *taz* results in midline separation defects in the hindbrain ventricle and mislocalization of apicobasal polarity components and F-actin. We observe an interaction between *taz* and the Wnt signaling pathway that supports a role for the Wnt signaling pathway in stabilizing Taz at rhombomere boundaries during ventricle morphogenesis. Furthermore, we determined that both β-catenin mediated transcription and Taz-mediated transcription are involved in morphogenesis of the hindbrain ventricle.

5.2 Results

5.2.1 Loss of function of *taz* results in midline separation defects

To investigate roles for *taz* during zebrafish development we created mutants for *taz* (*wwtr1*) using Transcription activator-like effector nuclease (TALEN) mediated mutagenesis (Cermak et al., 2011). *Taz*^{ua1015} mutants contain a 29bp deletion 25bp downstream of the start codon (I9KfsX12) that results in a frameshift mutation and truncation within the TEAD binding domain (Fig 5.1 B). This predicted protein lacks all functional domains. Utilizing a previously identified Taz antibody (Miesfeld et al., 2015), we find that Taz protein localizes to the rhombomere boundaries in the hindbrain (Fig 5.1 C). This antibody recognizes an epitope surrounding Asp362 in the transactivation domain of the human TAZ protein (Asp353 in zebrafish). Full length Taz protein should not be made in *taz*$^{ua1015/ua1015}$ homozygous mutants, and we do see a substantial loss of Taz antibody localization to the rhombomere boundaries in *taz*$^{ua1015/ua1015}$ mutants (hereafter referred to as *taz*$^{-/-}$ mutants). Any residual staining may be due to cross-reactivity between the antibody and endogenous Yap protein.

Previous reports of *taz* mutants have not identified any overt morphological phenotypes by 24hpf (Miesfeld et al., 2015), although Taz has been reported to be involved in thyroid development (Pappalardo et al., 2015), kidney development (Tian et al., 2007), and differentiation of mesenchymal stem cells into osteoblasts and adipocytes (Hong et al., 2005a). Further roles for Taz in combination with Yap have been identified in the neural retina and RPE (Miesfeld et al., 2015), neural progenitors and stem cells (Han et al., 2015; Lavado et al., 2013), epidermal morphogenesis and posterior body elongation (Kimelman et al., 2017), dorsal caudal vein plexus regression (Nagasawa-Masuda and Terai, 2017) and in sprouting angiogenesis and vascular barrier maturation (Kim et al., 2017a). Our examination of *taz*$^{-/-}$ mutants reveals defects in the hindbrain ventricle morphology (Fig 5.2 A). This defect can be clearly visualized utilizing the injection of fluorescently labeled dextran into the CSF of the hindbrain ventricle (Gutzman and Sive, 2009) (Fig 5.2B). Apart from the alteration to ventricle morphology, *taz*$^{-/-}$ mutants largely lack any other major morphological defects (Fig 5.2 A).

Aberrations to hindbrain ventricle morphology are broadly characterized as either defects in the initial shaping of the brain and opening of the ventricle, which is apparent by 20-21 hpf (hours post fertilization), or as defects in the later phases of brain expansion, which become apparent by 28 hpf or later (Lowery et al., 2009). To determine which phase of ventricle development may be affected by the loss of Taz, we undertook a time course from 22 – 36 hpf, using expression of *atoh1a* mRNA in the upper and lower rhombic lips (Kani et al., 2010) to define the edges of the hindbrain ventricle. Decreased ventricle size is observed at 22hpf (Fig 5.2 C-D) where the area of *taz*$^{-/-}$ mutant ventricles is 53% of that of wildtype ventricles (wildtype: 18645 μm^2, *taz*$^{-/-}$ mutants: 9998 μm^2, p-value 0.001). This trend persists to 36hpf (24hpf - wildtype: 20762 μm^2, *taz*$^{-/-}$ mutants: 10208 μm^2, 49%, p-value 0.0002; 28hpf - wildtype: 22696 μm^2, *taz*$^{-/-}$ mutants: 10255 μm^2, 45%, p-value 0.0001; 36hpf - wildtype: 28114 μm^2, *taz*$^{-/-}$ mutants: 15862 μm^2, 56%, p-value 0.0003; Fig 5.2 C-D). *Taz*$^{-/-}$ mutants show a characteristic midline separation defect, similar to those observed in *nok* (*nagie oko/membrane protein, palmitoylated 5a (mpp5a)*), *ome* (*oko meduzy/crumbs family member 2a (crb2a)*), *has* (*heart and soul/protein kinase C, iota (prkci)*), *zon* (*zonderzen*) and *atl* (*atlantis*) mutants (Lowery et al., 2009). This class of mutants is uniquely characterized by neuroepithelial cells that fail to separate at the midline (Lowery et al., 2009).

5.2.2 Localization of actin and apicobasal polarity complexes is abnormal in *taz* mutants

We next wished to determine if there are any changes in apically localized proteins in *taz* mutants. Previous work (Lowery et al., 2009; Lowery and Sive, 2005) has shown that components of the Crumbs complex are required for brain ventricle formation, and loss of *mpp5a (membrane protein, palmitoylated 5a (MAGUK p55 subfamily member 5, crb2a (crumbs family member 2a)* or *prkci (protein kinase C, iota)* results in a disorganized epithelium, and a failure of the ventricle to open, similar to the phenotype we see in *taz*$^{-/-}$ mutants. Crumbs is a type I transmembrane protein and together with Mpp5a, Prkci and Lin7c scaffolding proteins they form an evolutionarily conserved complex that is an integral component of apicobasal polarity (Bachmann et

al., 2001; Hong et al., 2001; Horne-Badovinac et al., 2001; Hsu et al., 2006; Kamberov et al., 2000; Omori and Malicki, 2006; Yang et al., 2009). This complex may also be involved in stabilization of the actin cytoskeleton through interactions of Mpp5a through its FERM (Protein 4.1/Ezrin/Radixin/Moesin) binding domain with FERM family members, which have a conserved role in stabilizing actin (Bretscher et al., 2002).

To determine if apicobasal polarity, or actin stabilization is affected by the loss of *taz*, we assayed for Crb2a (*crumbs family member 2a*) and actin localization. In wildtype embryos, Crb2a and actin are localized consistently along the apical surface of the ventricle (Fig 5.3 A-C). At points where the midline fails to separate in *taz*$^{-/-}$ mutants, there is a lack of midline localization of Crb2a and actin (Fig 5.3 A-C). This is consistent with the disorganization of midline localized proteins observed in *mpp5a, crb2a* and *prkci* mutants (Lowery et al., 2009; Lowery and Sive, 2005), and may indicate that *taz* is required for the correct distribution of apicobasal polarity components, and actin organization.

We investigated potential FERM family members that may be mis-regulated in *taz*$^{-/-}$ mutants. Homologs of the FERM family members Merlin and Expanded (Ex), have already been associated with the Hippo signaling pathway, both as upstream regulators and as downstream effectors (Hamaratoglu et al., 2006). The vertebrate homologs of Merlin are *nf2a* and *nf2b*, while the homologs of Expanded is less clear. Researchers have suggested that *frmd6* and/or *angiomotin* may fulfill the roles of Ex in vertebrates (Angus et al., 2012; Bossuyt et al., 2014; Genevet and Tapon, 2011; Gunn-Moore et al., 2005; Moleirinho et al., 2013). To determine if there are any changes in these FERM family members we assayed for changes in the mRNA expression levels of Merlin and Ex homologs in mutant hindbrains. We found that *nf2b* mRNA levels are significantly altered in *taz*$^{-/-}$ mutants (Fig 5.3 D, Wildtype – 1, *taz*$^{-/-}$ mutants – 1.6663; p-value 0.0118), while the expression of other paralogs/homologs of Merlin/Ex are not changed (Fig 5.4). This supports a role for Taz in ensuring the apical localization of the Crumbs complex, actin and regulating expression of *nf2b*, which may be involved in this process.

5.2.3 Taz interacts with the β-catenin destruction complex in ventricle morphogenesis

As Taz is known to interact with multiple signaling pathways, we wanted to determine if Taz is interacting with any other signaling pathways in the hindbrain to regulate ventricle morphogenesis. The Wnt signaling pathway is a potential candidate that may be interacting with Taz in this process. There are multiple Wnt ligands expressed in the hindbrain (Brand et al., 1996; Buckles et al., 2004; Elsen et al., 2008; Lekven et al., 2003; Riley et al., 2004; Thisse and Thisse, 2005), and at least 4 *wnt* genes have enriched expression at rhombomere boundaries (*wnt1*, *wnt10b*, *wnt3a* and *wnt8b*) (Lekven et al., 2003; Riley et al., 2004), suggesting that Wnt signaling involved in hindbrain development. Additionally, knockdown of *wnt1* results in midline separation defects (Elsen et al., 2008), similar to those observed in *taz*$^{-/-}$ mutants. In combination with previous research that has characterized a role for Taz in Wnt/β-catenin signaling (Azzolin et al., 2014; Azzolin et al., 2012), this supports a hypothesis where Taz cooperates with Wnt signaling in ventricle morphogenesis.

To determine if the Wnt signaling pathway is involved in generating the midline separation defect observed in *taz*$^{-/-}$ mutants, we used Wnt agonists and antagonists to assay for their effect on Taz stabilization and localization, and midline separation of the ventricle. First we used the Wnt antagonist XAV939, which stabilizes Axin by inhibiting Tankyrase enzymes (which stimulate Axin degradation via ubiquitin proteasomal degradation) (Huang et al., 2009). XAV939 has previously been used in zebrafish to inhibit canonical Wnt signaling (Angbohang et al., 2016; Nishiya et al., 2014; Robertson et al., 2014; Wincent et al., 2015). The stabilization of Axin, should also stabilize the β-catenin destruction complex, and consequently the interaction between Taz with β-TrCP, resulting in constitutive proteasomal degradation of both Taz and β-catenin (Fig 5.5 A). If this is the case, then treatment with XAV939 should phenocopy *taz*$^{-/-}$ mutants, as Taz protein will no longer be stabilized at rhombomere boundaries. Wildtype embryos treated with DMSO exhibit normal ventricle morphogenesis and Taz localization to rhombomere boundaries (Fig 5.5 B), however upon treatment with 5 μM XAV939, embryos exhibit a striking phenocopy of the *taz*$^{-/-}$ mutant phenotype. XAV939 treated embryos have midline separation defects and a decrease in Taz localization to

rhombomere boundaries, which we hypothesize is due to increased proteasomal degradation of Taz (DMSO: 22229 μm^2, 5 μM XAV939: 10266 μm^2, 46%; p-value ≤ 0.0001, Fig 5.5 B-C).

We next used the Wnt agonist SB216763, which inhibits Gsk3 through competitive binding of the ATP pocket (Coghlan et al., 2000; Jacobs et al., 2012). SB216763 has previously been used in zebrafish as a Gsk3 inhibitor, and it has been shown to have an activating effect on the Wnt pathway (Anichtchik et al., 2008; Chelko et al., 2016; Zhong et al., 2009). We predict that Gsk3 inhibition will prevent the proteasomal degradation mediated by the β-catenin destruction complex, resulting in increased stabilization of Taz and β-catenin (Fig 5.6 A). Taz and β-catenin are then free to enter the nucleus and regulate target gene expression (Coghlan et al., 2000). While DMSO-treated wildtype controls show normal ventricle morphogenesis and Taz localization to rhombomere boundaries (Fig 5.6 C), treatment with 10 μM SB216763 results in a decrease in ventricle size, but most strikingly, there is an overall increase in Taz protein immunofluorescence throughout the hindbrain, indicating that Gsk3 inhibition, results in Taz stabilization (Between rhombomeres: DMSO - 1366221 AU, 10 μM SB216763 – 2397700 AU, 175%, p-value ≤ 0.0001; At rhombomere boundaries: DMSO - 3910998 AU, 10 μM SB216763 – 5677218 AU, 145%; p-value ≤ 0.0001, Fig 5.6 C-D). The increase in Taz protein levels throughout the hindbrain, and not just at rhombomere boundaries, may be explained by the expression of *taz* mRNA. *In situ* hybridization for *taz* reveals ubiquitous expression throughout the brain, with an enrichment of *taz* mRNA in the roof plate (Fig 5.6 D). As taz mRNA is present throughout the brain, Wnt signaling at rhombomere boundaries may be required for the specific maintenance of Taz protein at these boundaries, and pharmacologically stimulating Wnt signaling throughout the hindbrain results the in the stabilization of Taz protein throughout the hindbrain as well.

Together these experiments support the model (Azzolin et al., 2014; Azzolin et al., 2012) showing an interaction between Taz and the β-catenin destruction complex. We present evidence for a role for this interaction in a novel developmental context, ventricle morphogenesis.

5.2.4 Both β-catenin and Taz mediated transcription are required for ventricle morphogenesis

As the interaction between Taz and Wnt/β-catenin signaling is involved in ventricle morphogenesis, we wanted to determine if β-catenin-mediated transcription through Tcf/Lef, and Taz-mediated transcription, are required for ventricle development. To determine if β-catenin-mediated transcription is required for ventricle midline separation, we first used two inhibitors, ICG-001 and Windorphen to specifically block the interaction of β-catenin with the transcriptional co-activators, cyclic AMP response element-binding protein (CBP) and p300 (Emami et al., 2004; Hao et al., 2013; Hecht et al., 2000; Takemaru and Moon, 2000). Both ICG-001 and Windorphen have previously been characterized in zebrafish as having inhibitory effects on β-catenin (Delgado et al., 2014; Hao et al., 2013; Maftouh et al., 2014; Nishiya et al., 2014). Treatment of wildtype embryos with 200 μM ICG-001 + 100 μM Windorphen results in defects in ventricle morphogenesis, specifically the ventricles are smaller, and some have midline separation defects (DMSO: 18990 μm^2, 200 μM ICG-001 + 100 μM Windorphen: 10178 μm^2, 54%; p-value 0.0015, Fig 5.7 A-B). To verify that these effects are due to the specific loss of β-catenin mediated transcription, we employed a second approach. We utilized a dominant repressive Tcf3 (drTcf3) construct (courtesy of Richard Dorsky) in which the first 47 amino acids of the protein are truncated, removing the β-catenin interaction domain, and preventing β-catenin mediated transcriptional activation. This construct was overexpressed mosaically in developing embryos. Mosaic overexpression ensures that not all cells have disrupted Wnt signaling, which in early development would result in gross defects in dorsoventral patterning and a failure of the embryo to develop to the point where we can observe ventricle development. In the cells that contain the overexpressed construct, the drTcf3 will competitively bind to target genes and inhibit β-catenin/Tcf3 mediated transcription. The drTcf3 construct was overexpressed with eGFP as a marker, so we can identify cells in which β-catenin/Tcf3 mediated transcription is being repressed. In control embryos with mosaic expression of eGFP alone, ventricle morphogenesis proceeds normally (Fig 5.7 C). In embryos that have mosaic co-expression of eGFP and drTcf3 we see aberrant ventricle morphogenesis and midline separation defects, indicating that β-catenin/Tcf3 mediated transcription is

required for normal ventricle development (Fig 5.7 C). Additionally, as we do not see ventricle defects only in cells with eGFP expression, this may indicate a cell non-autonomous requirement for β-catenin mediated transcription.

Next, to determine if Taz-mediated transcription is required for ventricle development, we overexpressed full length and various truncated forms of *taz* mRNA in *taz*$^{-/-}$ mutants, and assayed for rescue of ventricle size (Fig 5.8 A). We predict that if transcriptional activation activity mediated by Taz is required for ventricle morphogenesis then only mRNA overexpression of *taz* constructs containing the full length transcription activation domain should be able to rescue ventricle morphogenesis in *taz*$^{-/-}$ mutants. To first validate that *taz* mRNA is able to rescue the ventricle phenotype in *taz*$^{-/-}$ mutants we overexpressed wildtype (WT) *taz* mRNA and measured ventricle size (Fig 5.8 B). Wildtype ventricles in embryos treated with control RNA (eGFP) have an average area of 26863 μm^2 while mutant embryos have an average area of 15000 μm^2 (56%, p-value 0.001). Injection of WT *taz* mRNA increased mutant ventricle size to 20571 μm^2 (77%, p-value 0.1155; Fig 5.8 B). Injection of *taz* mRNA lacking the transcription activation domain (Taz ΔWW and Taz ΔCC) fails to increase ventricle size, resulting in average areas of 8045 μm^2 and 13394 μm^2 respectively (Taz ΔWW – 30%, p-value 0.001; Taz ΔCC - 50%, p-value 0.001; Fig 5.8 B). Truncation of the transcriptional activation domain (Taz ΔTA) also fails to increase ventricle size in *taz*$^{-/-}$ mutants, resulting in an average area of 14064 μm^2 (52%, p-value 0.001; Fig 5.8 B). The truncation of just the PDZ binding domain (Taz ΔPDZ) is able to rescue ventricle size in *taz*$^{-/-}$ mutants to 23688 μm^2 (88%, p-value 0.6458; Fig 5.8 B), indicating that the PDZ binding domain is not required for ventricle morphogenesis. Overexpression of WT *taz* or any of the truncated versions of *taz* in wildtype embryos did not result in a statistically significant change in ventricle size (Fig 5.9). Together, this supports a requirement for Taz-mediated transcription, and not just Taz interactions with the β-catenin destruction complex in ventricle morphogenesis.

5.3 Discussion

5.3.1 Taz localization to rhombomere boundaries is required for 4th ventricle morphogenesis

Taz protein is localized specifically at rhombomere boundaries, and loss of *taz* results in defective ventricle morphogenesis. Ventricle defects can be observed as early as 22 hpf, where ventricle size is reduced by 53% due to failure of the midline to separate. This phenotype is similar to that observed in *mpp5a* (*membrane protein, palmitoylated 5a*), *crb2a* (*crumbs family member 2a*), *prkci* (*protein kinase C, iota*), *zon* (*zonderzen*) and *atl* (*atlantis*) mutants (Lowery et al., 2009).

The alterations in ventricle morphogenesis we observe in $taz^{-/-}$ mutants are associated with defects in apicobasal polarity. Mutations in components of the crumbs complex (*mpp5a crb2a* and *prkci*) (Lowery et al., 2009; Lowery and Sive, 2005) cause midline separation defects, similar to those we observe in $taz^{-/-}$ mutants. Membrane association of Crb has been shown to be necessary and sufficient to confer apical character (Wodarz et al., 1995). Crb is required to target Mpp5a to the apical surface, and loss of *crb* results in mis-localization of Mpp5a (Zou et al., 2013). Mpp5a and Crb contain FERM (4.1/Ezrin/Radixin/Moesin) binding domains, which allow them to interact with proteins such as Merlin (Mer) and Expanded (Ex) (Bretscher et al., 2002; Grzeschik et al., 2010; Hamaratoglu et al., 2006; Ling et al., 2010; Pellock et al., 2007; Robinson et al., 2010). FERM domain containing proteins link trans-membrane proteins with the actin cytoskeleton (Bretscher et al., 2002), and mislocalization, or loss of one component may result in mislocalization of the other components. Mer and Ex have previously been linked to the Hippo pathway, not only as upstream regulators of Yki, but also as transcriptional targets of Yki (Hamaratoglu et al., 2006). The vertebrate homologs of *Merlin*, are *nf2a* and *nf2b* in zebrafish, while the vertebrate homolog of *Expanded* is less clear. Sequence homology suggests that *frmd6* is homologous to *Ex*, and it may fulfill some of the functions of Ex in vertebrates (Angus et al., 2012), while other research has suggested that Angiomotin may fulfill some of the functions of Ex (Bossuyt et al., 2014; Genevet and Tapon, 2011; Gunn-Moore et al., 2005; Moleirinho et

al., 2013).

Our work supports a role for apicobasal polarity proteins, actin and FERM-domain containing proteins in ventricle morphogenesis. *Taz*$^{-/-}$ mutants have disruptions in the apical localization of both Crb2a and actin, and misregulation of *nf2b* expression. The changes in mRNA levels of *nf2b*, or localization of Crb2a or actin may result in the mislocalization or mis-regulation of the other apicobasal polarity components, and may underlie the failure of the midline to separate (similar to the midline separation defects observed in mutants for other components of the Crumbs complex (Lowery et al., 2009; Lowery and Sive, 2005)). Additionally, while our experiments have shown that *nf2b* mRNA levels are altered, there may be further changes in the subcellular localization of Nf2b, or other homologs of Mer and Ex.

5.3.2 Taz and Wnt/β-catenin signaling interact to facilitate midline separation

Previous work has proposed that Taz is required for Wnt/β-catenin signaling (Azzolin et al., 2014; Azzolin et al., 2012). Axin binds to Taz and upon phosphorylation of β-catenin by Gsk3, Taz recruits β-TrCP which ubiquitinates and targets Taz and β-catenin for proteasomal degradation. Wnt binding sequesters the β-catenin destruction complex, preventing degradation of both Taz and β-catenin, and allowing nuclear translocation and regulation of target gene expression. Our experiments support this role for Taz in the β-catenin destruction complex. Stabilization of the β-catenin destruction complex reduces Taz protein levels, and phenocopies the loss of *taz*, while inhibition of the β-catenin destruction complex stabilizes Taz protein throughout the hindbrain. Furthermore, while this interaction has been shown to occur *in vitro* and in the murine intestine and liver, we provide new evidence that this interaction is required for hindbrain ventricle morphogenesis in zebrafish. This is a novel developmental context for Taz involvement in Wnt/β-catenin signaling.

Wnt ligands such as *wnt1*, *wnt10b*, *wnt3a* and *wnt8b* are enriched at rhombomere boundaries (Lekven et al., 2003; Riley et al., 2004), and given the localization of Taz to rhombomere boundaries and the interaction with Wnt/β-catenin signaling, this supports a model in which Wnt signaling at rhombomere boundaries stabilizes Taz and β-catenin,

while decreased levels of Wnts between rhombomere boundaries results in reduced Taz localization (Fig 5.10). The requirement for Taz at rhombomere boundaries is supported by previous work, that indicates rhombomere boundary associated genes are involved in ventricle morphogenesis. Loss of function of *sfpq (splicing factor proline/glutamine-rich)*, *med12* and *mindbomb* result in disruption of rhombomere boundaries, loss of rhombomere boundary associated gene expression, and defects in ventricle development (Appel et al., 1999; Hong and Dawid, 2011; Itoh et al., 2003; Qiu et al., 2004; Riley et al., 2004; Schier et al., 1996; Thomas-Jinu et al., 2017) Furthermore, knockdown of rhombomere boundary associated genes such as *wnt1* and *rfng* also results in midline separation defects (Amoyel et al., 2005; Cheng et al., 2004; Elsen et al., 2008). Morpholino mediated knockdowns have been shown to disrupt expression of rhombomere boundary markers, as an off-target activation of the Tp-53-mediated cell death pathway. So although the knockdowns of rhombomere boundary genes themselves may not be the cause of midline separation defects, morpholino-mediated disruption of rhombomere boundary gene expression may still cause midline separation defects. In combination with our examination of *taz*$^{-/-}$ mutants, this supports a role for rhombomere boundaries and rhombomere boundary associated genes in ventricle morphogenesis.

Given the localization of Taz protein in the hindbrain in wildtype embryos, it is likely that Taz and β-catenin are required at rhombomere boundaries for the regulation of target gene expression. Selective inhibition of the interaction of β-catenin with cyclic AMP response element-binding protein (CBP) and p300 (Emami et al., 2004; Hao et al., 2013; Hecht et al., 2000; Takemaru and Moon, 2000) prevents the majority of β-catenin mediated transcription, and results in ventricle defects. Our results support a role for β-catenin mediated transcription in ventricle morphogenesis, however previous research has suggested that knockdown of Yap/Taz results in activation of β-catenin target genes in the absence of Wnt signals (Azzolin et al., 2014; Tschaharganeh et al., 2013). Therefore, in *taz*$^{-/-}$ mutants, not only is there a loss of Taz at rhombomere boundaries, but there may also be ectopic β-catenin between rhombomere boundaries, that fails to be degraded. This may support a complex role for the activation and repression of β-catenin in specific domains in the hindbrain. While incorporation of Taz into the β-catenin destruction complex is undoubtedly important for stabilizing Taz, and presumably β-

catenin at rhombomere boundaries, we provide evidence that Taz-mediated transcription is also important for ventricle morphogenesis. The absence of the Taz transcription activation domain results in defects in ventricle midline separation defects. Overexpression of full-length *taz* is able to rescue ventricle development in *taz*$^{-/-}$ mutants, while *taz* that does not contain the full transcription activation domain fails to rescue ventricle development in *taz*$^{-/-}$ mutants. Together this supports the role of Taz as a component of the β-catenin destruction complex, while also suggesting roles for Taz and β-catenin mediated transcription in separation of the midline and ventricle morphogenesis.

5.4 Figures

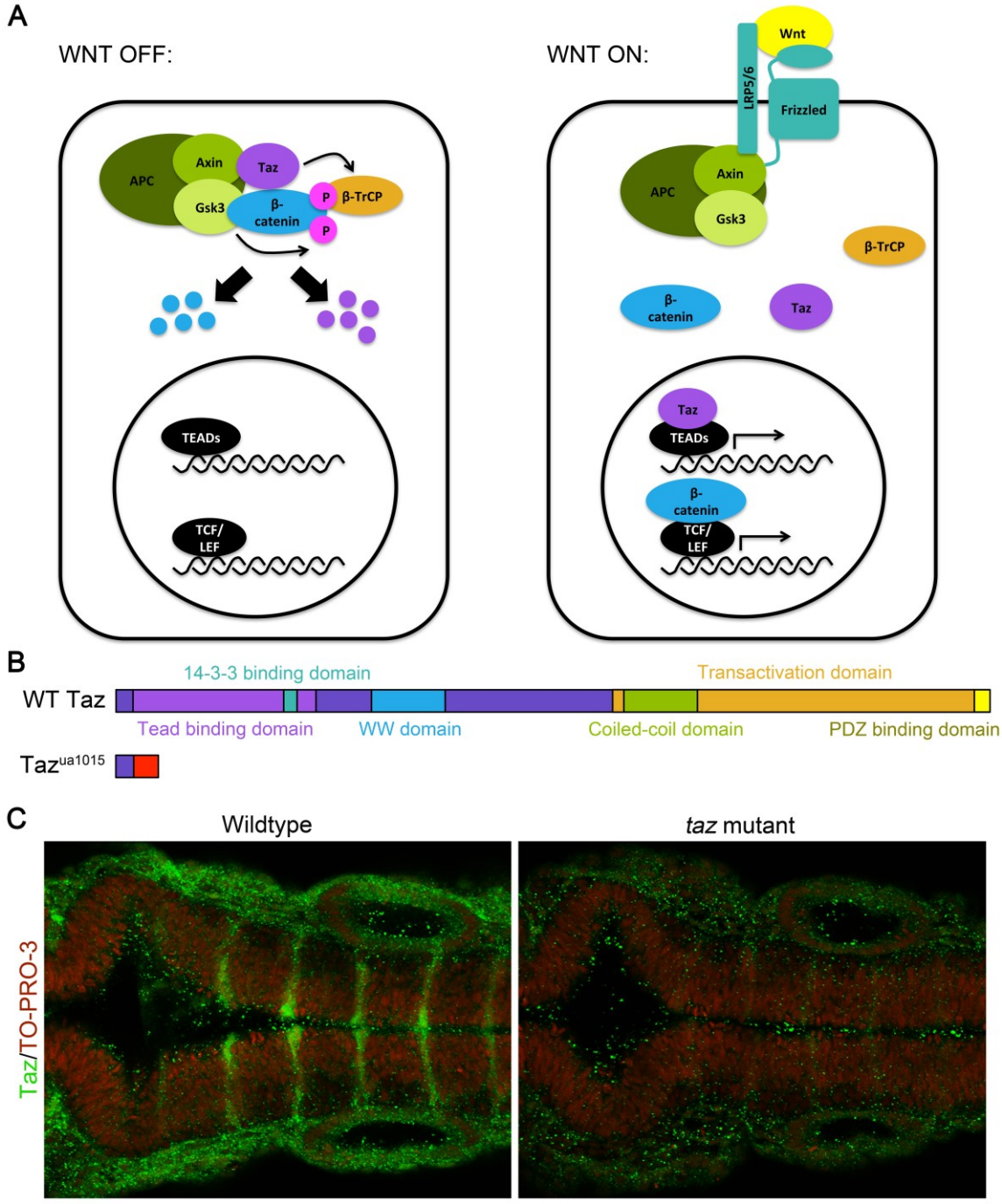

Figure 5.1. *Taz*^{ua1015} mutations.

(A) Taz is a component of the β-catenin destruction complex. In the absence of Wnt ligands, Taz is bound by Axin and upon β-catenin phosphorylation by Gsk3, Taz recruits β-TrCP which ubiquitinates both Taz and β-catenin, targeting them for proteasomal

degradation. Upon Wnt binding, the β-catenin destruction complex is inactivated and both β-catenin and Taz are free to translocate to the nucleus and regulate target gene transcription. (B) Wildtype Taz encodes a 391 amino acid protein. The protein has a Tead binding domain, and 14-3-3 binding domain, a WW domain, a transactivation domain, containing a coiled-coil domain and a PDZ binding domain. *Taz*^{ua1015} mutants have a 29 bp deletion 25 bp downstream of the start codon (I9KfsX12), resulting in a loss of all functional domains. (C) In wildtype embryos Taz protein localizes to the rhombomere boundaries (green). Nuclei are labeled in red with TO-PRO-3. In *taz*$^{-/-}$ mutants, this localization is largely lost. Any residual staining may be due to cross-reactivity of the antibody with endogenous Yap protein. Embryos are dorsal view, anterior to the left, 24 hpf.

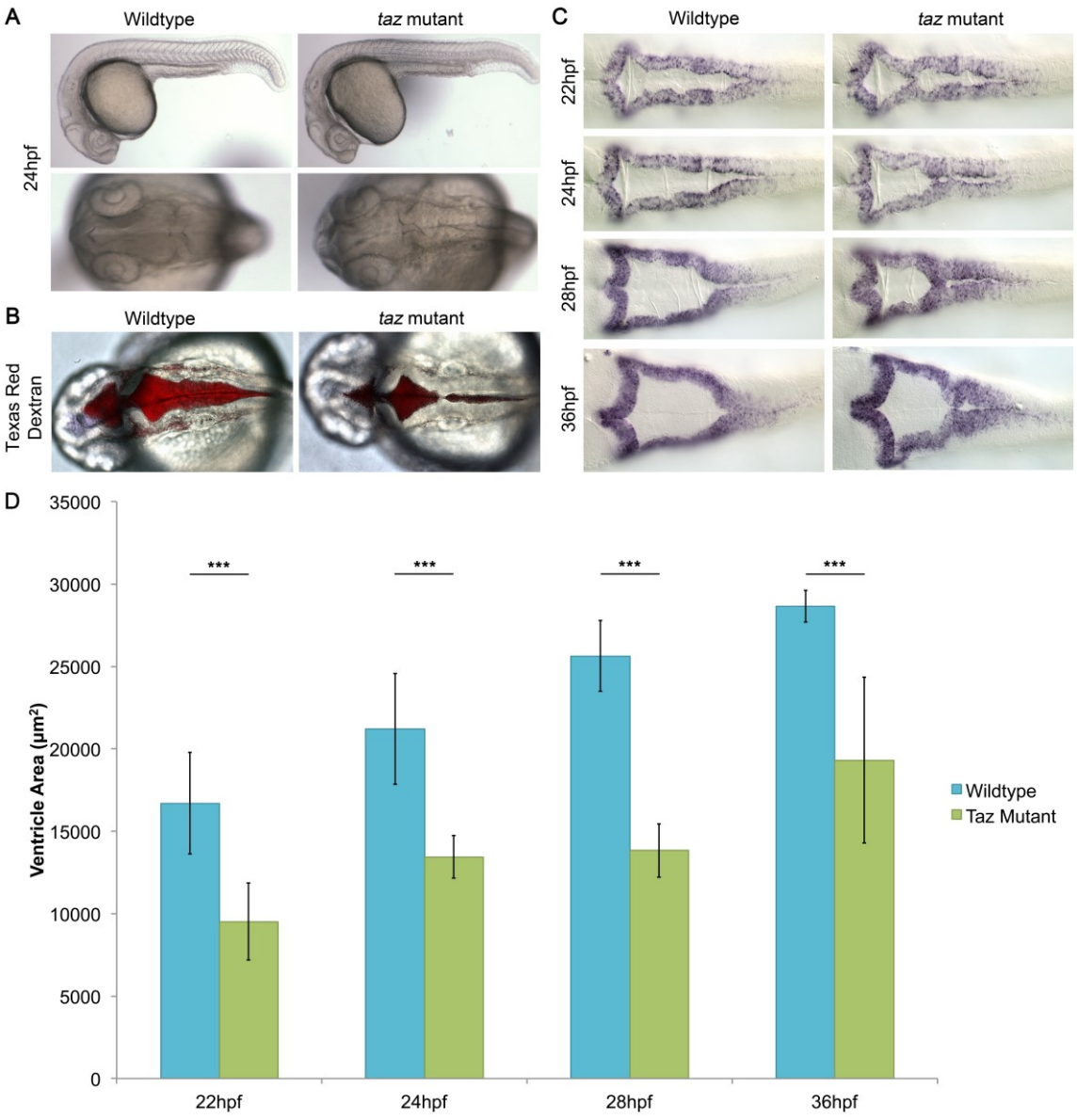

Figure 5.2. *Taz* mutants have defects in hindbrain ventricle morphogenesis.

(A) Live images of wildtype and *taz*$^{-/-}$ mutants show that *taz* mutants have alterations in hindbrain ventricle morphology, but do not have any other major morphological defects at 24 hpf. (B) Injection of Texas-Red labeled Dextran into the CSF of the hindbrain ventricle clearly illustrates the hindbrain ventricle midline separation defect observed in *taz*$^{-/-}$ mutants as compared to wildtype. (C) Ventricle defects are apparent from 22-36 hpf in *taz*$^{-/-}$ mutants, as visualized by *in situ* hybridization with the upper and lower rhombic lip marker, *atoh1a*. (D) Ventricle area was measured from 22-36 hpf in

wildtype and *taz*$^{-/-}$ mutant embryos. At 22 hpf *taz*$^{-/-}$ mutant ventricles are 53% of the size of wildtype ventricles (wildtype: 18645 μm^2, *taz*$^{-/-}$ mutants: 9998 μm^2, p-value 0.001). At 24 hpf *taz*$^{-/-}$ mutant ventricles are 49% of the size of wildtype ventricles (24hpf - wildtype: 20762 μm^2, *taz*$^{-/-}$ mutants: 10208 μm^2, p-value 0.0002). At 28 hpf *taz*$^{-/-}$ mutant ventricles are 45% of the size of wildtype ventricles (wildtype: 22696 μm^2, *taz*$^{-/-}$ mutants: 10255 μm^2, p-value 0.0001). At 36 hpf *taz*$^{-/-}$ mutant ventricles are 56% of the size of wildtype ventricles (wildtype: 28114 μm^2, *taz*$^{-/-}$ mutants: 15862 μm^2, p-value 0.0003). Statistical analysis was performed by Two-way ANOVA with a post-hoc Tukey test. All images are anterior to the left, (A, top row) lateral views, (A, bottom row; B-C) dorsal views, (A-B) 24 hpf, (C) are stages indicated on the left of panel.

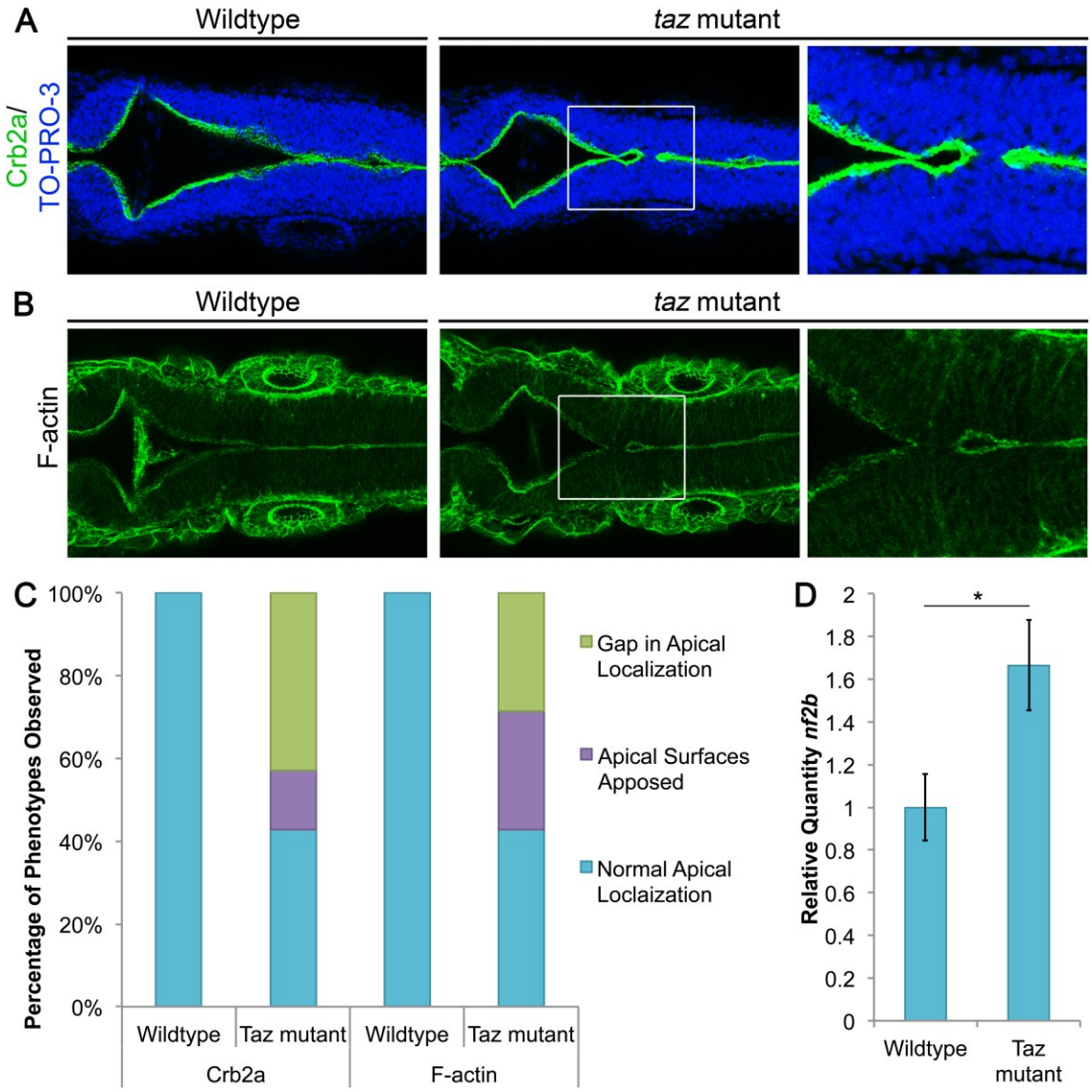

Figure 5.3. *Taz* mutants have abnormal localization of actin and apicobasal polarity components.

(A) Crb2a localization is shown in green, nuclei are labeled in blue with TO-PRO-3. In *taz*$^{-/-}$ mutants, there are disruptions in apical localization of Crb2a. (B) F-actin is labeled in green. In *taz*$^{-/-}$ mutants there are disruptions in the apical localization of F-actin. (C) Quantification of the phenotypes observed in *taz*$^{-/-}$ mutants. 57% of *taz*$^{-/-}$ mutants have abnormal localization of Crb2a (43% have gaps in apical localization). 57% of *taz*$^{-/-}$ mutants have abnormal localization of F-actin (29% have gaps in apical localization). (D) Real-time quantitative PCR analysis was performed on cDNA generated from dissected wildtype and *taz*$^{-/-}$ mutant hindbrain tissue for *nf2b*. *Nf2b* expression levels are

increased in *taz*$^{-/-}$ mutants (1.6663) as compared to wildtype (1), p-value: 0.0118, T-test. All images are dorsal views, anterior to the left, 22 hpf.

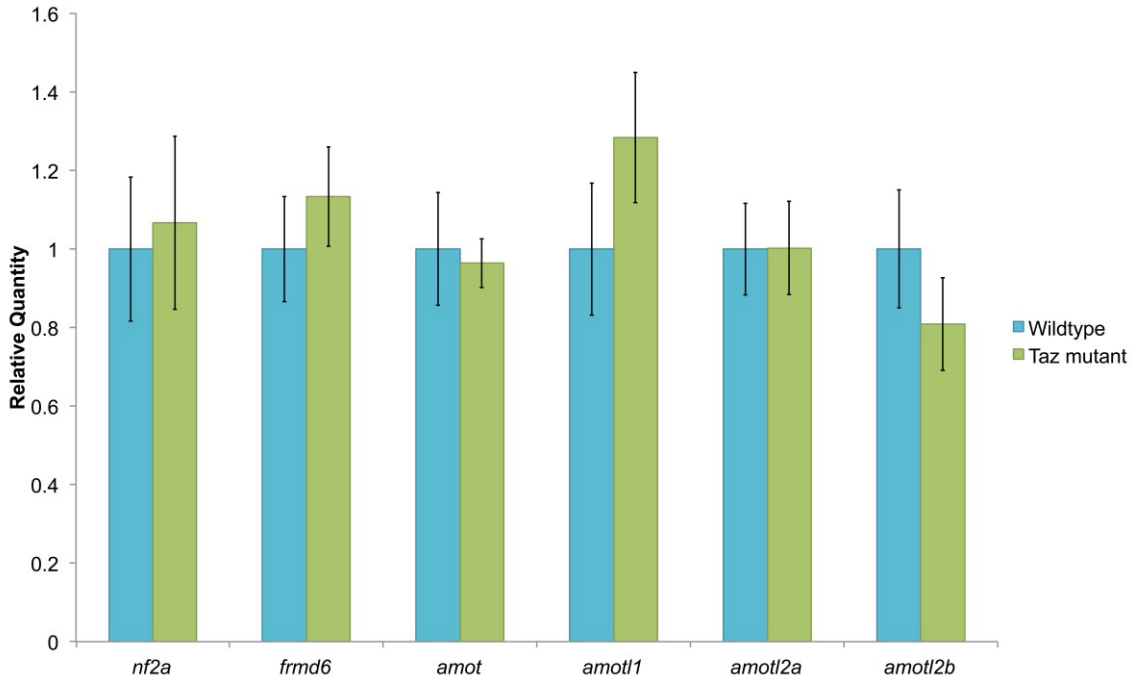

Figure 5.4. qPCR analysis of other FERM domain family members

Real-time quantitative PCR analysis was performed on cDNA generated from dissected wildtype and *taz*$^{-/-}$ mutant hindbrain tissue. The relative quantity for each gene was normalized to 1 for wildtype embryos. In *taz*$^{-/-}$ mutant embryos the relative quantity for each gene was: 1.0668 for *nf2a* (p-value 0.7075, T-test), 1.1329 for *frmd6* (p-value 0.2795, T-test), 0.9637 for *amot* (p-value 0.7082, T-test), 1.2834 for *amotl1* (p-value 0.1064, T-test), 1.0023 for *amotl2a* (p-value 0.982, T-test), and 0.8085 for *amotl2b* (p-value 0.1571, T-test).

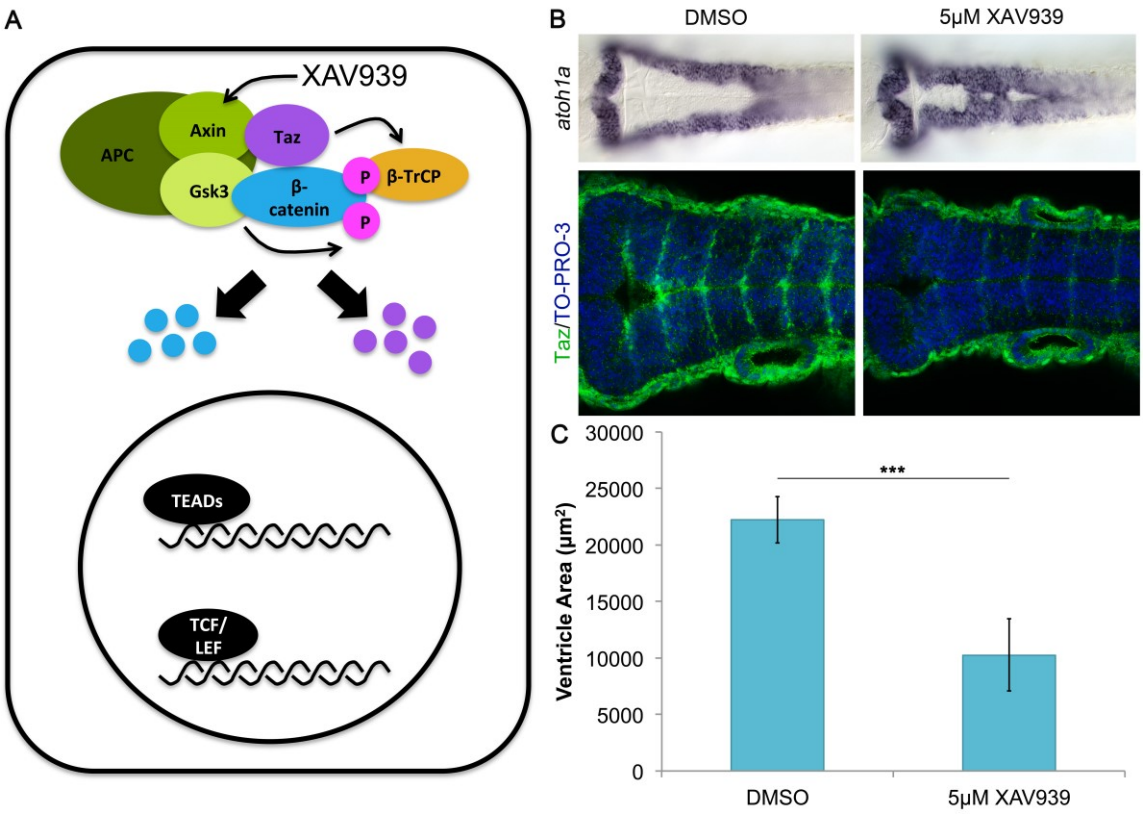

Figure 5.5. Stabilization of the β-catenin destruction complex phenocopies the *taz* mutant phenotype.

(A) The Wnt antagonist XAV939 is a Tankyrase inhibitor. Inhibition of Tankyrase stabilizes Axin, and the β-catenin destruction complex. If Taz is incorporated into the β-catenin destruction complex in zebrafish, then stabilization of the β-catenin destruction complex should cause constitutive degradation of both β-catenin and Taz, and result in phenotypes similar to *taz* loss of function. (B) Treatment of embryos with 5 μM XAV939 results in midline separation defects and a loss of Taz protein (shown in green) at rhombomere boundaries, while control treatments with DMSO does not affect ventricle morphogenesis or Taz localization. Nuclei are labeled in blue with TO-PRO-3. (C) Measurement of ventricle area shows that treatment of embryos with 5 μM XAV939 results in a 46% decrease in size as compared to DMSO controls (DMSO: 22229 μm^2, 5 μM XAV939: 10266 μm^2, p-value $\leq$ 0.0001, T-test). All embryos are dorsal views, anterior to the left, 24 hpf.

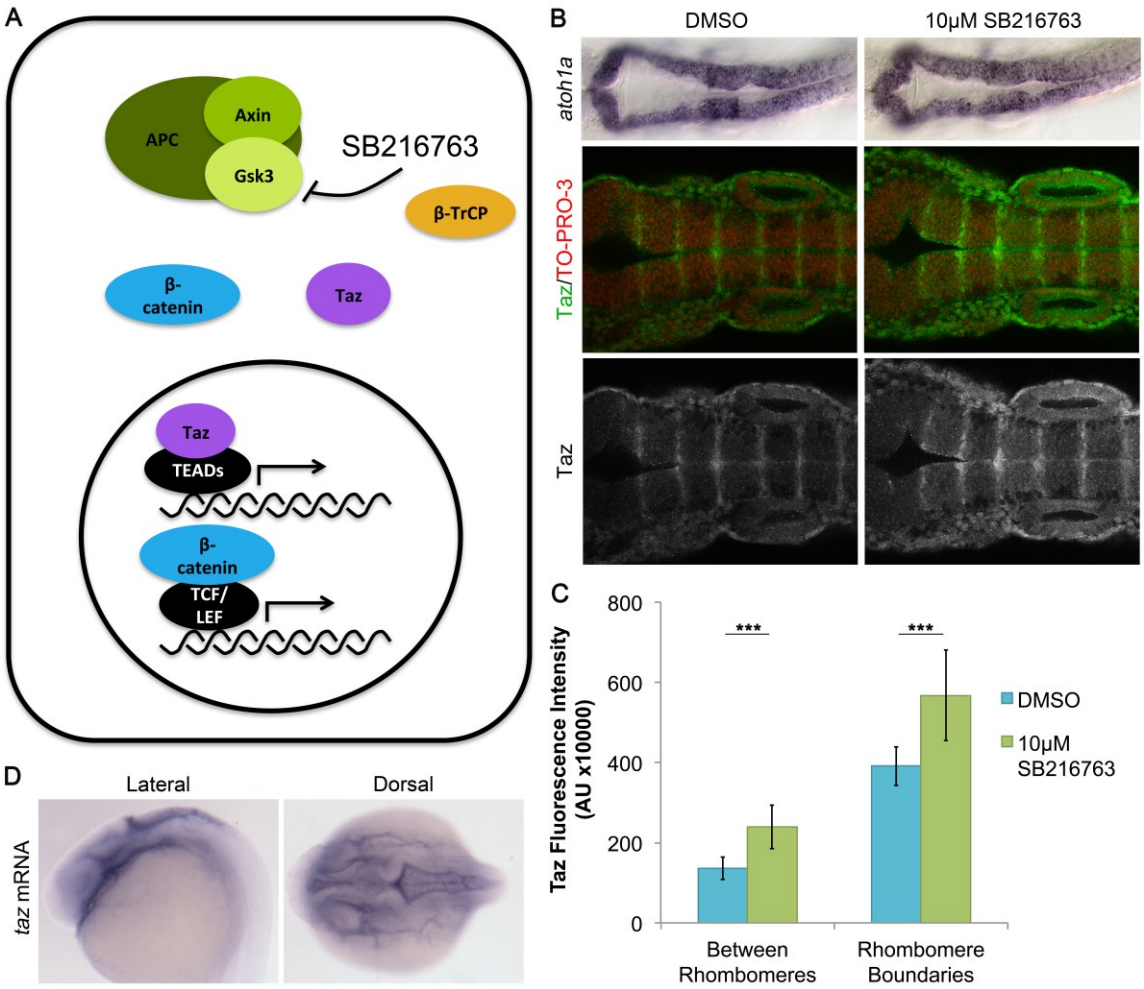

Figure 5.6. Inhibition of the β-catenin destruction complex stabilizes Taz throughout the hindbrain.

(A) The Wnt agonist SB216763 inhibits Gsk3, preventing phosphorylation of β-catenin, and the degradation of both Taz and β-catenin. (B) Treatment with 10 μM SB216763 results in slightly smaller ventricles, and an increase in Taz protein localization throughout the hindbrain as compared to DMSO treated controls. (C) Taz immunofluorescence at rhombomere boundaries and between rhombomere boundaries was measured. Taz fluorescence in embryos treated with 10 μM SB216763 was increased by 175% between rhombomeres (DMSO - 1366221 AU, 10 μM SB216763 – 2397700 AU, p-value ≤ 0.0001, T-test) and by 145% at rhombomere boundaries (DMSO - 3910998 AU, 10 μM SB216763 – 5677218 AU, p-value ≤ 0.0001, T-test). (D) The increase in Taz immunofluorescence throughout the hindbrain can be explained by the detection of *taz* transcripts throughout the hindbrain by *in situ* hybridization. All

embryos are anterior to the left, 24 hpf, (B, D-right side) are dorsal views, (D – right side) is a lateral view.

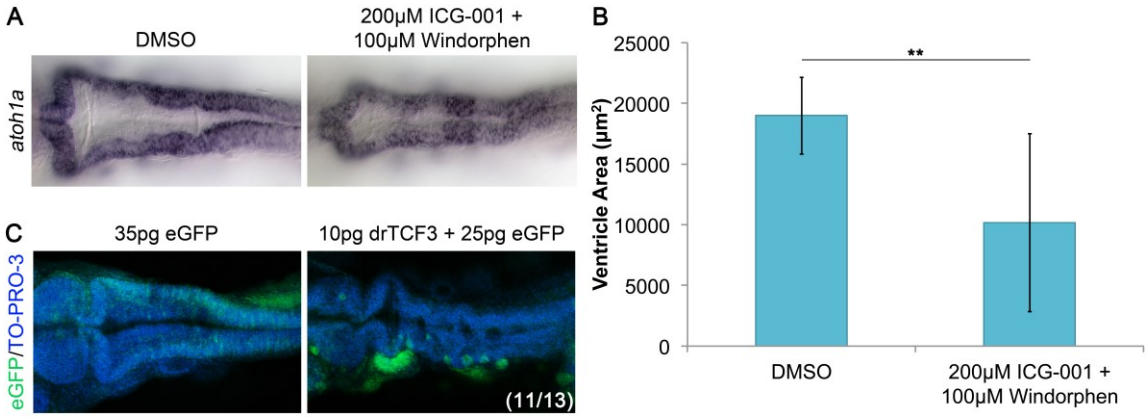

Figure 5.7. β-catenin mediated transcription is required for ventricle morphogenesis.

(A) Treatment of embryos with 200 μM ICG-001 and 100 μM Windorphen prevents β-catenin from interacting with the transcriptional co-activators CBP (cAMP response element binding protein) and p300. Compared to control treatment with DMSO, this results in a decrease in ventricle size. (B) Measurement of ventricle area shows that treatment of embryos with 200 μM ICG-001 and 100 μM Windorphen results in a 54% decrease in size (DMSO: 18990 μm^2, 200 μM ICG-001 + 100 μM Windorphen: 10178 μm^2, p-value 0.0015, T-test). (C) Mosaic co-expression of a dominant repressive form of TCF3 that lacks the β-catenin interaction domain with eGFP causes defects in ventricle development (11/13 embryos), as compared to control embryos overexpressing eGFP alone. All embryos are dorsal views, anterior to the left, 24 hpf.

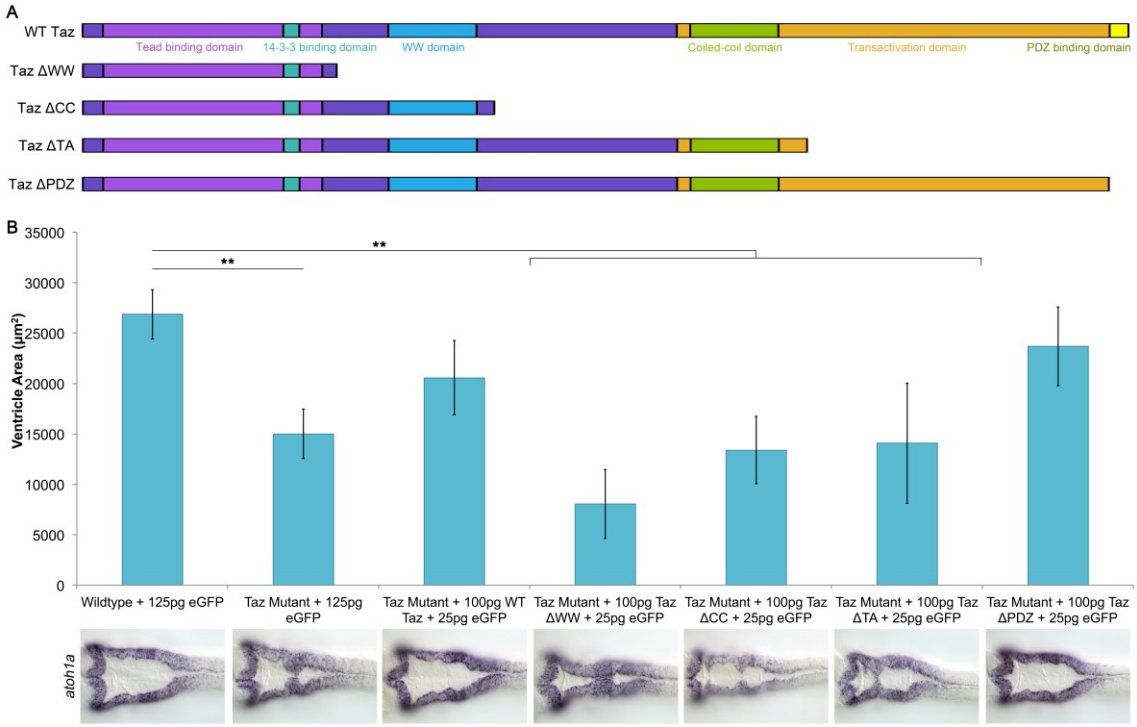

Figure 5.8. The Taz Transcription Activation Domain is required to rescue ventricle morphogenesis in taz mutants.

(A) Schematics of the *taz* overexpression constructs used. WT Taz encodes the full length protein. Taz ΔWW contains the Tead-binding domain and the 14-3-3 binding domain. Taz ΔCC contains the Tead-binding domain, the 14-3-3 binding domain and the WW domain. Taz ΔTA contains the Tead-binding domain, the 14-3-3 binding domain and the WW domain, and truncates the transcription activation domain after the Coiled-coil domain. Taz ΔPDZ contains the Tead-binding domain, the 14-3-3 binding domain and the WW domain, and the transcription activation domain including the Coiled-coil domain, but lacks the PDZ binding domain. (B) The *taz* overexpression constructs, or eGFP were injected into embryos, and the ventricle area was measured. Injection of eGFP was used as a control, and *taz*$^{-/-}$ mutant embryos injected with eGFP had a decrease in area of 56% compared to wildtype embryos (p-value 0.001). Injection of 100 pg WT Taz into *taz*$^{-/-}$ mutants increased ventricle area to 77% of Wildtype + 125 pg eGFP (p-value 0.1155). Injection of 100 pg of Taz ΔWW, Taz ΔCC or Taz ΔTA, did not increase ventricle size in *taz*$^{-/-}$ mutants (Taz ΔWW – 30%, p-value 0.001; Taz ΔCC - 50%, p-value 0.001; Taz ΔTA - 52%, p-value 0.001). Injection of 100 pg Taz ΔPDZ

increased ventricle size in *taz*$^{-/-}$ mutants to 88% of Wildtype + 125 pg eGFP (p-value 0.6458). Ventricle area: Wildtype + 125 pg eGFP - 26863 μm^2; *taz* mutant + 125 pg eGFP - 15000 μm^2; *taz* mutant + 100 pg WT Taz + 25 pg eGFP - 20571 μm^2; *taz* mutant + 100 pg Taz ΔWW + 25 pg eGFP - 8045 μm^2; *taz* mutant + 100 pg Taz ΔCC + 25 pg eGFP - 13394 μm^2; *taz* mutant + 100 pg Taz ΔTA + 25 pg eGFP - 14064 μm^2; *taz* mutant + 100 pg Taz ΔPDZ + 25 pg eGFP - 23688 μm^2. Statistical analysis was performed by ANOVA with a post-hoc Tukey test. All embryos are dorsal views, anterior to the left, 24 hpf.

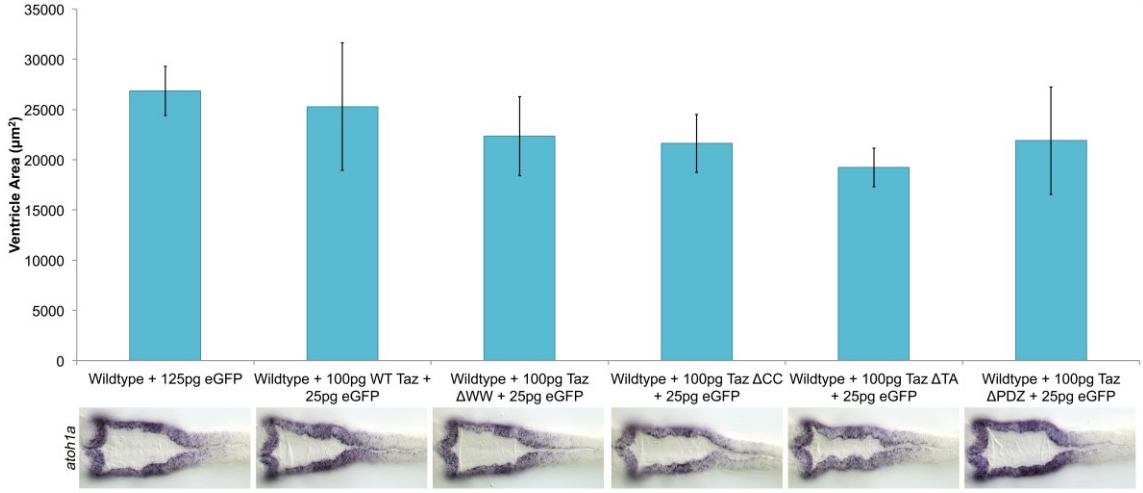

Figure 5.9. Overexpression of truncated forms of Taz does not have a significant effect on ventricle morphogenesis in wildtype embryos.

Overexpression of *taz* constructs did not have a significant effect on ventricle size in wildtype embryos. Ventricle area: Wildtype + 125 pg eGFP - 26863 μm^2; Wildtype + 100 pg WT Taz + 25 pg eGFP - 25280 μm^2; Wildtype + 100 pg Taz ΔWW + 25 pg eGFP - 22341 μm^2; Wildtype + 100 pg Taz ΔCC + 25 pg eGFP - 21632 μm^2; Wildtype + 100 pg Taz ΔTA + 25 pg eGFP - 19237 μm^2; Wildtype + 100 pg Taz ΔPDZ + 25 pg eGFP - 21892 μm^2. Statistical analysis was performed by ANOVA with a post-hoc Tukey test. All embryos are dorsal views, anterior to the left, 24 hpf.

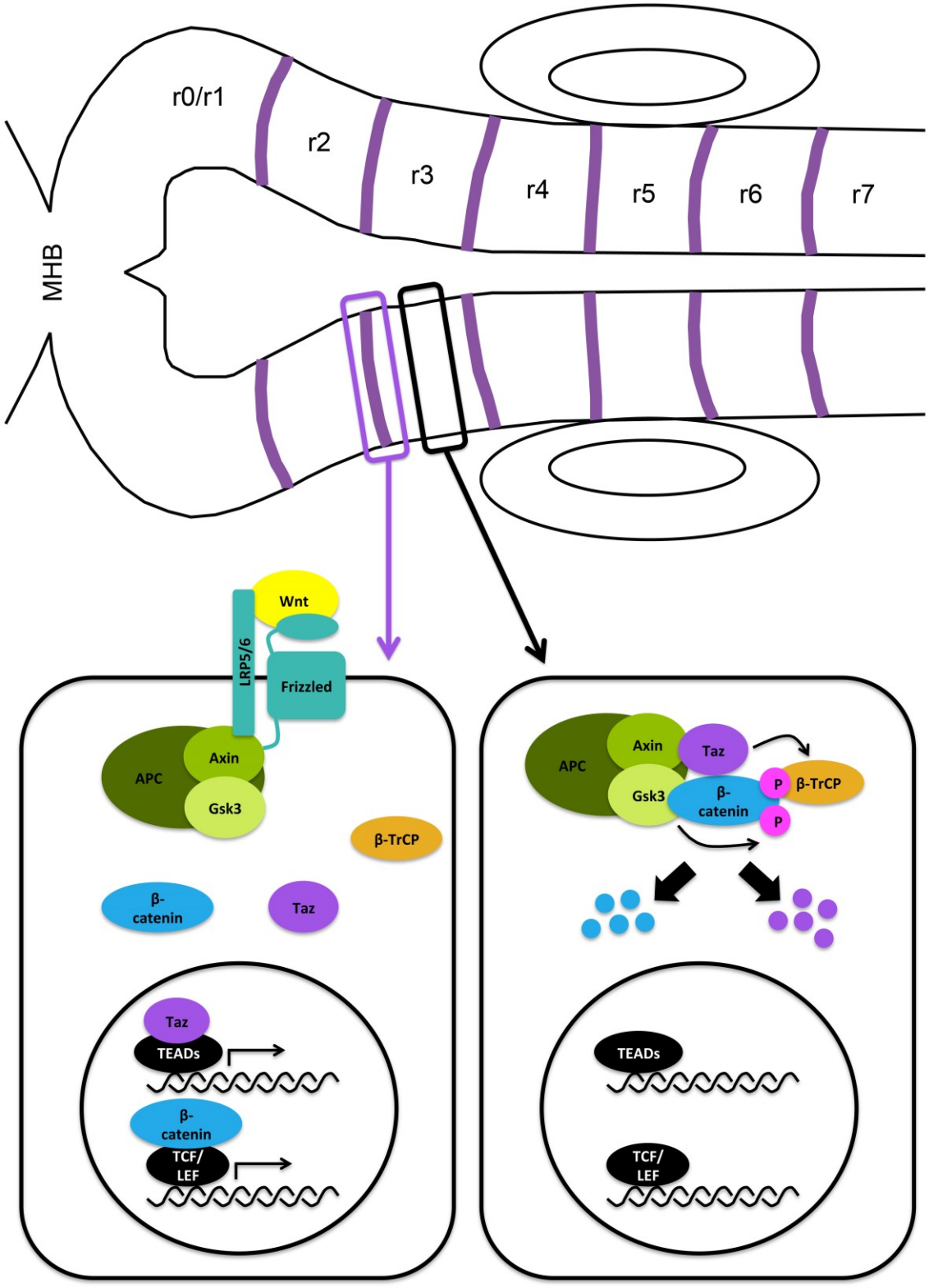
r0/r1
r2
r3
r4
r5
r6
r7
MHB
Wnt
LRP5/6
Frizzled
APC
Axin
Gsk3
β-TrCP
β-
catenin
Taz
TEADs
TCF/
LEF
P

Figure 5.10. Model for Wnt/Taz interactions at rhombomere boundaries.

We propose a model where Wnt signaling at rhombomere boundaries results in stabilization and nuclear localization of Taz and β-catenin. Between rhombomere boundaries, where Wnts are not enriched, Taz and β-catenin are degraded. This interaction is required for hindbrain ventricle morphogenesis.

Chapter 6: Preliminary Investigations of Interactions between Taz and the Notch Signaling Pathway in Ventricle Morphogenesis

6.1 Introduction

Notch signaling mediates cell-cell communication and is involved in establishing complex patterns within tissues and determining cell fate (Artavanis-Tsakonas et al., 1999; Irvine and Rauskolb, 2001; Lewis, 1998; Pourquie, 2001; Rida et al., 2004). Notch receptors are located on the plasma membrane, and binding of Notch to Delta/Serrate (Jagged) induces S2 cleavage of the Notch extracellular domain, mediated by the ADAM metalloprotease family (Pan and Rubin, 1997; Rooke et al., 1996). Subsequently the γ-secretase complex performs S3 cleavage releasing the Notch intracellular domain (NICD) (Donoviel et al., 1999; Levitan and Greenwald, 1995; Mumm et al., 2000; Schroeter et al., 1998; Struhl and Greenwald, 1999) which can then translocate into the nucleus, where it regulates target gene transcription by binding to Rbpj (recombination signal binding protein for immunoglobulin kappa J region a; suppressor of hairless (Su(H))) (Fryer et al., 2002; Kao et al., 1998). Following synthesis, the Notch receptors can be glycosylated in the Golgi by Fringe homologs, thereby making Notch more susceptible to activation by the ligand Delta, instead of Serrate. Fringe genes are important in Notch mediated establishment of boundaries between neighbouring cell populations (Irvine and Rauskolb, 2001). This is achieved by one population expressing Notch and Delta, while the other population expresses Notch, Serrate and Fringe, resulting in a strong activation of Notch at the interface, where glycosylated Notch encounters Delta (Panin et al., 1997).

Notch signaling at rhombomere boundaries is important for both boundary formation, and neurogenesis in the hindbrain. Notch activation at rhombomere boundaries suppresses neuronal differentiation, and Delta expression is restricted from rhombomere boundaries (Cheng et al., 2004). Notch receptors are expressed in neural progenitors (Del Amo et al., 1992; Higuchi et al., 1995; Lardelli et al., 1994; Lindsell et al., 1996; Weinmaster et al., 1991; Weinmaster et al., 1992), while early neuroblasts express Delta (Cheng et al., 2004). Notch activation also regulates cell affinity at rhombomere boundaries (Cheng et al., 2004), and induces boundary expression of F-actin and actin-binding molecules at adherens junctions (Major and Irvine, 2005; Major and Irvine, 2006).

Loss of function of components of the Notch signaling pathway results in

neurogenic phenotypes (Appel et al., 1999; Bingham et al., 2003; Cheng et al., 2004; Gray et al., 2001; Holley et al., 2000; Holley et al., 2002; Itoh et al., 2003; Jiang et al., 1996; Park and Appel, 2003; Riley et al., 1999; Schier et al., 1996; van Eeden et al., 1996). One of the strongest neurogenic phenotypes is observed in *mindbomb* mutants, which have ectopic expression of neurogenic genes at early stages (Bingham et al., 2003; Itoh et al., 2003; Jiang et al., 1996; Park and Appel, 2003; Schier et al., 1996), resulting in expression of the pan-neuronal marker HuC/D throughout the hindbrain by 24 hpf (Bingham et al.; Cheng et al., 2004), as opposed to its normal pattern where it is restricted to rhombomere centers. This results in overproduction of rhombomere centre neurons such as reticulospinal neurons (Riley et al., 2004), increased numbers of rohon-beard neurons (Bingham et al., 2003), and a loss of commissural and later-born neurons (Itoh et al., 2003; Jiang et al., 1996; Park and Appel, 2003; Riley et al., 2004; Schier et al., 1996). The neurogenic phenotype observed in *mindbomb* mutants is due to defective lateral inhibition, resulting in the premature differentiation of precursors, and depletion of neuroepithelial cells, which also leads to defects in segmental gene expression (Bingham et al., 2003). Rhombomere boundaries initially form, but they fail to be maintained in *mindbomb* mutants (Riley et al., 2004).

In zebrafish, two *fringe* genes are expressed in the hindbrain. *Lunatic fringe* (*lfng*) is expressed in even-numbered rhombomeres and at lower levels in odd-numbered rhombomeres (Prince et al., 2001), while *radical fringe* (*rfng*) is expressed specifically at rhombomere boundaries (Amoyel et al., 2005; Qiu et al., 2004). *Lfng* limits neuronal differentiation, and is required cell autonomously to maintain cells in a progenitor state (Nikolaou et al., 2009). *Rfng* is required for boundary specific *wnt1* expression (Cheng et al., 2004), and knockdown of *rfng* results defects in the hindbrain ventricle (Elsen et al., 2008). Loss of *rfng* expression and defects in ventricle formation have been associated with a number of mutants in which rhombomere boundaries or neurogenesis are disrupted. Loss of function of *mindbomb, med12/14* and *sfpq* results in a loss of *rfng* expression at rhombomere boundaries, disorganization or disruption of hindbrain neurons, and defects in ventricle morphogenesis (Appel et al., 1999; Bingham et al., 2003; Cheng et al., 2004; Conaway et al., 2005; Guo et al., 1999; Hong et al., 2005b; Itoh et al., 2003; Lowery et al., 2009; Lowery et al., 2007; Mawdsley et al., 2004; Riley

et al., 2004; Schier et al., 1996; Thomas-Jinu et al., 2017; Wang et al., 2006).

We are investigating roles for Taz in ventricle morphogenesis, and the role of Notch signaling in this developmental process. Yap/Taz are transcriptional co-activators/repressors whose stabilization and localization are canonically controlled by the Hippo pathway kinases. When Yap/Taz are phosphorylated that are either sequestered in the cytoplasm or degraded (Chan et al., 2005; Dong et al., 2007; Huang et al., 2005; Lei et al., 2008; Liu et al., 2010; Oh and Irvine, 2008; Praskova et al., 2008; Zhao et al., 2010; Zhao et al., 2007), while un-phosphorylated Yap/Taz are able to translocate to the nucleus where they bind to the promoters of target genes (Dong et al., 2007; Kanai et al., 2000; Lei et al., 2008; Oh and Irvine, 2008; Ren et al., 2010; Zhao et al., 2007) primarily through interactions with the TEAD (TEA domain) family of transcription factors (Goulev et al., 2008; Vassilev et al., 2001; Wu et al., 2008; Zhang et al., 2008; Zhao et al., 2008a).

Yap/Taz are involved in body axis specification, posterior body elongation, development of the thyroid, kidney, lateral line, heart, vascular system, and retina (Agarwala et al., 2015; Gee et al., 2011; Hu et al., 2013; Kim et al., 2017a; Kimelman et al., 2017; Miesfeld et al., 2015; Miesfeld and Link, 2014; Nagasawa-Masuda and Terai, 2017; Nakajima et al., 2017; Pappalardo et al., 2015; Tian et al., 2007). Yap/Taz activity is often associated with the maintenance of neural progenitors (Cao et al., 2008; Gee et al., 2011; Han et al., 2015; Hindley et al., 2016; Lavado et al., 2013; Milewski et al., 2004; Ramalho-Santos et al., 2002; Zhang et al., 2011a) and *Yap* is required for the generation of ependymal cells within the brain ventricles (Park et al., 2016). Yap/Taz have also been shown to activate the Notch signaling pathway (Camargo et al., 2007; Zhou et al., 2011). In different contexts, Yap/Taz have been shown to both induce (Kim et al., 2017b; Tschaharganeh et al., 2013) and repress Jagged (Serrate) expression (Kim et al., 2017b; Manderfield et al., 2015), and regulate the expression of Notch inhibitors in response to mechanical forces, thereby controlling epidermal stem cell differentiation (Totaro et al., 2017).

In this Chapter, we have performed a preliminary investigation of interactions between Taz and the Notch signaling pathway that may be involved in ventricle morphogenesis. We provide evidence that Taz regulates the expression of *rfng* and *wnt1*

at rhombomere boundaries. Loss of function of *taz* also mildly reduces proliferation in the hindbrain, which may contribute to ventricle defects. We demonstrate that Notch signaling is important for ventricle morphogenesis, but disruption of Notch signaling does not affect Taz localization to rhombomere boundaries. This suggests roles for Taz upstream of Notch in ventricle morphogenesis. Additionally, while defects in Notch signaling in the hindbrain are commonly associated with alterations in neurogenesis, we do not see significant changes in neurogenesis in *taz*$^{-/-}$ mutants.

6.2 Results

6.2.1 Loss of function of *taz* results in a loss of rhombomere boundary markers

Zebrafish *taz*$^{-/-}$ mutants have defects in hindbrain ventricle development (as shown in Chapter 5). As Taz is a transcriptional co-regulator, we sought to determine if there were any changes in gene expression in the hindbrain accompanying the ventricle defects. We found that expression of *rfng* at hindbrain boundaries is lost (Fig 6.1 A-B) and *wnt1* rhombomere boundary expression is disrupted (Figure 6.1 C-D). Previous work has suggested that *rfng* may regulate *wnt1* expression at rhombomere boundaries (Cheng et al., 2004). Our results suggest that Taz may be upstream of this interaction. Tp53 (Tumor protein 53) has also been shown to regulate *rfng* expression (Gerety and Wilkinson, 2011), and Taz has been shown to mediate tissue and organ size through regulation of cell proliferation (reviewed in (Watt et al., 2017)). Therefore, we examined *taz*$^{-/-}$ mutants for changes in cell proliferation and apoptosis. Proliferating cells were labeled with Phospho-histone H3, and in wildtype embryos proliferating cells can be seen lining the apical surface of the ventricle (Fig 6.1 E). There is a mild decrease in the number of proliferating cells on the apical surface of the ventricle in *taz*$^{-/-}$ mutants (Fig 6.1 E-F). To determine if there are any changes in cell death, we also assayed for apoptosis with anti-active Caspase 3 immunofluorescence. In both wildtype embryos and *taz*$^{-/-}$ mutants very few cells are labeled with anti-active Caspase 3 (Fig 6.1 G-H), indicating a very low rate of cell death in the hindbrain at this stage. *Taz*$^{-/-}$ mutants do

not appear to have a change in the number of cells undergoing apoptosis, as compared to wildtype embryos (Fig 6.1 G-H). This suggests that activation of the Tp53 pathway is not involved *taz*-mediated regulation of *rfng*, although the loss of *taz* may affect proliferation in the hindbrain.

6.2.2 Notch signaling pathway genes and proneural genes are not affected in *taz* mutants

Fringe genes are important in establishing Notch signaling at boundaries between compartments, and *rfng* may be required for Notch activation at rhombomere boundaries. The loss of *rfng* expression has be reported in *mindbomb* mutants which have a loss of rhombomere boundaries (Riley et al., 2004), and often loss of *rfng* expression is mirrored by a loss of other rhombomere boundary markers like *mariposa* (*foxb1a)* (Riley et al., 2004). The disruption of rhombomere boundaries is also often accompanied by mis-expression of other components of the Notch signaling pathway such as *deltaA* (Riley et al., 2004). We examined expression of the Notch ligands *deltaC* and *deltaD*, as well as expression of *her6 (hairy-related 6),* a transcriptional target of Notch signaling. *DeltaC* is expressed in small puncta at 22hpf, which may be differentiating neuroblasts (Fig 6.2 A), while *deltaD* is expressed primarily in rhombomere centers (Fig 6.2 C)(Amoyel et al.). *Her6* is expressed weakly in cells throughout the hindbrain, but is expressed more strongly in r5/6, and in ventral regions of the hindbrain (Fig 6.2 E, data not shown). *Taz*$^{-/-}$ mutants do not have any significant changes in the expression of *deltaC*, *deltaD* or *her6* (Fig 6.2 A-F).

Notch activation at rhombomere boundaries is also important to prevent pro-neural gene expression at rhombomere boundaries (Cheng et al., 2004). Proneural genes such as *ascl1a (achaete-scute family bHLH transcription factor 1a*), *ascl1b(achaete-scute family bHLH transcription factor 1b*) and *ngn1 (neurogenin 1; neurog1)* are first expressed at the onset of neuronal differentiation in rhombomere centers (Allende and Weinberg, 1994; Haddon et al., 1998; Korzh et al., 1998). Initial expression of proneural genes then induces expression of *delta* ligands and other proneural genes such as *neurod4 (neuronal differentiation 4)* (Park et al., 2003; Wang et al., 2003). The expression of Delta is required to activate Notch signaling in adjacent cells and inhibits

proneural gene expression and neuronal differentiation via lateral inhibition (Chitnis et al., 1995; de la Pompa et al., 1997). Loss of function of components of the Notch signaling pathway, such as *deltaD*, *notch1*, and *mindbomb*, results in neurogenic phenotypes, resulting in alterations in proneural gene expression (Gray et al., 2001; Holley et al., 2000; Holley et al., 2002; Jiang et al., 1996; Schier et al., 1996; van Eeden et al., 1996). To determine if *taz*$^{-/-}$ mutants have defects in proneural gene expression similar to those seen in loss of function of Notch pathway components, we examined the expression of multiple families of proneural genes. *Ascl1a*, *ascl1b*, *insm1a*, *ngn1* and *neurod4* are primarily expressed in rhombomere centers (Fig 6.3 A-J). *Ascl1a* expressed is observed in the lateral portions of the rhombomere (Fig 6.3 A), while *insm1a* is expressed closer to the midline (Lukowski et al., 2006) (Fig 6.3 E). *Ascl1b*, *ngn1* and *neurod4* are expressed more broadly across the rhombomeres (Fig 6.3 C, G, I). *Neurod1* and *ngn1* are expressed in the cranial ganglia (Sperber et al., 2008) (Fig 6.3 G, K-L), and *neurod4* is also expressed in the branchial arches (Thisse et al., 2004) (Fig 6.3 I). The expression of *ascl1a*, *ascl1b*, *insm1a*, *ngn1*, *neurod4,* and *neurod1* does not appear to be altered in *taz*$^{-/-}$ mutants (Fig 6.3 A-J). This suggests that the loss of *taz* does not affect specification of rhombomere centre proneural domains, or the specification of cranial ganglia and branchial arch proneural domains.

Sox1b, *sox2* and *sox3* are members of the SoxB1 family of genes, which are primarily involved in activation of gene expression during neural development (Bylund et al., 2003; Kamachi et al., 1998; Uchikawa et al., 1999). *Sox1b* is specifically expressed in the forebrain and the lens (Fig 6.3 M-N), while *sox2* and *sox3* are expressed more broadly across the developing brain (Fig 6.3 O-R). Examination of *taz*$^{-/-}$ mutants does not reveal any changes in the expression of *sox1b*, *sox2* or *sox3* (Fig 6.3 M-R). This indicates that the loss of *taz* does not interfere with SoxB1 family gene expression in neural development.

6.2.3 Loss of function of *taz* mutants results in minor changes to some neuronal sub-populations

Although there were no changes in the expression of proneural genes we have examined in *taz*$^{-/-}$ mutants, a number of mutants in which *rfng* expression is lost also

have changes in neurogenesis. Mutants for *sfpq* lose reticulospinal neurons in the hindbrain, (except for the Mauthner neuron), and have reduced numbers of axons throughout the forebrain midbrain and hindbrain (Lowery et al., 2007). Further investigation has indicated that Sfpq is required in the axons of motor neurons, and its loss results in disorganized axon tracts, loss of both facial and trigeminal axons projections and defects in spinal motor neuron projections (Thomas-Jinu et al., 2017). *Med12* mutants also have reduced numbers of reticulospinal neuron cell bodies and axons, and reduced numbers of commissural neurons in the hindbrain (Lowery et al., 2009). Finally, *mindbomb* mutants have increased numbers of early born neurons and rhombomere centre neurons, at the expense of late born neurons, disorganization of the branchiomotor neurons and increased numbers of rohon-beard neurons (Appel et al., 1999; Bingham et al., 2003; Itoh et al., 2003; Riley et al., 2004; Schier et al., 1996). To determine if the loss of *rfng* is correlated with any of these changes in neuronal development, we examined a variety of neuronal populations in *taz*$^{-/-}$ mutants. *Taz*$^{-/-}$ mutants have normal branchiomotor neuron organization, and axonal projections (Fig 6.4 A-D), unlike what is observed in *mindbomb* and *sfpq* mutants. Examination of acetylated tubulin (Fig 6.4 E-H), and spinal cord motor neurons (Znp1, Fig 6.4 I-J) did not reveal any major defects in axon numbers or projections as is observed in *sfpq* mutants. *Taz*$^{-/-}$ mutants also do not show any major changes to reticulospinal neuron numbers, organization or axons (Fig 6.4 K-L), unlike *sfpq* and *med12* mutants. There is an alteration in abducens neurons labeled by zn5 in some *taz*$^{-/-}$ mutants (Fig 6.4 M-N) and there is an increase in Rohon-beard neurons visible in *Tg(islet2b:GFP)* in some *taz*$^{-/-}$ mutants (Fig 6.4 O-P), which is similar to reported phenotypes for *mindbomb* mutants (Cheng et al., 2004). Further quantification and characterization of the changes in these neuronal populations will be required. Interestingly, abducens neurons have not been identified as being altered in *sfpq*, *med12* and *mib* mutants.

6.2.4 Notch signaling and *rfng* involvement in ventricle morphogenesis

We wished to determine if *rfng* is involved in ventricle morphogenesis. To first determine if Notch signaling is required for ventricle morphogenesis we used two γ-secretase inhibitors to prevent cleavage of the NICD, thereby preventing activation of

Notch target genes. Both Compound E (Cpd E) and DAPT are well-characterized γ-secretase inhibitors that have previously been used in zebrafish to inhibit Notch signaling (Da'as et al., 2012; Jurisch-Yaksi et al., 2013; Kitzmann et al., 2006; Liu et al., 2007; Yang et al., 2008; Zecchin et al., 2007). Treatment of embryos with 100 μM DAPT (Fig 6.5 A-H) or 100 μM Cpd E (Fig 6.5 I-P), results in a reduction in ventricle size (Fig 6.5 A-B, I-J). Interestingly, it does not result in a phenocopy of the midline separation defect observed in *taz*$^{-/-}$ mutants (Fig 5.2 A-D). Rhombomere boundary specific expression of *wnt1*, *rfng* and Taz localization are still observed in embryos treated with 100 μM DAPT (Fig 6.5 C-H), or 100 μM Cpd E (Fig 6.5 K-P). This suggests that Notch signaling is not an upstream regulator of Taz, *rfng* or *wnt1*. Treatment with 100 μM Cpd E does slightly increase the midline expression of *rfng* and localization of Taz (Fig 6.5 M-P). This is similar to results seen by (Qiu et al., 2009), however the significance of this alteration in expression and localization has not been explored. Together these results support a role for Notch signaling in ventricle development, however it suggests that Notch signaling does not operate upstream of Taz, and notably, although pharmacological inhibition of Notch signaling does reduce ventricle size, it does not result in midline separation defects as are seen in *taz*$^{-/-}$ mutants.

Loss of *rfng* rhombomere boundary expression has been observed in mutants that have ventricle defects. (Cheng et al., 2004; Lowery et al., 2009; Lowery et al., 2007; Thomas-Jinu et al., 2017). Additionally, knockdown of *rfng* has been shown to result in midline separation defects, similar to those observed in *taz*$^{-/-}$ mutants (Elsen et al., 2008). To determine if the loss of *rfng* is involved in the ventricle defects observed in *taz*$^{-/-}$ mutants, we used CRISPR (Clustered regularly interspersed palindromic repeats) mediated mutagenesis to generate loss of function alleles targeting the signal peptide and transmembrane region of *rfng*. In P0 incrosses of CRISPR injected zebrafish we identified 4 alleles with homozygous deletions, which should result in frameshift mutations in *rfng*. In all cases, homozygous mutations in *rfng* did not result in defects in ventricle morphogenesis (Fig 6.6 A-E).

6.3 Discussion

6.3.1 Roles for Notch and rhombomere boundaries in ventricle development

Notch signaling has previously been implicated in ventricle development. *Mindbomb* mutants have disrupted Delta/Notch signaling, which results in a failure to maintain rhombomere boundaries, and a reduction in ventricle size (Appel et al., 1999; Bingham et al., 2003; Cheng et al., 2004; Itoh et al., 2003; Riley et al., 2004; Schier et al., 1996). Knockdown of *rfng* also results in midline separation defects (Elsen et al., 2008), and a loss of *rfng* expression is observed in *mindbomb*, *sfpq*, and *med12/14* mutants which all have defects in ventricle morphogenesis (Appel et al., 1999; Bingham et al., 2003; Cheng et al., 2004; Hong and Dawid, 2011; Itoh et al., 2003; Lowery et al., 2009; Lowery et al., 2007; Riley et al., 2004; Schier et al., 1996; Thomas-Jinu et al., 2017).. Not only does this suggest a role for *rfng* in ventricle morphogenesis, but it also supports roles for the Notch signaling pathway and rhombomere boundaries in this process.

As shown in Chapter 5, Taz protein is localized to rhombomere boundaries, and loss of function of *taz* results in midline separation defects. Additionally, *taz*$^{-/-}$ mutants have a loss of *rfng* expression at rhombomere boundaries, as is seen in *mindbomb*, *sfpq*, and *med12/14* mutants (Cheng et al., 2004; Hong and Dawid, 2011; Thomas-Jinu et al., 2017). Together, this supports a role for rhombomere boundaries in ventricle development, however examination of additional rhombomere boundary markers and assaying for characteristic properties of rhombomere boundary cells such as their elongated shape, large intercellular space, and reduced proliferation and interkinetic nuclear migration (Guthrie et al., 1991; Guthrie and Lumsden, 1991; Heyman et al., 1995; Heyman et al., 1993; Lumsden and Keynes, 1989) will be required to determine if rhombomere boundaries are completely abolished in *taz*$^{-/-}$ mutants. Additionally, while *taz*, *mindbomb*, *sfpq*, and *med12/14* mutants all exhibit ventricle defects and a loss of *rfng* expression at rhombomere boundaries, the other phenotypes observed in these mutants are not identical. While they all have neuronal defects to some degree, they do not all affect the same neuronal populations, and the effect that they have on neurons

also varies. This suggests that the loss of *rfng* expression at rhombomere boundaries is not the only factor that influences neurogenesis in these mutants.

We also wished to determine the contribution of *rfng* and Notch signaling to ventricle development. Disruption of rhombomere boundaries, as is observed in *mindbomb* mutants does result in smaller ventricles, however *taz*$^{-/-}$ mutants do not have just a small ventricle, instead the midline of the ventricle fails to separate. To determine how disruption of Notch signaling affects ventricle development, pharmacological inhibitors were used to prevent cleavage and release of the Notch intracellular domain. We find that inhibition of Notch signaling does results in a reduced ventricle size, but does not cause midline separation defects. While this does support a role for Notch signaling in ventricle development, it indicates that there are other factors that contribute to the ventricle defect observed in *taz* mutants. Additionally, pharmacological inhibition of the Notch pathway does not result in a loss of Taz localization or *rfng* and *wnt1* expression at rhombomere boundaries, supporting a role for Taz upstream of the Notch pathway. As pharmacological inhibitors will affect Notch signaling throughout the hindbrain, we also wanted to determine the effect of the loss of *rfng* alone. It is possible that loss of function of *rfng* will result in a different phenotype than is observed in embryos treated with γ-secretase inhibitors. In fact, previous research has shown that *rfng* morphants have midline separation defects (Elsen et al., 2008). To determine if the loss of *rfng* is involved in the generation of midline separation defects in *taz* mutants, we used CRISPR meditated mutagenesis to generate frameshift mutation in *rfng*. In contrast to the phenotype observed in *rfng* morphants (Elsen et al., 2008), we do not observe defects in the ventricle of *rfng* homozygous mutants. There are a number of reasons why *rfng* mutants do not have the same phenotype as *rfng* morphants. First, morpholino knockdown has been shown to result in ectopic expression of *rfng* via the Tp-53 pathway (Amoyel et al., 2005; Gerety and Wilkinson, 2011), so the phenotype observed in *rfng* morphants may be due to ectopic boundary marker expression, as opposed to the loss of *rfng*. Alternatively, maternal expression of *rfng* transcripts (Qiu et al., 2004) may be sufficient to prevent defects in ventricle morphogenesis in zygotic *taz* mutants. As previous studies used a translation blocking morpholino oligonucleotide (Elsen et al., 2008), this would prevent the translation of both maternal and zygotic transcripts, which

may be required for ventricle defects to be apparent. Additionally, there is increasing evidence that mutants undergo different compensation mechanisms than morphants. Changes in the expression of related genes and paralogs can compensate for loss of function (Rossi et al., 2015). In the case of *rfng* mutants, it is possible that one of the other zebrafish *fringe* homologs may be differentially regulated and compensate for the loss of *rfng*. Alterations to mRNA processing has also been shown to occur in zebrafish mutants, allowing for the translation of partially functional proteins (Anderson et al., 2017). Therefore, careful analysis of changes in expression of *fringe* homologs in zebrafish, cDNA sequencing, and generation of maternal zygotic mutants is required to determine the reason for the absence of ventricle defects in *rfng* mutants.

6.3.2 Changes in cell proliferation may contribute to ventricle defects in *taz* mutants

Changes in cell proliferation have previously been associated with defects in ventricle development. *Zic1 (zic family member 1)* and *zic4 (zic family member 4)* regulate neural proliferation and knockdown of *zic1* and *zic4* results in midline separation defects in the hindbrain ventricle (Elsen et al., 2008). Knockdown of *zic2a,* which is involved in promoting proliferation the midbrain, also results in reductions in ventricle size (Nyholm et al., 2007). *Curly fry* mutants also have abnormal proliferation and reduced ventricles (Song et al., 2004) and loss of function of *sfpq*, which promotes cell survival, also causes defects in ventricle development (Lowery et al., 2007). The Hippo pathway is also involved in the regulation of cell proliferation (reviewed in (Watt et al., 2017)). In zebrafish, Yap has been linked to regulation of cell proliferation following injury (Mateus et al., 2015), and in the posterior lateral line primordium (Agarwala et al., 2015). Taz has also been linked to regulating the size of the thyroid gland in zebrafish (Pappalardo et al., 2015). We find that *taz*$^{-/-}$ mutants have a mild decrease in proliferating cells on the apical surface of the hindbrain ventricle. Together, this suggests that there may be roles for Taz in regulating proliferation in the hindbrain, and this may be involved in ventricle morphogenesis. However further characterization of the proliferation defect observed in *taz*$^{-/-}$ mutants should be performed. Determination of the mitotic index, and analysis of cell proliferation by other methods, such as BrD-U

labeling will provide additional support for changes in cell proliferation. Furthermore, the mechanism by which changes in cell proliferation result in defects in ventricle development has not been fully explored, and *taz*$^{-/-}$ mutants may provide a model in which to explore this mechanism.

6.3.3 Loss of function of *taz* mutants does not cause extensive defects in neurogenesis

Previous research has suggested roles for Yap/Taz in the regulation of neurogenesis. Yap is expressed by neural progenitor cells, neural stem cells and cells of the ventricular progenitor zone (Cao et al., 2008; Gee et al., 2011; Ramalho-Santos et al., 2002). Knockdown of Yap in zebrafish results in defects in proneural, neuronal, and neural crest markers (Jiang et al., 2009). Multiple models have provided evidence for roles for Yap in maintaining neural progenitors and preventing neural cell cycle exit and differentiation (Alarcon et al., 2009; Cao et al., 2008; Han et al., 2015; Milewski et al., 2004; Zhang et al., 2012; Zhang et al., 2011a). Additionally, other proteins such as Nf2, FatJ cadherin and FAT4/Dchs1 act through Yap/Taz to regulate neural progenitor cell numbers (Cappello et al., 2013; Lavado et al., 2013; Van Hateren et al., 2011). Although much of the previous research has focused on role for Yap in neurogenesis, our results may support a role for Taz in neurogenesis.

Alterations in neurogenesis have also been observed in mutants with ventricle defects. Mutations in components of the mediator complex (*mediator complex subunit 12 (med12)* and *mediator complex subunit 14 (med14)*) have defects in select neuronal subtypes, and a reduction in ventricle size (Guo et al., 1999; Hong et al., 2005b; Lowery et al., 2009; Wang et al., 2006)). Mutants for *sfpq* have reduced numbers of reticulospinal neurons, reduced numbers and disorganization of axon tracts and projections and small ventricles (Lowery et al., 2007; Thomas-Jinu et al., 2017). Similarly, *her9*, *zic1* and *zic4*, which are involved in neural progenitor maintenance (Bae et al., 2005; Elsen et al., 2008) and *neogenin* which is required for neuronal differentiation (Lowery et al., 2007; Mawdsley et al., 2004; Thomas-Jinu et al., 2017), also result in defective ventricle morphogenesis when they are lost or knocked down (Bae et al., 2005; Elsen et al., 2008; Lowery et al., 2007; Mawdsley et al., 2004). Loss of

function of *mindbomb* results not only in reduced ventricle size, but also causes ectopic expression of proneural genes at early stages (Bingham et al., 2003; Itoh et al., 2003; Jiang et al., 1996; Park and Appel, 2003; Schier et al., 1996), resulting in overproduction of rhombomere centre neurons such as reticulospinal neurons (Riley et al., 2004), increased numbers of rohon-beard neurons (Bingham et al., 2003), and a loss of commissural and later-born neurons (Itoh et al., 2003; Jiang et al., 1996; Park and Appel, 2003; Riley et al., 2004; Schier et al., 1996). Additionally, neurons in *mindbomb* mutants have defects in axonal pathfinding and fasciculation (Riley et al., 2004). Unlike *mindbomb* mutants, we do not observe any changes in proneural gene expression in *taz*$^{-/-}$ mutants, however there may be changes in other proneural genes which we have not examined. Consistent with the unaltered expression of proneural genes, we find that most neuronal populations examined are unchanged in *taz*$^{-/-}$ mutants. We do find that abducens neurons and rohon-beard neurons are altered in some *taz*$^{-/-}$ mutants. Rohon-beard neurons are increased in *mindbomb* mutants, but they are not affected in any other mutants with ventricle defects, and alterations in abducens neurons have also not been observed in any mutants with ventricle defects. The neuronal alterations observed in other mutants with ventricle defects tend to be more widespread than we have observed in our *taz*$^{-/-}$ mutants, so while it is possible that neuronal defects contribute to the ventricle defects in *taz*$^{-/-}$ mutants, it is unlikely that they are the sole cause.

6.4 Figures

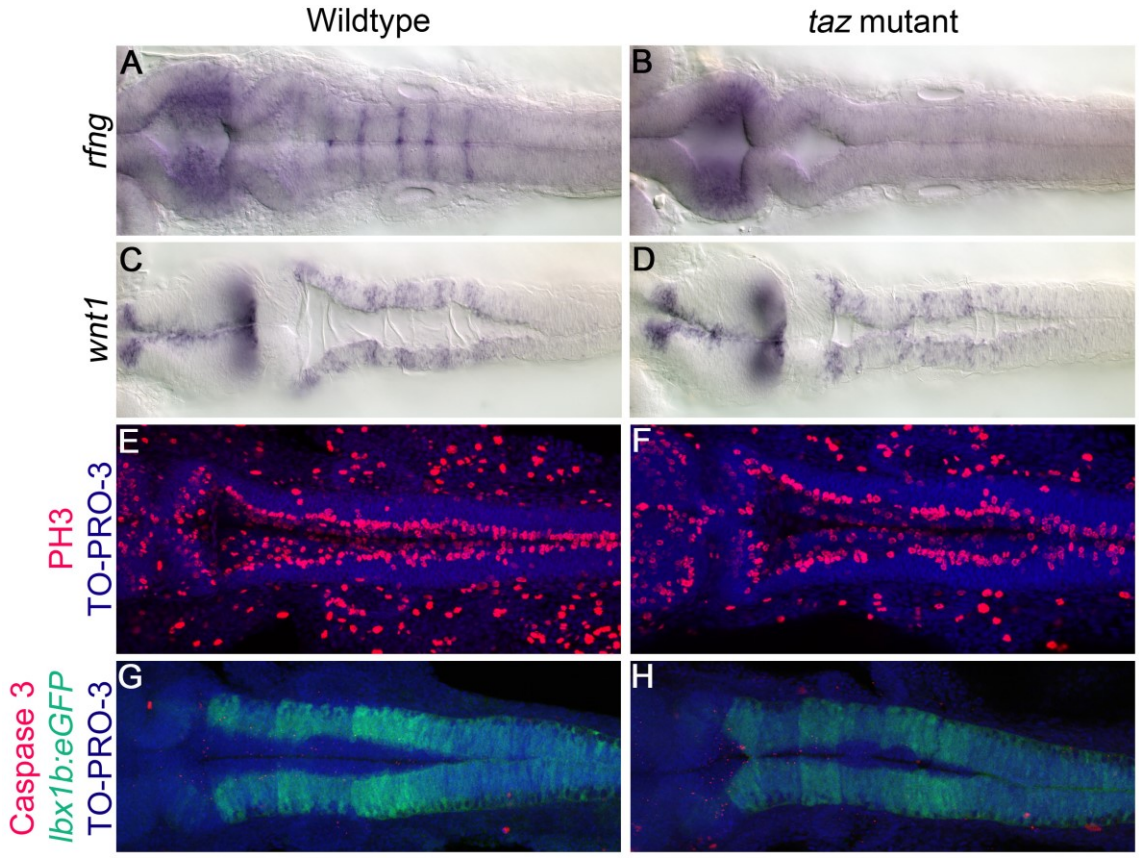

Figure 6.1. *Taz* mutants have a loss of *rfng* and *wnt1* expression at rhombomere boundaries, but may only have mild changes to cell

(A) *rfng* is expressed at rhombomere boundaries in wildtype embryos, (B) *rfng* expression at rhombomere boundaries is lost in *taz*$^{-/-}$ mutants. (C) *Wnt1* is expressed in the dorsal neural tube, and is enriched at rhombomere boundaries, (D) *wnt1* rhombomere boundary expression is disrupted in *taz*$^{-/-}$ mutants. (E) Phospho-histone H3 (PH3) labels proliferating cells (red), nuclei are labeled with TO-PRO-3 (blue) in wildtype embryos. (F) There may be a slight reduction in the number of proliferating cells in *taz*$^{-/-}$ mutants. (G) Anti-active Caspase 3 labels cells undergoing apoptosis (red), nuclei are labeled with TO-PRO-3 (blue) in an *Tg(lbx1b:eGFP)* background which is expressed in the neural tube. (H) *Taz*$^{-/-}$ mutants do not appear to have changes in apoptosis in the hindbrain. All embryos are dorsal views, anterior to the left, 22 hpf.

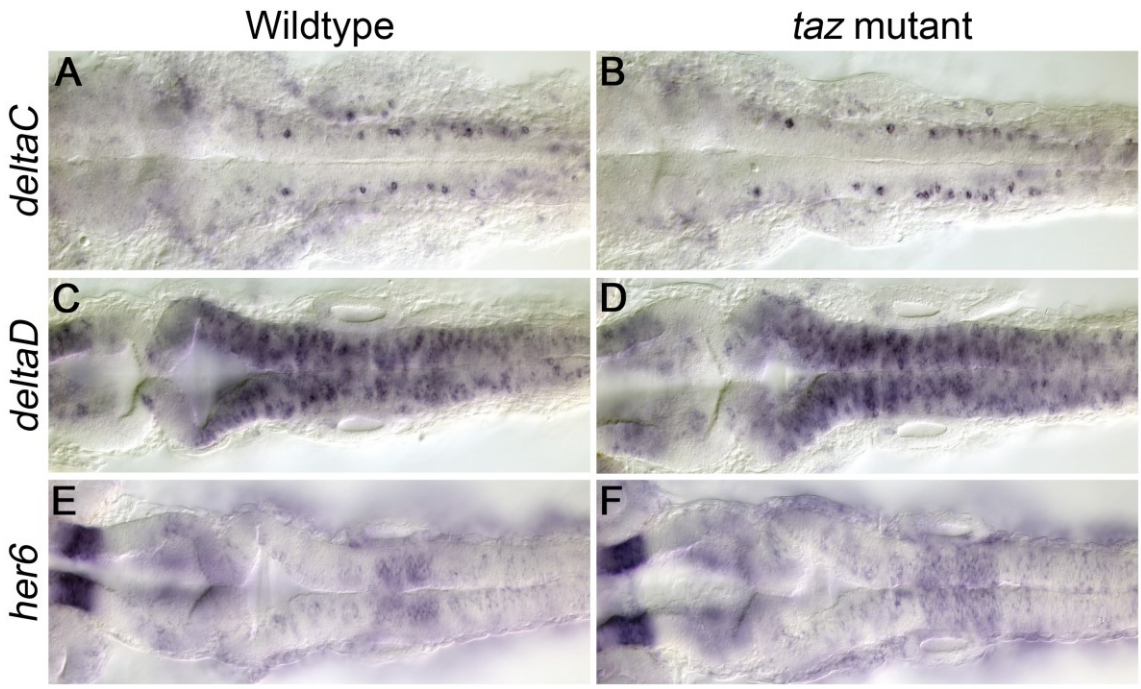

Figure 6.2. Components of the Notch signaling pathway, and Notch responsive genes are not changed in *taz* mutants.

DeltaC is expressed in a distinct sub-population of cells in the ventral neural tube in both wildtype (A) and *taz*$^{-/-}$ mutants (B). *DeltaD* is expressed in stripes along the hindbrain in wildtype (C) and *taz*$^{-/-}$ mutants (D). *Her6* is responsive to notch signaling and expressed similarly in wildtype (E) and *taz*$^{-/-}$ mutants (F). All embryos are dorsal views, anterior to the left, 22 hpf.

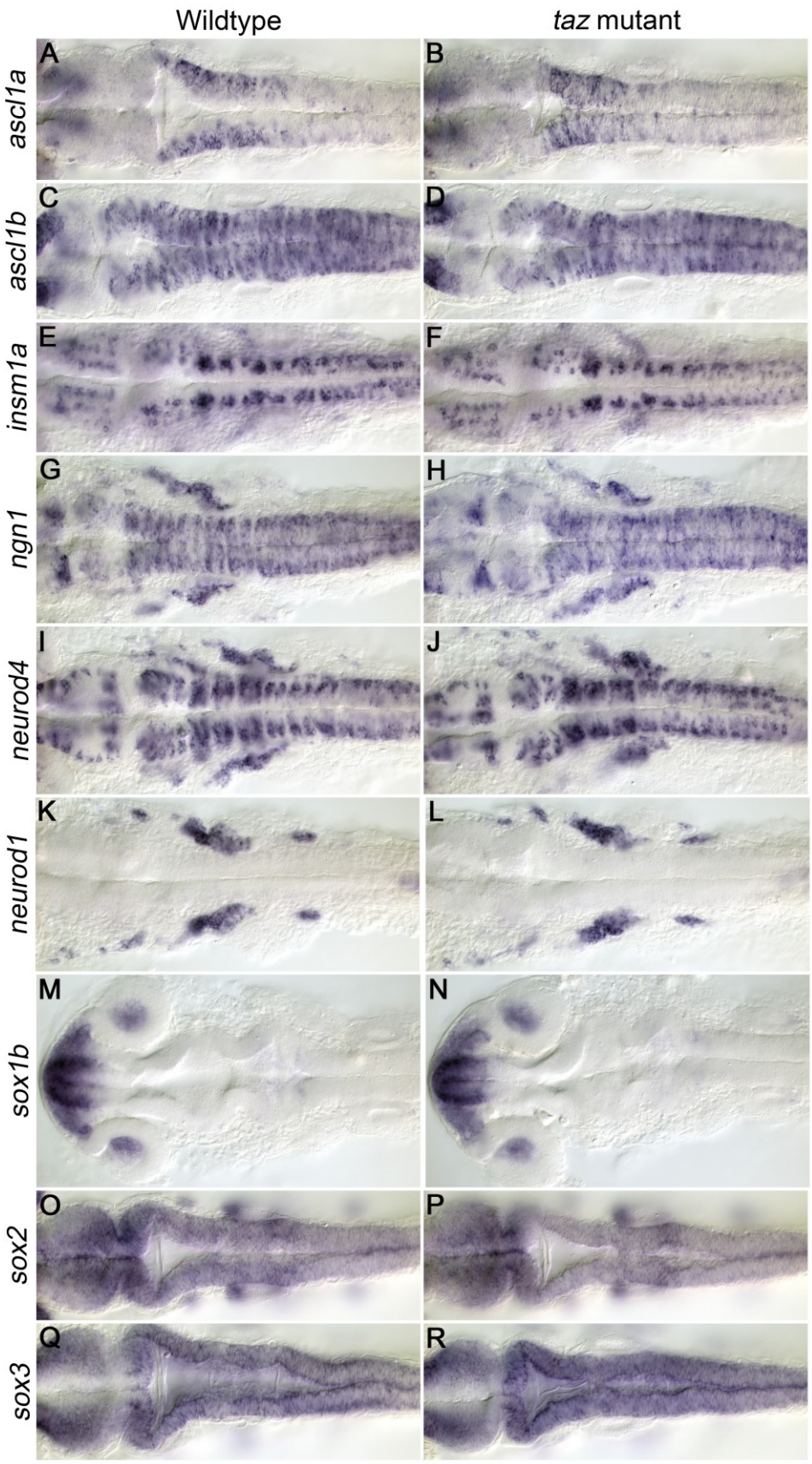
Wildtype
taz mutant
A
B
ascl1a
C
D
ascl1b
E
F
insm1a
G
H
ngn1
I
J
neurod4
K
L
neurod1
M
N
sox1b
O
P
sox2
Q
R
sox3

Figure 6.3. Proneural gene expression is unaffected in taz mutants.

The proneural genes *ascl1a* (A-B), *ascl1b* (C-D), *insm1a* (E-F), *ngn1* (G-H) and *neurod4* (I-J) are expressed in stripes along the hindbrain in both wildtype (A,C,E,G,I) and *taz*$^{-/-}$ mutants (B,D,F,H,J). *Neurod1* expression in tissues adjacent to the hindbrain is observed in both wildtype (K) and *taz*$^{-/-}$ mutant (L) embryos. Expression of *sox* genes, *sox1b* (M-N), *sox2* (O-P) and *sox3* (Q-R) is unchanged from wildtype (M,O,Q) in *taz*$^{-/-}$ mutants (N,P,R). All embryos are dorsal views, anterior to the left, 22 hpf.

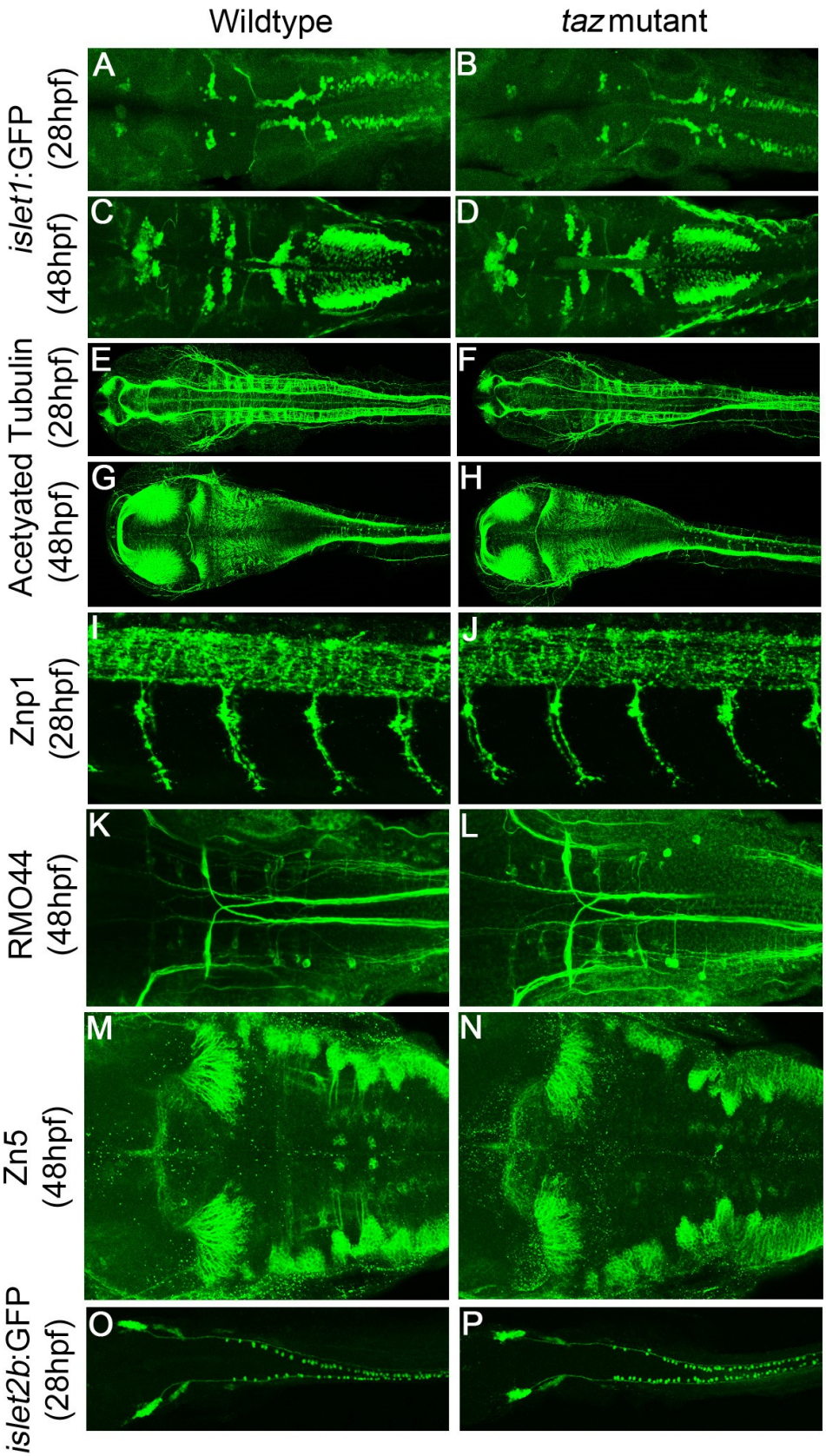
Wildtype
taz mutant
islet1:GFP (28hpf)
A
B
(48hpf)
C
D
Acetyated Tubulin (28hpf)
E
F
(48hpf)
G
H
Znp1 (28hpf)
I
J
RMO44 (48hpf)
K
L
Zn5 (48hpf)
M
N
islet2b:GFP (28hpf)
O
P

Figure 6.4. *Taz* mutants may have changes in abducens and rohon-beard neurons, but not in other neuronal populations.

Branchiomotor neuron organization and axon projections observed by *Tg(isl1:GFP)* is the same in wildtype (A,C) and *taz*$^{-/-}$ mutant embryos (B,D) at 28 hpf (A-B) and 48 hpf (C-D). Acetylated tubulin labeling of axon projections does not show any major differences at 28 hpf (E-F) or 48 hpf (G-H) between wildtype (E,G) and *taz*$^{-/-}$ mutants (F, H). Spinal cord motor neuron axon projections labeled by Znp1 are normal in wildtype (I) and *taz*$^{-/-}$ mutants (J). Reticulospinal neuron numbers, organization and axon projections in wildtype (K) and *taz*$^{-/-}$ mutants are similar (L). Zn5 labels abducens neurons in the centre of the hindbrain in wildtype embryos (M) and these neurons are variably affected in *taz*$^{-/-}$ mutants (N). Rohon-beard neurons are labeled in the spinal cord by *Tg(isl2b:GFP),* and there appears to be an increase in the number of rohon-beard neurons in *taz*$^{-/-}$ mutants (although this effect can be variable) (P) as compared to wildtype (O). All images are anterior to the left, (A-H, K-P) are dorsal views, (I-J) are lateral views, stages are indicated on the left of the images.

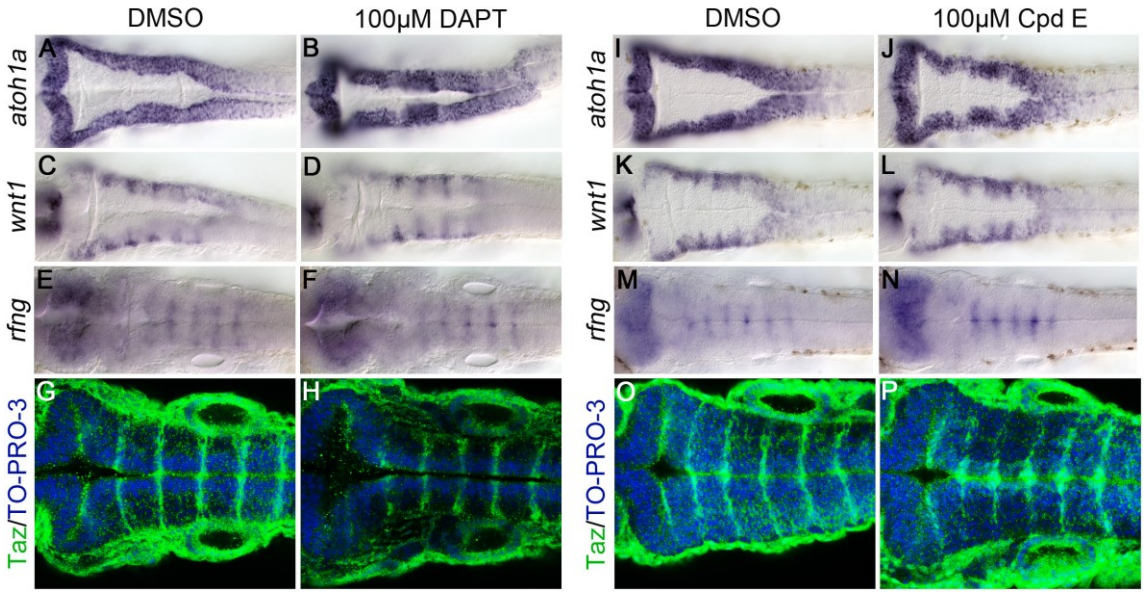

Figure 6.5. Pharmacological inhibition of the Notch Signaling pathway may result in smaller ventricles, but does not affect rhombomere boundary specific gene expression and localization.

Embryos were treated with either DMSO as a control (A, C, E, G, I, K, M, O), 100 μM DAPT (B, D, F, H) or 100 μM Cpd E (J, L, N, P) and *atoh1a* (A-B, I-J), *wnt1* (C-D, K-L) and *rfng* (E-F, M-N) expression and Taz localization (G-H, O-P) was examined. Treatment with 100 μM DAPT or 100 μM Cpd E results in a reduction in ventricle size (B, J), compared to controls (A, I). Rhombomere boundary specific expression of *wnt1* and *rfng* is maintained embryos treated with 100 μM DAPT (D, F) or 100 μM Cpd E (L, N), and localization of Taz to rhombomere boundaries is also maintained in embryos treated with 100 μM DAPT (H) or 100 μM Cpd E (P). Treatment with 100 μM Cpd E does result in a slight increase in the midline expression of *rfng* (N) and midline localization of Taz (P) compared to untreated embryos (M, O). All embryos are dorsal views, anterior to the left, 24 hpf.

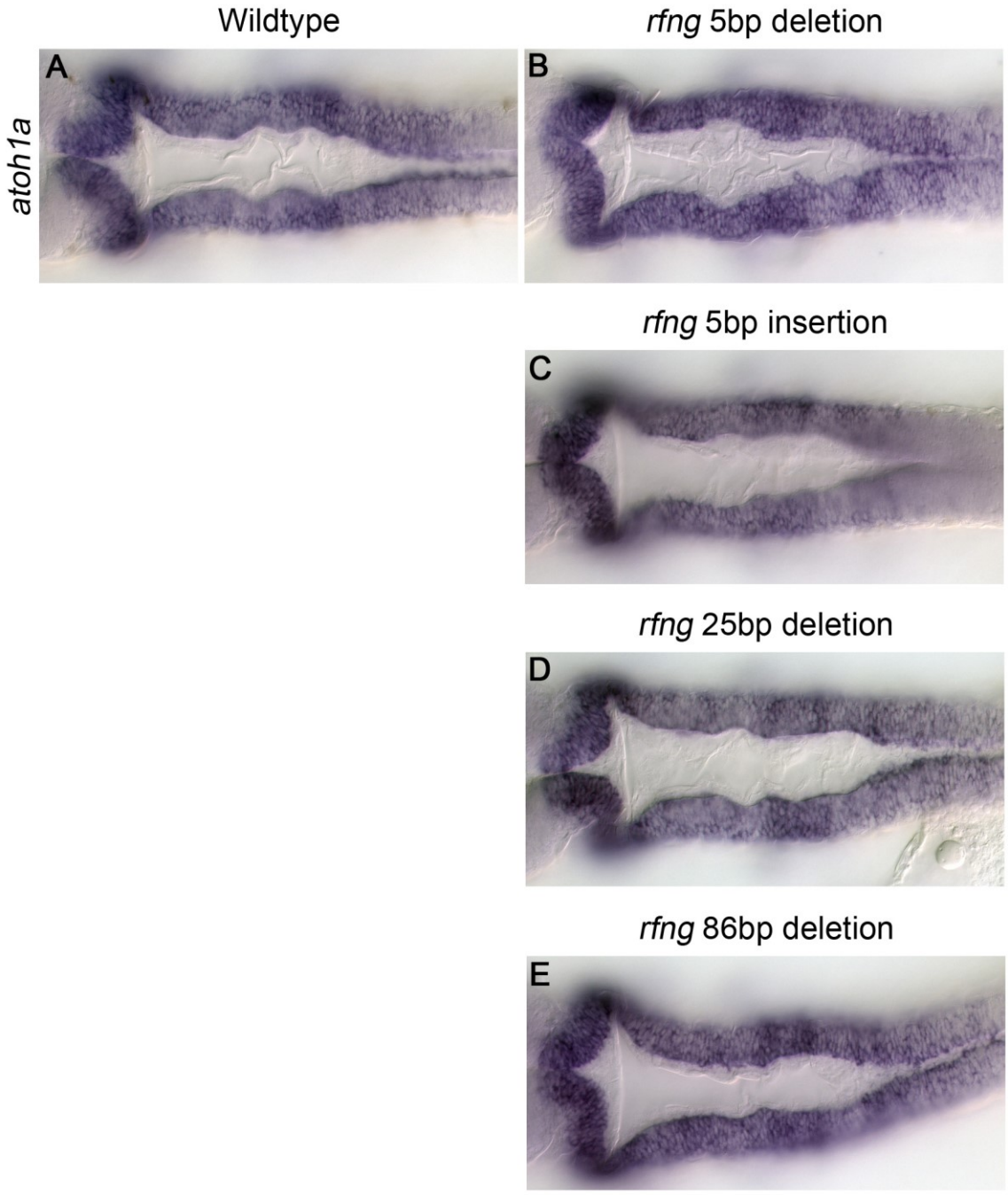

Figure 6.6. Loss of function of *rfng* does not cause ventricle defects.

CRISPRs targeting the signal peptide and transmembrane region of *rfng* were injected into 1-2 cell stage embryos. Embryos were grown to adulthood, and founders containing germline mutations were identified and incrossed. F1 embryos from these P0 incrosses were examined for alterations in ventricle morphogenesis using *atoh1a.* Sequencing identified embryos with homozygous mutations in *rfng*, 4 alleles were identified, a 5 bp

deletion (B), a 5 bp insertion (C), a 25 bp deletion (D) and an 86 bp deletion (E). None of the homozygous mutations in *rfng* resulted in defects in ventricle morphogenesis (B-E), as compared to wildtype embryos (A). All embryos are dorsal views, anterior to the left, 22 hpf.

Chapter 7: Conclusions and Future Directions

7.1 Links between segmental gene expression and rhombomere boundaries in hindbrain development

Segmental gene expression and the division of the developing hindbrain into rhombomeres, is essential for the development of adult tissues that arise from the hindbrain, but is also required for specification and development of neuronal populations associated with the hindbrain, craniofacial tissues, and development of tissues adjacent to the hindbrain such as the ear. To establish rhombomere patterning, regionalization of the hindbrain through FGF and RA signaling is required (Gavalas, 2002; Maroon et al., 2002; Maves et al., 2002; Niederreither and Dolle, 2008; Phillips et al., 2001). Loss of RA signaling results in a loss of posterior hindbrain identity (Begemann et al., 2001; Dupe and Lumsden, 2001; Maden et al., 1996), while loss of FGF signaling results in disruption of the anterior hindbrain, and the r4 signaling centre, affecting the specification of the surrounding rhombomeres (r3-6) (Maroon et al., 2002; Maves et al., 2002; Phillips et al., 2001). A complex network of transcription factors is established in the hindbrain, with each transcription factor being expressed in a unique domain and performing a specific function. Paralog group 1-4 *hox* genes display nested expression domains, where PG 2 *hox* genes are expressed up to the r2/3 boundary, PG1 *hox* gene are expressed up to the r3/4 boundary, PG 3 *hox* genes are expressed up to the r4/5 boundary, and PG 4 *hox* genes are expressed up to the r6/7 boundary (with some exceptions) (Hunt et al., 1991; Keynes and Krumlauf, 1994; Lumsden and Krumlauf, 1996; Maconochie et al., 1996; Wilkinson et al., 1989). *Hox* gene expression is required for segmental identity, and loss of *hox* genes is associated with homeotic transformations and loss of segmental identity (Carpenter et al., 1993; Davenne et al., 1999; Gaufo et al., 2003; Gavalas et al., 1997; Gavalas et al., 2003; Gavalas et al., 1998; Mark et al., 1993; McClintock et al., 2002; McNulty et al., 2005; Rijli et al., 1998; Rossel and Capecchi, 1999; Studer et al., 1998; Trainor and Krumlauf, 2000; Weicksel et al., 2014; Zigman et al., 2014). Previous work has suggested roles for paralog group 1 *hox* genes as master regulators of hindbrain patterning. Paralog Group 1 (PG1) *hox* genes are the first to be expressed in the nascent hindbrain (Alexandre et al., 1996). Loss of the *hox* cofactors *pbx2* and *pbx4* results in a loss of segmental identity from r2-6, however that expression of *hoxb1b* is unaffected (Waskiewicz et al., 2002). As such, it was proposed that Pbx-

Hox-1 complexes are required to regulate and initiate patterning of segmental gene expression throughout the hindbrain. Consistent with this model, knockdown of *hoxa1/b1/d1* in *Xenopus laevis* results in a loss of segmental identity similar to that observed in Pbx-depleted zebrafish embryos (McNulty et al., 2005; Waskiewicz et al., 2002). However our work and others have shown that in mouse and zebrafish, the loss of PG1 *hox* genes does not result in a complete loss of hindbrain identity, instead affecting patterning and segmentation more locally from r3-6 (Gavalas et al., 1998; Rossel and Capecchi, 1999; Selland et al., 2018; Studer et al., 1998; Weicksel et al., 2014; Zigman et al., 2014). We have shown that the loss of both *hoxb1b* and *pbx4* is sufficient to revert the hindbrain to the r1 ground state (Selland et al., 2018). This provides evidence that *pbx* plays a central role in hindbrain specification, as more than just a cofactor to PG1 *hox* genes. Additionally, our work supports roles for *hoxb1b* in regulating Fgf signaling, and for *pbx* genes in regulating RA signaling (Selland et al., 2018).

Not only does segmental gene expression establish rhombomere identity, it is also required for the generation of rhombomere boundaries. Expression of Ephs and Ephrins in alternating segments is an important step in sorting and segregating cells into the appropriate compartments (Bovenkamp and Greer, 1997; Cooke et al., 2001; Mellitzer et al., 1999; Xu et al., 1995a). Ephrins and Eph receptors are expressed in alternating rhombomeres, with receptors being expressed in r3/5 and ligands being expressed in r2/4/6 (Bovenkamp and Greer, 1997; Cooke et al., 2001; Mellitzer et al., 1999; Xu et al., 1995a); reviewed by (Cooke and Moens, 2002; Lumsden, 1999)). Segment specific gene expression promotes the expression of Ephs and Ephrins. *Krox20* activates *epha4a* expression in r3/5 (Maconochie et al., 1996; Nonchev et al., 1996a; Nonchev et al., 1996b), and loss of *val* results in expanded *ephrinb2a* expression across r4-7, as opposed to the normal 2-segment periodicity (Cooke et al., 2001; Moens et al., 1998; Moens et al., 1996). Similarly, the loss of segmental identity seen in *pbx*-nulls and in *hoxb1b;pbx4* double mutants results in an expansion of *epha4a* across the entire hindbrain (Selland et al., 2018; Waskiewicz et al., 2002). The segregation of cells into separate compartments is accompanied by the establishment of a distinct population of cells at the boundaries between rhombomere. These boundary cells express specific markers, have an elongated shape and larger intercellular spaces, while also

experiencing reduced proliferation and interkinetic nuclear migration (Guthrie et al., 1991; Guthrie and Lumsden, 1991; Heyman et al., 1995; Heyman et al., 1993; Lumsden and Keynes, 1989). Interactions between Ephs and Ephrins in odd/even numbered rhombomeres are required for the formation of rhombomere boundary cells (Cooke et al., 2005; Guthrie and Lumsden, 1991; Terriente et al., 2012; Xu et al., 1995a). Knockdown of *epha4a* and *ephrinb3b* results in a partial loss of rhombomere boundary markers (Terriente et al., 2012). Defects in segmental gene expression resulting in alterations to Eph/Ephrin expression also result in defects in the expression of rhombomere boundary markers. *Val* mutants do not have rhombomere boundaries posterior to the r3/4 boundary, and this includes a loss of *mariposa* (*foxb1a*) expression (Cooke et al., 2001; Moens et al., 1998; Moens et al., 1996). Similarly, *pbx*-nulls have a loss of *mariposa* expression throughout the hindbrain (Waskiewicz et al., 2002). In contrast to these results, loss of *hoxb1b* results in a loss of rhombomere boundaries expression of *mariposa* anterior to r5/6 and compound loss of *hoxb1a* and *hoxb1b* disrupts *mariposa* expression throughout the hindbrain (Selland et al., 2018). Despite this apparent disruption of rhombomere boundaries, *hoxb1b* mutants and *hoxb1a;hoxb1b* double mutants still have expression of *epha4a* in r3/5. Although *epha4a* expression is unaffected in *hoxb1b* mutants and *hoxb1a;hoxb1b* double mutants, it is possible that the expression of other Ephs and Ephrins in the hindbrain may be affected.

Boundaries are important to coordinate patterns of growth and differentiation in adjacent compartments (Blair, 2003; Blair and Ralston, 1997; Clarke and Lumsden, 1993; Dahmann and Basler, 1999; Gaunt et al., 1997; Gaunt, 1997; Irvine, 1999; Irvine and Rauskolb, 2001; Lumsden and Krumlauf, 1996; Sanson, 2001; Trevarrow et al., 1990; Wingate and Lumsden, 1996), and within the hindbrain, rhombomere boundary cells are a source of signals that function to organize neurons and glia within each rhombomere (Hanneman et al., 1988; Metcalfe et al., 1986; Trevarrow et al., 1990). Notch activation at rhombomere boundaries suppresses neuronal differentiation, and Delta expression is restricted from rhombomere boundaries (Cheng et al., 2004). Loss of function of components of the Notch signaling pathway results in neurogenic phenotypes (Appel et al., 1999; Bingham et al., 2003; Cheng et al., 2004; Gray et al., 2001; Holley et al., 2000; Holley et al., 2002; Itoh et al., 2003; Jiang et al., 1996; Park

and Appel, 2003; Riley et al., 1999; Schier et al., 1996; van Eeden et al., 1996). In particular, *mindbomb* mutants initially form rhombomere boundaries, but they are not maintained (Riley et al., 2004). As a result, *mindbomb* mutants also have ectopic expression of proneural and neuronal markers at early stages, indicative of overproduction of early born neurons and rhombomere centre neurons (Bingham et al., 2003; Cheng et al., 2004; Itoh et al., 2003; Jiang et al., 1996; Park and Appel, 2003; Riley et al., 2004; Schier et al., 1996).

Elevated levels of *wnt* at rhombomere boundaries also regulate patterning of the rhombomeres and Notch signaling provides feedback to maintain the rhombomere boundaries as Wnt signaling centers (Riley et al., 2004). Our work also suggests a role for Taz and Wnt/β-catenin signaling at rhombomere boundaries that is important for ventricle morphogenesis. Previous research has found that Taz can be incorporated into the β-catenin destruction complex, where it recruits the E3 ubiquitin ligase, β-TrCP, mediating ubiquitination and degradation of both Taz and β-catenin (Azzolin et al., 2014; Azzolin et al., 2012). Wnt ligand binding sequesters the β-catenin destruction complex at the cell membrane, preventing degradation of both Taz and β-catenin, thus allowing them to enter the nucleus and regulate target gene expression. Consistent with the elevated expression of *wnt* ligands at rhombomere boundaries, we find that Taz protein is localized specifically to rhombomere boundaries as well. This supports a model where Wnt signals at rhombomere boundaries not only stabilize β-catenin, but they also stabilize Taz. Additionally, we demonstrate that both β-catenin mediated transcription and Taz mediated transcription are involved in ventricle morphogenesis. We also find that Taz mutants have defects in the expression of other rhombomere boundary associated genes. *Rfng* expression at rhombomere boundaries is lost in *taz* mutants, and enrichment of *wnt1* expression at rhombomere boundaries is disrupted. The loss of *wnt1* rhombomere boundary expression may be due to the loss of *rfng* expression, as *rfng* has been shown to regulate *wnt1* expression at rhombomere boundaries (Cheng et al., 2004). Our work also suggests that Taz is upstream of Notch signaling, as inhibition of Notch signaling does not disrupt localization of Taz to rhombomere boundaries, although it does reduce the size of the ventricle.

Together our research supports a model in which Hoxb1b in combination with Pbx4 are essential for the establishment of segmental identity in the hindbrain, and this is achieved at least in part through regulation of Fgf signaling by Hoxb1b, and regulation of RA signaling by Pbx genes. Segmental identity facilitates the appropriate expression of Ephs and Ephrins in the hindbrain, which mediate cell sorting and is involved in establishing rhombomere boundaries. Rhombomere boundary cells then regulate both neurogenesis and ventricle morphogenesis. However, there is one key step in this model that has not been investigated. It is unclear how the alternating expression of Ephs and Ephrins induce rhombomere boundary specific characteristics and markers, however we present two possible models for how this could be achieved.

Previous research has shown that actin is enriched along segment borders and at the interface between transplanted cells with different segmental identities (Calzolari et al., 2014; Cooke et al., 2001). Eph/Ephrin signaling may be responsible for changes in the cytoskeleton specifically at rhombomere boundaries. Eph forward signaling activates tyrosine kinase activity, which can then regulate the activity of Rho GTPases and Rho kinase, which in turn modulate cytoskeletal dynamics and mediate cortical tension (reviewed in (Amano et al., 2010)). Furthermore, knockdown of *epha4a* disrupts the formation of actomyosin cables at rhombomere boundaries (Calzolari et al., 2014). Actomyosin cables induced at rhombomere boundaries by Eph/Ephrin may then go on to induce either Taz nuclear localization, or Wnt signaling at rhombomere boundaries. *Ephb2/Ephrinb1* interactions have been shown to promote nuclear localization of Taz to promote osteoblast differentiation (Arthur et al., 2011; Xing et al., 2010). Yap/Taz have also previously been shown to respond to changes in actin. Reduced cellular tension or reduced actin polymerization results in cytosolic Yap/Taz (Dupont et al., 2011), while stabilization of actin has been shown to increase the nuclear localization of Yap (Reddy et al., 2013). Although changes in cytoskeletal dynamics are most often seen downstream of non-canonical Wnt signaling, there is some evidence that the cytoskeleton may also regulate components of the canonical Wnt signaling pathway. Apc (Adenomatous polyposis coli), a component of the β-catenin destruction complex has been shown to be localized to the plasma membrane via interactions with actin (Langford et al., 2006; Rosin-Arbesfeld et al., 2001) The plasma membrane localization

of Apc may interfere with the function of the β-catenin destruction complex, resulting in stabilization of Taz and β-catenin. Therefore, one potential model for how Eph/Ephrin signaling induces rhombomere boundary cells may be that stabilization of Taz, either directly by the cytoskeletal signals, or by cytoskeletal mediated activation of Wnt signaling at rhombomere boundaries, drives the expression of rhombomere boundary markers, such as *rfng*. *Rfng* subsequently activates *wnt1* expression at rhombomere boundaries, which provides feedback to maintain Taz localization and Wnt signaling at rhombomere boundaries. This feedback may also be involved in the maintenance of the cytoskeleton and apicobasal polarity at rhombomere boundaries during ventricle morphogenesis.

Alternatively, Eph/Ephrin signaling may directly activate the expression of Wnt ligands at rhombomere boundaries (or a factor which subsequently induces the expression of Wnt ligands). Eph/Ephrins have been shown to regulate gene transcription. Forward signaling by EphrinB1 regulates a subset of genes that are indicative of receptor tyrosine kinase signaling pathways, and suggests roles for signal transduction through the Erk/Mapk cascade (Bush and Soriano, 2010). The intracellular domain of EphrinB1 can also be cleaved by presenilins. This intracellular domain has been shown to by involved in maintaining neural progenitor cells by enhancing Zhx2 transcriptional activity (Georgakopoulos et al., 2006; Tomita et al., 2006; Wu et al., 2009). Eph/Ephrin mediated activation of gene expression at rhombomere boundaries, may then directly or indirectly activate Wnt signaling at rhombomere boundaries, resulting in stabilization of β-catenin and Taz. Similar to the previous model, Taz then activates *rfng* expression at rhombomere boundaries, which then activates *wnt1*. This provides feedback to maintain Wnt signaling and Taz protein at rhombomere boundaries. *Rfng* expression at rhombomere boundaries may then mediate activation of Notch at rhombomere boundaries. Notch activation regulates cell affinity at rhombomere boundaries (Cheng et al., 2004), and has also been shown to induce boundary expression of F-actin and actin-binding molecules at adherens junctions (Major and Irvine, 2005; Major and Irvine, 2006). *Mindbomb* ubiquitinates the FERM family member Epb41l5 (Matsuda et al., 2016), which is involved in establishing neuroepithelial apical-basal polarity (Gosens et al., 2007; Hsu et al., 2006; Jensen et al., 2001; Jensen and Westerfield, 2004; Laprise et

al., 2006). Therefore, Taz mediated activation of Notch signaling via *rfng*, may be responsible for actin localization to rhombomere boundaries, and establishment or maintenance of apicobasal polarity at rhombomere boundaries, and ventricle morphogenesis. A role for Notch signaling in the establishment of actomyosin bundles downstream of Eph/Ephrin signals is supported by the timing of actomyosin accumulation, and Eph expression. *Epha4a* is expressed at 11 hpf, while actomyosin accumulation at rhombomere boundaries is not observed until 15 hpf (Calzolari et al., 2014). This delay between Eph expression and actomyosin bundle formation, may suggest that there are multiple steps between Eph and changes in the cytoskeleton.

In both models we would expect that disruption of Eph/Ephrin signals should affect Taz localization at rhombomere boundaries. However, if changes in the cytoskeleton are responsible for Taz stabilization at rhombomere boundaries, then disruption of the actomyosin bundles at rhombomere boundaries, should also result in a loss of Taz rhombomere boundary localization. On the other hand, if establishment of the actomyosin bundles at rhombomere boundaries is a result of Eph/Ephrin activation of Wnt signaling and Taz, then disruption of the actomyosin bundles may affect ventricle morphogenesis, but should not affect Taz stabilization at rhombomere boundaries.

7.2 Roles for segmental gene expression and rhombomere boundaries in hindbrain neurogenesis

Our research and others have illustrated the importance of segmental gene expression. It is required for segmental identity, establishment of rhombomere boundaries and neurogenesis. Loss of function of *hoxb1b* disrupts gene expression in r4/5 and rhombomere boundaries anterior to r5/6. As a result, *hoxb1b* mutants have defects in r4 and r6 associated reticulospinal neurons, and reduced numbers of the r4 born facial BMN (Selland et al., 2018; Weicksel et al., 2014). Loss of function of *hoxb1a* in combination with *hoxb1b* exacerbates these phenotypes, resulting is disruption of all rhombomere boundaries, loss of r3/4/6 reticulospinal neurons and defects in both the number and posterior migration of the facial BMNs (Selland et al., 2018; Weicksel et al., 2014). Similarly, the loss of other segment specific genes results

in rhombomere boundary and neuronal defects. Loss of function of *val* affects gene expression in r5/6, disrupts rhombomere boundaries posterior to r3/4, and results in defects in reticulospinal neurons, commissural neurons, and abducens neurons (Cooke et al., 2001; Moens et al., 1998; Moens et al., 1996; Riley et al., 2004). *Pbx*-nulls have a complete loss of segmental identity, where the entire hindbrain acquires an r1 identity and rhombomere boundaries are lost throughout the hindbrain (Waskiewicz et al., 2002). This results in severe neuronal defects. The trochlear (nIV) CMNs in r0 are still present, and vagal (nX) BMN that are normally located in the caudal hindbrain are still present, but they are not organized as they are in wildtype. Additionally while there are some presumptive BMNs between these two populations, they are not identifiable as trigeminal (nV), facial (nVII) or glossopharyngeal (nIX) neurons. Additionally, at early stages of development while wildtype embryos have a distinctive organization of developing BMN and engrailed-positive neurons, *pbx*-nulls have homogeneous localization of developing BMN and engrailed-positive neurons throughout the hindbrain. Together these results support essential roles for segmental gene expression in establishing rhombomere boundaries, and regulating neurogenesis.

Further support for the role of rhombomere boundaries in neurogenesis comes from examination of mutants that have a loss of rhombomere boundaries. *Mindbomb* mutants fail to maintain rhombomere boundaries, and while they do have segmental gene expression at early stages, it is disrupted later on in development (Bingham et al., 2003; Cheng et al., 2004; Riley et al., 2004). *Mindbomb* mutants do have extensive neurogenesis defects however, that have been attributed to the loss of lateral inhibition mediated by rhombomere boundaries. *Mindbomb* mutants have increased numbers of early born neurons, at the expense of late born neurons, disorganization of the branchiomotor neurons, increased numbers of rhombomere centre neurons (such as reticulospinal neurons), increased numbers of rohon-beard neurons and a loss of commissural neurons (Appel et al., 1999; Bingham et al., 2003; Cheng et al., 2004; Itoh et al., 2003; Riley et al., 2004; Schier et al., 1996). Similarly, *deltaA* mutants have disrupted rhombomere boundaries and overproduction of rhombomere centre reticulospinal neurons (Riley et al., 2004). The loss of rhombomere boundaries without significant disruption to rhombomere specific gene expression also results in disruptions

in neurogenesis. *Sfpq* mutants have a loss of *rfng* expression at rhombomere boundaries, but do not appear to have defects in rhombomere specific gene expression (Lowery et al., 2007; Thomas-Jinu et al., 2017). Examination of neurogenesis in *sfpq* mutants reveals a loss of reticulospinal neurons in the hindbrain, (except for the Mauthner neuron), reduced numbers of axons throughout the forebrain midbrain and hindbrain, and defects in axon tract organization and projection (Lowery et al., 2007; Thomas-Jinu et al., 2017). Similarly, *med12* mutants have a loss of rhombomere boundary markers, including *rfng*, yet still appear to maintain rhombomere patterning, and have reduced numbers of reticulospinal neurons and commissural neurons in the hindbrain (Hong and Dawid, 2011; Lowery et al., 2009).

In contrast to these studies, our work suggests that Taz mutants have a loss of rhombomere boundaries, however there is almost no effect on neurogenesis in the hindbrain. *Taz* mutants have a loss of rhombomere boundary expression of *rfng* and *wnt1*, and while this supports a loss of rhombomere boundary specific regions, examination of further rhombomere boundary markers such as *mariposa* would be beneficial to confirm this. Additionally, while rhombomere boundaries may be lost, segmental gene expression does not appear to be affected. The expression of *Tg(lbx1b:eGFP)* (Fig 6.1 G-H) shows segment specific expression, that is decreased specifically in r3/5 in both wildtype and *taz* mutant embryos, suggesting that rhombomere patterning has not been disrupted. However, further examination of rhombomere specific markers will be required to unequivocally determine if rhombomere patterning is normal. Finally, examination of *taz* mutants finds that they do not have defects in branchiomotor neuron organization or projection, reticulospinal neuron organization or numbers, and no defects in axon numbers or projections are observed by acetylated tubulin staining. The only populations of neurons found to be affected were abducens neurons and rohon-beard neurons, and the effect was variable. In comparison to the literature, the lack of significant changes in neuronal populations in the hindbrain of *taz* mutants is at odds with the apparent importance of rhombomere boundaries in neurogenesis. Although the neuronal subtypes we have examined are often affected in mutants with rhombomere boundary defects, examination of HuC/D immunohistochemistry may allow us to observe defects in early born neurons that are

not apparent with the methods we have utilized thus far.

While the results in the literature support roles for rhombomere boundaries in neurogenesis, these studies along with ours also suggest roles for rhombomere boundaries in ventricle morphogenesis. *Mindbomb*, *sfpq* and *med12* mutants, all have defects in ventricle development, in addition to the defects in rhombomere boundary specific expression of *rfng* (Appel et al., 1999; Bingham et al., 2003; Cheng et al., 2004; Hong and Dawid, 2011; Itoh et al., 2003; Lowery et al., 2009; Lowery et al., 2007; Riley et al., 2004; Schier et al., 1996; Thomas-Jinu et al., 2017). These observations are consistent with the phenotype of *taz* mutants. Therefore, we propose a model in which *fringe* mediated activation of Notch at rhombomere boundaries is important for two separate developmental processes. Notch signaling not only mediates lateral inhibition to ensure appropriate organization of neurons and glia within each rhombomere, but it is also required for ventricle development. We hypothesize that different *fringe* genes may mediate these two functions of Notch at rhombomere boundaries.

Lunatic fringe (*lfng*) is expressed primarily in even-numbered rhombomeres and at lower levels in odd-numbered rhombomeres (Prince et al., 2001; Qiu et al., 2004). We propose that *lfng* may mediate lateral inhibition in the hindbrain. In support of this role, previous research has shown that *lfng* cell autonomously maintains cells as neural progenitors (Nikolaou et al., 2009). *Rfng* is expressed specifically at rhombomere boundaries, and we propose that *rfng* is required to mediate Notch signaling required for ventricle morphogenesis. Consistent with this hypothesis, knockdown of *rfng* does result in ventricle defects (Elsen et al., 2008). *Mindbomb* is required for efficient activation of Notch signaling, and is expressed throughout the hindbrain (Itoh et al., 2003; Thisse et al., 2004). *Mindbomb* mutants have disrupted Delta/Notch signaling throughout the hindbrain, so the presence of both ventricle and neurogenesis defects may be due to the inability of both *rfng* and *lfng* to activate Notch signaling. Similarly, in *sfpq* and *med12* mutants, where both neurogenesis and ventricle development are disrupted, we would expect to see a loss or reduction in *lfng* expression in addition to the loss of *rfng* expression previously observed (Hong and Dawid, 2011; Thomas-Jinu et al., 2017). Conversely, in *taz* mutants where neurogenesis is largely unchanged, we would expect to see little to no change in *lfng* expression. Additionally, provided *lfng* and *rfng* do not

compensate for each other, we would expect that loss of function of *lfng* should cause defects in neurogenesis, but not in ventricle development, while loss of function of *rfng* should cause defects in ventricle development and not in neurogenesis

7.3 Utilizing hindbrain genes to elucidate the differences between morphants and mutants

The advent of genome editing tools has greatly improved the ability of scientists to study how genetic changes affects phenotypes, however it does not come without challenges. Our lab has had success using Zinc-Finger Nucleases (ZFNs), Transcription Activator-like Effector Nucleases (TALENs) and Clustered Regularly Interspersed Palindromic Repeats (CRISPRs) to generate targeted mutations. Genome editing techniques use different methods to create double strand breaks (DSB) in genes of interest which are primarily repaired by Non-Homologous End-Joining (NHEJ), but also can be repaired by Homology Directed Repair (HDR). NHEJ can give rise to insertions and deletions, resulting in frameshifts. ZFNs were first used in zebrafish in 2008 to generate targeted mutations (Doyon et al., 2008; Meng et al., 2008), while TALENs first came into use in 2011 (Huang et al., 2011; Sander et al., 2011a). Both ZFNs and TALENs use a fusion of the nuclease domain from the Type IIS restriction Enzyme FokI, while the DNA recognition component of ZFNs is composed of multiple 3-base recognition motifs. TALENs rely on arrays of repeat modules containing a repeat variable di-residue, which specifies recognition of a particular DNA base. Pairs of ZFs or TALEs then target the nuclease to the gene of interest. ZFNs have a more limited targeting capability, while TALENs have almost no restrictions in targeting capability, greater specificity and fewer off target cleavages (Christian et al., 2010; Li et al., 2011b; Miller et al., 2007). However, generation of both ZFNs and TALENs can be relatively expensive and time consuming.

A great deal of research has gone into improvements in genome editing technologies. We have investigated the effectiveness of the *sharkey* FokI variant (Guo et al., 2010) in improving the mutagenesis efficiency of these technologies. We found that while the *sharkey* FokI variant does increase target-site cleavage of both ZFNs and TALENs in vitro, it only improves mutagenesis in vivo for ZFNs. *Sharkey* TALENs fail

to generate mutations in vivo. This is important for those attempting to increase mutagenesis efficiency with TALENs.

However, recent technological advances in genome editing have utilized the CRISPR-Cas9 system. CRISPRs were initially identified in *Escherichia coli* in 1987 as clusters of 29bp repeats by Nakata et al (Ishino et al., 1987). Cas (CRISPR associated genes) were subsequently identified, including the RNA-directed endonuclease, Cas9 (Garneau et al., 2010). Further work generated a single guide RNA method (?) that could successfully target the Cas9 endonuclease to specific targets (Jinek et al., 2012), and this system was first used in zebrafish in 2013 (Hwang et al., 2013). The CRISPR system is advantageous as it only requires a gene specific sgRNA, and Cas9, and unique sgRNAs can be easily synthesized from overlapping oligos (Varshney et al., 2015). Since the advent of CRISPR technology, much of the field has adopted it as the technique of choice. CRISPRs are commonly used for targeted gene knockouts, and knock ins via HDR. HDR has been used in investigating, and researching therapies for disease causing loci (such as thalassemia (Niu et al., 2016; Xu et al., 2015), Alzheimer's disease (Paquet et al., 2016) sickle cell anemia (Huang et al., 2015), HIV-resistance (Kang et al., 2015) and Duchenne muscular dystrophy (Li et al., 2015a)). Furthermore, HDR could be used to insert epitope tags, manipulate promoters, and introduce full-length genes.

A variety of applications for the CRISPR system have also been developed using catalytically inactive Cas9 (dead Cas9 or dCas9) (Bikard et al., 2013; Chen et al., 2013a; Dominguez et al., 2016; Gilbert et al., 2013; Ma et al., 2015; Polstein and Gersbach, 2015; Qi et al., 2013). Transcription initiation and elongation can be blocked with dCas9, (Qi et al., 2013), it can also be fused to transcriptional activators or repressors (Bikard et al., 2013; Dominguez et al., 2016), and a version has been created which activates genes in response to blue light stimulation (Polstein and Gersbach, 2015).

While the advancements in genome editing have significantly improved our ability to investigate the role of genes in development, it has not been without challenges. One of the major challenges is the disparity between phenotypes generated by antisense morpholino oligonucleotides (MO) and mutants. Kok *et al.* (Kok et al., 2015) examined mutants for 24 genes, and found that only 3 had phenotypes similar to those observed in morphants. MOs are known to induce p53 dependent apoptosis and

off-target effects (Amoyel et al., 2005; Ekker and Larson, 2001; Gerety and Wilkinson, 2011; Pickart et al., 2006; Robu et al., 2007), and this may be one explanation for the presence of phenotypes in morphants, that are not observed in mutants. However, Rossi et al (Rossi et al., 2015) determined that these phenotypic differences may in fact be due to genetic compensation. Egfl7 mutants have an upregulation in the expression of Emilins that does not occur in morphants, which may be compensating for the loss of Egfl7. This upregulation also occurs in embryos injected with egfl7 TALENs, but does not occur in egfl7 morphants. Compensation in mutants can also occur at the mRNA. Anderson et al (Anderson et al., 2017) found that in 5 of 7 mutant lines altered mRNA processing; including alternative mRNA splicing and the use of cryptic slice sites can be used to restore ORFs in homozygous mutants. This allows for the translation of at least a partially functional protein and may allow the embryo to cope with the loss of function. It is also possible that other mechansims may allow for production of full-length proteins from mutant mRNAs, such as ribosomal frameshifting and non-sense readthrough (Baradaran-Heravi et al., 2017). These compensatory mechanisms are supported by the identification of deleterious mutations in essential genes in humans (Jagannathan and Bradley, 2016). A final confounding factor is the contribution of maternally expressed genes. Sequencing of transcripts before and after the maternal-zygotic transition has shown that 34% of genes are exclusively maternal, while 61% are maternal and zygotic, and only 5% are exclusively zygotic (Harvey et al., 2013). Genes that are maternally expressed will be affected by translation blocking MOs, while heterozygous incrosses for mutants of these genes will still retain the maternal contribution, and as a result may not have a phenotype or may have a less severe phenotype.

From the initial advent of genome editing technologies to now, we have made significant advances. The time required and the ease with which mutations in a gene of interest can be obtained have been significantly improved. HDR has been shown to be possible, however there is still room for improvement in terms of efficiency. Further research has expanded the use of genome editing tools to modulate gene expression via different methods. Advances in our understanding of how the embryo responds to deleterious mutations have helped us to understand the disparity between morphants and mutant phenotypes, and come up with guidelines and strategies for the generation of

mutants, and the analysis of such mutants. However the mechanism(s) of how mutant embryos detect and compensate for deleterious mutations have not been elucidated. This is further complicated by the fact that while some mutants do not recapitulate morphants phenotypes, some mutants do have the same phenotypes as morphants. Within our own research we have encountered both situations. The phenotypes we observe in *hoxb1a* and *hoxb1b* mutants are consistent with those observed in *hoxb1a* and *hoxb1b* morphants (McClintock et al., 2002). Conversely, our examination of *rfng* mutants does not yield the same phenotype as *rfng* morphants (Elsen et al., 2008).

Our identification and characterization of these genes, provides an opportunity to examine the mechanisms by which mutant embryos identify and respond to mutations. Through analysis of the transcriptome of *hoxb1b* morphants, *hoxb1b* mutants, *rfng* morphants and *rfng* mutants, pathways that are used to identify deleterious mutations and compensate for them may be identified. Comparison of *hoxb1b* morphants to *hoxb1b* mutants should not yield any differences in the transcriptome, while the comparison of *rfng* morphants to *rfng* mutants may identify transcripts that are being upregulated specifically in response to the presence of a mutation in *rfng*. These transcripts should not be upregulated in *rfng* morphants, or in *hoxb1b* mutants, where compensatory mechanisms are not active. Identification of pathways that mediate compensatory responses in zebrafish, may provide the opportunity to generate zebrafish lines in which these pathways are inactive. This would facilitate characterization of gene function without the added complexity of compensation. This approach could also be used to determine if there is any correlation between different types of mutations, or mutations that targeting certain domains, and their ability to induce compensation.

References

Aberle, H., Bauer, A., Stappert, J., Kispert, A. and Kemler, R., 1997. beta-catenin is a target for the ubiquitin-proteasome pathway. EMBO J. 16, 3797-804.

Abu-Abed, S., Dolle, P., Metzger, D., Beckett, B., Chambon, P. and Petkovich, M., 2001. The retinoic acid-metabolizing enzyme, CYP26A1, is essential for normal hindbrain patterning, vertebral identity, and development of posterior structures. Genes Dev. 15, 226-40.

Abu-Shaar, M., Ryoo, H.D. and Mann, R.S., 1999. Control of the nuclear localization of Extradenticle by competing nuclear import and export signals. Genes Dev. 13, 935-45.

Adler, J.J., Heller, B.L., Bringman, L.R., Ranahan, W.P., Cocklin, R.R., Goebl, M.G., Oh, M., Lim, H.S., Ingham, R.J. and Wells, C.D., 2013. Amot130 adapts atrophin-1 interacting protein 4 to inhibit yes-associated protein signaling and cell growth. J Biol Chem. 288, 15181-93.

Agarwala, S., Duquesne, S., Liu, K., Boehm, A., Grimm, L., Link, S., Konig, S., Eimer, S., Ronneberger, O. and Lecaudey, V., 2015. Amotl2a interacts with the Hippo effector Yap1 and the Wnt/beta-catenin effector Lef1 to control tissue size in zebrafish. Elife. 4, e08201.

Aires, R., Jurberg, A.D., Leal, F., Novoa, A., Cohn, M.J. and Mallo, M., 2016. Oct4 Is a Key Regulator of Vertebrate Trunk Length Diversity. Dev Cell. 38, 262-74.

Akai, J., Halley, P.A. and Storey, K.G., 2005. FGF-dependent Notch signaling maintains the spinal cord stem zone. Genes Dev. 19, 2877-87.

Akam, M., 1989. Hox and HOM: homologous gene clusters in insects and vertebrates. Cell. 57, 347-9.

Alarcon, C., Zaromytidou, A.I., Xi, Q., Gao, S., Yu, J., Fujisawa, S., Barlas, A., Miller, A.N., Manova-Todorova, K., Macias, M.J., Sapkota, G., Pan, D. and Massague, J., 2009. Nuclear CDKs drive Smad transcriptional activation and turnover in BMP and TGF-beta pathways. Cell. 139, 757-69.

Alexandre, D., Clarke, J.D.W., Oxtoby, E., Yan, Y.-L., Jowett, T. and Holder, N., 1996. Ectopic expression of *Hoxa-1* in the zebrafish alters the fate of the mandibular arch neural crest and phenocopies a retinoic acid-induced phenotype. Development. 122, 735-746.

Alper, J., 2009. One-off therapy for HIV. Nat Biotechnol. 27, 300.

Alwin, S., Gere, M.B., Guhl, E., Effertz, K., Barbas, C.F., 3rd, Segal, D.J., Weitzman, M.D. and Cathomen, T., 2005. Custom zinc-finger nucleases for use in human cells. Mol Ther. 12, 610-7.

Amano, M., Nakayama, M. and Kaibuchi, K., 2010. Rho-kinase/ROCK: A key regulator of the cytoskeleton and cell polarity. Cytoskeleton (Hoboken). 67, 545-54.

Amaya, E., Musci, T.J. and Kirschner, M.W., 1991. Expression of a dominant negative mutant of the FGF receptor disrupts mesoderm formation in Xenopus embryos. Cell. 66, 257-70.

Amoyel, M., Cheng, Y.C., Jiang, Y.J. and Wilkinson, D.G., 2005. Wnt1 regulates neurogenesis and mediates lateral inhibition of boundary cell specification in the zebrafish hindbrain. Development. 132, 775-85.

Anderson, J.L., Mulligan, T.S., Shen, M.C., Wang, H., Scahill, C.M., Tan, F.J., Du, S.J., Busch-Nentwich, E.M. and Farber, S.A., 2017. mRNA processing in mutant zebrafish lines generated by chemical and CRISPR-mediated mutagenesis

produces unexpected transcripts that escape nonsense-mediated decay. PLoS Genet. 13, e1007105.
Angbohang, A., Wu, N., Charalambous, T., Eastlake, K., Lei, Y., Kim, Y.S., Sun, X.H. and Limb, G.A., 2016. Downregulation of the Canonical WNT Signaling Pathway by TGFbeta1 Inhibits Photoreceptor Differentiation of Adult Human Muller Glia with Stem Cell Characteristics. Stem Cells Dev. 25, 1-12.
Angus, L., Moleirinho, S., Herron, L., Sinha, A., Zhang, X., Niestrata, M., Dholakia, K., Prystowsky, M.B., Harvey, K.F., Reynolds, P.A. and Gunn-Moore, F.J., 2012. Willin/FRMD6 expression activates the Hippo signaling pathway kinases in mammals and antagonizes oncogenic YAP. Oncogene. 31, 238-50.
Anichtchik, O., Diekmann, H., Fleming, A., Roach, A., Goldsmith, P. and Rubinsztein, D.C., 2008. Loss of PINK1 function affects development and results in neurodegeneration in zebrafish. J Neurosci. 28, 8199-207.
Ansai, S., Sakuma, T., Yamamoto, T., Ariga, H., Uemura, N., Takahashi, R. and Kinoshita, M., 2013. Efficient targeted mutagenesis in medaka using custom-designed transcription activator-like effector nucleases. Genetics. 193, 739-49.
Appel, B., Fritz, A., Westerfield, M., Grunwald, D.J., Eisen, J.S. and Riley, B.B., 1999. Delta-mediated specification of midline cell fates in zebrafish embryos. Curr Biol. 9, 247-56.
Aragon, F., Vazquez-Echeverria, C., Ulloa, E., Reber, M., Cereghini, S., Alsina, B., Giraldez, F. and Pujades, C., 2005. vHnf1 regulates specification of caudal rhombomere identity in the chick hindbrain. Dev Dyn. 234, 567-76.
Aragona, M., Panciera, T., Manfrin, A., Giulitti, S., Michielin, F., Elvassore, N., Dupont, S. and Piccolo, S., 2013. A mechanical checkpoint controls multicellular growth through YAP/TAZ regulation by actin-processing factors. Cell. 154, 1047-1059.
Arenkiel, B.R., Tvrdik, P., Gaufo, G.O. and Capecchi, M.R., 2004. Hoxb1 functions in both motoneurons and in tissues of the periphery to establish and maintain the proper neuronal circuitry. Genes Dev. 18, 1539-52.
Artavanis-Tsakonas, S., Matsuno, K. and Fortini, M.E., 1995. Notch signaling. Science. 268, 225-32.
Artavanis-Tsakonas, S., Rand, M.D. and Lake, R.J., 1999. Notch signaling: cell fate control and signal integration in development. Science. 284, 770-6.
Arthur, A., Zannettino, A., Panagopoulos, R., Koblar, S.A., Sims, N.A., Stylianou, C., Matsuo, K. and Gronthos, S., 2011. EphB/ephrin-B interactions mediate human MSC attachment, migration and osteochondral differentiation. Bone. 48, 533-42.
Ashkenas, J., Muschler, J. and Bissell, M.J., 1996. The extracellular matrix in epithelial biology: shared molecules and common themes in distant phyla. Dev Biol. 180, 433-44.
Avantaggiato, V., Acampora, D., Tuorto, F. and Simeone, A., 1996. Retinoic acid induces stage-specific repatterning of the rostral central nervous system. Dev Biol. 175, 347-57.
Avilion, A.A., Nicolis, S.K., Pevny, L.H., Perez, L., Vivian, N. and Lovell-Badge, R., 2003. Multipotent cell lineages in early mouse development depend on SOX2 function. Genes Dev. 17, 126-40.
Azzolin, L., Panciera, T., Soligo, S., Enzo, E., Bicciato, S., Dupont, S., Bresolin, S., Frasson, C., Basso, G., Guzzardo, V., Fassina, A., Cordenonsi, M. and Piccolo,

S., 2014. YAP/TAZ incorporation in the beta-catenin destruction complex orchestrates the Wnt response. Cell. 158, 157-70.
Azzolin, L., Zanconato, F., Bresolin, S., Forcato, M., Basso, G., Bicciato, S., Cordenonsi, M. and Piccolo, S., 2012. Role of TAZ as mediator of Wnt signaling. Cell. 151, 1443-56.
Babalian, A.L. and Chmykhova, N.M., 1987. Morphophysiological characteristics of connexions between single ventrolateral tract fibres and individual motoneurones in the frog spinal cord. Brain Res. 407, 394-7.
Babalian, A.L. and Shapovalov, A.I., 1984. Synaptic actions produced by individual ventrolateral tract fibres in frog lumbar motoneurones. Exp Brain Res. 54, 551-63.
Bachmann, A., Schneider, M., Theilenberg, E., Grawe, F. and Knust, E., 2001. Drosophila Stardust is a partner of Crumbs in the control of epithelial cell polarity. Nature. 414, 638-43.
Bae, K.H., Kwon, Y.D., Shin, H.C., Hwang, M.S., Ryu, E.H., Park, K.S., Yang, H.Y., Lee, D.K., Lee, Y., Park, J., Kwon, H.S., Kim, H.W., Yeh, B.I., Lee, H.W., Sohn, S.H., Yoon, J., Seol, W. and Kim, J.S., 2003. Human zinc fingers as building blocks in the construction of artificial transcription factors. Nat Biotechnol. 21, 275-80.
Bae, Y.K., Shimizu, T. and Hibi, M., 2005. Patterning of proneuronal and inter-proneuronal domains by hairy- and enhancer of split-related genes in zebrafish neuroectoderm. Development. 132, 1375-85.
Bally-Cuif, L., Dubois, L. and Vincent, A., 1998. Molecular cloning of Zcoe2, the zebrafish homolog of Xenopus Xcoe2 and mouse EBF-2, and its expression during primary neurogenesis. Mech Dev. 77, 85-90.
Baradaran-Heravi, A., Niesser, J., Balgi, A.D., Choi, K., Zimmerman, C., South, A.P., Anderson, H.J., Strynadka, N.C., Bally, M.B. and Roberge, M., 2017. Gentamicin B1 is a minor gentamicin component with major nonsense mutation suppression activity. Proc Natl Acad Sci U S A. 114, 3479-3484.
Bateson, W., 1894. Materials for the Study of Variation Treated with Especial Regard to Discontinuity in the Origin of Species. Macmillan, London.
Baumgartner, R., Poernbacher, I., Buser, N., Hafen, E. and Stocker, H., 2010. The WW domain protein Kibra acts upstream of Hippo in Drosophila. Dev Cell. 18, 309-16.
Bedell, V.M., Wang, Y., Campbell, J.M., Poshusta, T.L., Starker, C.G., Krug, R.G., 2nd, Tan, W., Penheiter, S.G., Ma, A.C., Leung, A.Y., Fahrenkrug, S.C., Carlson, D.F., Voytas, D.F., Clark, K.J., Essner, J.J. and Ekker, S.C., 2012. In vivo genome editing using a high-efficiency TALEN system. Nature. 491, 114-8.
Beerli, R.R. and Barbas, C.F., 3rd, 2002. Engineering polydactyl zinc-finger transcription factors. Nat Biotechnol. 20, 135-41.
Begemann, G., Schilling, T.F., Rauch, G.J., Geisler, R. and Ingham, P.W., 2001. The zebrafish neckless mutation reveals a requirement for raldh2 in mesodermal signals that pattern the hindbrain. Development. 128, 3081-94.
Behrens, J., von Kries, J.P., Kuhl, M., Bruhn, L., Wedlich, D., Grosschedl, R. and Birchmeier, W., 1996. Functional interaction of beta-catenin with the transcription factor LEF-1. Nature. 382, 638-42.

Bell, E., Wingate, R.J. and Lumsden, A., 1999. Homeotic transformation of rhombomere identity after localized Hoxb1 misexpression. Science. 284, 2168-71.

Ben, J., Elworthy, S., Ng, A.S., van Eeden, F. and Ingham, P.W., 2011. Targeted mutation of the talpid3 gene in zebrafish reveals its conserved requirement for ciliogenesis and Hedgehog signalling across the vertebrates. Development. 138, 4969-78.

Berthelsen, J., Kilstrup-Nielsen, C., Blasi, F., Mavilio, F. and Zappavigna, V., 1999. The subcellular localization of PBX1 and EXD proteins depends on nuclear import and export signals and is modulated by association with PREP1 and HTH. Genes Dev. 13, 946-53.

Berthelsen, J., Zappavigna, V., Ferretti, E., Mavilio, F. and Blasi, F., 1998. The novel homeoprotein Prep1 modulates Pbx-Hox protein cooperativity. EMBO J. 17, 1434-45.

Beumer, K., Bhattacharyya, G., Bibikova, M., Trautman, J.K. and Carroll, D., 2006. Efficient gene targeting in Drosophila with zinc-finger nucleases. Genetics. 172, 2391-403.

Bhanot, P., Brink, M., Samos, C.H., Hsieh, J.C., Wang, Y., Macke, J.P., Andrew, D., Nathans, J. and Nusse, R., 1996. A new member of the frizzled family from Drosophila functions as a Wingless receptor. Nature. 382, 225-30.

Bibikova, M., Beumer, K., Trautman, J.K. and Carroll, D., 2003. Enhancing gene targeting with designed zinc finger nucleases. Science. 300, 764.

Bibikova, M., Carroll, D., Segal, D.J., Trautman, J.K., Smith, J., Kim, Y.G. and Chandrasegaran, S., 2001. Stimulation of homologous recombination through targeted cleavage by chimeric nucleases. Mol Cell Biol. 21, 289-97.

Bibikova, M., Golic, M., Golic, K.G. and Carroll, D., 2002. Targeted chromosomal cleavage and mutagenesis in Drosophila using zinc-finger nucleases. Genetics. 161, 1169-75.

Bienz, M. and Tremml, G., 1988. Domain of Ultrabithorax expression in Drosophila visceral mesoderm from autoregulation and exclusion. Nature. 333, 576-8.

Bikard, D., Jiang, W., Samai, P., Hochschild, A., Zhang, F. and Marraffini, L.A., 2013. Programmable repression and activation of bacterial gene expression using an engineered CRISPR-Cas system. Nucleic Acids Res. 41, 7429-37.

Bingham, S., Chaudhari, S., Vanderlaan, G., Itoh, M., Chitnis, A. and Chandrasekhar, A., 2003. Neurogenic phenotype of mind bomb mutants leads to severe patterning defects in the zebrafish hindbrain. Dev Dyn. 228, 451-63.

Blair, S.S., 2003. Developmental biology: boundary lines. Nature. 424, 379-81.

Blair, S.S. and Ralston, A., 1997. Smoothened-mediated Hedgehog signalling is required for the maintenance of the anterior-posterior lineage restriction in the developing wing of Drosophila. Development. 124, 4053-63.

Blaumueller, C.M., Qi, H., Zagouras, P. and Artavanis-Tsakonas, S., 1997. Intracellular cleavage of Notch leads to a heterodimeric receptor on the plasma membrane. Cell. 90, 281-91.

Boch, J. and Bonas, U., 2010. Xanthomonas AvrBs3 family-type III effectors: discovery and function. Annu Rev Phytopathol. 48, 419-36.

Bogdanove, A.J. and Voytas, D.F., 2011. TAL effectors: customizable proteins for DNA targeting. Science. 333, 1843-6.

Boggiano, J.C., Vanderzalm, P.J. and Fehon, R.G., 2011. Tao-1 phosphorylates Hippo/MST kinases to regulate the Hippo-Salvador-Warts tumor suppressor pathway. Dev Cell. 21, 888-95.

Bossuyt, W., Chen, C.L., Chen, Q., Sudol, M., McNeill, H., Pan, D., Kopp, A. and Halder, G., 2014. An evolutionary shift in the regulation of the Hippo pathway between mice and flies. Oncogene. 33, 1218-28.

Bovenkamp, D.E. and Greer, P., 1997. Novel Eph-family receptor tyrosine kinase is widely expressed in the developing zebrafish nervous system. Dev Dyn. 209, 166-81.

Bozas, A., Beumer, K.J., Trautman, J.K. and Carroll, D., 2009. Genetic analysis of zinc-finger nuclease-induced gene targeting in Drosophila. Genetics. 182, 641-51.

Brand, M., Heisenberg, C.P., Jiang, Y.J., Beuchle, D., Lun, K., Furutani-Seiki, M., Granato, M., Haffter, P., Hammerschmidt, M., Kane, D.A., Kelsh, R.N., Mullins, M.C., Odenthal, J., van Eeden, F.J. and Nusslein-Volhard, C., 1996. Mutations in zebrafish genes affecting the formation of the boundary between midbrain and hindbrain. Development. 123, 179-90.

Brault, E., Gautreau, A., Lamarine, M., Callebaut, I., Thomas, G. and Goutebroze, L., 2001. Normal membrane localization and actin association of the NF2 tumor suppressor protein are dependent on folding of its N-terminal domain. J Cell Sci. 114, 1901-12.

Brennan, R.J. and Schiestl, R.H., 1998. Free radicals generated in yeast by the Salmonella test-negative carcinogens benzene, urethane, thiourea and auramine O. Mutat Res. 403, 65-73.

Bretscher, A., Edwards, K. and Fehon, R.G., 2002. ERM proteins and merlin: integrators at the cell cortex. Nat Rev Mol Cell Biol. 3, 586-99.

Britto, J., Tannahill, D. and Keynes, R., 2002. A critical role for sonic hedgehog signaling in the early expansion of the developing brain. Nat Neurosci. 5, 103-10.

Bruckner, K., Pasquale, E.B. and Klein, R., 1997. Tyrosine phosphorylation of transmembrane ligands for Eph receptors. Science. 275, 1640-3.

Buckles, G.R., Thorpe, C.J., Ramel, M.C. and Lekven, A.C., 2004. Combinatorial Wnt control of zebrafish midbrain-hindbrain boundary formation. Mech Dev. 121, 437-47.

Buckley, C.E., Ren, X., Ward, L.C., Girdler, G.C., Araya, C., Green, M.J., Clark, B.S., Link, B.A. and Clarke, J.D., 2013. Mirror-symmetric microtubule assembly and cell interactions drive lumen formation in the zebrafish neural rod. EMBO J. 32, 30-44.

Burgess, A., Vigneron, S., Brioudes, E., Labbe, J.C., Lorca, T. and Castro, A., 2010. Loss of human Greatwall results in G2 arrest and multiple mitotic defects due to deregulation of the cyclin B-Cdc2/PP2A balance. Proc Natl Acad Sci U S A. 107, 12564-9.

Bush, J.O. and Soriano, P., 2010. Ephrin-B1 forward signaling regulates craniofacial morphogenesis by controlling cell proliferation across Eph-ephrin boundaries. Genes Dev. 24, 2068-80.

Bylund, M., Andersson, E., Novitch, B.G. and Muhr, J., 2003. Vertebrate neurogenesis is counteracted by Sox1-3 activity. Nat Neurosci. 6, 1162-8.

Cade, L., Reyon, D., Hwang, W.Y., Tsai, S.Q., Patel, S., Khayter, C., Joung, J.K., Sander, J.D., Peterson, R.T. and Yeh, J.R., 2012. Highly efficient generation of heritable zebrafish gene mutations using homo- and heterodimeric TALENs. Nucleic Acids Res. 40, 8001-10.

Callus, B.A., Verhagen, A.M. and Vaux, D.L., 2006. Association of mammalian sterile twenty kinases, Mst1 and Mst2, with hSalvador via C-terminal coiled-coil domains, leads to its stabilization and phosphorylation. FEBS J. 273, 4264-76.

Calzolari, S., Terriente, J. and Pujades, C., 2014. Cell segregation in the vertebrate hindbrain relies on actomyosin cables located at the interhombomeric boundaries. EMBO J. 33, 686-701.

Camargo, F.D., Gokhale, S., Johnnidis, J.B., Fu, D., Bell, G.W., Jaenisch, R. and Brummelkamp, T.R., 2007. YAP1 increases organ size and expands undifferentiated progenitor cells. Curr Biol. 17, 2054-60.

Cammas, L., Romand, R., Fraulob, V., Mura, C. and Dolle, P., 2007. Expression of the murine retinol dehydrogenase 10 (Rdh10) gene correlates with many sites of retinoid signalling during embryogenesis and organ differentiation. Dev Dyn. 236, 2899-908.

Campos-Ortega, J.A., 1988. Cellular interactions during early neurogenesis of Drosophila melanogaster. Trends Neurosci. 11, 400-5.

Camps, M., Nichols, A., Gillieron, C., Antonsson, B., Muda, M., Chabert, C., Boschert, U. and Arkinstall, S., 1998. Catalytic activation of the phosphatase MKP-3 by ERK2 mitogen-activated protein kinase. Science. 280, 1262-5.

Cannon, P. and June, C., 2011. Chemokine receptor 5 knockout strategies. Curr Opin HIV AIDS. 6, 74-9.

Cao, X., Pfaff, S.L. and Gage, F.H., 2008. YAP regulates neural progenitor cell number via the TEA domain transcription factor. Genes Dev. 22, 3320-34.

Cappello, S., Gray, M.J., Badouel, C., Lange, S., Einsiedler, M., Srour, M., Chitayat, D., Hamdan, F.F., Jenkins, Z.A., Morgan, T., Preitner, N., Uster, T., Thomas, J., Shannon, P., Morrison, V., Di Donato, N., Van Maldergem, L., Neuhann, T., Newbury-Ecob, R., Swinkells, M., Terhal, P., Wilson, L.C., Zwijnenburg, P.J., Sutherland-Smith, A.J., Black, M.A., Markie, D., Michaud, J.L., Simpson, M.A., Mansour, S., McNeill, H., Gotz, M. and Robertson, S.P., 2013. Mutations in genes encoding the cadherin receptor-ligand pair DCHS1 and FAT4 disrupt cerebral cortical development. Nat Genet. 45, 1300-8.

Carbery, I.D., Ji, D., Harrington, A., Brown, V., Weinstein, E.J., Liaw, L. and Cui, X., 2010. Targeted genome modification in mice using zinc-finger nucleases. Genetics. 186, 451-9.

Carlson, D.F., Tan, W., Lillico, S.G., Stverakova, D., Proudfoot, C., Christian, M., Voytas, D.F., Long, C.R., Whitelaw, C.B. and Fahrenkrug, S.C., 2012. Efficient TALEN-mediated gene knockout in livestock. Proc Natl Acad Sci U S A. 109, 17382-7.

Carpenter, E.M., Goddard, J.M., Chisaka, O., Manley, N.R. and Capecchi, M.R., 1993. Loss of Hox-A1 (Hox-1.6) function results in the reorganization of the murine hindbrain. Development. 118, 1063-75.

Casci, T., Vinos, J. and Freeman, M., 1999. Sprouty, an intracellular inhibitor of Ras signaling. Cell. 96, 655-65.

Castellanos, F.X., Giedd, J.N., Marsh, W.L., Hamburger, S.D., Vaituzis, A.C., Dickstein, D.P., Sarfatti, S.E., Vauss, Y.C., Snell, J.W., Lange, N., Kaysen, D., Krain, A.L., Ritchie, G.F., Rajapakse, J.C. and Rapoport, J.L., 1996. Quantitative brain magnetic resonance imaging in attention-deficit hyperactivity disorder. Arch Gen Psychiatry. 53, 607-16.

Cathomen, T. and Joung, J.K., 2008. Zinc-finger nucleases: the next generation emerges. Mol Ther. 16, 1200-7.

Cavallo, R.A., Cox, R.T., Moline, M.M., Roose, J., Polevoy, G.A., Clevers, H., Peifer, M. and Bejsovec, A., 1998. Drosophila Tcf and Groucho interact to repress Wingless signalling activity. Nature. 395, 604-8.

Cermak, T., Doyle, E., Christian, M., Wang, L., Zhang, Y., Schmidt, C., Baller, J., Somia, N., Bogdanove, A. and Voytas, D., 2011. Efficient design and assembly of custom TALEN and other TAL effector-based constructs for DNA targeting. Nucleic Acids Res. 39.

Chambers, D., Wilson, L., Maden, M. and Lumsden, A., 2007. RALDH-independent generation of retinoic acid during vertebrate embryogenesis by CYP1B1. Development. 134, 1369-83.

Chan, E.H., Nousiainen, M., Chalamalasetty, R.B., Schafer, A., Nigg, E.A. and Sillje, H.H., 2005. The Ste20-like kinase Mst2 activates the human large tumor suppressor kinase Lats1. Oncogene. 24, 2076-86.

Chan, S.K., Jaffe, L., Capovilla, M., Botas, J. and Mann, R.S., 1994. The DNA binding specificity of Ultrabithorax is modulated by cooperative interactions with extradenticle, another homeoprotein. Cell. 78, 603-15.

Chan, S.W., Lim, C.J., Chong, Y.F., Pobbati, A.V., Huang, C. and Hong, W., 2011a. Hippo pathway-independent restriction of TAZ and YAP by angiomotin. J Biol Chem. 286, 7018-26.

Chan, S.W., Lim, C.J., Huang, C., Chong, Y.F., Gunaratne, H.J., Hogue, K.A., Blackstock, W.P., Harvey, K.F. and Hong, W., 2011b. WW domain-mediated interaction with Wbp2 is important for the oncogenic property of TAZ. Oncogene. 30, 600-10.

Chandrasekhar, A., 2004. Turning heads: development of vertebrate branchiomotor neurons. Dev Dyn. 229, 143-61.

Chandrasekhar, A., Moens, C.B., Warren Jr, J.T., Kimmel, C.B. and Kuwada, J.Y., 1997. Development of branchiomotor neurons in zebrafish. Development. 124, 2633-2644.

Chang, C.P., Jacobs, Y., Nakamura, T., Jenkins, N.A., Copeland, N.G. and Cleary, M.L., 1997. Meis proteins are major in vivo DNA binding partners for wild-type but not chimeric Pbx proteins. Mol Cell Biol. 17, 5679-87.

Chang, C.P., Shen, W.F., Rozenfeld, S., Lawrence, H.J., Largman, C. and Cleary, M.L., 1995. Pbx proteins display hexapeptide-dependent cooperative DNA binding with a subset of Hox proteins. Genes Dev. 9, 663-74.

Chavrier, P., Zerial, M., Lemaire, P., Almendral, J., Bravo, R. and Charnay, P., 1988. A gene encoding a protein with zinc fingers is activated during G0/G1 transition in cultured cells. EMBO J. 7, 29-35.

Chelko, S.P., Asimaki, A., Andersen, P., Bedja, D., Amat-Alarcon, N., DeMazumder, D., Jasti, R., MacRae, C.A., Leber, R., Kleber, A.G., Saffitz, J.E. and Judge,

D.P., 2016. Central role for GSK3beta in the pathogenesis of arrhythmogenic cardiomyopathy. JCI Insight. 1.
Chen, B., Gilbert, L.A., Cimini, B.A., Schnitzbauer, J., Zhang, W., Li, G.W., Park, J., Blackburn, E.H., Weissman, J.S., Qi, L.S. and Huang, B., 2013a. Dynamic imaging of genomic loci in living human cells by an optimized CRISPR/Cas system. Cell. 155, 1479-91.
Chen, C.L., Gajewski, K.M., Hamaratoglu, F., Bossuyt, W., Sansores-Garcia, L., Tao, C. and Halder, G., 2010. The apical-basal cell polarity determinant Crumbs regulates Hippo signaling in Drosophila. Proc Natl Acad Sci U S A. 107, 15810-5.
Chen, C.L., Schroeder, M.C., Kango-Singh, M., Tao, C. and Halder, G., 2012. Tumor suppression by cell competition through regulation of the Hippo pathway. Proc Natl Acad Sci U S A. 109, 484-9.
Chen, H.I., Einbond, A., Kwak, S.J., Linn, H., Koepf, E., Peterson, S., Kelly, J.W. and Sudol, M., 1997. Characterization of the WW domain of human yes-associated protein and its polyproline-containing ligands. J Biol Chem. 272, 17070-7.
Chen, J. and Verheyen, E.M., 2012. Homeodomain-interacting protein kinase regulates Yorkie activity to promote tissue growth. Curr Biol. 22, 1582-6.
Chen, M., Wang, M., Xu, S., Guo, X. and Jiang, J., 2015. Upregulation of miR-181c contributes to chemoresistance in pancreatic cancer by inactivating the Hippo signaling pathway. Oncotarget. 6, 44466-79.
Chen, S., Oikonomou, G., Chiu, C.N., Niles, B.J., Liu, J., Lee, D.A., Antoshechkin, I. and Prober, D.A., 2013b. A large-scale in vivo analysis reveals that TALENs are significantly more mutagenic than ZFNs generated using context-dependent assembly. Nucleic Acids Res. 41, 2769-78.
Cheng, Y.C., Amoyel, M., Qiu, X., Jiang, Y.J., Xu, Q. and Wilkinson, D.G., 2004. Notch activation regulates the segregation and differentiation of rhombomere boundary cells in the zebrafish hindbrain. Dev Cell. 6, 539-50.
Chisaka, O., Musci, T.S. and Capecchi, M.R., 1992. Developmental defects of the ear, cranial nerves and hindbrain resulting from targeted disruption of the mouse homeobox gene Hox-1.6. Nature. 355, 516-20.
Chithalen, J.V., Luu, L., Petkovich, M. and Jones, G., 2002. HPLC-MS/MS analysis of the products generated from all-trans-retinoic acid using recombinant human CYP26A. J Lipid Res. 43, 1133-42.
Chitnis, A., Henrique, D., Lewis, J., Ish-Horowicz, D. and Kintner, C., 1995. Primary neurogenesis in Xenopus embryos regulated by a homologue of the Drosophila neurogenic gene Delta. Nature. 375, 761-6.
Chizhikov, V.V. and Millen, K.J., 2005. Roof plate-dependent patterning of the vertebrate dorsal central nervous system. Dev Biol. 277, 287-95.
Chodobski, A. and Szmydynger-Chodobska, J., 2001. Choroid plexus: target for polypeptides and site of their synthesis. Microsc Res Tech. 52, 65-82.
Choe, S.K., Vlachakis, N. and Sagerstrom, C.G., 2002. Meis family proteins are required for hindbrain development in the zebrafish. Development. 129, 585-95.
Choe, S.K., Zhang, X., Hirsch, N., Straubhaar, J. and Sagerstrom, C.G., 2011. A screen for hoxb1-regulated genes identifies ppp1r14al as a regulator of the rhombomere 4 Fgf-signaling center. Dev Biol. 358, 356-67.

Chomette, D., Frain, M., Cereghini, S., Charnay, P. and Ghislain, J., 2006. Krox20 hindbrain cis-regulatory landscape: interplay between multiple long-range initiation and autoregulatory elements. Development. 133, 1253-62.

Chouinard, S. and Kaufman, T.C., 1991. Control of expression of the homeotic labial (lab) locus of Drosophila melanogaster: evidence for both positive and negative autogenous regulation. Development. 113, 1267-80.

Choulika, A., Perrin, A., Dujon, B. and Nicolas, J.F., 1995. Induction of homologous recombination in mammalian chromosomes by using the I-SceI system of Saccharomyces cerevisiae. Mol Cell Biol. 15, 1968-73.

Christian, M., Cermak, T., Doyle, E.L., Schmidt, C., Zhang, F., Hummel, A., Bogdanove, A.J. and Voytas, D.F., 2010. Targeting DNA double-strand breaks with TAL effector nucleases. Genetics. 186, 757-61.

Clark, B.S., Winter, M., Cohen, A.R. and Link, B.A., 2011. Generation of Rab-based transgenic lines for in vivo studies of endosome biology in zebrafish. Dev Dyn. 240, 2452-65.

Clarke, J., 2009. Role of polarized cell divisions in zebrafish neural tube formation. Curr Opin Neurobiol. 19, 134-8.

Clarke, J.D. and Lumsden, A., 1993. Segmental repetition of neuronal phenotype sets in the chick embryo hindbrain. Development. 118, 151-62.

Coghlan, M.P., Culbert, A.A., Cross, D.A., Corcoran, S.L., Yates, J.W., Pearce, N.J., Rausch, O.L., Murphy, G.J., Carter, P.S., Roxbee Cox, L., Mills, D., Brown, M.J., Haigh, D., Ward, R.W., Smith, D.G., Murray, K.J., Reith, A.D. and Holder, J.C., 2000. Selective small molecule inhibitors of glycogen synthase kinase-3 modulate glycogen metabolism and gene transcription. Chem Biol. 7, 793-803.

Conaway, R.C., Sato, S., Tomomori-Sato, C., Yao, T. and Conaway, J.W., 2005. The mammalian Mediator complex and its role in transcriptional regulation. Trends Biochem Sci. 30, 250-5.

Conlon, R.A. and Rossant, J., 1992. Exogenous retinoic acid rapidly induces anterior ectopic expression of murine Hox-2 genes in vivo. Development. 116, 357-68.

Cooke, J., Moens, C., Roth, L., Durbin, L., Shiomi, K., Brennan, C., Kimmel, C., Wilson, S. and Holder, N., 2001. Eph signalling functions downstream of Val to regulate cell sorting and boundary formation in the caudal hindbrain. Development. 128, 571-80.

Cooke, J.E., Kemp, H.A. and Moens, C.B., 2005. EphA4 is required for cell adhesion and rhombomere-boundary formation in the zebrafish. Curr Biol. 15, 536-42.

Cooke, J.E. and Moens, C.B., 2002. Boundary formation in the hindbrain: Eph only it were simple. Trends Neurosci. 25, 260-7.

Cooper, K.L., Leisenring, W.M. and Moens, C.B., 2003. Autonomous and nonautonomous functions for Hox/Pbx in branchiomotor neuron development. Dev Biol. 253, 200-13.

Cordenonsi, M., Zanconato, F., Azzolin, L., Forcato, M., Rosato, A., Frasson, C., Inui, M., Montagner, M., Parenti, A.R., Poletti, A., Daidone, M.G., Dupont, S., Basso, G., Bicciato, S. and Piccolo, S., 2011. The Hippo transducer TAZ confers cancer stem cell-related traits on breast cancer cells. Cell. 147, 759-72.

Cordes, S.P. and Barsh, G.S., 1994. The mouse segmentation gene kr encodes a novel basic domain-leucine zipper transcription factor. Cell. 79, 1025-34.

Cornu, T.I., Thibodeau-Beganny, S., Guhl, E., Alwin, S., Eichtinger, M., Joung, J.K. and Cathomen, T., 2008. DNA-binding specificity is a major determinant of the activity and toxicity of zinc-finger nucleases. Mol Ther. 16, 352-8.

Couso, J.P., Bishop, S.A. and Martinez Arias, A., 1994. The wingless signalling pathway and the patterning of the wing margin in Drosophila. Development. 120, 621-36.

Couso, J.P., Knust, E. and Martinez Arias, A., 1995. Serrate and wingless cooperate to induce vestigial gene expression and wing formation in Drosophila. Curr Biol. 5, 1437-48.

Couso, J.P. and Martinez Arias, A., 1994. Notch is required for wingless signaling in the epidermis of Drosophila. Cell. 79, 259-72.

Cruce, W.L., 1974. The anatomical organization of hindlimb motoneurons in the lumbar spinal cord of the frog, Rana catesbiana. J Comp Neurol. 153, 59-76.

Cruciat, C.M. and Niehrs, C., 2013. Secreted and transmembrane wnt inhibitors and activators. Cold Spring Harb Perspect Biol. 5, a015081.

Cushing, H., 1914. Studies on the Cerebro-Spinal Fluid : I. Introduction. J Med Res. 31, 1-19.

Da'as, S.I., Coombs, A.J., Balci, T.B., Grondin, C.A., Ferrando, A.A. and Berman, J.N., 2012. The zebrafish reveals dependence of the mast cell lineage on Notch signaling in vivo. Blood. 119, 3585-94.

Dahlem, T.J., Hoshijima, K., Jurynec, M.J., Gunther, D., Starker, C.G., Locke, A.S., Weis, A.M., Voytas, D.F. and Grunwald, D.J., 2012. Simple methods for generating and detecting locus-specific mutations induced with TALENs in the zebrafish genome. PLoS Genet. 8, e1002861.

Dahmann, C. and Basler, K., 1999. Compartment boundaries: at the edge of development. Trends Genet. 15, 320-6.

Dai, X., Liu, H., Shen, S., Guo, X., Yan, H., Ji, X., Li, L., Huang, J., Feng, X.H. and Zhao, B., 2015. YAP activates the Hippo pathway in a negative feedback loop. Cell Res. 25, 1175-8.

Das Thakur, M., Feng, Y., Jagannathan, R., Seppa, M.J., Skeath, J.B. and Longmore, G.D., 2010. Ajuba LIM proteins are negative regulators of the Hippo signaling pathway. Curr Biol. 20, 657-62.

Davenne, M., Maconochie, M.K., Neun, R., Pattyn, A., Chambon, P., Krumlauf, R. and Rijli, F.M., 1999. Hoxa2 and Hoxb2 control dorsoventral patterns of neuronal development in the rostral hindbrain. Neuron. 22, 677-91.

de Celis, J.F. and Bray, S., 1997. Feed-back mechanisms affecting Notch activation at the dorsoventral boundary in the Drosophila wing. Development. 124, 3241-51.

de Celis, J.F., Garcia-Bellido, A. and Bray, S.J., 1996. Activation and function of Notch at the dorsal-ventral boundary of the wing imaginal disc. Development. 122, 359-69.

de la Pompa, J.L., Wakeham, A., Correia, K.M., Samper, E., Brown, S., Aguilera, R.J., Nakano, T., Honjo, T., Mak, T.W., Rossant, J. and Conlon, R.A., 1997. Conservation of the Notch signalling pathway in mammalian neurogenesis. Development. 124, 1139-48.

De Robertis, E.M. and Kuroda, H., 2004. Dorsal-ventral patterning and neural induction in Xenopus embryos. Annu Rev Cell Dev Biol. 20, 285-308.

De Robertis, E.M., Larrain, J., Oelgeschlager, M. and Wessely, O., 2000. The establishment of Spemann's organizer and patterning of the vertebrate embryo. Nat Rev Genet. 1, 171-81.

de Roos, K., Sonneveld, E., Compaan, B., ten Berge, D., Durston, A.J. and van der Saag, P.T., 1999. Expression of retinoic acid 4-hydroxylase (CYP26) during mouse and Xenopus laevis embryogenesis. Mech Dev. 82, 205-11.

DeCamillis, M., Cheng, N.S., Pierre, D. and Brock, H.W., 1992. The polyhomeotic gene of Drosophila encodes a chromatin protein that shares polytene chromosome-binding sites with Polycomb. Genes Dev. 6, 223-32.

Deflorian, G., Tiso, N., Ferretti, E., Meyer, D., Blasi, F., Bortolussi, M. and Argenton, F., 2004. Prep1.1 has essential genetic functions in hindbrain development and cranial neural crest cell differentiation. Development. 131, 613-27.

Dekker, E.J., Pannese, M., Houtzager, E., Boncinelli, E. and Durston, A., 1993. Colinearity in the Xenopus laevis Hox-2 complex. Mech Dev. 40, 3-12.

Del Amo, F.F., Smith, D.E., Swiatek, P.J., Gendron-Maguire, M., Greenspan, R.J., McMahon, A.P. and Gridley, T., 1992. Expression pattern of Motch, a mouse homolog of Drosophila Notch, suggests an important role in early postimplantation mouse development. Development. 115, 737-44.

Delaune, E., Lemaire, P. and Kodjabachian, L., 2005. Neural induction in Xenopus requires early FGF signalling in addition to BMP inhibition. Development. 132, 299-310.

Delgado, E.R., Yang, J., So, J., Leimgruber, S., Kahn, M., Ishitani, T., Shin, D., Mustata Wilson, G. and Monga, S.P., 2014. Identification and characterization of a novel small-molecule inhibitor of beta-catenin signaling. Am J Pathol. 184, 2111-22.

Deng, D., Yan, C., Pan, X., Mahfouz, M., Wang, J., Zhu, J.K., Shi, Y. and Yan, N., 2012. Structural basis for sequence-specific recognition of DNA by TAL effectors. Science. 335, 720-3.

DeRan, M., Yang, J., Shen, C.H., Peters, E.C., Fitamant, J., Chan, P., Hsieh, M., Zhu, S., Asara, J.M., Zheng, B., Bardeesy, N., Liu, J. and Wu, X., 2014. Energy stress regulates hippo-YAP signaling involving AMPK-mediated regulation of angiomotin-like 1 protein. Cell Rep. 9, 495-503.

Desjarlais, J.R. and Berg, J.M., 1993. Use of a zinc-finger consensus sequence framework and specificity rules to design specific DNA binding proteins. Proc Natl Acad Sci U S A. 90, 2256-60.

Ding, Q., Lee, Y.K., Schaefer, E.A., Peters, D.T., Veres, A., Kim, K., Kuperwasser, N., Motola, D.L., Meissner, T.B., Hendriks, W.T., Trevisan, M., Gupta, R.M., Moisan, A., Banks, E., Friesen, M., Schinzel, R.T., Xia, F., Tang, A., Xia, Y., Figueroa, E., Wann, A., Ahfeldt, T., Daheron, L., Zhang, F., Rubin, L.L., Peng, L.F., Chung, R.T., Musunuru, K. and Cowan, C.A., 2013. A TALEN Genome-Editing System for Generating Human Stem Cell-Based Disease Models. Cell Stem Cell. 12, 238-51.

Dolle, P., Izpisua-Belmonte, J.C., Boncinelli, E. and Duboule, D., 1991. The Hox-4.8 gene is localized at the 5' extremity of the Hox-4 complex and is expressed in the most posterior parts of the body during development. Mech Dev. 36, 3-13.

Dolle, P., Izpisua-Belmonte, J.C., Falkenstein, H., Renucci, A. and Duboule, D., 1989. Coordinate expression of the murine Hox-5 complex homoeobox-containing genes during limb pattern formation. Nature. 342, 767-72.

Dominguez, A.A., Lim, W.A. and Qi, L.S., 2016. Beyond editing: repurposing CRISPR-Cas9 for precision genome regulation and interrogation. Nat Rev Mol Cell Biol. 17, 5-15.

Dominguez, M. and de Celis, J.F., 1998. A dorsal/ventral boundary established by Notch controls growth and polarity in the Drosophila eye. Nature. 396, 276-8.

Dong, J., Feldmann, G., Huang, J., Wu, S., Zhang, N., Comerford, S.A., Gayyed, M.F., Anders, R.A., Maitra, A. and Pan, D., 2007. Elucidation of a universal size-control mechanism in Drosophila and mammals. Cell. 130, 1120-33.

Dong, Z., Ge, J., Li, K., Xu, Z., Liang, D., Li, J., Jia, W., Li, Y., Dong, X., Cao, S., Wang, X., Pan, J. and Zhao, Q., 2011. Heritable targeted inactivation of myostatin gene in yellow catfish (Pelteobagrus fulvidraco) using engineered zinc finger nucleases. PLoS One. 6, e28897.

Donoviel, D.B., Hadjantonakis, A.K., Ikeda, M., Zheng, H., Hyslop, P.S. and Bernstein, A., 1999. Mice lacking both presenilin genes exhibit early embryonic patterning defects. Genes Dev. 13, 2801-10.

Downs, K.M., 2008. Systematic localization of Oct-3/4 to the gastrulating mouse conceptus suggests manifold roles in mammalian development. Dev Dyn. 237, 464-75.

Doyon, Y., McCammon, J.M., Miller, J.C., Faraji, F., Ngo, C., Katibah, G.E., Amora, R., Hocking, T.D., Zhang, L., Rebar, E.J., Gregory, P.D., Urnov, F.D. and Amacher, S.L., 2008. Heritable targeted gene disruption in zebrafish using designed zinc-finger nucleases. Nat Biotechnol. 26, 702-8.

Dreier, B., Segal, D.J. and Barbas, C.F., 3rd, 2000. Insights into the molecular recognition of the 5'-GNN-3' family of DNA sequences by zinc finger domains. J Mol Biol. 303, 489-502.

Drummond, D.L., Cheng, C.S., Selland, L.G., Hocking, J.C., Prichard, L.B. and Waskiewicz, A.J., 2013. The role of Zic transcription factors in regulating hindbrain retinoic acid signaling. BMC Dev Biol. 13, 31.

Duboule, D., 1992. The vertebrate limb: a model system to study the Hox/HOM gene network during development and evolution. Bioessays. 14, 375-84.

Duboule, D. and Dolle, P., 1989. The structural and functional organization of the murine HOX gene family resembles that of Drosophila homeotic genes. EMBO J. 8, 1497-505.

Duncan, R.N., Panahi, S., Piotrowski, T. and Dorsky, R.I., 2015. Identification of Wnt Genes Expressed in Neural Progenitor Zones during Zebrafish Brain Development. PLoS One. 10, e0145810.

Dupe, V., Davenne, M., Brocard, J., Dolle, P., Mark, M., Dierich, A., Chambon, P. and Rijli, F.M., 1997. In vivo functional analysis of the Hoxa-1 3' retinoic acid response element (3'RARE). Development. 124, 399-410.

Dupe, V., Ghyselinck, N.B., Wendling, O., Chambon, P. and Mark, M., 1999. Key roles of retinoic acid receptors alpha and beta in the patterning of the caudal hindbrain, pharyngeal arches and otocyst in the mouse. Development. 126, 5051-9.

Dupe, V. and Lumsden, A., 2001. Hindbrain patterning involves graded responses to retinoic acid signalling. Development. 128, 2199-208.

Dupont, S., Morsut, L., Aragona, M., Enzo, E., Giulitti, S., Cordenonsi, M., Zanconato, F., Le Digabel, J., Forcato, M., Bicciato, S., Elvassore, N. and Piccolo, S., 2011. Role of YAP/TAZ in mechanotransduction. Nature. 474, 179-83.

Durai, S., Mani, M., Kandavelou, K., Wu, J., Porteus, M.H. and Chandrasegaran, S., 2005. Zinc finger nucleases: custom-designed molecular scissors for genome engineering of plant and mammalian cells. Nucleic Acids Res. 33, 5978-90.

Ebner, A., Cabernard, C., Affolter, M. and Merabet, S., 2005. Recognition of distinct target sites by a unique Labial/Extradenticle/Homothorax complex. Development. 132, 1591-600.

Ekker, S.C. and Larson, J.D., 2001. Morphant technology in model developmental systems. Genesis. 30, 89-93.

Elrod-Erickson, M., Rould, M.A., Nekludova, L. and Pabo, C.O., 1996. Zif268 protein-DNA complex refined at 1.6 A: a model system for understanding zinc finger-DNA interactions. Structure. 4, 1171-80.

Elsen, G.E., Choi, L.Y., Millen, K.J., Grinblat, Y. and Prince, V.E., 2008. Zic1 and Zic4 regulate zebrafish roof plate specification and hindbrain ventricle morphogenesis. Dev Biol. 314, 376-92.

Emami, K.H., Nguyen, C., Ma, H., Kim, D.H., Jeong, K.W., Eguchi, M., Moon, R.T., Teo, J.L., Kim, H.Y., Moon, S.H., Ha, J.R. and Kahn, M., 2004. A small molecule inhibitor of beta-catenin/CREB-binding protein transcription [corrected]. Proc Natl Acad Sci U S A. 101, 12682-7.

Emerich, D.F., Skinner, S.J., Borlongan, C.V. and Thanos, C.G., 2005. A role of the choroid plexus in transplantation therapy. Cell Transplant. 14, 715-25.

Enzo, E., Santinon, G., Pocaterra, A., Aragona, M., Bresolin, S., Forcato, M., Grifoni, D., Pession, A., Zanconato, F., Guzzo, G., Bicciato, S. and Dupont, S., 2015. Aerobic glycolysis tunes YAP/TAZ transcriptional activity. EMBO J. 34, 1349-70.

Erickson, T., Scholpp, S., Brand, M., Moens, C.B. and Waskiewicz, A.J., 2007. Pbx proteins cooperate with Engrailed to pattern the midbrain-hindbrain and diencephalic-mesencephalic boundaries. Dev Biol. 301, 504-17.

Erter, C.E., Wilm, T.P., Basler, N., Wright, C.V. and Solnica-Krezel, L., 2001. Wnt8 is required in lateral mesendodermal precursors for neural posteriorization in vivo. Development. 128, 3571-83.

Eto, M., Kirkbride, J.A. and Brautigan, D.L., 2005. Assembly of MYPT1 with protein phosphatase-1 in fibroblasts redirects localization and reorganizes the actin cytoskeleton. Cell Motil Cytoskeleton. 62, 100-9.

Feldman, B., Dougan, S.T., Schier, A.F. and Talbot, W.S., 2000. Nodal-related signals establish mesendodermal fate and trunk neural identity in zebrafish. Curr Biol. 10, 531-4.

Fernandez, B.G., Gaspar, P., Bras-Pereira, C., Jezowska, B., Rebelo, S.R. and Janody, F., 2011. Actin-Capping Protein and the Hippo pathway regulate F-actin and tissue growth in Drosophila. Development. 138, 2337-46.

Fernandez, L.A., Northcott, P.A., Dalton, J., Fraga, C., Ellison, D., Angers, S., Taylor, M.D. and Kenney, A.M., 2009. YAP1 is amplified and up-regulated in hedgehog-associated medulloblastomas and mediates Sonic hedgehog-driven neural precursor proliferation. Genes Dev. 23, 2729-41.

Ferretti, E., Marshall, H., Popperl, H., Maconochie, M., Krumlauf, R. and Blasi, F., 2000. Segmental expression of Hoxb2 in r4 requires two separate sites that integrate cooperative interactions between Prep1, Pbx and Hox proteins. Development. 127, 155-66.

Ferrigno, O., Lallemand, F., Verrecchia, F., L'Hoste, S., Camonis, J., Atfi, A. and Mauviel, A., 2002. Yes-associated protein (YAP65) interacts with Smad7 and potentiates its inhibitory activity against TGF-beta/Smad signaling. Oncogene. 21, 4879-84.

Fiedler, M., Mendoza-Topaz, C., Rutherford, T.J., Mieszczanek, J. and Bienz, M., 2011. Dishevelled interacts with the DIX domain polymerization interface of Axin to interfere with its function in down-regulating beta-catenin. Proc Natl Acad Sci U S A. 108, 1937-42.

Flenniken, A.M., Gale, N.W., Yancopoulos, G.D. and Wilkinson, D.G., 1996. Distinct and overlapping expression patterns of ligands for Eph-related receptor tyrosine kinases during mouse embryogenesis. Dev Biol. 179, 382-401.

Foley, J.E., Maeder, M.L., Pearlberg, J., Joung, J.K., Peterson, R.T. and Yeh, J.R., 2009a. Targeted mutagenesis in zebrafish using customized zinc-finger nucleases. Nat Protoc. 4, 1855-67.

Foley, J.E., Yeh, J.R., Maeder, M.L., Reyon, D., Sander, J.D., Peterson, R.T. and Joung, J.K., 2009b. Rapid mutation of endogenous zebrafish genes using zinc finger nucleases made by Oligomerized Pool ENgineering (OPEN). PLoS One. 4, e4348.

Frangou, S., Aylward, E., Warren, A., Sharma, T., Barta, P. and Pearlson, G., 1997. Small planum temporale volume in Down's syndrome: a volumetric MRI study. Am J Psychiatry. 154, 1424-9.

Franke, A., DeCamillis, M., Zink, D., Cheng, N., Brock, H.W. and Paro, R., 1992. Polycomb and polyhomeotic are constituents of a multimeric protein complex in chromatin of Drosophila melanogaster. EMBO J. 11, 2941-50.

Frasch, M., Chen, X. and Lufkin, T., 1995. Evolutionary-conserved enhancers direct region-specific expression of the murine Hoxa-1 and Hoxa-2 loci in both mice and Drosophila. Development. 121, 957-74.

Fraser, S., Keynes, R. and Lumsden, A., 1990. Segmentation in the chick embryo hindbrain is defined by cell lineage restrictions. Nature. 344, 431-5.

French, C.R., Erickson, T., Callander, D., Berry, K.M., Koss, R., Hagey, D.W., Stout, J., Wuennenberg-Stapleton, K., Ngai, J., Moens, C.B. and Waskiewicz, A.J., 2007. Pbx homeodomain proteins pattern both the zebrafish retina and tectum. BMC Dev Biol. 7, 85.

Fristrom, D., 1988. The cellular basis of epithelial morphogenesis. A review. Tissue Cell. 20, 645-90.

Frohman, M.A., Martin, G.R., Cordes, S.P., Halamek, L.P. and Barsh, G.S., 1993. Altered rhombomere-specific gene expression and hyoid bone differentiation in the mouse segmentation mutant, kreisler (kr). Development. 117, 925-36.

Fryer, C.J., Lamar, E., Turbachova, I., Kintner, C. and Jones, K.A., 2002. Mastermind mediates chromatin-specific transcription and turnover of the Notch enhancer complex. Genes Dev. 16, 1397-411.

Furthauer, M., Van Celst, J., Thisse, C. and Thisse, B., 2004. Fgf signalling controls the dorsoventral patterning of the zebrafish embryo. Development. 131, 2853-64.

Furukawa, K.T., Yamashita, K., Sakurai, N. and Ohno, S., 2017. The Epithelial Circumferential Actin Belt Regulates YAP/TAZ through Nucleocytoplasmic Shuttling of Merlin. Cell Rep. 20, 1435-1447.

Galant, R., Walsh, C.M. and Carroll, S.B., 2002. Hox repression of a target gene: extradenticle-independent, additive action through multiple monomer binding sites. Development. 129, 3115-26.

Gale, E., Zile, M. and Maden, M., 1999. Hindbrain respecification in the retinoid-deficient quail. Mech Dev. 89, 43-54.

Garcia-Dominguez, M., Gilardi-Hebenstreit, P. and Charnay, P., 2006. PIASxbeta acts as an activator of Hoxb1 and is antagonized by Krox20 during hindbrain segmentation. EMBO J. 25, 2432-42.

Garneau, J.E., Dupuis, M.E., Villion, M., Romero, D.A., Barrangou, R., Boyaval, P., Fremaux, C., Horvath, P., Magadan, A.H. and Moineau, S., 2010. The CRISPR/Cas bacterial immune system cleaves bacteriophage and plasmid DNA. Nature. 468, 67-71.

Gato, A., Moro, J.A., Alonso, M.I., Pastor, J.F., Represa, J.J. and Barbosa, E., 1993. Chondroitin sulphate proteoglycan and embryonic brain enlargement in the chick. Anat Embryol (Berl). 188, 101-6.

Gaufo, G.O., Thomas, K.R. and Capecchi, M.R., 2003. Hox3 genes coordinate mechanisms of genetic suppression and activation in the generation of branchial and somatic motoneurons. Development. 130, 5191-201.

Gaunt, M.W., Jones, L.D., Laurenson, K., Hudson, P.J., Reid, H.W. and Gould, E.A., 1997. Definitive identification of louping ill virus by RT-PCR and sequencing in field populations of Ixodes ricinus on the Lochindorb estate. Arch Virol. 142, 1181-91.

Gaunt, S.J., 1991. Expression patterns of mouse Hox genes: clues to an understanding of developmental and evolutionary strategies. Bioessays. 13, 505-13.

Gaunt, S.J., 1997. Chick limbs, fly wings and homology at the fringe. Nature. 386, 324-5.

Gavalas, A., 2002. ArRAnging the hindbrain. Trends Neurosci. 25, 61-4.

Gavalas, A., Davenne, M., Lumsden, A., Chambon, P. and Rijli, F.M., 1997. Role of Hoxa-2 in axon pathfinding and rostral hindbrain patterning. Development. 124, 3693-702.

Gavalas, A. and Krumlauf, R., 2000. Retinoid signalling and hindbrain patterning. Curr Opin Genet Dev. 10, 380-6.

Gavalas, A., Ruhrberg, C., Livet, J., Henderson, C.E. and Krumlauf, R., 2003. Neuronal defects in the hindbrain of Hoxa1, Hoxb1 and Hoxb2 mutants reflect regulatory interactions among these Hox genes. Development. 130, 5663-79.

Gavalas, A., Studer, M., Lumsden, A., Rijli, F.M., Krumlauf, R. and Chambon, P., 1998. Hoxa1 and Hoxb1 synergize in patterning the hindbrain, cranial nerves and second pharyngeal arch. Development. 125, 1123-36.

Gebelein, B., McKay, D.J. and Mann, R.S., 2004. Direct integration of Hox and segmentation gene inputs during Drosophila development. Nature. 431, 653-9.

Gee, S.T., Milgram, S.L., Kramer, K.L., Conlon, F.L. and Moody, S.A., 2011. Yes-associated protein 65 (YAP) expands neural progenitors and regulates Pax3 expression in the neural plate border zone. PLoS One. 6, e20309.

Gendron-Maguire, M., Mallo, M., Zhang, M. and Gridley, T., 1993. Hoxa-2 mutant mice exhibit homeotic transformation of skeletal elements derived from cranial neural crest. Cell. 75, 1317-31.

Genevet, A. and Tapon, N., 2011. The Hippo pathway and apico-basal cell polarity. Biochem J. 436, 213-24.

Genevet, A., Wehr, M.C., Brain, R., Thompson, B.J. and Tapon, N., 2010. Kibra is a regulator of the Salvador/Warts/Hippo signaling network. Dev Cell. 18, 300-8.

Georgakopoulos, A., Litterst, C., Ghersi, E., Baki, L., Xu, C., Serban, G. and Robakis, N.K., 2006. Metalloproteinase/Presenilin1 processing of ephrinB regulates EphB-induced Src phosphorylation and signaling. EMBO J. 25, 1242-52.

Gerety, S.S. and Wilkinson, D.G., 2011. Morpholino artifacts provide pitfalls and reveal a novel role for pro-apoptotic genes in hindbrain boundary development. Dev Biol. 350, 279-89.

Geurts, A.M., Cost, G.J., Freyvert, Y., Zeitler, B., Miller, J.C., Choi, V.M., Jenkins, S.S., Wood, A., Cui, X., Meng, X., Vincent, A., Lam, S., Michalkiewicz, M., Schilling, R., Foeckler, J., Kalloway, S., Weiler, H., Menoret, S., Anegon, I., Davis, G.D., Zhang, L., Rebar, E.J., Gregory, P.D., Urnov, F.D., Jacob, H.J. and Buelow, R., 2009. Knockout rats via embryo microinjection of zinc-finger nucleases. Science. 325, 433.

Gilbert, L.A., Larson, M.H., Morsut, L., Liu, Z., Brar, G.A., Torres, S.E., Stern-Ginossar, N., Brandman, O., Whitehead, E.H., Doudna, J.A., Lim, W.A., Weissman, J.S. and Qi, L.S., 2013. CRISPR-mediated modular RNA-guided regulation of transcription in eukaryotes. Cell. 154, 442-51.

Gilmore, J.H., van Tol, J.J., Lewis Streicher, H., Williamson, K., Cohen, S.B., Greenwood, R.S., Charles, H.C., Kliewer, M.A., Whitt, J.K., Silva, S.G., Hertzberg, B.S. and Chescheir, N.C., 2001. Outcome in children with fetal mild ventriculomegaly: a case series. Schizophr Res. 48, 219-26.

Giudicelli, F., Gilardi-Hebenstreit, P., Mechta-Grigoriou, F., Poquet, C. and Charnay, P., 2003. Novel activities of Mafb underlie its dual role in hindbrain segmentation and regional specification. Dev Biol. 253, 150-62.

Gladden, A.B., Hebert, A.M., Schneeberger, E.E. and McClatchey, A.I., 2010. The NF2 tumor suppressor, Merlin, regulates epidermal development through the establishment of a junctional polarity complex. Dev Cell. 19, 727-39.

Glinka, A., Wu, W., Delius, H., Monaghan, A.P., Blumenstock, C. and Niehrs, C., 1998. Dickkopf-1 is a member of a new family of secreted proteins and functions in head induction. Nature. 391, 357-62.

Glucksmann, A., 1951. Cell deaths in normal vertebrate ontogeny. Biol Rev Camb Philos Soc. 26, 59-86.

Goddard, J.M., Rossel, M., Manley, N.R. and Capecchi, M.R., 1996. Mice with targeted disruption of Hoxb-1 fail to form the motor nucleus of the VIIth nerve. Development. 122, 3217-28.

Goetz, R. and Mohammadi, M., 2013. Exploring mechanisms of FGF signalling through the lens of structural biology. Nat Rev Mol Cell Biol. 14, 166-80.

Gonzalez, B., Schwimmer, L.J., Fuller, R.P., Ye, Y., Asawapornmongkol, L. and Barbas, C.F., 3rd, 2010. Modular system for the construction of zinc-finger libraries and proteins. Nat Protoc. 5, 791-810.

Gordon, W.R., Vardar-Ulu, D., L'Heureux, S., Ashworth, T., Malecki, M.J., Sanchez-Irizarry, C., McArthur, D.G., Histen, G., Mitchell, J.L., Aster, J.C. and Blacklow, S.C., 2009. Effects of S1 cleavage on the structure, surface export, and signaling activity of human Notch1 and Notch2. PLoS One. 4, e6613.

Gosens, I., Sessa, A., den Hollander, A.I., Letteboer, S.J., Belloni, V., Arends, M.L., Le Bivic, A., Cremers, F.P., Broccoli, V. and Roepman, R., 2007. FERM protein EPB41L5 is a novel member of the mammalian CRB-MPP5 polarity complex. Exp Cell Res. 313, 3959-70.

Gould, A., Itasaki, N. and Krumlauf, R., 1998. Initiation of rhombomeric Hoxb4 expression requires induction by somites and a retinoid pathway. Neuron. 21, 39-51.

Gould, A., Morrison, A., Sproat, G., White, R.A. and Krumlauf, R., 1997. Positive cross-regulation and enhancer sharing: two mechanisms for specifying overlapping Hox expression patterns. Genes Dev. 11, 900-13.

Goulev, Y., Fauny, J.D., Gonzalez-Marti, B., Flagiello, D., Silber, J. and Zider, A., 2008. SCALLOPED interacts with YORKIE, the nuclear effector of the hippo tumor-suppressor pathway in Drosophila. Curr Biol. 18, 435-41.

Graham, A., Papalopulu, N. and Krumlauf, R., 1989. The murine and Drosophila homeobox gene complexes have common features of organization and expression. Cell. 57, 367-78.

Grandel, H., Lun, K., Rauch, G.J., Rhinn, M., Piotrowski, T., Houart, C., Sordino, P., Kuchler, A.M., Schulte-Merker, S., Geisler, R., Holder, N., Wilson, S.W. and Brand, M., 2002. Retinoic acid signalling in the zebrafish embryo is necessary during pre-segmentation stages to pattern the anterior-posterior axis of the CNS and to induce a pectoral fin bud. Development. 129, 2851-65.

Gray, H. and Clemente, C.D., 1985. Anatomy of the human body, 30th American ed. Lea & Febiger, Philadelphia.

Gray, M., Moens, C.B., Amacher, S.L., Eisen, J.S. and Beattie, C.E., 2001. Zebrafish deadly seven functions in neurogenesis. Dev Biol. 237, 306-23.

Greisman, H.A. and Pabo, C.O., 1997. A general strategy for selecting high-affinity zinc finger proteins for diverse DNA target sites. Science. 275, 657-61.

Griffin, K., Patient, R. and Holder, N., 1995. Analysis of FGF function in normal and no tail zebrafish embryos reveals separate mechanisms for formation of the trunk and the tail. Development. 121, 2983-94.

Grzeschik, N.A., Parsons, L.M., Allott, M.L., Harvey, K.F. and Richardson, H.E., 2010. Lgl, aPKC, and Crumbs regulate the Salvador/Warts/Hippo pathway through two distinct mechanisms. Curr Biol. 20, 573-81.

Gullberg, D. and Ekblom, P., 1995. Extracellular matrix and its receptors during development. Int J Dev Biol. 39, 845-54.

Gunn-Moore, F.J., Welsh, G.I., Herron, L.R., Brannigan, F., Venkateswarlu, K., Gillespie, S., Brandwein-Gensler, M., Madan, R., Tavare, J.M., Brophy, P.J., Prystowsky, M.B. and Guild, S., 2005. A novel 4.1 ezrin radixin moesin (FERM)-containing protein, 'Willin'. FEBS Lett. 579, 5089-94.

Guo, C., Qiu, H.Y., Huang, Y., Chen, H., Yang, R.Q., Chen, S.D., Johnson, R.L., Chen, Z.F. and Ding, Y.Q., 2007. Lmx1b is essential for Fgf8 and Wnt1 expression in the isthmic organizer during tectum and cerebellum development in mice. Development. 134, 317-25.

Guo, J., Gaj, T. and Barbas, C.F., 3rd, 2010. Directed evolution of an enhanced and highly efficient FokI cleavage domain for zinc finger nucleases. J Mol Biol. 400, 96-107.

Guo, S., Brush, J., Teraoka, H., Goddard, A., Wilson, S.W., Mullins, M.C. and Rosenthal, A., 1999. Development of noradrenergic neurons in the zebrafish hindbrain requires BMP, FGF8, and the homeodomain protein soulless/Phox2a. Neuron. 24, 555-66.

Gupta, A., Hall, V.L., Kok, F.O., Shin, M., McNulty, J.C., Lawson, N.D. and Wolfe, S.A., 2013. Targeted Chromosomal Deletions and Inversions in Zebrafish. Genome Res.

Guthrie, S., Butcher, M. and Lumsden, A., 1991. Patterns of cell division and interkinetic nuclear migration in the chick embryo hindbrain. J Neurobiol. 22, 742-54.

Guthrie, S. and Lumsden, A., 1991. Formation and regeneration of rhombomere boundaries in the developing chick hindbrain. Development. 112, 221-9.

Gutzman, J.H., Graeden, E.G., Lowery, L.A., Holley, H.S. and Sive, H., 2008. Formation of the zebrafish midbrain-hindbrain boundary constriction requires laminin-dependent basal constriction. Mech Dev. 125, 974-83.

Gutzman, J.H. and Sive, H., 2009. Zebrafish brain ventricle injection. J Vis Exp.

Gutzman, J.H. and Sive, H., 2010. Epithelial relaxation mediated by the myosin phosphatase regulator Mypt1 is required for brain ventricle lumen expansion and hindbrain morphogenesis. Development. 137, 795-804.

Hagmann, M., Bruggmann, R., Xue, L., Georgiev, O., Schaffner, W., Rungger, D., Spaniol, P. and Gerster, T., 1998. Homologous recombination and DNA-end joining reactions in zygotes and early embryos of zebrafish (Danio rerio) and Drosophila melanogaster. Biol Chem. 379, 673-81.

Hajdu, S.I., 2003. A note from history: discovery of the cerebrospinal fluid. Ann Clin Lab Sci. 33, 334-6.

Halder, G. and Johnson, R.L., 2011. Hippo signaling: growth control and beyond. Development. 138, 9-22.

Haliassos, A., Chomel, J.C., Grandjouan, S., Kruh, J., Kaplan, J.C. and Kitzis, A., 1989. Detection of minority point mutations by modified PCR technique: a new approach for a sensitive diagnosis of tumor-progression markers. Nucleic Acids Res. 17, 8093-9.

Hamaratoglu, F., Willecke, M., Kango-Singh, M., Nolo, R., Hyun, E., Tao, C., Jafar-Nejad, H. and Halder, G., 2006. The tumour-suppressor genes NF2/Merlin and Expanded act through Hippo signalling to regulate cell proliferation and apoptosis. Nat Cell Biol. 8, 27-36.

Han, D., Byun, S.H., Park, S., Kim, J., Kim, I., Ha, S., Kwon, M. and Yoon, K., 2015. YAP/TAZ enhance mammalian embryonic neural stem cell characteristics in a Tead-dependent manner. Biochem Biophys Res Commun. 458, 110-6.

Handel, E.M., Alwin, S. and Cathomen, T., 2009. Expanding or restricting the target site repertoire of zinc-finger nucleases: the inter-domain linker as a major determinant of target site selectivity. Mol Ther. 17, 104-11.

Hanneman, E., Trevarrow, B., Metcalfe, W.K., Kimmel, C.B. and Westerfield, M., 1988. Segmental pattern of development of the hindbrain and spinal cord of the zebrafish embryo. Development. 103, 49-58.

Hao, J., Ao, A., Zhou, L., Murphy, C.K., Frist, A.Y., Keel, J.J., Thorne, C.A., Kim, K., Lee, E. and Hong, C.C., 2013. Selective small molecule targeting beta-catenin function discovered by in vivo chemical genetic screen. Cell Rep. 4, 898-904.

Hardan, A.Y., Minshew, N.J., Mallikarjuhn, M. and Keshavan, M.S., 2001. Brain volume in autism. J Child Neurol. 16, 421-4.

Hartenstein, V., 1993. Early pattern of neuronal differentiation in the Xenopus embryonic brainstem and spinal cord. J Comp Neurol. 328, 213-31.

Hartshorne, D.J., Ito, M. and Erdodi, F., 2004. Role of protein phosphatase type 1 in contractile functions: myosin phosphatase. J Biol Chem. 279, 37211-4.

Harvey, K.F., Pfleger, C.M. and Hariharan, I.K., 2003. The Drosophila Mst ortholog, hippo, restricts growth and cell proliferation and promotes apoptosis. Cell. 114, 457-67.

Harvey, S.A., Sealy, I., Kettleborough, R., Fenyes, F., White, R., Stemple, D. and Smith, J.C., 2013. Identification of the zebrafish maternal and paternal transcriptomes. Development. 140, 2703-10.

Hecht, A., Vleminckx, K., Stemmler, M.P., van Roy, F. and Kemler, R., 2000. The p300/CBP acetyltransferases function as transcriptional coactivators of beta-catenin in vertebrates. EMBO J. 19, 1839-50.

Hefferin, M.L. and Tomkinson, A.E., 2005. Mechanism of DNA double-strand break repair by non-homologous end joining. DNA Repair (Amst). 4, 639-48.

Heisenberg, C.P., Houart, C., Take-Uchi, M., Rauch, G.J., Young, N., Coutinho, P., Masai, I., Caneparo, L., Concha, M.L., Geisler, R., Dale, T.C., Wilson, S.W. and Stemple, D.L., 2001. A mutation in the Gsk3-binding domain of zebrafish Masterblind/Axin1 leads to a fate transformation of telencephalon and eyes to diencephalon. Genes Dev. 15, 1427-34.

Helmbacher, F., Pujades, C., Desmarquet, C., Frain, M., Rijli, F.M., Chambon, P. and Charnay, P., 1998. Hoxa1 and Krox-20 synergize to control the development of rhombomere 3. Development. 125, 4739-48.

Hernandez, R.E., Putzke, A.P., Myers, J.P., Margaretha, L. and Moens, C.B., 2007. Cyp26 enzymes generate the retinoic acid response pattern necessary for hindbrain development. Development. 134, 177-87.

Hernandez, R.E., Rikhof, H.A., Bachmann, R. and Moens, C.B., 2004. vhnf1 integrates global RA patterning and local FGF signals to direct posterior hindbrain development in zebrafish. Development. 131, 4511-20.

Heyman, I., Faissner, A. and Lumsden, A., 1995. Cell and matrix specialisations of rhombomere boundaries. Dev Dyn. 204, 301-15.

Heyman, I., Kent, A. and Lumsden, A., 1993. Cellular morphology and extracellular space at rhombomere boundaries in the chick embryo hindbrain. Dev Dyn. 198, 241-53.

Higashijima, S., Hotta, Y. and Okamoto, H., 2000. Visualization of cranial motor neurons in live transgenic zebrafish expressing green fluorescent protein under the control of the islet-1 promoter/enhancer. J Neurosci. 20, 206-18.

Higuchi, M., Kiyama, H., Hayakawa, T., Hamada, Y. and Tsujimoto, Y., 1995. Differential expression of Notch1 and Notch2 in developing and adult mouse brain. Brain Res Mol Brain Res. 29, 263-72.

Hill, J., Clarke, J.D., Vargesson, N., Jowett, T. and Holder, N., 1995. Exogenous retinoic acid causes specific alterations in the development of the midbrain and hindbrain of the zebrafish embryo including positional respecification of the Mauthner neuron. Mech Dev. 50, 3-16.

Hindley, C.J., Condurat, A.L., Menon, V., Thomas, R., Azmitia, L.M., Davis, J.A. and Pruszak, J., 2016. The Hippo pathway member YAP enhances human neural crest cell fate and migration. Sci Rep. 6, 23208.

Hirate, Y., Hirahara, S., Inoue, K., Suzuki, A., Alarcon, V.B., Akimoto, K., Hirai, T., Hara, T., Adachi, M., Chida, K., Ohno, S., Marikawa, Y., Nakao, K., Shimono, A. and Sasaki, H., 2013. Polarity-dependent distribution of angiomotin localizes Hippo signaling in preimplantation embryos. Curr Biol. 23, 1181-94.

Hjorth, J.T., Connor, R.M. and Key, B., 2002. Role of hlx1 in zebrafish brain morphogenesis. Int J Dev Biol. 46, 583-96.

Hockemeyer, D., Wang, H., Kiani, S., Lai, C.S., Gao, Q., Cassady, J.P., Cost, G.J., Zhang, L., Santiago, Y., Miller, J.C., Zeitler, B., Cherone, J.M., Meng, X., Hinkley, S.J., Rebar, E.J., Gregory, P.D., Urnov, F.D. and Jaenisch, R., 2011. Genetic engineering of human pluripotent cells using TALE nucleases. Nat Biotechnol. 29, 731-4.

Holder, N. and Hill, J., 1991. Retinoic acid modifies development of the midbrain-hindbrain border and affects cranial ganglion formation in zebrafish embryos. Development. 113, 1159-70.

Holland, S.J., Gale, N.W., Mbamalu, G., Yancopoulos, G.D., Henkemeyer, M. and Pawson, T., 1996. Bidirectional signalling through the EPH-family receptor Nuk and its transmembrane ligands. Nature. 383, 722-5.

Holley, S.A., Geisler, R. and Nusslein-Volhard, C., 2000. Control of her1 expression during zebrafish somitogenesis by a delta-dependent oscillator and an independent wave-front activity. Genes Dev. 14, 1678-90.

Holley, S.A., Julich, D., Rauch, G.J., Geisler, R. and Nusslein-Volhard, C., 2002. her1 and the notch pathway function within the oscillator mechanism that regulates zebrafish somitogenesis. Development. 129, 1175-83.

Holly, V.L., Widen, S.A., Famulski, J.K. and Waskiewicz, A.J., 2014. Sfrp1a and Sfrp5 function as positive regulators of Wnt and BMP signaling during early retinal development. Dev Biol. 388, 192-204.

Hong, E. and Brewster, R., 2006. N-cadherin is required for the polarized cell behaviors that drive neurulation in the zebrafish. Development. 133, 3895-905.

Hong, J.H., Hwang, E.S., McManus, M.T., Amsterdam, A., Tian, Y., Kalmukova, R., Mueller, E., Benjamin, T., Spiegelman, B.M., Sharp, P.A., Hopkins, N. and Yaffe, M.B., 2005a. TAZ, a transcriptional modulator of mesenchymal stem cell differentiation. Science. 309, 1074-8.

Hong, S.K. and Dawid, I.B., 2011. The transcriptional mediator component Med12 is required for hindbrain boundary formation. PLoS One. 6, e19076.

Hong, S.K., Haldin, C.E., Lawson, N.D., Weinstein, B.M., Dawid, I.B. and Hukriede, N.A., 2005b. The zebrafish kohtalo/trap230 gene is required for the development of the brain, neural crest, and pronephric kidney. Proc Natl Acad Sci U S A. 102, 18473-8.

Hong, Y., Stronach, B., Perrimon, N., Jan, L.Y. and Jan, Y.N., 2001. Drosophila Stardust interacts with Crumbs to control polarity of epithelia but not neuroblasts. Nature. 414, 634-8.

Horan, G.S., Ramirez-Solis, R., Featherstone, M.S., Wolgemuth, D.J., Bradley, A. and Behringer, R.R., 1995. Compound mutants for the paralogous hoxa-4, hoxb-4, and hoxd-4 genes show more complete homeotic transformations and a dose-

dependent increase in the number of vertebrae transformed. Genes Dev. 9, 1667-77.
Horne-Badovinac, S., Lin, D., Waldron, S., Schwarz, M., Mbamalu, G., Pawson, T., Jan, Y., Stainier, D.Y. and Abdelilah-Seyfried, S., 2001. Positional cloning of heart and soul reveals multiple roles for PKC lambda in zebrafish organogenesis. Curr Biol. 11, 1492-502.
Hsieh, J.C., Kodjabachian, L., Rebbert, M.L., Rattner, A., Smallwood, P.M., Samos, C.H., Nusse, R., Dawid, I.B. and Nathans, J., 1999a. A new secreted protein that binds to Wnt proteins and inhibits their activities. Nature. 398, 431-6.
Hsieh, J.C., Rattner, A., Smallwood, P.M. and Nathans, J., 1999b. Biochemical characterization of Wnt-frizzled interactions using a soluble, biologically active vertebrate Wnt protein. Proc Natl Acad Sci U S A. 96, 3546-51.
Hsu, Y.C., Willoughby, J.J., Christensen, A.K. and Jensen, A.M., 2006. Mosaic Eyes is a novel component of the Crumbs complex and negatively regulates photoreceptor apical size. Development. 133, 4849-59.
Hu, J., Sun, S., Jiang, Q., Sun, S., Wang, W., Gui, Y. and Song, H., 2013. Yes-associated protein (yap) is required for early embryonic development in zebrafish (danio rerio). Int J Biol Sci. 9, 267-78.
Huang, H., Ruan, H., Aw, M.Y., Hussain, A., Guo, L., Gao, C., Qian, F., Leung, T., Song, H., Kimelman, D., Wen, Z. and Peng, J., 2008. Mypt1-mediated spatial positioning of Bmp2-producing cells is essential for liver organogenesis. Development. 135, 3209-18.
Huang, H.L., Wang, S., Yin, M.X., Dong, L., Wang, C., Wu, W., Lu, Y., Feng, M., Dai, C., Guo, X., Li, L., Zhao, B., Zhou, Z., Ji, H., Jiang, J., Zhao, Y., Liu, X.Y. and Zhang, L., 2013a. Par-1 regulates tissue growth by influencing hippo phosphorylation status and hippo-salvador association. PLoS Biol. 11, e1001620.
Huang, J., Wu, S., Barrera, J., Matthews, K. and Pan, D., 2005. The Hippo signaling pathway coordinately regulates cell proliferation and apoptosis by inactivating Yorkie, the Drosophila Homolog of YAP. Cell. 122, 421-34.
Huang, J.M., Nagatomo, I., Suzuki, E., Mizuno, T., Kumagai, T., Berezov, A., Zhang, H., Karlan, B., Greene, M.I. and Wang, Q., 2013b. YAP modifies cancer cell sensitivity to EGFR and survivin inhibitors and is negatively regulated by the non-receptor type protein tyrosine phosphatase 14. Oncogene. 32, 2220-9.
Huang, P., Xiao, A., Zhou, M., Zhu, Z., Lin, S. and Zhang, B., 2011. Heritable gene targeting in zebrafish using customized TALENs. Nat Biotechnol. 29, 699-700.
Huang, S.M., Mishina, Y.M., Liu, S., Cheung, A., Stegmeier, F., Michaud, G.A., Charlat, O., Wiellette, E., Zhang, Y., Wiessner, S., Hild, M., Shi, X., Wilson, C.J., Mickanin, C., Myer, V., Fazal, A., Tomlinson, R., Serluca, F., Shao, W., Cheng, H., Shultz, M., Rau, C., Schirle, M., Schlegl, J., Ghidelli, S., Fawell, S., Lu, C., Curtis, D., Kirschner, M.W., Lengauer, C., Finan, P.M., Tallarico, J.A., Bouwmeester, T., Porter, J.A., Bauer, A. and Cong, F., 2009. Tankyrase inhibition stabilizes axin and antagonizes Wnt signalling. Nature. 461, 614-20.
Huang, X., Wang, Y., Yan, W., Smith, C., Ye, Z., Wang, J., Gao, Y., Mendelsohn, L. and Cheng, L., 2015. Production of Gene-Corrected Adult Beta Globin Protein in Human Erythrocytes Differentiated from Patient iPSCs After Genome Editing of the Sickle Point Mutation. Stem Cells. 33, 1470-9.

Hunt, P., Gulisano, M., Cook, M., Sham, M.H., Faiella, A., Wilkinson, D., Boncinelli, E. and Krumlauf, R., 1991. A distinct Hox code for the branchial region of the vertebrate head. Nature. 353, 861-4.

Hurt, J.A., Thibodeau, S.A., Hirsh, A.S., Pabo, C.O. and Joung, J.K., 2003. Highly specific zinc finger proteins obtained by directed domain shuffling and cell-based selection. Proc Natl Acad Sci U S A. 100, 12271-6.

Hwang, W.Y., Fu, Y., Reyon, D., Maeder, M.L., Tsai, S.Q., Sander, J.D., Peterson, R.T., Yeh, J.R. and Joung, J.K., 2013. Efficient genome editing in zebrafish using a CRISPR-Cas system. Nat Biotechnol. 31, 227-9.

Ibanez-Tallon, I., Pagenstecher, A., Fliegauf, M., Olbrich, H., Kispert, A., Ketelsen, U.P., North, A., Heintz, N. and Omran, H., 2004. Dysfunction of axonemal dynein heavy chain Mdnah5 inhibits ependymal flow and reveals a novel mechanism for hydrocephalus formation. Hum Mol Genet. 13, 2133-41.

Ikeda, M., Kawata, A., Nishikawa, M., Tateishi, Y., Yamaguchi, M., Nakagawa, K., Hirabayashi, S., Bao, Y., Hidaka, S., Hirata, Y. and Hata, Y., 2009. Hippo pathway-dependent and -independent roles of RASSF6. Sci Signal. 2, ra59.

Irvine, K.D., 1999. Fringe, Notch, and making developmental boundaries. Curr Opin Genet Dev. 9, 434-41.

Irvine, K.D. and Rauskolb, C., 2001. Boundaries in development: formation and function. Annu Rev Cell Dev Biol. 17, 189-214.

Irvine, K.D. and Wieschaus, E., 1994. fringe, a Boundary-specific signaling molecule, mediates interactions between dorsal and ventral cells during Drosophila wing development. Cell. 79, 595-606.

Isalan, M. and Choo, Y., 2001. Rapid, high-throughput engineering of sequence-specific zinc finger DNA-binding proteins. Methods Enzymol. 340, 593-609.

Isalan, M., Choo, Y. and Klug, A., 1997. Synergy between adjacent zinc fingers in sequence-specific DNA recognition. Proc Natl Acad Sci U S A. 94, 5617-21.

Isalan, M., Klug, A. and Choo, Y., 1998. Comprehensive DNA recognition through concerted interactions from adjacent zinc fingers. Biochemistry. 37, 12026-33.

Ishibashi, S., Cliffe, R. and Amaya, E., 2012. Highly efficient bi-allelic mutation rates using TALENs in Xenopus tropicalis. Biol Open. 1, 1273-6.

Ishino, Y., Shinagawa, H., Makino, K., Amemura, M. and Nakata, A., 1987. Nucleotide sequence of the iap gene, responsible for alkaline phosphatase isozyme conversion in Escherichia coli, and identification of the gene product. J Bacteriol. 169, 5429-33.

Ito, M., Nakano, T., Erdodi, F. and Hartshorne, D.J., 2004. Myosin phosphatase: structure, regulation and function. Mol Cell Biochem. 259, 197-209.

Itoh, M., Kim, C.H., Palardy, G., Oda, T., Jiang, Y.J., Maust, D., Yeo, S.Y., Lorick, K., Wright, G.J., Ariza-McNaughton, L., Weissman, A.M., Lewis, J., Chandrasekharappa, S.C. and Chitnis, A.B., 2003. Mind bomb is a ubiquitin ligase that is essential for efficient activation of Notch signaling by Delta. Dev Cell. 4, 67-82.

Izpisua-Belmonte, J.C., Falkenstein, H., Dolle, P., Renucci, A. and Duboule, D., 1991. Murine genes related to the Drosophila AbdB homeotic genes are sequentially expressed during development of the posterior part of the body. EMBO J. 10, 2279-89.

Jacobs, K.M., Bhave, S.R., Ferraro, D.J., Jaboin, J.J., Hallahan, D.E. and Thotala, D., 2012. GSK-3beta: A Bifunctional Role in Cell Death Pathways. Int J Cell Biol. 2012, 930710.

Jacobs, Y., Schnabel, C.A. and Cleary, M.L., 1999. Trimeric association of Hox and TALE homeodomain proteins mediates Hoxb2 hindbrain enhancer activity. Mol Cell Biol. 19, 5134-42.

Jagannathan, S. and Bradley, R.K., 2016. Translational plasticity facilitates the accumulation of nonsense genetic variants in the human population. Genome Res. 26, 1639-1650.

James, M.F., Manchanda, N., Gonzalez-Agosti, C., Hartwig, J.H. and Ramesh, V., 2001. The neurofibromatosis 2 protein product merlin selectively binds F-actin but not G-actin, and stabilizes the filaments through a lateral association. Biochem J. 356, 377-86.

Janda, C.Y., Dang, L.T., You, C., Chang, J., de Lau, W., Zhong, Z.A., Yan, K.S., Marecic, O., Siepe, D., Li, X., Moody, J.D., Williams, B.O., Clevers, H., Piehler, J., Baker, D., Kuo, C.J. and Garcia, K.C., 2017. Surrogate Wnt agonists that phenocopy canonical Wnt and beta-catenin signalling. Nature. 545, 234-237.

Jaw, T.J., You, L.R., Knoepfler, P.S., Yao, L.C., Pai, C.Y., Tang, C.Y., Chang, L.P., Berthelsen, J., Blasi, F., Kamps, M.P. and Sun, Y.H., 2000. Direct interaction of two homeoproteins, homothorax and extradenticle, is essential for EXD nuclear localization and function. Mech Dev. 91, 279-91.

Jensen, A.M., Walker, C. and Westerfield, M., 2001. mosaic eyes: a zebrafish gene required in pigmented epithelium for apical localization of retinal cell division and lamination. Development. 128, 95-105.

Jensen, A.M. and Westerfield, M., 2004. Zebrafish mosaic eyes is a novel FERM protein required for retinal lamination and retinal pigmented epithelial tight junction formation. Curr Biol. 14, 711-7.

Jia, J., Zhang, W., Wang, B., Trinko, R. and Jiang, J., 2003. The Drosophila Ste20 family kinase dMST functions as a tumor suppressor by restricting cell proliferation and promoting apoptosis. Genes Dev. 17, 2514-9.

Jiang, Q., Liu, D., Gong, Y., Wang, Y., Sun, S., Gui, Y. and Song, H., 2009. yap is required for the development of brain, eyes, and neural crest in zebrafish. Biochem Biophys Res Commun. 384, 114-9.

Jiang, Y.J., Brand, M., Heisenberg, C.P., Beuchle, D., Furutani-Seiki, M., Kelsh, R.N., Warga, R.M., Granato, M., Haffter, P., Hammerschmidt, M., Kane, D.A., Mullins, M.C., Odenthal, J., van Eeden, F.J. and Nusslein-Volhard, C., 1996. Mutations affecting neurogenesis and brain morphology in the zebrafish, Danio rerio. Development. 123, 205-16.

Jinek, M., Chylinski, K., Fonfara, I., Hauer, M., Doudna, J.A. and Charpentier, E., 2012. A programmable dual-RNA-guided DNA endonuclease in adaptive bacterial immunity. Science. 337, 816-21.

Johnston, S.H., Rauskolb, C., Wilson, R., Prabhakaran, B., Irvine, K.D. and Vogt, T.F., 1997. A family of mammalian Fringe genes implicated in boundary determination and the Notch pathway. Development. 124, 2245-54.

Judson, R.N., Tremblay, A.M., Knopp, P., White, R.B., Urcia, R., De Bari, C., Zammit, P.S., Camargo, F.D. and Wackerhage, H., 2012. The Hippo pathway member

Yap plays a key role in influencing fate decisions in muscle satellite cells. J Cell Sci. 125, 6009-19.
Jungbluth, S., Bell, E. and Lumsden, A., 1999. Specification of distinct motor neuron identities by the singular activities of individual Hox genes. Development. 126, 2751-8.
Jurberg, A.D., Aires, R., Varela-Lasheras, I., Novoa, A. and Mallo, M., 2013. Switching axial progenitors from producing trunk to tail tissues in vertebrate embryos. Dev Cell. 25, 451-62.
Jurisch-Yaksi, N., Rose, A.J., Lu, H., Raemaekers, T., Munck, S., Baatsen, P., Baert, V., Vermeire, W., Scales, S.J., Verleyen, D., Vandepoel, R., Tylzanowski, P., Yaksi, E., de Ravel, T., Yost, H.J., Froyen, G., Arrington, C.B. and Annaert, W., 2013. Rer1p maintains ciliary length and signaling by regulating gamma-secretase activity and Foxj1a levels. J Cell Biol. 200, 709-20.
Justice, R.W., Zilian, O., Woods, D.F., Noll, M. and Bryant, P.J., 1995. The Drosophila tumor suppressor gene warts encodes a homolog of human myotonic dystrophy kinase and is required for the control of cell shape and proliferation. Genes Dev. 9, 534-46.
Kahane, N. and Kalcheim, C., 1998. Identification of early postmitotic cells in distinct embryonic sites and their possible roles in morphogenesis. Cell Tissue Res. 294, 297-307.
Kallen, B., 1955. Cell degeneration during normal ontogenesis of the rabbit brain. J Anat. 89, 153-61.
Kamachi, Y., Uchikawa, M., Collignon, J., Lovell-Badge, R. and Kondoh, H., 1998. Involvement of Sox1, 2 and 3 in the early and subsequent molecular events of lens induction. Development. 125, 2521-32.
Kamberov, E., Makarova, O., Roh, M., Liu, A., Karnak, D., Straight, S. and Margolis, B., 2000. Molecular cloning and characterization of Pals, proteins associated with mLin-7. J Biol Chem. 275, 11425-31.
Kanai, F., Marignani, P.A., Sarbassova, D., Yagi, R., Hall, R.A., Donowitz, M., Hisaminato, A., Fujiwara, T., Ito, Y., Cantley, L.C. and Yaffe, M.B., 2000. TAZ: a novel transcriptional co-activator regulated by interactions with 14-3-3 and PDZ domain proteins. EMBO J. 19, 6778-91.
Kandavelou, K., Mani, M., Durai, S. and Chandrasegaran, S., 2005. "Magic" scissors for genome surgery. Nat Biotechnol. 23, 686-7.
Kandel, E.R., Schwartz, J.H. and Jessell, T.M., 2000. Principles of neural science, 4th ed. McGraw-Hill, Health Professions Division, New York.
Kang, H., Minder, P., Park, M.A., Mesquitta, W.T., Torbett, B.E. and Slukvin, II, 2015. CCR5 Disruption in Induced Pluripotent Stem Cells Using CRISPR/Cas9 Provides Selective Resistance of Immune Cells to CCR5-tropic HIV-1 Virus. Mol Ther Nucleic Acids. 4, e268.
Kango-Singh, M., Nolo, R., Tao, C., Verstreken, P., Hiesinger, P.R., Bellen, H.J. and Halder, G., 2002. Shar-pei mediates cell proliferation arrest during imaginal disc growth in Drosophila. Development. 129, 5719-30.
Kani, S., Bae, Y.K., Shimizu, T., Tanabe, K., Satou, C., Parsons, M.J., Scott, E., Higashijima, S. and Hibi, M., 2010. Proneural gene-linked neurogenesis in zebrafish cerebellum. Dev Biol. 343, 1-17.

Kao, H.Y., Ordentlich, P., Koyano-Nakagawa, N., Tang, Z., Downes, M., Kintner, C.R., Evans, R.M. and Kadesch, T., 1998. A histone deacetylase corepressor complex regulates the Notch signal transduction pathway. Genes Dev. 12, 2269-77.

Kappen, C., Schughart, K. and Ruddle, F.H., 1989. Two steps in the evolution of Antennapedia-class vertebrate homeobox genes. Proc Natl Acad Sci U S A. 86, 5459-63.

Kawakami, Y., Rodriguez-Leon, J., Koth, C.M., Buscher, D., Itoh, T., Raya, A., Ng, J.K., Esteban, C.R., Takahashi, S., Henrique, D., Schwarz, M.F., Asahara, H. and Izpisua Belmonte, J.C., 2003. MKP3 mediates the cellular response to FGF8 signalling in the vertebrate limb. Nat Cell Biol. 5, 513-9.

Keino, H., Masaki, S., Kawarada, Y. and Naruse, I., 1994. Apoptotic degeneration in the arhinencephalic brain of the mouse mutant Pdn/Pdn. Brain Res Dev Brain Res. 78, 161-8.

Kessel, M. and Gruss, P., 1990. Murine developmental control genes. Science. 249, 374-9.

Kessel, M. and Gruss, P., 1991. Homeotic transformations of murine vertebrae and concomitant alteration of Hox codes induced by retinoic acid. Cell. 67, 89-104.

Kettleborough, R.N., Busch-Nentwich, E.M., Harvey, S.A., Dooley, C.M., de Bruijn, E., van Eeden, F., Sealy, I., White, R.J., Herd, C., Nijman, I.J., Fenyes, F., Mehroke, S., Scahill, C., Gibbons, R., Wali, N., Carruthers, S., Hall, A., Yen, J., Cuppen, E. and Stemple, D.L., 2013. A systematic genome-wide analysis of zebrafish protein-coding gene function. Nature. 496, 494-7.

Keynes, R. and Krumlauf, R., 1994. Hox genes and regionalization of the nervous system. Annu Rev Neurosci. 17, 109-32.

Kim, C.A. and Berg, J.M., 1996. A 2.2 A resolution crystal structure of a designed zinc finger protein bound to DNA. Nat Struct Biol. 3, 940-5.

Kim, C.H., Oda, T., Itoh, M., Jiang, D., Artinger, K.B., Chandrasekharappa, S.C., Driever, W. and Chitnis, A.B., 2000. Repressor activity of Headless/Tcf3 is essential for vertebrate head formation. Nature. 407, 913-6.

Kim, D.H., Kim, S.H., Lee, O.J., Huang, S.M., Kwon, J.L., Kim, J.M., Kim, J.Y., Seong, I.O., Song, K.S. and Kim, K.H., 2013a. Differential expression of Yes-associated protein and phosphorylated Yes-associated protein is correlated with expression of Ki-67 and phospho-ERK in colorectal adenocarcinoma. Histol Histopathol. 28, 1483-90.

Kim, F.A., Sing l, A., Kaneko, T., Bieman, M., Stallwood, N., Sadl, V.S. and Cordes, S.P., 2005. The vHNF1 homeodomain protein establishes early rhombomere identity by direct regulation of Kreisler expression. Mech Dev. 122, 1300-9.

Kim, H.J., Lee, H.J., Kim, H., Cho, S.W. and Kim, J.S., 2009. Targeted genome editing in human cells with zinc finger nucleases constructed via modular assembly. Genome Res. 19, 1279-88.

Kim, J., Irvine, K.D. and Carroll, S.B., 1995. Cell recognition, signal induction, and symmetrical gene activation at the dorsal-ventral boundary of the developing Drosophila wing. Cell. 82, 795-802.

Kim, J., Kim, Y.H., Kim, J., Park, D.Y., Bae, H., Lee, D.H., Kim, K.H., Hong, S.P., Jang, S.P., Kubota, Y., Kwon, Y.G., Lim, D.S. and Koh, G.Y., 2017a. YAP/TAZ regulates sprouting angiogenesis and vascular barrier maturation. J Clin Invest. 127, 3441-3461.

Kim, J., Sebring, A., Esch, J.J., Kraus, M.E., Vorwerk, K., Magee, J. and Carroll, S.B., 1996. Integration of positional signals and regulation of wing formation and identity by Drosophila vestigial gene. Nature. 382, 133-8.
Kim, M., Kim, M., Lee, S., Kuninaka, S., Saya, H., Lee, H., Lee, S. and Lim, D.S., 2013b. cAMP/PKA signalling reinforces the LATS-YAP pathway to fully suppress YAP in response to actin cytoskeletal changes. EMBO J. 32, 1543-55.
Kim, M., Kim, T., Johnson, R.L. and Lim, D.S., 2015. Transcriptional co-repressor function of the hippo pathway transducers YAP and TAZ. Cell Rep. 11, 270-82.
Kim, N.G., Koh, E., Chen, X. and Gumbiner, B.M., 2011. E-cadherin mediates contact inhibition of proliferation through Hippo signaling-pathway components. Proc Natl Acad Sci U S A. 108, 11930-5.
Kim, S., Kim, E.J. and Kim, J.S., 2010. Construction of combinatorial libraries that encode zinc finger-based transcription factors. Methods Mol Biol. 649, 133-47.
Kim, W., Khan, S.K., Gvozdenovic-Jeremic, J., Kim, Y., Dahlman, J., Kim, H., Park, O., Ishitani, T., Jho, E.H., Gao, B. and Yang, Y., 2017b. Hippo signaling interactions with Wnt/beta-catenin and Notch signaling repress liver tumorigenesis. J Clin Invest. 127, 137-152.
Kimelman, D., Smith, N.L., Lai, J.K.H. and Stainier, D.Y., 2017. Regulation of posterior body and epidermal morphogenesis in zebrafish by localized Yap1 and Wwtr1. Elife. 6.
Kimmel, C.B., Ballard, W.W., Kimmel, S.R., Ullmann, B. and Schilling, T.F., 1995. Stages of embryonic development of the zebrafish. Dev Dyn. 203, 253-310.
Kimmel, C.B., Hatta, K. and Metcalfe, W.K., 1990. Early axonal contacts during development of an identified dendrite in the brain of the zebrafish. Neuron. 4, 535-45.
Kimmel, C.B., Powell, S.L. and Metcalfe, W.K., 1982. Brain neurons which project to the spinal cord in young larvae of the zebrafish. J Comp Neurol. 205, 112-27.
Kitagawa, M., Hatakeyama, S., Shirane, M., Matsumoto, M., Ishida, N., Hattori, K., Nakamichi, I., Kikuchi, A., Nakayama, K. and Nakayama, K., 1999. An F-box protein, FWD1, mediates ubiquitin-dependent proteolysis of beta-catenin. EMBO J. 18, 2401-10.
Kitzmann, M., Bonnieu, A., Duret, C., Vernus, B., Barro, M., Laoudj-Chenivesse, D., Verdi, J.M. and Carnac, G., 2006. Inhibition of Notch signaling induces myotube hypertrophy by recruiting a subpopulation of reserve cells. J Cell Physiol. 208, 538-48.
Knoepfler, P.S. and Kamps, M.P., 1995. The pentapeptide motif of Hox proteins is required for cooperative DNA binding with Pbx1, physically contacts Pbx1, and enhances DNA binding by Pbx1. Mol Cell Biol. 15, 5811-9.
Knoepfler, P.S., Lu, Q. and Kamps, M.P., 1996. Pbx-1 Hox heterodimers bind DNA on inseparable half-sites that permit intrinsic DNA binding specificity of the Hox partner at nucleotides 3' to a TAAT motif. Nucleic Acids Res. 24, 2288-94.
Kobayashi, M., Fujioka, M., Tolkunova, E.N., Deka, D., Abu-Shaar, M., Mann, R.S. and Jaynes, J.B., 2003. Engrailed cooperates with extradenticle and homothorax to repress target genes in Drosophila. Development. 130, 741-51.
Koentges, G. and Matsuoka, T., 2002. Evolution. Jaws of the fates. Science. 298, 371-3.
Kok, F.O., Shin, M., Ni, C.W., Gupta, A., Grosse, A.S., van Impel, A., Kirchmaier, B.C., Peterson-Maduro, J., Kourkoulis, G., Male, I., DeSantis, D.F., Sheppard-

Tindell, S., Ebarasi, L., Betsholtz, C., Schulte-Merker, S., Wolfe, S.A. and Lawson, N.D., 2015. Reverse genetic screening reveals poor correlation between morpholino-induced and mutant phenotypes in zebrafish. Dev Cell. 32, 97-108.

Komisarczuk, A.Z., Topp, S., Stigloher, C., Kapsimali, M., Bally-Cuif, L. and Becker, T.S., 2008. Enhancer detection and developmental expression of zebrafish sprouty1, a member of the fgf8 synexpression group. Dev Dyn. 237, 2594-603.

Komuro, A., Nagai, M., Navin, N.E. and Sudol, M., 2003. WW domain-containing protein YAP associates with ErbB-4 and acts as a co-transcriptional activator for the carboxyl-terminal fragment of ErbB-4 that translocates to the nucleus. J Biol Chem. 278, 33334-41.

Koshida, S., Shinya, M., Nikaido, M., Ueno, N., Schulte-Merker, S., Kuroiwa, A. and Takeda, H., 2002. Inhibition of BMP activity by the FGF signal promotes posterior neural development in zebrafish. Dev Biol. 244, 9-20.

Koster, R.W. and Fraser, S.E., 2001. Direct imaging of in vivo neuronal migration in the developing cerebellum. Curr Biol. 11, 1858-63.

Kouhara, H., Hadari, Y.R., Spivak-Kroizman, T., Schilling, J., Bar-Sagi, D., Lax, I. and Schlessinger, J., 1997. A lipid-anchored Grb2-binding protein that links FGF-receptor activation to the Ras/MAPK signaling pathway. Cell. 89, 693-702.

Kovalchuk, I., Pelczar, P. and Kovalchuk, O., 2004. High frequency of nucleotide misincorporations upon the processing of double-strand breaks. DNA Repair (Amst). 3, 217-23.

Krumlauf, R., 1992a. Evolution of the vertebrate Hox homeobox genes. Bioessays. 14, 245-52.

Krumlauf, R., 1992b. Transforming the Hox code. Curr Biol. 2, 641-3.

Krumlauf, R., 1993. Hox genes and pattern formation in the branchial region of the vertebrate head. Trends Genet. 9, 106-12.

Kudoh, T., Wilson, S.W. and Dawid, I.B., 2002. Distinct roles for Fgf, Wnt and retinoic acid in posteriorizing the neural ectoderm. Development. 129, 4335-46.

Kuida, K., Zheng, T.S., Na, S., Kuan, C., Yang, D., Karasuyama, H., Rakic, P. and Flavell, R.A., 1996. Decreased apoptosis in the brain and premature lethality in CPP32-deficient mice. Nature. 384, 368-72.

Kurokawa, K., Nakamura, K., Sumiyoshi, T., Hagino, H., Yotsutsuji, T., Yamashita, I., Suzuki, M., Matsui, M. and Kurachi, M., 2000. Ventricular enlargement in schizophrenia spectrum patients with prodromal symptoms of obsessive-compulsive disorder. Psychiatry Res. 99, 83-91.

Kurooka, H. and Honjo, T., 2000. Functional interaction between the mouse notch1 intracellular region and histone acetyltransferases PCAF and GCN5. J Biol Chem. 275, 17211-20.

Lai, D. and Yang, X., 2013. BMP4 is a novel transcriptional target and mediator of mammary cell migration downstream of the Hippo pathway component TAZ. Cell Signal. 25, 1720-8.

Lai, Z.C., Wei, X., Shimizu, T., Ramos, E., Rohrbaugh, M., Nikolaidis, N., Ho, L.L. and Li, Y., 2005. Control of cell proliferation and apoptosis by mob as tumor suppressor, mats. Cell. 120, 675-85.

Lallemand, D., Curto, M., Saotome, I., Giovannini, M. and McClatchey, A.I., 2003. NF2 deficiency promotes tumorigenesis and metastasis by destabilizing adherens junctions. Genes Dev. 17, 1090-100.

Langford, K.J., Askham, J.M., Lee, T., Adams, M. and Morrison, E.E., 2006. Examination of actin and microtubule dependent APC localisations in living mammalian cells. BMC Cell Biol. 7, 3.

Langston, A.W. and Gudas, L.J., 1992. Identification of a retinoic acid responsive enhancer 3' of the murine homeobox gene Hox-1.6. Mech Dev. 38, 217-27.

Laprise, P., Beronja, S., Silva-Gagliardi, N.F., Pellikka, M., Jensen, A.M., McGlade, C.J. and Tepass, U., 2006. The FERM protein Yurt is a negative regulatory component of the Crumbs complex that controls epithelial polarity and apical membrane size. Dev Cell. 11, 363-74.

Lardelli, M., Dahlstrand, J. and Lendahl, U., 1994. The novel Notch homologue mouse Notch 3 lacks specific epidermal growth factor-repeats and is expressed in proliferating neuroepithelium. Mech Dev. 46, 123-36.

Lavado, A., He, Y., Pare, J., Neale, G., Olson, E.N., Giovannini, M. and Cao, X., 2013. Tumor suppressor Nf2 limits expansion of the neural progenitor pool by inhibiting Yap/Taz transcriptional coactivators. Development. 140, 3323-34.

Lavado, A., Ware, M., Pare, J. and Cao, X., 2014. The tumor suppressor Nf2 regulates corpus callosum development by inhibiting the transcriptional coactivator Yap. Development. 141, 4182-93.

Le Douarin, N. and Kalcheim, C., 1999. The neural crest, 2nd ed. Cambridge University Press, Cambridge, UK ; New York, NY, USA.

Lecaudey, V., Anselme, I., Rosa, F. and Schneider-Maunoury, S., 2004. The zebrafish Iroquois gene iro7 positions the r4/r5 boundary and controls neurogenesis in the rostral hindbrain. Development. 131, 3121-31.

Lecuit, T. and Lenne, P.F., 2007. Cell surface mechanics and the control of cell shape, tissue patterns and morphogenesis. Nat Rev Mol Cell Biol. 8, 633-44.

Lee, H.J., Kim, E. and Kim, J.S., 2010. Targeted chromosomal deletions in human cells using zinc finger nucleases. Genome Res. 20, 81-9.

Lee, R.K. and Eaton, R.C., 1991. Identifiable reticulospinal neurons of the adult zebrafish, Brachydanio rerio. J Comp Neurol. 304, 34-52.

Lei, Q.Y., Zhang, H., Zhao, B., Zha, Z.Y., Bai, F., Pei, X.H., Zhao, S., Xiong, Y. and Guan, K.L., 2008. TAZ promotes cell proliferation and epithelial-mesenchymal transition and is inhibited by the hippo pathway. Mol Cell Biol. 28, 2426-36.

Lei, Y., Guo, X., Liu, Y., Cao, Y., Deng, Y., Chen, X., Cheng, C.H., Dawid, I.B., Chen, Y. and Zhao, H., 2012. Efficient targeted gene disruption in Xenopus embryos using engineered transcription activator-like effector nucleases (TALENs). Proc Natl Acad Sci U S A. 109, 17484-9.

Lekven, A.C., Buckles, G.R., Kostakis, N. and Moon, R.T., 2003. Wnt1 and wnt10b function redundantly at the zebrafish midbrain-hindbrain boundary. Dev Biol. 254, 172-87.

Lele, Z., Folchert, A., Concha, M., Rauch, G.J., Geisler, R., Rosa, F., Wilson, S.W., Hammerschmidt, M. and Bally-Cuif, L., 2002. parachute/n-cadherin is required for morphogenesis and maintained integrity of the zebrafish neural tube. Development. 129, 3281-94.

Levitan, D. and Greenwald, I., 1995. Facilitation of lin-12-mediated signalling by sel-12, a Caenorhabditis elegans S182 Alzheimer's disease gene. Nature. 377, 351-4.

Lewis, E.B., 1978. A gene complex controlling segmentation in Drosophila. Nature. 276, 565-70.

Lewis, J., 1998. Notch signalling and the control of cell fate choices in vertebrates. Semin Cell Dev Biol. 9, 583-9.

Li, H.L., Fujimoto, N., Sasakawa, N., Shirai, S., Ohkame, T., Sakuma, T., Tanaka, M., Amano, N., Watanabe, A., Sakurai, H., Yamamoto, T., Yamanaka, S. and Hotta, A., 2015a. Precise correction of the dystrophin gene in duchenne muscular dystrophy patient induced pluripotent stem cells by TALEN and CRISPR-Cas9. Stem Cell Reports. 4, 143-54.

Li, L., Piatek, M.J., Atef, A., Piatek, A., Wibowo, A., Fang, X., Sabir, J.S., Zhu, J.K. and Mahfouz, M.M., 2012. Rapid and highly efficient construction of TALE-based transcriptional regulators and nucleases for genome modification. Plant Mol Biol. 78, 407-16.

Li, T., Huang, S., Jiang, W.Z., Wright, D., Spalding, M.H., Weeks, D.P. and Yang, B., 2011a. TAL nucleases (TALNs): hybrid proteins composed of TAL effectors and FokI DNA-cleavage domain. Nucleic Acids Res. 39, 359-72.

Li, T., Huang, S., Zhao, X., Wright, D.A., Carpenter, S., Spalding, M.H., Weeks, D.P. and Yang, B., 2011b. Modularly assembled designer TAL effector nucleases for targeted gene knockout and gene replacement in eukaryotes. Nucleic Acids Res. 39, 6315-25.

Li, Y., Zhou, H., Li, F., Chan, S.W., Lin, Z., Wei, Z., Yang, Z., Guo, F., Lim, C.J., Xing, W., Shen, Y., Hong, W., Long, J. and Zhang, M., 2015b. Angiomotin binding-induced activation of Merlin/NF2 in the Hippo pathway. Cell Res. 25, 801-17.

Lindsell, C.E., Boulter, J., diSibio, G., Gossler, A. and Weinmaster, G., 1996. Expression patterns of Jagged, Delta1, Notch1, Notch2, and Notch3 genes identify ligand-receptor pairs that may function in neural development. Mol Cell Neurosci. 8, 14-27.

Ling, C., Zheng, Y., Yin, F., Yu, J., Huang, J., Hong, Y., Wu, S. and Pan, D., 2010. The apical transmembrane protein Crumbs functions as a tumor suppressor that regulates Hippo signaling by binding to Expanded. Proc Natl Acad Sci U S A. 107, 10532-7.

Link, V., Shevchenko, A. and Heisenberg, C.P., 2006. Proteomics of early zebrafish embryos. BMC Dev Biol. 6, 1.

Linville, A., Gumusaneli, E., Chandraratna, R.A.S. and Schilling, T.F., 2004. Independent roles for retinoic acid in segmentation and neuronal differentiation in the zebrafish hindbrain. Developmental Biology. 270, 186-199.

Liu, C., Li, Y., Semenov, M., Han, C., Baeg, G.H., Tan, Y., Zhang, Z., Lin, X. and He, X., 2002. Control of beta-catenin phosphorylation/degradation by a dual-kinase mechanism. Cell. 108, 837-47.

Liu, C.Y., Zha, Z.Y., Zhou, X., Zhang, H., Huang, W., Zhao, D., Li, T., Chan, S.W., Lim, C.J., Hong, W., Zhao, S., Xiong, Y., Lei, Q.Y. and Guan, K.L., 2010. The hippo tumor pathway promotes TAZ degradation by phosphorylating a phosphodegron and recruiting the SCF{beta}-TrCP E3 ligase. J Biol Chem. 285, 37159-69.

Liu, J., Li, C., Yu, Z., Huang, P., Wu, H., Wei, C., Zhu, N., Shen, Y., Chen, Y., Zhang, B., Deng, W.M. and Jiao, R., 2012. Efficient and specific modifications of the Drosophila genome by means of an easy TALEN strategy. J Genet Genomics. 39, 209-15.

Liu, J.P., 2006. The function of growth/differentiation factor 11 (Gdf11) in rostrocaudal patterning of the developing spinal cord. Development. 133, 2865-74.
Liu, Q., Segal, D.J., Ghiara, J.B. and Barbas, C.F., 3rd, 1997. Design of polydactyl zinc-finger proteins for unique addressing within complex genomes. Proc Natl Acad Sci U S A. 94, 5525-30.
Liu, X., Xiong, C., Jia, S., Zhang, Y., Chen, Y.G., Wang, Q. and Meng, A., 2013a. Araf kinase antagonizes Nodal-Smad2 activity in mesendoderm development by directly phosphorylating the Smad2 linker region. Nat Commun. 4, 1728.
Liu, X., Yang, N., Figel, S.A., Wilson, K.E., Morrison, C.D., Gelman, I.H. and Zhang, J., 2013b. PTPN14 interacts with and negatively regulates the oncogenic function of YAP. Oncogene. 32, 1266-73.
Liu, Y., Pathak, N., Kramer-Zucker, A. and Drummond, I.A., 2007. Notch signaling controls the differentiation of transporting epithelia and multiciliated cells in the zebrafish pronephros. Development. 134, 1111-22.
Livak, K.J. and Schmittgen, T.D., 2001. Analysis of relative gene expression data using real-time quantitative PCR and the 2(-Delta Delta C(T)) Method. Methods. 25, 402-8.
Lloyd, A., Plaisier, C.L., Carroll, D. and Drews, G.N., 2005. Targeted mutagenesis using zinc-finger nucleases in Arabidopsis. Proc Natl Acad Sci U S A. 102, 2232-7.
Logeat, F., Bessia, C., Brou, C., LeBail, O., Jarriault, S., Seidah, N.G. and Israel, A., 1998. The Notch1 receptor is cleaved constitutively by a furin-like convertase. Proc Natl Acad Sci U S A. 95, 8108-12.
Lohnes, D., Kastner, P., Dierich, A., Mark, M., LeMeur, M. and Chambon, P., 1993. Function of retinoic acid receptor gamma in the mouse. Cell. 73, 643-58.
Lombardo, A., Genovese, P., Beausejour, C.M., Colleoni, S., Lee, Y.L., Kim, K.A., Ando, D., Urnov, F.D., Galli, C., Gregory, P.D., Holmes, M.C. and Naldini, L., 2007. Gene editing in human stem cells using zinc finger nucleases and integrase-defective lentiviral vector delivery. Nat Biotechnol. 25, 1298-306.
Lombardo, A., Isaacs, H.V. and Slack, J.M., 1998. Expression and functions of FGF-3 in Xenopus development. Int J Dev Biol. 42, 1101-7.
Longobardi, E. and Blasi, F., 2003. Overexpression of PREP-1 in F9 teratocarcinoma cells leads to a functionally relevant increase of PBX-2 by preventing its degradation. J Biol Chem. 278, 39235-41.
Lowery, L.A., De Rienzo, G., Gutzman, J.H. and Sive, H., 2009. Characterization and classification of zebrafish brain morphology mutants. Anat Rec (Hoboken). 292, 94-106.
Lowery, L.A., Rubin, J. and Sive, H., 2007. Whitesnake/sfpq is required for cell survival and neuronal development in the zebrafish. Dev Dyn. 236, 1347-57.
Lowery, L.A. and Sive, H., 2005. Initial formation of zebrafish brain ventricles occurs independently of circulation and requires the nagie oko and snakehead/atp1a1a.1 gene products. Development. 132, 2057-67.
Lowery, L.A. and Sive, H., 2009. Totally tubular: the mystery behind function and origin of the brain ventricular system. Bioessays. 31, 446-58.
Lufkin, T., Dierich, A., LeMeur, M., Mark, M. and Chambon, P., 1991. Disruption of the Hox-1.6 homeobox gene results in defects in a region corresponding to its rostral domain of expression. Cell. 66, 1105-19.

Lukowski, C.M., Ritzel, R.G. and Waskiewicz, A.J., 2006. Expression of two insm1-like genes in the developing zebrafish nervous system. Gene Expr Patterns. 6, 711-8.
Lumsden, A., 1999. Closing in on rhombomere boundaries. Nat Cell Biol. 1, E83-5.
Lumsden, A. and Keynes, R., 1989. Segmental patterns of neuronal development in the chick hindbrain. Nature. 337, 424-8.
Lumsden, A. and Krumlauf, R., 1996. Patterning the vertebrate neuraxis. Science. 274, 1109-15.
Lumsden, A., Sprawson, N. and Graham, A., 1991. Segmental origin and migration of neural crest cells in the hindbrain region of the chick embryo. Development. 113, 1281-91.
Ma, H., Naseri, A., Reyes-Gutierrez, P., Wolfe, S.A., Zhang, S. and Pederson, T., 2015. Multicolor CRISPR labeling of chromosomal loci in human cells. Proc Natl Acad Sci U S A. 112, 3002-7.
Ma, S., Zhang, S., Wang, F., Liu, Y., Xu, H., Liu, C., Lin, Y., Zhao, P. and Xia, Q., 2012. Highly efficient and specific genome editing in silkworm using custom TALENs. PLoS One. 7, e45035.
Maclean, G., Dolle, P. and Petkovich, M., 2009. Genetic disruption of CYP26B1 severely affects development of neural crest derived head structures, but does not compromise hindbrain patterning. Dev Dyn. 238, 732-45.
Maconochie, M., Nonchev, S., Morrison, A. and Krumlauf, R., 1996. Paralogous Hox genes: function and regulation. Annu Rev Genet. 30, 529-56.
Maconochie, M.K., Nonchev, S., Studer, M., Chan, S.K., Popperl, H., Sham, M.H., Mann, R.S. and Krumlauf, R., 1997. Cross-regulation in the mouse HoxB complex: the expression of Hoxb2 in rhombomere 4 is regulated by Hoxb1. Genes Dev. 11, 1885-95.
Maden, M., 2002. Retinoid signalling in the development of the central nervous system. Nat Rev Neurosci. 3, 843-53.
Maden, M., Gale, E., Kostetskii, I. and Zile, M., 1996. Vitamin A-deficient quail embryos have half a hindbrain and other neural defects. Curr Biol. 6, 417-26.
Maden, M. and Holder, N., 1991. The involvement of retinoic acid in the development of the vertebrate central nervous system. Dev Suppl. Suppl 2, 87-94.
Maden, M. and Holder, N., 1992. Retinoic acid and development of the central nervous system. Bioessays. 14, 431-8.
Maeder, M.L., Thibodeau-Beganny, S., Osiak, A., Wright, D.A., Anthony, R.M., Eichtinger, M., Jiang, T., Foley, J.E., Winfrey, R.J., Townsend, J.A., Unger-Wallace, E., Sander, J.D., Muller-Lerch, F., Fu, F., Pearlberg, J., Gobel, C., Dassie, J.P., Pruett-Miller, S.M., Porteus, M.H., Sgroi, D.C., Iafrate, A.J., Dobbs, D., McCray, P.B., Jr., Cathomen, T., Voytas, D.F. and Joung, J.K., 2008. Rapid "open-source" engineering of customized zinc-finger nucleases for highly efficient gene modification. Mol Cell. 31, 294-301.
Maftouh, M., Belo, A.I., Avan, A., Funel, N., Peters, G.J., Giovannetti, E. and Van Die, I., 2014. Galectin-4 expression is associated with reduced lymph node metastasis and modulation of Wnt/beta-catenin signalling in pancreatic adenocarcinoma. Oncotarget. 5, 5335-49.
Mahfouz, M.M., Li, L., Shamimuzzaman, M., Wibowo, A., Fang, X. and Zhu, J.K., 2011. De novo-engineered transcription activator-like effector (TALE) hybrid

nuclease with novel DNA binding specificity creates double-strand breaks. Proc Natl Acad Sci U S A. 108, 2623-8.
Mahmood, R., Kiefer, P., Guthrie, S., Dickson, C. and Mason, I., 1995. Multiple roles for FGF-3 during cranial neural development in the chicken. Development. 121, 1399-410.
Mahmood, R., Mason, I.J. and Morriss-Kay, G.M., 1996. Expression of Fgf-3 in relation to hindbrain segmentation, otic pit position and pharyngeal arch morphology in normal and retinoic acid-exposed mouse embryos. Anat Embryol (Berl). 194, 13-22.
Major, R.J. and Irvine, K.D., 2005. Influence of Notch on dorsoventral compartmentalization and actin organization in the Drosophila wing. Development. 132, 3823-33.
Major, R.J. and Irvine, K.D., 2006. Localization and requirement for Myosin II at the dorsal-ventral compartment boundary of the Drosophila wing. Dev Dyn. 235, 3051-8.
Mak, A.N., Bradley, P., Bogdanove, A.J. and Stoddard, B.L., 2012. TAL effectors: function, structure, engineering and applications. Curr Opin Struct Biol. 23, 93-9.
Malicki, J., Neuhauss, S.C., Schier, A.F., Solnica-Krezel, L., Stemple, D.L., Stainier, D.Y., Abdelilah, S., Zwartkruis, F., Rangini, Z. and Driever, W., 1996. Mutations affecting development of the zebrafish retina. Development. 123, 263-73.
Mandell, J.G. and Barbas, C.F., 3rd, 2006. Zinc Finger Tools: custom DNA-binding domains for transcription factors and nucleases. Nucleic Acids Res. 34, W516-23.
Manderfield, L.J., Aghajanian, H., Engleka, K.A., Lim, L.Y., Liu, F., Jain, R., Li, L., Olson, E.N. and Epstein, J.A., 2015. Hippo signaling is required for Notch-dependent smooth muscle differentiation of neural crest. Development. 142, 2962-71.
Mani, M., Kandavelou, K., Dy, F.J., Durai, S. and Chandrasegaran, S., 2005. Design, engineering, and characterization of zinc finger nucleases. Biochem Biophys Res Commun. 335, 447-57.
Manley, N.R. and Capecchi, M.R., 1997. Hox group 3 paralogous genes act synergistically in the formation of somitic and neural crest-derived structures. Dev Biol. 192, 274-88.
Mann, R.S., 1995. The specificity of homeotic gene function. Bioessays. 17, 855-63.
Mann, R.S. and Affolter, M., 1998. Hox proteins meet more partners. Curr Opin Genet Dev. 8, 423-9.
Mann, R.S. and Chan, S.K., 1996. Extra specificity from extradenticle: the partnership between HOX and PBX/EXD homeodomain proteins. Trends Genet. 12, 258-62.
Manzanares, M., Bel-Vialar, S., Ariza-McNaughton, L., Ferretti, E., Marshall, H., Maconochie, M.M., Blasi, F. and Krumlauf, R., 2001. Independent regulation of initiation and maintenance phases of Hoxa3 expression in the vertebrate hindbrain involve auto- and cross-regulatory mechanisms. Development. 128, 3595-607.
Manzanares, M., Cordes, S., Ariza-McNaughton, L., Sadl, V., Maruthainar, K., Barsh, G. and Krumlauf, R., 1999a. Conserved and distinct roles of kreisler in

regulation of the paralogous Hoxa3 and Hoxb3 genes. Development. 126, 759-69.
Manzanares, M., Cordes, S., Kwan, C.T., Sham, M.H., Barsh, G.S. and Krumlauf, R., 1997. Segmental regulation of Hoxb-3 by kreisler. Nature. 387, 191-5.
Manzanares, M., Nardelli, J., Gilardi-Hebenstreit, P., Marshall, H., Giudicelli, F., Martinez-Pastor, M.T., Krumlauf, R. and Charnay, P., 2002. Krox20 and kreisler co-operate in the transcriptional control of segmental expression of Hoxb3 in the developing hindbrain. EMBO J. 21, 365-76.
Manzanares, M., Trainor, P.A., Ariza-McNaughton, L., Nonchev, S. and Krumlauf, R., 2000. Dorsal patterning defects in the hindbrain, roof plate and skeleton in the dreher (dr(J)) mouse mutant. Mech Dev. 94, 147-56.
Manzanares, M., Trainor, P.A., Nonchev, S., Ariza-McNaughton, L., Brodie, J., Gould, A., Marshall, H., Morrison, A., Kwan, C.T., Sham, M.H., Wilkinson, D.G. and Krumlauf, R., 1999b. The role of kreisler in segmentation during hindbrain development. Dev Biol. 211, 220-37.
Marin, F. and Charnay, P., 2000. Hindbrain patterning: FGFs regulate Krox20 and mafB/kr expression in the otic/preotic region. Development. 127, 4925-35.
Mark, M., Lufkin, T., Vonesch, J.L., Ruberte, E., Olivo, J.C., Dolle, P., Gorry, P., Lumsden, A. and Chambon, P., 1993. Two rhombomeres are altered in Hoxa-1 mutant mice. Development. 119, 319-38.
Maroon, H., Walshe, J., Mahmood, R., Kiefer, P., Dickson, C. and Mason, I., 2002. Fgf3 and Fgf8 are required together for formation of the otic placode and vesicle. Development. 129, 2099-108.
Marshall, H., Morrison, A., Studer, M., Popperl, H. and Krumlauf, R., 1996. Retinoids and Hox genes. FASEB J. 10, 969-78.
Marshall, H., Nonchev, S., Sham, M.H., Muchamore, I., Lumsden, A. and Krumlauf, R., 1992. Retinoic acid alters hindbrain Hox code and induces transformation of rhombomeres 2/3 into a 4/5 identity. Nature. 360, 737-41.
Marshall, H., Studer, M., Popperl, H., Aparicio, S., Kuroiwa, A., Brenner, S. and Krumlauf, R., 1994. A conserved retinoic acid response element required for early expression of the homeobox gene Hoxb-1. Nature. 370, 567-71.
Mashayekhi, F., Draper, C.E., Bannister, C.M., Pourghasem, M., Owen-Lynch, P.J. and Miyan, J.A., 2002. Deficient cortical development in the hydrocephalic Texas (H-Tx) rat: a role for CSF. Brain. 125, 1859-74.
Mashimo, T., Kaneko, T., Sakuma, T., Kobayashi, J., Kunihiro, Y., Voigt, B., Yamamoto, T. and Serikawa, T., 2013. Efficient gene targeting by TAL effector nucleases coinjected with exonucleases in zygotes. Sci Rep. 3, 1253.
Mateus, R., Lourenco, R., Fang, Y., Brito, G., Farinho, A., Valerio, F. and Jacinto, A., 2015. Control of tissue growth by Yap relies on cell density and F-actin in zebrafish fin regeneration. Development. 142, 2752-63.
Matsuda, M., Rand, K., Palardy, G., Shimizu, N., Ikeda, H., Dalle Nogare, D., Itoh, M. and Chitnis, A.B., 2016. Epb41l5 competes with Delta as a substrate for Mib1 to coordinate specification and differentiation of neurons. Development. 143, 3085-96.
Maves, L., Jackman, W. and Kimmel, C., 2002. FGF3 and FGF8 mediate a rhombomere 4 signaling activity in the zebrafish hindbrain. Development (Cambridge, England). 129, 3825-3837.

Maves, L. and Kimmel, C.B., 2005. Dynamic and sequential patterning of the zebrafish posterior hindbrain by retinoic acid. Dev Biol. 285, 593-605.
Maves, L., Waskiewicz, A.J., Paul, B., Cao, Y., Tyler, A., Moens, C.B. and Tapscott, S.J., 2007. Pbx homeodomain proteins direct Myod activity to promote fast-muscle differentiation. Development. 134, 3371-82.
Mawdsley, D.J., Cooper, H.M., Hogan, B.M., Cody, S.H., Lieschke, G.J. and Heath, J.K., 2004. The Netrin receptor Neogenin is required for neural tube formation and somitogenesis in zebrafish. Dev Biol. 269, 302-15.
McCartney, B.M., Kulikauskas, R.M., LaJeunesse, D.R. and Fehon, R.G., 2000. The neurofibromatosis-2 homologue, Merlin, and the tumor suppressor expanded function together in Drosophila to regulate cell proliferation and differentiation. Development. 127, 1315-24.
McClintock, J., Carlson, R., Mann, D. and Prince, V., 2001. Consequences of Hox gene duplication in the vertebrates: an investigation of the zebrafish Hox paralogue group 1 genes. Development (Cambridge, England). 128, 2471-2484.
McClintock, J., Kheirbek, M. and Prince, V., 2002. Knockdown of duplicated zebrafish hoxb1 genes reveals distinct roles in hindbrain patterning and a novel mechanism of duplicate gene retention. Development (Cambridge, England). 129, 2339-2354.
McGinnis, W., Garber, R.L., Wirz, J., Kuroiwa, A. and Gehring, W.J., 1984. A homologous protein-coding sequence in Drosophila homeotic genes and its conservation in other metazoans. Cell. 37, 403-8.
McGinnis, W. and Krumlauf, R., 1992. Homeobox genes and axial patterning. Cell. 68, 283-302.
McGrew, L.L., Hoppler, S. and Moon, R.T., 1997. Wnt and FGF pathways cooperatively pattern anteroposterior neural ectoderm in Xenopus. Mech Dev. 69, 105-14.
McKay, I.J., Lewis, J. and Lumsden, A., 1996. The role of FGF-3 in early inner ear development: an analysis in normal and kreisler mutant mice. Dev Biol. 174, 370-8.
McKay, I.J., Muchamore, I., Krumlauf, R., Maden, M., Lumsden, A. and Lewis, J., 1994. The kreisler mouse: a hindbrain segmentation mutant that lacks two rhombomeres. Development. 120, 2199-211.
McNulty, C.L., Peres, J.N., Bardine, N., van den Akker, W.M. and Durston, A.J., 2005. Knockdown of the complete Hox paralogous group 1 leads to dramatic hindbrain and neural crest defects. Development. 132, 2861-71.
McPherron, A.C., Lawler, A.M. and Lee, S.J., 1999. Regulation of anterior/posterior patterning of the axial skeleton by growth/differentiation factor 11. Nat Genet. 22, 260-4.
Meeker, N.D., Hutchinson, S.A., Ho, L. and Trede, N.S., 2007. Method for isolation of PCR-ready genomic DNA from zebrafish tissues. Biotechniques. 43, 610, 612, 614.
Mellitzer, G., Xu, Q. and Wilkinson, D.G., 1999. Eph receptors and ephrins restrict cell intermingling and communication. Nature. 400, 77-81.
Mendelson, B., 1986. Development of reticulospinal neurons of the zebrafish. I. Time of origin. J Comp Neurol. 251, 160-71.

Menendez, J., Perez-Garijo, A., Calleja, M. and Morata, G., 2010. A tumor-suppressing mechanism in Drosophila involving cell competition and the Hippo pathway. Proc Natl Acad Sci U S A. 107, 14651-6.

Meng, X., Noyes, M.B., Zhu, L.J., Lawson, N.D. and Wolfe, S.A., 2008. Targeted gene inactivation in zebrafish using engineered zinc-finger nucleases. Nat Biotechnol. 26, 695-701.

Menoret, S., Fontaniere, S., Jantz, D., Tesson, L., Thinard, R., Remy, S., Usal, C., Ouisse, L.H., Fraichard, A. and Anegon, I., 2013. Generation of Rag1-knockout immunodeficient rats and mice using engineered meganucleases. FASEB J. 27, 703-11.

Merabet, S., Kambris, Z., Capovilla, M., Berenger, H., Pradel, J. and Graba, Y., 2003. The hexapeptide and linker regions of the AbdA Hox protein regulate its activating and repressive functions. Dev Cell. 4, 761-8.

Mercader, N., Leonardo, E., Azpiazu, N., Serrano, A., Morata, G., Martinez, C. and Torres, M., 1999. Conserved regulation of proximodistal limb axis development by Meis1/Hth. Nature. 402, 425-9.

Metcalfe, W.K., Mendelson, B. and Kimmel, C.B., 1986. Segmental homologies among reticulospinal neurons in the hindbrain of the zebrafish larva. J Comp Neurol. 251, 147-59.

Meyers, E.N., Lewandoski, M. and Martin, G.R., 1998. An Fgf8 mutant allelic series generated by Cre- and Flp-mediated recombination. Nat Genet. 18, 136-41.

Micchelli, C.A. and Blair, S.S., 1999. Dorsoventral lineage restriction in wing imaginal discs requires Notch. Nature. 401, 473-6.

Micchelli, C.A., Rulifson, E.J. and Blair, S.S., 1997. The function and regulation of cut expression on the wing margin of Drosophila: Notch, Wingless and a dominant negative role for Delta and Serrate. Development. 124, 1485-95.

Miesfeld, J.B., Gestri, G., Clark, B.S., Flinn, M.A., Poole, R.J., Bader, J.R., Besharse, J.C., Wilson, S.W. and Link, B.A., 2015. Yap and Taz regulate retinal pigment epithelial cell fate. Development. 142, 3021-32.

Miesfeld, J.B. and Link, B.A., 2014. Establishment of transgenic lines to monitor and manipulate Yap/Taz-Tead activity in zebrafish reveals both evolutionarily conserved and divergent functions of the Hippo pathway. Mech Dev. 133, 177-88.

Milewski, R.C., Chi, N.C., Li, J., Brown, C., Lu, M.M. and Epstein, J.A., 2004. Identification of minimal enhancer elements sufficient for Pax3 expression in neural crest and implication of Tead2 as a regulator of Pax3. Development. 131, 829-37.

Milhorat, T.H., Hammock, M.K., Fenstermacher, J.D. and Levin, V.A., 1971. Cerebrospinal fluid production by the choroid plexus and brain. Science. 173, 330-2.

Miller, E., Yang, J., DeRan, M., Wu, C., Su, A.I., Bonamy, G.M., Liu, J., Peters, E.C. and Wu, X., 2012. Identification of serum-derived sphingosine-1-phosphate as a small molecule regulator of YAP. Chem Biol. 19, 955-62.

Miller, J.C., Holmes, M.C., Wang, J., Guschin, D.Y., Lee, Y.L., Rupniewski, I., Beausejour, C.M., Waite, A.J., Wang, N.S., Kim, K.A., Gregory, P.D., Pabo, C.O. and Rebar, E.J., 2007. An improved zinc-finger nuclease architecture for highly specific genome editing. Nat Biotechnol. 25, 778-85.

Millonig, J.H., Millen, K.J. and Hatten, M.E., 2000. The mouse Dreher gene Lmx1a controls formation of the roof plate in the vertebrate CNS. Nature. 403, 764-9.
Miyan, J.A., Nabiyouni, M. and Zendah, M., 2003. Development of the brain: a vital role for cerebrospinal fluid. Can J Physiol Pharmacol. 81, 317-28.
Mo, J.S., Meng, Z., Kim, Y.C., Park, H.W., Hansen, C.G., Kim, S., Lim, D.S. and Guan, K.L., 2015. Cellular energy stress induces AMPK-mediated regulation of YAP and the Hippo pathway. Nat Cell Biol. 17, 500-10.
Mo, J.S., Yu, F.X., Gong, R., Brown, J.H. and Guan, K.L., 2012. Regulation of the Hippo-YAP pathway by protease-activated receptors (PARs). Genes Dev. 26, 2138-43.
Moehle, E.A., Rock, J.M., Lee, Y.L., Jouvenot, Y., DeKelver, R.C., Gregory, P.D., Urnov, F.D. and Holmes, M.C., 2007. Targeted gene addition into a specified location in the human genome using designed zinc finger nucleases. Proc Natl Acad Sci U S A. 104, 3055-60.
Moens, C. and Prince, V., 2002. Constructing the hindbrain: insights from the zebrafish. Dev Dyn. 224, 1-17.
Moens, C.B., Cordes, S.P., Giorgianni, M.W., Barsh, G.S. and Kimmel, C.B., 1998. Equivalence in the genetic control of hindbrain segmentation in fish and mouse. Development. 125, 381-91.
Moens, C.B., Yan, Y.L., Appel, B., Force, A.G. and Kimmel, C.B., 1996. valentino: a zebrafish gene required for normal hindbrain segmentation. Development. 122, 3981-90.
Mohseni, M., Sun, J., Lau, A., Curtis, S., Goldsmith, J., Fox, V.L., Wei, C., Frazier, M., Samson, O., Wong, K.K., Kim, C. and Camargo, F.D., 2014. A genetic screen identifies an LKB1-MARK signalling axis controlling the Hippo-YAP pathway. Nat Cell Biol. 16, 108-17.
Moleirinho, S., Chang, N., Sims, A.H., Tilston-Lunel, A.M., Angus, L., Steele, A., Boswell, V., Barnett, S.C., Ormandy, C., Faratian, D., Gunn-Moore, F.J. and Reynolds, P.A., 2013. KIBRA exhibits MST-independent functional regulation of the Hippo signaling pathway in mammals. Oncogene. 32, 1821-30.
Molenaar, M., van de Wetering, M., Oosterwegel, M., Peterson-Maduro, J., Godsave, S., Korinek, V., Roose, J., Destree, O. and Clevers, H., 1996. XTcf-3 transcription factor mediates beta-catenin-induced axis formation in Xenopus embryos. Cell. 86, 391-9.
Moore, C.A., 2006. Classification of Neural Tube Defects, in: Wyszynski, D.F. (Ed.), Neural tube defects: from origin to treatment. Oxford University Press, Oxford, pp. 66-75.
Moore, F.E., Reyon, D., Sander, J.D., Martinez, S.A., Blackburn, J.S., Khayter, C., Ramirez, C.L., Joung, J.K. and Langenau, D.M., 2012. Improved somatic mutagenesis in zebrafish using transcription activator-like effector nucleases (TALENs). PLoS One. 7, e37877.
Moreno, C., Hoffman, M., Stodola, T.J., Didier, D.N., Lazar, J., Geurts, A.M., North, P.E., Jacob, H.J. and Greene, A.S., 2011. Creation and characterization of a renin knockout rat. Hypertension. 57, 614-9.
Morgan, T.H. and Bridges, C.B., 1916. Sex-linked inheritance in Drosophila, Carnegie Institution of Washington, Washington,.

Morrison, A., Ariza-McNaughton, L., Gould, A., Featherstone, M. and Krumlauf, R., 1997. HOXD4 and regulation of the group 4 paralog genes. Development. 124, 3135-46.

Morriss, G.M., 1972. Morphogenesis of the malformations induced in rat embryos by maternal hypervitaminosis A. J Anat. 113, 241-50.

Morriss-Kay, G., 1993. Retinoic acid and craniofacial development: molecules and morphogenesis. Bioessays. 15, 9-15.

Morriss-Kay, G.M. and Crutch, B., 1982. Culture of rat embryos with beta-D-xyloside: evidence of a role for proteoglycans in neurulation. J Anat. 134, 491-506.

Morton, J., Davis, M.W., Jorgensen, E.M. and Carroll, D., 2006. Induction and repair of zinc-finger nuclease-targeted double-strand breaks in Caenorhabditis elegans somatic cells. Proc Natl Acad Sci U S A. 103, 16370-5.

Mosimann, C., Hausmann, G. and Basler, K., 2006. Parafibromin/Hyrax activates Wnt/Wg target gene transcription by direct association with beta-catenin/Armadillo. Cell. 125, 327-41.

Mukhopadhyay, M., Shtrom, S., Rodriguez-Esteban, C., Chen, L., Tsukui, T., Gomer, L., Dorward, D.W., Glinka, A., Grinberg, A., Huang, S.P., Niehrs, C., Izpisua Belmonte, J.C. and Westphal, H., 2001. Dickkopf1 is required for embryonic head induction and limb morphogenesis in the mouse. Dev Cell. 1, 423-34.

Mumm, J.S., Schroeter, E.H., Saxena, M.T., Griesemer, A., Tian, X., Pan, D.J., Ray, W.J. and Kopan, R., 2000. A ligand-induced extracellular cleavage regulates gamma-secretase-like proteolytic activation of Notch1. Mol Cell. 5, 197-206.

Munke, M., Cox, D.R., Jackson, I.J., Hogan, B.L. and Francke, U., 1986. The murine Hox-2 cluster of homeo box containing genes maps distal on chromosome 11 near the tail-short (Ts) locus. Cytogenet Cell Genet. 42, 236-40.

Mussolino, C., Morbitzer, R., Lutge, F., Dannemann, N., Lahaye, T. and Cathomen, T., 2011. A novel TALE nuclease scaffold enables high genome editing activity in combination with low toxicity. Nucleic Acids Res. 39, 9283-93.

Nagasawa-Masuda, A. and Terai, K., 2017. Yap/Taz transcriptional activity is essential for vascular regression via Ctgf expression and actin polymerization. PLoS One. 12, e0174633.

Nakajima, H., Yamamoto, K., Agarwala, S., Terai, K., Fukui, H., Fukuhara, S., Ando, K., Miyazaki, T., Yokota, Y., Schmelzer, E., Belting, H.G., Affolter, M., Lecaudey, V. and Mochizuki, N., 2017. Flow-Dependent Endothelial YAP Regulation Contributes to Vessel Maintenance. Dev Cell. 40, 523-536 e6.

Nakashima, M., Toyono, T., Akamine, A. and Joyner, A., 1999. Expression of growth/differentiation factor 11, a new member of the BMP/TGFbeta superfamily during mouse embryogenesis. Mech Dev. 80, 185-9.

Nasevicius, A. and Ekker, S.C., 2000. Effective targeted gene 'knockdown' in zebrafish. Nat Genet. 26, 216-20.

Neuteboom, S.T., Peltenburg, L.T., van Dijk, M.A. and Murre, C., 1995. The hexapeptide LFPWMR in Hoxb-8 is required for cooperative DNA binding with Pbx1 and Pbx2 proteins. Proc Natl Acad Sci U S A. 92, 9166-70.

Niederreither, K., Abu-Abed, S., Schuhbaur, B., Petkovich, M., Chambon, P. and Dolle, P., 2002. Genetic evidence that oxidative derivatives of retinoic acid are not involved in retinoid signaling during mouse development. Nat Genet. 31, 84-8.

Niederreither, K. and Dolle, P., 2008. Retinoic acid in development: towards an integrated view. Nat Rev Genet. 9, 541-53.
Niederreither, K., Subbarayan, V., Dolle, P. and Chambon, P., 1999. Embryonic retinoic acid synthesis is essential for early mouse post-implantation development. Nat Genet. 21, 444-8.
Niederreither, K., Vermot, J., Schuhbaur, B., Chambon, P. and Dolle, P., 2000. Retinoic acid synthesis and hindbrain patterning in the mouse embryo. Development. 127, 75-85.
Niehrs, C., 2012. The complex world of WNT receptor signalling. Nat Rev Mol Cell Biol. 13, 767-79.
Nikolaou, N., Watanabe-Asaka, T., Gerety, S., Distel, M., Koster, R.W. and Wilkinson, D.G., 2009. Lunatic fringe promotes the lateral inhibition of neurogenesis. Development. 136, 2523-33.
Nishiya, N., Oku, Y., Kumagai, Y., Sato, Y., Yamaguchi, E., Sasaki, A., Shoji, M., Ohnishi, Y., Okamoto, H. and Uehara, Y., 2014. A zebrafish chemical suppressor screening identifies small molecule inhibitors of the Wnt/beta-catenin pathway. Chem Biol. 21, 530-540.
Nittenberg, R., Patel, K., Joshi, Y., Krumlauf, R., Wilkinson, D.G., Brickell, P.M., Tickle, C. and Clarke, J.D., 1997. Cell movements, neuronal organisation and gene expression in hindbrains lacking morphological boundaries. Development. 124, 2297-306.
Niu, X., He, W., Song, B., Ou, Z., Fan, D., Chen, Y., Fan, Y. and Sun, X., 2016. Combining Single Strand Oligodeoxynucleotides and CRISPR/Cas9 to Correct Gene Mutations in beta-Thalassemia-induced Pluripotent Stem Cells. J Biol Chem. 291, 16576-85.
Nonchev, S., Maconochie, M., Vesque, C., Aparicio, S., Ariza-McNaughton, L., Manzanares, M., Maruthainar, K., Kuroiwa, A., Brenner, S., Charnay, P. and Krumlauf, R., 1996a. The conserved role of Krox-20 in directing Hox gene expression during vertebrate hindbrain segmentation. Proc Natl Acad Sci U S A. 93, 9339-45.
Nonchev, S., Vesque, C., Maconochie, M., Seitanidou, T., Ariza-McNaughton, L., Frain, M., Marshall, H., Sham, M.H., Krumlauf, R. and Charnay, P., 1996b. Segmental expression of Hoxa-2 in the hindbrain is directly regulated by Krox-20. Development. 122, 543-54.
Nopoulos, P., Richman, L., Andreasen, N.C., Murray, J.C. and Schutte, B., 2007. Abnormal brain structure in adults with Van der Woude syndrome. Clin Genet. 71, 511-7.
Nusse, R. and Varmus, H.E., 1982. Many tumors induced by the mouse mammary tumor virus contain a provirus integrated in the same region of the host genome. Cell. 31, 99-109.
Nyholm, M.K., Wu, S.F., Dorsky, R.I. and Grinblat, Y., 2007. The zebrafish zic2a-zic5 gene pair acts downstream of canonical Wnt signaling to control cell proliferation in the developing tectum. Development. 134, 735-46.
O'Hara, F.P., Beck, E., Barr, L.K., Wong, L.L., Kessler, D.S. and Riddle, R.D., 2005. Zebrafish Lmx1b.1 and Lmx1b.2 are required for maintenance of the isthmic organizer. Development. 132, 3163-73.

Ochiai, H., Fujita, K., Suzuki, K., Nishikawa, M., Shibata, T., Sakamoto, N. and Yamamoto, T., 2010. Targeted mutagenesis in the sea urchin embryo using zinc-finger nucleases. Genes Cells. 15, 875-85.

Oh, H. and Irvine, K.D., 2008. In vivo regulation of Yorkie phosphorylation and localization. Development. 135, 1081-8.

Ojeda, J.L. and Piedra, S., 2000. Evidence of a new transitory extracellular structure within the developing rhombencephalic cavity. An ultrastructural and immunoelectron-microscopic study in the chick. Anat Embryol (Berl). 202, 257-64.

Oka, T., Remue, E., Meerschaert, K., Vanloo, B., Boucherie, C., Gfeller, D., Bader, G.D., Sidhu, S.S., Vandekerckhove, J., Gettemans, J. and Sudol, M., 2010. Functional complexes between YAP2 and ZO-2 are PDZ domain-dependent, and regulate YAP2 nuclear localization and signalling. Biochem J. 432, 461-72.

Omerovic, J., Puggioni, E.M., Napoletano, S., Visco, V., Fraioli, R., Frati, L., Gulino, A. and Alimandi, M., 2004. Ligand-regulated association of ErbB-4 to the transcriptional co-activator YAP65 controls transcription at the nuclear level. Exp Cell Res. 294, 469-79.

Omori, Y. and Malicki, J., 2006. oko meduzy and related crumbs genes are determinants of apical cell features in the vertebrate embryo. Curr Biol. 16, 945-57.

Ong, S.H., Guy, G.R., Hadari, Y.R., Laks, S., Gotoh, N., Schlessinger, J. and Lax, I., 2000. FRS2 proteins recruit intracellular signaling pathways by binding to diverse targets on fibroblast growth factor and nerve growth factor receptors. Mol Cell Biol. 20, 979-89.

Ornitz, D.M. and Leder, P., 1992. Ligand specificity and heparin dependence of fibroblast growth factor receptors 1 and 3. J Biol Chem. 267, 16305-11.

Ornitz, D.M., Yayon, A., Flanagan, J.G., Svahn, C.M., Levi, E. and Leder, P., 1992. Heparin is required for cell-free binding of basic fibroblast growth factor to a soluble receptor and for mitogenesis in whole cells. Mol Cell Biol. 12, 240-7.

Osorno, R., Tsakiridis, A., Wong, F., Cambray, N., Economou, C., Wilkie, R., Blin, G., Scotting, P.J., Chambers, I. and Wilson, V., 2012. The developmental dismantling of pluripotency is reversed by ectopic Oct4 expression. Development. 139, 2288-98.

Packer, A.I., Crotty, D.A., Elwell, V.A. and Wolgemuth, D.J., 1998. Expression of the murine Hoxa4 gene requires both autoregulation and a conserved retinoic acid response element. Development. 125, 1991-8.

Pan, D. and Rubin, G.M., 1997. Kuzbanian controls proteolytic processing of Notch and mediates lateral inhibition during Drosophila and vertebrate neurogenesis. Cell. 90, 271-80.

Panin, V.M., Papayannopoulos, V., Wilson, R. and Irvine, K.D., 1997. Fringe modulates Notch-ligand interactions. Nature. 387, 908-12.

Pantalacci, S., Tapon, N. and Leopold, P., 2003. The Salvador partner Hippo promotes apoptosis and cell-cycle exit in Drosophila. Nat Cell Biol. 5, 921-7.

Papalopulu, N., Clarke, J.D., Bradley, L., Wilkinson, D., Krumlauf, R. and Holder, N., 1991. Retinoic acid causes abnormal development and segmental patterning of the anterior hindbrain in Xenopus embryos. Development. 113, 1145-58.

Papan, C. and Campos-Ortega, J.A., 1994. On the formation of the neural keel and neural tube in the zebrafishDanio (Brachydanio) rerio. Roux Arch Dev Biol. 203, 178-186.

Papayannopoulos, V., Tomlinson, A., Panin, V.M., Rauskolb, C. and Irvine, K.D., 1998. Dorsal-ventral signaling in the Drosophila eye. Science. 281, 2031-4.

Pappalardo, A., Porreca, I., Caputi, L., De Felice, E., Schulte-Merker, S., Zannini, M. and Sordino, P., 2015. Thyroid development in zebrafish lacking Taz. Mech Dev. 138 Pt 3, 268-78.

Paquet, D., Kwart, D., Chen, A., Sproul, A., Jacob, S., Teo, S., Olsen, K.M., Gregg, A., Noggle, S. and Tessier-Lavigne, M., 2016. Efficient introduction of specific homozygous and heterozygous mutations using CRISPR/Cas9. Nature. 533, 125-9.

Paramasivam, M., Sarkeshik, A., Yates, J.R., 3rd, Fernandes, M.J. and McCollum, D., 2011. Angiomotin family proteins are novel activators of the LATS2 kinase tumor suppressor. Mol Biol Cell. 22, 3725-33.

Park, H.C. and Appel, B., 2003. Delta-Notch signaling regulates oligodendrocyte specification. Development. 130, 3747-55.

Park, R., Moon, U.Y., Park, J.Y., Hughes, L.J., Johnson, R.L., Cho, S.H. and Kim, S., 2016. Yap is required for ependymal integrity and is suppressed in LPA-induced hydrocephalus. Nat Commun. 7, 10329.

Paro, R., 1990. Imprinting a determined state into the chromatin of Drosophila. Trends Genet. 6, 416-21.

Paro, R. and Hogness, D.S., 1991. The Polycomb protein shares a homologous domain with a heterochromatin-associated protein of Drosophila. Proc Natl Acad Sci U S A. 88, 263-7.

Paro, R. and Zink, B., 1993. The Polycomb gene is differentially regulated during oogenesis and embryogenesis of Drosophila melanogaster. Mech Dev. 40, 37-46.

Passner, J.M., Ryoo, H.D., Shen, L., Mann, R.S. and Aggarwal, A.K., 1999. Structure of a DNA-bound Ultrabithorax-Extradenticle homeodomain complex. Nature. 397, 714-9.

Pavletich, N.P. and Pabo, C.O., 1991. Zinc finger-DNA recognition: crystal structure of a Zif268-DNA complex at 2.1 A. Science. 252, 809-17.

Peifer, M. and Wieschaus, E., 1990. Mutations in the Drosophila gene extradenticle affect the way specific homeo domain proteins regulate segmental identity. Genes Dev. 4, 1209-23.

Pellock, B.J., Buff, E., White, K. and Hariharan, I.K., 2007. The Drosophila tumor suppressors Expanded and Merlin differentially regulate cell cycle exit, apoptosis, and Wingless signaling. Dev Biol. 304, 102-15.

Perez, E.E., Wang, J., Miller, J.C., Jouvenot, Y., Kim, K.A., Liu, O., Wang, N., Lee, G., Bartsevich, V.V., Lee, Y.L., Guschin, D.Y., Rupniewski, I., Waite, A.J., Carpenito, C., Carroll, R.G., Orange, J.S., Urnov, F.D., Rebar, E.J., Ando, D., Gregory, P.D., Riley, J.L., Holmes, M.C. and June, C.H., 2008. Establishment of HIV-1 resistance in CD4+ T cells by genome editing using zinc-finger nucleases. Nat Biotechnol. 26, 808-16.

Phelan, M.L., Rambaldi, I. and Featherstone, M.S., 1995. Cooperative interactions between HOX and PBX proteins mediated by a conserved peptide motif. Mol Cell Biol. 15, 3989-97.

Phelan, M.L., Sadoul, R. and Featherstone, M.S., 1994. Functional differences between HOX proteins conferred by two residues in the homeodomain N-terminal arm. Mol Cell Biol. 14, 5066-75.

Phillips, B.T., Bolding, K. and Riley, B.B., 2001. Zebrafish fgf3 and fgf8 encode redundant functions required for otic placode induction. Dev Biol. 235, 351-65.

Pickart, M.A., Klee, E.W., Nielsen, A.L., Sivasubbu, S., Mendenhall, E.M., Bill, B.R., Chen, E., Eckfeldt, C.E., Knowlton, M., Robu, M.E., Larson, J.D., Deng, Y., Schimmenti, L.A., Ellis, L.B., Verfaillie, C.M., Hammerschmidt, M., Farber, S.A. and Ekker, S.C., 2006. Genome-wide reverse genetics framework to identify novel functions of the vertebrate secretome. PLoS One. 1, e104.

Piper, D.E., Batchelor, A.H., Chang, C.P., Cleary, M.L. and Wolberger, C., 1999. Structure of a HoxB1-Pbx1 heterodimer bound to DNA: role of the hexapeptide and a fourth homeodomain helix in complex formation. Cell. 96, 587-97.

Piven, J., Arndt, S., Bailey, J., Havercamp, S., Andreasen, N.C. and Palmer, P., 1995. An MRI study of brain size in autism. Am J Psychiatry. 152, 1145-9.

Poernbacher, I., Baumgartner, R., Marada, S.K., Edwards, K. and Stocker, H., 2012. Drosophila Pez acts in Hippo signaling to restrict intestinal stem cell proliferation. Curr Biol. 22, 389-96.

Pollay, M. and Curl, F., 1967. Secretion of cerebrospinal fluid by the ventricular ependyma of the rabbit. Am J Physiol. 213, 1031-8.

Polstein, L.R. and Gersbach, C.A., 2015. A light-inducible CRISPR-Cas9 system for control of endogenous gene activation. Nat Chem Biol. 11, 198-200.

Poon, C.L., Lin, J.I., Zhang, X. and Harvey, K.F., 2011. The sterile 20-like kinase Tao-1 controls tissue growth by regulating the Salvador-Warts-Hippo pathway. Dev Cell. 21, 896-906.

Poon, C.L., Mitchell, K.A., Kondo, S., Cheng, L.Y. and Harvey, K.F., 2016. The Hippo Pathway Regulates Neuroblasts and Brain Size in Drosophila melanogaster. Curr Biol. 26, 1034-42.

Poon, C.L., Zhang, X., Lin, J.I., Manning, S.A. and Harvey, K.F., 2012. Homeodomain-interacting protein kinase regulates Hippo pathway-dependent tissue growth. Curr Biol. 22, 1587-94.

Popperl, H., Bienz, M., Studer, M., Chan, S.K., Aparicio, S., Brenner, S., Mann, R.S. and Krumlauf, R., 1995. Segmental expression of Hoxb-1 is controlled by a highly conserved autoregulatory loop dependent upon exd/pbx. Cell. 81, 1031-42.

Popperl, H. and Featherstone, M.S., 1993. Identification of a retinoic acid response element upstream of the murine Hox-4.2 gene. Mol Cell Biol. 13, 257-65.

Pöpperl, H., Rikhof, H., Chang, H., Haffter, P., Kimmel, C. and Moens, C., 2000. lazarus is a novel pbx gene that globally mediates hox gene function in zebrafish. Molecular cell. 6, 255-267.

Porazinski, S., Wang, H., Asaoka, Y., Behrndt, M., Miyamoto, T., Morita, H., Hata, S., Sasaki, T., Krens, S.F.G., Osada, Y., Asaka, S., Momoi, A., Linton, S., Miesfeld, J.B., Link, B.A., Senga, T., Shimizu, N., Nagase, H., Matsuura, S., Bagby, S., Kondoh, H., Nishina, H., Heisenberg, C.P. and Furutani-Seiki, M., 2015. YAP is essential for tissue tension to ensure vertebrate 3D body shape. Nature. 521, 217-221.

Porteus, M.H., 2006. Mammalian gene targeting with designed zinc finger nucleases. Mol Ther. 13, 438-46.
Porteus, M.H. and Baltimore, D., 2003. Chimeric nucleases stimulate gene targeting in human cells. Science. 300, 763.
Porteus, M.H. and Carroll, D., 2005. Gene targeting using zinc finger nucleases. Nat Biotechnol. 23, 967-73.
Pouilhe, M., Gilardi-Hebenstreit, P., Desmarquet-Trin Dinh, C. and Charnay, P., 2007. Direct regulation of vHnf1 by retinoic acid signaling and MAF-related factors in the neural tube. Dev Biol. 309, 344-57.
Pourghasem, M., Mashayekhi, F., Bannister, C.M. and Miyan, J., 2001. Changes in the CSF fluid pathways in the developing rat fetus with early onset hydrocephalus. Eur J Pediatr Surg. 11 Suppl 1, S10-3.
Pourquie, O., 2001. The vertebrate segmentation clock. J Anat. 199, 169-75.
Pownall, M.E., Isaacs, H.V. and Slack, J.M., 1998. Two phases of Hox gene regulation during early Xenopus development. Curr Biol. 8, 673-6.
Pownall, M.E., Tucker, A.S., Slack, J.M. and Isaacs, H.V., 1996. eFGF, Xcad3 and Hox genes form a molecular pathway that establishes the anteroposterior axis in Xenopus. Development. 122, 3881-92.
Praskova, M., Khoklatchev, A., Ortiz-Vega, S. and Avruch, J., 2004. Regulation of the MST1 kinase by autophosphorylation, by the growth inhibitory proteins, RASSF1 and NORE1, and by Ras. Biochem J. 381, 453-62.
Praskova, M., Xia, F. and Avruch, J., 2008. MOBKL1A/MOBKL1B phosphorylation by MST1 and MST2 inhibits cell proliferation. Curr Biol. 18, 311-21.
Prassopoulos, P., Cavouras, D. and Golfinopoulos, S., 1996. Developmental changes in the posterior cranial fossa of children studied by CT. Neuroradiology. 38, 80-3.
Prince, V.E., Holley, S.A., Bally-Cuif, L., Prabhakaran, B., Oates, A.C., Ho, R.K. and Vogt, T.F., 2001. Zebrafish lunatic fringe demarcates segmental boundaries. Mech Dev. 105, 175-80.
Prince, V.E., Moens, C.B., Kimmel, C.B. and Ho, R.K., 1998. Zebrafish hox genes: expression in the hindbrain region of wild-type and mutants of the segmentation gene, valentino. Development. 125, 393-406.
Pruett-Miller, S.M., Connelly, J.P., Maeder, M.L., Joung, J.K. and Porteus, M.H., 2008. Comparison of zinc finger nucleases for use in gene targeting in mammalian cells. Mol Ther. 16, 707-17.
Qi, L.S., Larson, M.H., Gilbert, L.A., Doudna, J.A., Weissman, J.S., Arkin, A.P. and Lim, W.A., 2013. Repurposing CRISPR as an RNA-guided platform for sequence-specific control of gene expression. Cell. 152, 1173-83.
Qiu, X., Lim, C.H., Ho, S.H., Lee, K.H. and Jiang, Y.J., 2009. Temporal Notch activation through Notch1a and Notch3 is required for maintaining zebrafish rhombomere boundaries. Dev Genes Evol. 219, 339-51.
Qiu, X., Xu, H., Haddon, C., Lewis, J. and Jiang, Y.J., 2004. Sequence and embryonic expression of three zebrafish fringe genes: lunatic fringe, radical fringe, and manic fringe. Dev Dyn. 231, 621-30.
Raible, F. and Brand, M., 2001. Tight transcriptional control of the ETS domain factors Erm and Pea3 by Fgf signaling during early zebrafish development. Mech Dev. 107, 105-17.

Ramalho-Santos, M., Yoon, S., Matsuzaki, Y., Mulligan, R.C. and Melton, D.A., 2002. "Stemness": transcriptional profiling of embryonic and adult stem cells. Science. 298, 597-600.

Ramirez, C.L., Foley, J.E., Wright, D.A., Muller-Lerch, F., Rahman, S.H., Cornu, T.I., Winfrey, R.J., Sander, J.D., Fu, F., Townsend, J.A., Cathomen, T., Voytas, D.F. and Joung, J.K., 2008. Unexpected failure rates for modular assembly of engineered zinc fingers. Nat Methods. 5, 374-5.

Rapraeger, A.C., Krufka, A. and Olwin, B.B., 1991. Requirement of heparan sulfate for bFGF-mediated fibroblast growth and myoblast differentiation. Science. 252, 1705-8.

Rauskolb, C., Pan, G., Reddy, B.V., Oh, H. and Irvine, K.D., 2011. Zyxin links fat signaling to the hippo pathway. PLoS Biol. 9, e1000624.

Rauskolb, C., Peifer, M. and Wieschaus, E., 1993. extradenticle, a regulator of homeotic gene activity, is a homolog of the homeobox-containing human proto-oncogene pbx1. Cell. 74, 1101-12.

Rauskolb, C., Smith, K.M., Peifer, M. and Wieschaus, E., 1995. extradenticle determines segmental identities throughout Drosophila development. Development. 121, 3663-73.

Reddy, P., Deguchi, M., Cheng, Y. and Hsueh, A.J., 2013. Actin cytoskeleton regulates Hippo signaling. PLoS One. 8, e73763.

Rehn, A.E. and Rees, S.M., 2005. Investigating the neurodevelopmental hypothesis of schizophrenia. Clin Exp Pharmacol Physiol. 32, 687-96.

Reich, A., Sapir, A. and Shilo, B., 1999. Sprouty is a general inhibitor of receptor tyrosine kinase signaling. Development. 126, 4139-47.

Reifers, F., Bohli, H., Walsh, E.C., Crossley, P.H., Stainier, D.Y. and Brand, M., 1998. Fgf8 is mutated in zebrafish acerebellar (ace) mutants and is required for maintenance of midbrain-hindbrain boundary development and somitogenesis. Development. 125, 2381-95.

Reiss, A.L., Abrams, M.T., Greenlaw, R., Freund, L. and Denckla, M.B., 1995. Neurodevelopmental effects of the FMR-1 full mutation in humans. Nat Med. 1, 159-67.

Remacle, S., Abbas, L., De Backer, O., Pacico, N., Gavalas, A., Gofflot, F., Picard, J.J. and Rezsohazy, R., 2004. Loss of function but no gain of function caused by amino acid substitutions in the hexapeptide of Hoxa1 in vivo. Mol Cell Biol. 24, 8567-75.

Remacle, S., Shaw-Jackson, C., Matis, C., Lampe, X., Picard, J. and Rezsohazy, R., 2002. Changing homeodomain residues 2 and 3 of Hoxa1 alters its activity in a cell-type and enhancer dependent manner. Nucleic Acids Res. 30, 2663-8.

Remue, E., Meerschaert, K., Oka, T., Boucherie, C., Vandekerckhove, J., Sudol, M. and Gettemans, J., 2010. TAZ interacts with zonula occludens-1 and -2 proteins in a PDZ-1 dependent manner. FEBS Lett. 584, 4175-80.

Ren, F., Zhang, L. and Jiang, J., 2010. Hippo signaling regulates Yorkie nuclear localization and activity through 14-3-3 dependent and independent mechanisms. Dev Biol. 337, 303-12.

Rhinn, M., Schuhbaur, B., Niederreither, K. and Dolle, P., 2011. Involvement of retinol dehydrogenase 10 in embryonic patterning and rescue of its loss of function by maternal retinaldehyde treatment. Proc Natl Acad Sci U S A. 108, 16687-92.

Ribeiro, P.S., Josue, F., Wepf, A., Wehr, M.C., Rinner, O., Kelly, G., Tapon, N. and Gstaiger, M., 2010. Combined functional genomic and proteomic approaches identify a PP2A complex as a negative regulator of Hippo signaling. Mol Cell. 39, 521-34.

Rida, P.C., Le Minh, N. and Jiang, Y.J., 2004. A Notch feeling of somite segmentation and beyond. Dev Biol. 265, 2-22.

Riddle, R.D., Johnson, R.L., Laufer, E. and Tabin, C., 1993. Sonic hedgehog mediates the polarizing activity of the ZPA. Cell. 75, 1401-16.

Rieckhof, G.E., Casares, F., Ryoo, H.D., Abu-Shaar, M. and Mann, R.S., 1997. Nuclear translocation of extradenticle requires homothorax, which encodes an extradenticle-related homeodomain protein. Cell. 91, 171-83.

Rijli, F.M., Gavalas, A. and Chambon, P., 1998. Segmentation and specification in the branchial region of the head: the role of the Hox selector genes. Int J Dev Biol. 42, 393-401.

Rijli, F.M., Mark, M., Lakkaraju, S., Dierich, A., Dolle, P. and Chambon, P., 1993. A homeotic transformation is generated in the rostral branchial region of the head by disruption of Hoxa-2, which acts as a selector gene. Cell. 75, 1333-49.

Riley, B.B., Chiang, M., Farmer, L. and Heck, R., 1999. The deltaA gene of zebrafish mediates lateral inhibition of hair cells in the inner ear and is regulated by pax2.1. Development. 126, 5669-78.

Riley, B.B., Chiang, M.Y., Storch, E.M., Heck, R., Buckles, G.R. and Lekven, A.C., 2004. Rhombomere boundaries are Wnt signaling centers that regulate metameric patterning in the zebrafish hindbrain. Dev Dyn. 231, 278-91.

Robertson, J.K., Danzmann, K., Charles, S., Blake, K., Olivares, A., Bamikole, S., Olson, M. and Van Raay, T.J., 2014. Targeting the Wnt pathway in zebrafish as a screening method to identify novel therapeutic compounds. Exp Biol Med (Maywood). 239, 169-76.

Robinson, B.S., Huang, J., Hong, Y. and Moberg, K.H., 2010. Crumbs regulates Salvador/Warts/Hippo signaling in Drosophila via the FERM-domain protein Expanded. Curr Biol. 20, 582-90.

Robu, M.E., Larson, J.D., Nasevicius, A., Beiraghi, S., Brenner, C., Farber, S.A. and Ekker, S.C., 2007. p53 activation by knockdown technologies. PLoS Genet. 3, e78.

Rochette-Egly, C. and Germain, P., 2009. Dynamic and combinatorial control of gene expression by nuclear retinoic acid receptors (RARs). Nucl Recept Signal. 7, e005.

Rodriguez-Boulan, E. and Macara, I.G., 2014. Organization and execution of the epithelial polarity programme. Nat Rev Mol Cell Biol. 15, 225-42.

Roehl, H. and Nusslein-Volhard, C., 2001. Zebrafish pea3 and erm are general targets of FGF8 signaling. Curr Biol. 11, 503-7.

Romand, R., Kondo, T., Cammas, L., Hashino, E. and Dolle, P., 2008. Dynamic expression of the retinoic acid-synthesizing enzyme retinol dehydrogenase 10 (rdh10) in the developing mouse brain and sensory organs. J Comp Neurol. 508, 879-92.

Rooke, J., Pan, D., Xu, T. and Rubin, G.M., 1996. KUZ, a conserved metalloprotease-disintegrin protein with two roles in Drosophila neurogenesis. Science. 273, 1227-31.

Roose, J., Molenaar, M., Peterson, J., Hurenkamp, J., Brantjes, H., Moerer, P., van de Wetering, M., Destree, O. and Clevers, H., 1998. The Xenopus Wnt effector XTcf-3 interacts with Groucho-related transcriptional repressors. Nature. 395, 608-12.

Rosin-Arbesfeld, R., Ihrke, G. and Bienz, M., 2001. Actin-dependent membrane association of the APC tumour suppressor in polarized mammalian epithelial cells. EMBO J. 20, 5929-39.

Rossel, M. and Capecchi, M.R., 1999. Mice mutant for both Hoxa1 and Hoxb1 show extensive remodeling of the hindbrain and defects in craniofacial development. Development. 126, 5027-40.

Rossi, A., Kontarakis, Z., Gerri, C., Nolte, H., Holper, S., Kruger, M. and Stainier, D.Y., 2015. Genetic compensation induced by deleterious mutations but not gene knockdowns. Nature. 524, 230-3.

Roth, D.B. and Wilson, J.H., 1986. Nonhomologous recombination in mammalian cells: role for short sequence homologies in the joining reaction. Mol Cell Biol. 6, 4295-304.

Rowitch, D.H., Echelard, Y., Danielian, P.S., Gellner, K., Brenner, S. and McMahon, A.P., 1998. Identification of an evolutionarily conserved 110 base-pair cis-acting regulatory sequence that governs Wnt-1 expression in the murine neural plate. Development. 125, 2735-46.

Roy, N.M. and Sagerstrom, C.G., 2004. An early Fgf signal required for gene expression in the zebrafish hindbrain primordium. Brain Res Dev Brain Res. 148, 27-42.

Rubenstein, J.L., 2000. Intrinsic and extrinsic control of cortical development. Novartis Found Symp. 228, 67-75; discussion 75-82, 109-13.

Rubenstein, J.L., Shimamura, K., Martinez, S. and Puelles, L., 1998. Regionalization of the prosencephalic neural plate. Annu Rev Neurosci. 21, 445-77.

Rulifson, E.J. and Blair, S.S., 1995. Notch regulates wingless expression and is not required for reception of the paracrine wingless signal during wing margin neurogenesis in Drosophila. Development. 121, 2813-24.

Rulifson, E.J., Micchelli, C.A., Axelrod, J.D., Perrimon, N. and Blair, S.S., 1996. wingless refines its own expression domain on the Drosophila wing margin. Nature. 384, 72-4.

Ryoo, H.D., Marty, T., Casares, F., Affolter, M. and Mann, R.S., 1999. Regulation of Hox target genes by a DNA bound Homothorax/Hox/Extradenticle complex. Development. 126, 5137-48.

Sagerstrom, C.G., Kao, B.A., Lane, M.E. and Sive, H., 2001. Isolation and characterization of posteriorly restricted genes in the zebrafish gastrula. Dev Dyn. 220, 402-8.

Sajwan, S., Takasu, Y., Tamura, T., Uchino, K., Sezutsu, H. and Zurovec, M., 2013. Efficient disruption of endogenous Bombyx gene by TAL effector nucleases. Insect Biochem Mol Biol. 43, 17-23.

Sakai, Y., Meno, C., Fujii, H., Nishino, J., Shiratori, H., Saijoh, Y., Rossant, J. and Hamada, H., 2001. The retinoic acid-inactivating enzyme CYP26 is essential for establishing an uneven distribution of retinoic acid along the anterio-posterior axis within the mouse embryo. Genes Dev. 15, 213-25.

Sakuma, T., Hosoi, S., Woltjen, K., Suzuki, K.I., Kashiwagi, K., Wada, H., Ochiai, H., Miyamoto, T., Kawai, N., Sasakura, Y., Matsuura, S., Okada, Y., Kawahara, A.,

Hayashi, S. and Yamamoto, T., 2013. Efficient TALEN construction and evaluation methods for human cell and animal applications. Genes Cells.

Saleh, M., Rambaldi, I., Yang, X.J. and Featherstone, M.S., 2000. Cell signaling switches HOX-PBX complexes from repressors to activators of transcription mediated by histone deacetylases and histone acetyltransferases. Mol Cell Biol. 20, 8623-33.

Samad, O.A., Geisen, M.J., Caronia, G., Varlet, I., Zappavigna, V., Ericson, J., Goridis, C. and Rijli, F.M., 2004. Integration of anteroposterior and dorsoventral regulation of Phox2b transcription in cranial motoneuron progenitors by homeodomain proteins. Development. 131, 4071-83.

Sandell, L.L., Sanderson, B.W., Moiseyev, G., Johnson, T., Mushegian, A., Young, K., Rey, J.P., Ma, J.X., Staehling-Hampton, K. and Trainor, P.A., 2007. RDH10 is essential for synthesis of embryonic retinoic acid and is required for limb, craniofacial, and organ development. Genes Dev. 21, 1113-24.

Sander, J.D., Cade, L., Khayter, C., Reyon, D., Peterson, R.T., Joung, J.K. and Yeh, J.R., 2011a. Targeted gene disruption in somatic zebrafish cells using engineered TALENs. Nat Biotechnol. 29, 697-8.

Sander, J.D., Dahlborg, E.J., Goodwin, M.J., Cade, L., Zhang, F., Cifuentes, D., Curtin, S.J., Blackburn, J.S., Thibodeau-Beganny, S., Qi, Y., Pierick, C.J., Hoffman, E., Maeder, M.L., Khayter, C., Reyon, D., Dobbs, D., Langenau, D.M., Stupar, R.M., Giraldez, A.J., Voytas, D.F., Peterson, R.T., Yeh, J.R. and Joung, J.K., 2011b. Selection-free zinc-finger-nuclease engineering by context-dependent assembly (CoDA). Nat Methods. 8, 67-9.

Sander, J.D., Maeder, M.L., Reyon, D., Voytas, D.F., Joung, J.K. and Dobbs, D., 2010. ZiFiT (Zinc Finger Targeter): an updated zinc finger engineering tool. Nucleic Acids Res. 38, W462-8.

Sander, J.D., Yeh, J.R., Peterson, R.T. and Joung, J.K., 2011c. Engineering zinc finger nucleases for targeted mutagenesis of zebrafish. Methods Cell Biol. 104, 51-8.

Sander, J.D., Zaback, P., Joung, J.K., Voytas, D.F. and Dobbs, D., 2007. Zinc Finger Targeter (ZiFiT): an engineered zinc finger/target site design tool. Nucleic Acids Res. 35, W599-605.

Sanderson, T.L., Best, J.J., Doody, G.A., Owens, D.G. and Johnstone, E.C., 1999. Neuroanatomy of comorbid schizophrenia and learning disability: a controlled study. Lancet. 354, 1867-71.

Sanjana, N.E., Cong, L., Zhou, Y., Cunniff, M.M., Feng, G. and Zhang, F., 2012. A transcription activator-like effector toolbox for genome engineering. Nat Protoc. 7, 171-92.

Sanson, B., 2001. Generating patterns from fields of cells. Examples from Drosophila segmentation. EMBO Rep. 2, 1083-8.

Sansores-Garcia, L., Atkins, M., Moya, I.M., Shahmoradgoli, M., Tao, C., Mills, G.B. and Halder, G., 2013. Mask is required for the activity of the Hippo pathway effector Yki/YAP. Curr Biol. 23, 229-35.

Sasai, Y., 1998. Identifying the missing links: genes that connect neural induction and primary neurogenesis in vertebrate embryos. Neuron. 21, 455-8.

Sausedo, R.A., Smith, J.L. and Schoenwolf, G.C., 1997. Role of nonrandomly oriented cell division in shaping and bending of the neural plate. J Comp Neurol. 381, 473-88.

Sawamoto, K., Wichterle, H., Gonzalez-Perez, O., Cholfin, J.A., Yamada, M., Spassky, N., Murcia, N.S., Garcia-Verdugo, J.M., Marin, O., Rubenstein, J.L., Tessier-Lavigne, M., Okano, H. and Alvarez-Buylla, A., 2006. New neurons follow the flow of cerebrospinal fluid in the adult brain. Science. 311, 629-32.

Schier, A.F., Neuhauss, S.C., Harvey, M., Malicki, J., Solnica-Krezel, L., Stainier, D.Y., Zwartkruis, F., Abdelilah, S., Stemple, D.L., Rangini, Z., Yang, H. and Driever, W., 1996. Mutations affecting the development of the embryonic zebrafish brain. Development. 123, 165-78.

Schier, A.F. and Talbot, W.S., 2001. Nodal signaling and the zebrafish organizer. Int J Dev Biol. 45, 289-97.

Schilling, T.F. and Kimmel, C.B., 1994. Segment and cell type lineage restrictions during pharyngeal arch development in the zebrafish embryo. Development. 120, 483-94.

Schilling, T.F., Prince, V. and Ingham, P.W., 2001. Plasticity in zebrafish hox expression in the hindbrain and cranial neural crest. Dev Biol. 231, 201-16.

Schlegelmilch, K., Mohseni, M., Kirak, O., Pruszak, J., Rodriguez, J.R., Zhou, D., Kreger, B.T., Vasioukhin, V., Avruch, J., Brummelkamp, T.R. and Camargo, F.D., 2011. Yap1 acts downstream of alpha-catenin to control epidermal proliferation. Cell. 144, 782-95.

Schneider-Maunoury, S., Seitanidou, T., Charnay, P. and Lumsden, A., 1997. Segmental and neuronal architecture of the hindbrain of Krox-20 mouse mutants. Development. 124, 1215-26.

Schneider-Maunoury, S., Topilko, P., Seitandou, T., Levi, G., Cohen-Tannoudji, M., Pournin, S., Babinet, C. and Charnay, P., 1993. Disruption of Krox-20 results in alteration of rhombomeres 3 and 5 in the developing hindbrain. Cell. 75, 1199-214.

Schoenwolf, G.C. and Alvarez, I.S., 1989. Roles of neuroepithelial cell rearrangement and division in shaping of the avian neural plate. Development. 106, 427-39.

Schoenwolf, G.C. and Fisher, M., 1983. Analysis of the effects of Streptomyces hyaluronidase on formation of the neural tube. J Embryol Exp Morphol. 73, 1-15.

Schreiber, A.B., Kenney, J., Kowalski, J., Thomas, K.A., Gimenez-Gallego, G., Rios-Candelore, M., Di Salvo, J., Barritault, D., Courty, J., Courtois, Y., Moenner, M., Loret, C., Burgess, W.H., Mehlman, T., Friesel, R., Johnson, W. and Maciag, T., 1985a. A unique family of endothelial cell polypeptide mitogens: the antigenic and receptor cross-reactivity of bovine endothelial cell growth factor, brain-derived acidic fibroblast growth factor, and eye-derived growth factor-II. J Cell Biol. 101, 1623-6.

Schreiber, A.B., Kenney, J., Kowalski, W.J., Friesel, R., Mehlman, T. and Maciag, T., 1985b. Interaction of endothelial cell growth factor with heparin: characterization by receptor and antibody recognition. Proc Natl Acad Sci U S A. 82, 6138-42.

Schroeter, E.H., Kisslinger, J.A. and Kopan, R., 1998. Notch-1 signalling requires ligand-induced proteolytic release of intracellular domain. Nature. 393, 382-6.

Schwarz-Romond, T., Fiedler, M., Shibata, N., Butler, P.J., Kikuchi, A., Higuchi, Y. and Bienz, M., 2007a. The DIX domain of Dishevelled confers Wnt signaling by dynamic polymerization. Nat Struct Mol Biol. 14, 484-92.

Schwarz-Romond, T., Metcalfe, C. and Bienz, M., 2007b. Dynamic recruitment of axin by Dishevelled protein assemblies. J Cell Sci. 120, 2402-12.
Scott, M.P., Tamkun, J.W. and Hartzell, G.W., 3rd, 1989. The structure and function of the homeodomain. Biochim Biophys Acta. 989, 25-48.
Scott, M.P. and Weiner, A.J., 1984. Structural relationships among genes that control development: sequence homology between the Antennapedia, Ultrabithorax, and fushi tarazu loci of Drosophila. Proc Natl Acad Sci U S A. 81, 4115-9.
Segal, D.J., Beerli, R.R., Blancafort, P., Dreier, B., Effertz, K., Huber, A., Koksch, B., Lund, C.V., Magnenat, L., Valente, D. and Barbas, C.F., 3rd, 2003. Evaluation of a modular strategy for the construction of novel polydactyl zinc finger DNA-binding proteins. Biochemistry. 42, 2137-48.
Segal, M.B., 2001. Transport of nutrients across the choroid plexus. Microsc Res Tech. 52, 38-48.
Selland, L.G., Koch, S., Laraque, M. and Waskiewicz, A.J., 2018. Coordinate regulation of retinoic acid synthesis by pbx genes and fibroblast growth factor signaling by hoxb1b is required for hindbrain patterning and development. Mech Dev.
Selleri, L., Depew, M.J., Jacobs, Y., Chanda, S.K., Tsang, K.Y., Cheah, K.S., Rubenstein, J.L., O'Gorman, S. and Cleary, M.L., 2001. Requirement for Pbx1 in skeletal patterning and programming chondrocyte proliferation and differentiation. Development. 128, 3543-57.
Serinagaoglu, Y., Pare, J., Giovannini, M. and Cao, X., 2015. Nf2-Yap signaling controls the expansion of DRG progenitors and glia during DRG development. Dev Biol. 398, 97-109.
Serpente, P., Tumpel, S., Ghyselinck, N.B., Niederreither, K., Wiedemann, L.M., Dolle, P., Chambon, P., Krumlauf, R. and Gould, A.P., 2005. Direct crossregulation between retinoic acid receptor {beta} and Hox genes during hindbrain segmentation. Development. 132, 503-13.
Sham, M.H., Vesque, C., Nonchev, S., Marshall, H., Frain, M., Gupta, R.D., Whiting, J., Wilkinson, D., Charnay, P. and Krumlauf, R., 1993. The zinc finger gene Krox20 regulates HoxB2 (Hox2.8) during hindbrain segmentation. Cell. 72, 183-96.
Shamim, H. and Mason, I., 1999. Expression of Fgf4 during early development of the chick embryo. Mech Dev. 85, 189-92.
Shapovalov, A.I., 1972. Extrapyramidal monosynaptic and disynaptic control of mammalian alpha-motoneurons. Brain Res. 40, 105-15.
Shapovalov, A.I., 1975. Neuronal organization and synaptic mechanisms of supraspinal motor control in vertebrates. Rev Physiol Biochem Pharmacol. 72, 1-54.
Shenton, M.E., Dickey, C.C., Frumin, M. and McCarley, R.W., 2001. A review of MRI findings in schizophrenia. Schizophr Res. 49, 1-52.
Shukla, V.K., Doyon, Y., Miller, J.C., DeKelver, R.C., Moehle, E.A., Worden, S.E., Mitchell, J.C., Arnold, N.L., Gopalan, S., Meng, X., Choi, V.M., Rock, J.M., Wu, Y.Y., Katibah, G.E., Zhifang, G., McCaskill, D., Simpson, M.A., Blakeslee, B., Greenwalt, S.A., Butler, H.J., Hinkley, S.J., Zhang, L., Rebar, E.J., Gregory, P.D. and Urnov, F.D., 2009. Precise genome modification in the crop species Zea mays using zinc-finger nucleases. Nature. 459, 437-41.
Sidor, C.M., Brain, R. and Thompson, B.J., 2013. Mask proteins are cofactors of Yorkie/YAP in the Hippo pathway. Curr Biol. 23, 223-8.

Silvis, M.L., Mosher, T.J., Smetana, B.S., Chinchilli, V.M., Flemming, D.J., Walker, E.A. and Black, K.P., 2011. High prevalence of pelvic and hip magnetic resonance imaging findings in asymptomatic collegiate and professional hockey players. Am J Sports Med. 39, 715-21.

Simandi, Z., Horvath, A., Wright, L.C., Cuaranta-Monroy, I., De Luca, I., Karolyi, K., Sauer, S., Deleuze, J.F., Gudas, L.J., Cowley, S.M. and Nagy, L., 2016. OCT4 Acts as an Integrator of Pluripotency and Signal-Induced Differentiation. Mol Cell. 63, 647-661.

Simeone, A., Acampora, D., Arcioni, L., Andrews, P.W., Boncinelli, E. and Mavilio, F., 1990. Sequential activation of HOX2 homeobox genes by retinoic acid in human embryonal carcinoma cells. Nature. 346, 763-6.

Sirbu, I.O., Gresh, L., Barra, J. and Duester, G., 2005. Shifting boundaries of retinoic acid activity control hindbrain segmental gene expression. Development. 132, 2611-22.

Sleptsova-Friedrich, I., Li, Y., Emelyanov, A., Ekker, M., Korzh, V. and Ge, R., 2001. fgfr3 and regionalization of anterior neural tube in zebrafish. Mech Dev. 102, 213-7.

Smith, G.R., Amundsen, S.K., Dabert, P. and Taylor, A.F., 1995. The initiation and control of homologous recombination in Escherichia coli. Philos Trans R Soc Lond B Biol Sci. 347, 13-20.

Song, M.H., Brown, N.L. and Kuwada, J.Y., 2004. The cfy mutation disrupts cell divisions in a stage-dependent manner in zebrafish embryos. Dev Biol. 276, 194-206.

Sorrentino, G., Ruggeri, N., Specchia, V., Cordenonsi, M., Mano, M., Dupont, S., Manfrin, A., Ingallina, E., Sommaggio, R., Piazza, S., Rosato, A., Piccolo, S. and Del Sal, G., 2014. Metabolic control of YAP and TAZ by the mevalonate pathway. Nat Cell Biol. 16, 357-66.

Sperber, S.M., Saxena, V., Hatch, G. and Ekker, M., 2008. Zebrafish dlx2a contributes to hindbrain neural crest survival, is necessary for differentiation of sensory ganglia and functions with dlx1a in maturation of the arch cartilage elements. Dev Biol. 314, 59-70.

Stadeli, R., Hoffmans, R. and Basler, K., 2006. Transcription under the control of nuclear Arm/beta-catenin. Curr Biol. 16, R378-85.

Stamos, J.L., Chu, M.L., Enos, M.D., Shah, N. and Weis, W.I., 2014. Structural basis of GSK-3 inhibition by N-terminal phosphorylation and by the Wnt receptor LRP6. Elife. 3, e01998.

Stedman, A., Lecaudey, V., Havis, E., Anselme, I., Wassef, M., Gilardi-Hebenstreit, P. and Schneider-Maunoury, S., 2009. A functional interaction between Irx and Meis patterns the anterior hindbrain and activates krox20 expression in rhombomere 3. Dev Biol. 327, 566-77.

Strano, S., Munarriz, E., Rossi, M., Castagnoli, L., Shaul, Y., Sacchi, A., Oren, M., Sudol, M., Cesareni, G. and Blandino, G., 2001. Physical interaction with Yes-associated protein enhances p73 transcriptional activity. J Biol Chem. 276, 15164-73.

Streit, A., Berliner, A.J., Papanayotou, C., Sirulnik, A. and Stern, C.D., 2000. Initiation of neural induction by FGF signalling before gastrulation. Nature. 406, 74-8.

Streit, A., Sockanathan, S., Perez, L., Rex, M., Scotting, P.J., Sharpe, P.T., Lovell-Badge, R. and Stern, C.D., 1997. Preventing the loss of competence for neural induction: HGF/SF, L5 and Sox-2. Development. 124, 1191-202.

Stroud, D.A., Formosa, L.E., Wijeyeratne, X.W., Nguyen, T.N. and Ryan, M.T., 2013. Gene knockout using transcription activator-like effector nucleases (TALENs) reveals that human NDUFA9 protein is essential for stabilizing the junction between membrane and matrix arms of complex I. J Biol Chem. 288, 1685-90.

Struhl, G. and Akam, M., 1985. Altered distributions of Ultrabithorax transcripts in extra sex combs mutant embryos of Drosophila. EMBO J. 4, 3259-64.

Struhl, G. and Greenwald, I., 1999. Presenilin is required for activity and nuclear access of Notch in Drosophila. Nature. 398, 522-5.

Studer, M., Gavalas, A., Marshall, H., Ariza-McNaughton, L., Rijli, F.M., Chambon, P. and Krumlauf, R., 1998. Genetic interactions between Hoxa1 and Hoxb1 reveal new roles in regulation of early hindbrain patterning. Development. 125, 1025-36.

Sukumaran, S.K., Stumpf, M., Salamon, S., Ahmad, I., Bhattacharya, K., Fischer, S., Muller, R., Altmuller, J., Budde, B., Thiele, H., Tariq, M., Malik, N.A., Nurnberg, P., Baig, S.M., Hussain, M.S. and Noegel, A.A., 2017. CDK5RAP2 interaction with components of the Hippo signaling pathway may play a role in primary microcephaly. Mol Genet Genomics. 292, 365-383.

Sun, N., Liang, J., Abil, Z. and Zhao, H., 2012. Optimized TAL effector nucleases (TALENs) for use in treatment of sickle cell disease. Mol Biosyst. 8, 1255-63.

Sun, Z. and Hopkins, N., 2001. vhnf1, the MODY5 and familial GCKD-associated gene, regulates regional specification of the zebrafish gut, pronephros, and hindbrain. Genes Dev. 15, 3217-29.

Sung, Y.H., Baek, I.J., Kim, D.H., Jeon, J., Lee, J., Lee, K., Jeong, D., Kim, J.S. and Lee, H.W., 2013. Knockout mice created by TALEN-mediated gene targeting. Nat Biotechnol. 31, 23-4.

Swiatek, P.J. and Gridley, T., 1993. Perinatal lethality and defects in hindbrain development in mice homozygous for a targeted mutation of the zinc finger gene Krox20. Genes Dev. 7, 2071-84.

Swindell, E.C. and Eichele, G., 1999. Retinoid metabolizing enzymes in development. Biofactors. 10, 85-9.

Szczepek, M., Brondani, V., Buchel, J., Serrano, L., Segal, D.J. and Cathomen, T., 2007. Structure-based redesign of the dimerization interface reduces the toxicity of zinc-finger nucleases. Nat Biotechnol. 25, 786-93.

Szumska, D., Pieles, G., Essalmani, R., Bilski, M., Mesnard, D., Kaur, K., Franklyn, A., El Omari, K., Jefferis, J., Bentham, J., Taylor, J.M., Schneider, J.E., Arnold, S.J., Johnson, P., Tymowska-Lalanne, Z., Stammers, D., Clarke, K., Neubauer, S., Morris, A., Brown, S.D., Shaw-Smith, C., Cama, A., Capra, V., Ragoussis, J., Constam, D., Seidah, N.G., Prat, A. and Bhattacharya, S., 2008. VACTERL/caudal regression/Currarino syndrome-like malformations in mice with mutation in the proprotein convertase Pcsk5. Genes Dev. 22, 1465-77.

Takasu, Y., Kobayashi, I., Beumer, K., Uchino, K., Sezutsu, H., Sajwan, S., Carroll, D., Tamura, T. and Zurovec, M., 2010. Targeted mutagenesis in the silkworm Bombyx mori using zinc finger nuclease mRNA injection. Insect Biochem Mol Biol. 40, 759-65.

Takemaru, K.I. and Moon, R.T., 2000. The transcriptional coactivator CBP interacts with beta-catenin to activate gene expression. J Cell Biol. 149, 249-54.

Tannahill, D., Harris, L.W. and Keynes, R., 2005. Role of morphogens in brain growth. J Neurobiol. 64, 367-75.

Tannahill, D., Isaacs, H.V., Close, M.J., Peters, G. and Slack, J.M., 1992. Developmental expression of the Xenopus int-2 (FGF-3) gene: activation by mesodermal and neural induction. Development. 115, 695-702.

Tao, W. and Lai, E., 1992. Telencephalon-restricted expression of BF-1, a new member of the HNF-3/fork head gene family, in the developing rat brain. Neuron. 8, 957-66.

Tapon, N., Harvey, K.F., Bell, D.W., Wahrer, D.C., Schiripo, T.A., Haber, D. and Hariharan, I.K., 2002. salvador Promotes both cell cycle exit and apoptosis in Drosophila and is mutated in human cancer cell lines. Cell. 110, 467-78.

Tauriello, D.V., Jordens, I., Kirchner, K., Slootstra, J.W., Kruitwagen, T., Bouwman, B.A., Noutsou, M., Rudiger, S.G., Schwamborn, K., Schambony, A. and Maurice, M.M., 2012. Wnt/beta-catenin signaling requires interaction of the Dishevelled DEP domain and C terminus with a discontinuous motif in Frizzled. Proc Natl Acad Sci U S A. 109, E812-20.

Tawk, M., Araya, C., Lyons, D.A., Reugels, A.M., Girdler, G.C., Bayley, P.R., Hyde, D.R., Tada, M. and Clarke, J.D., 2007. A mirror-symmetric cell division that orchestrates neuroepithelial morphogenesis. Nature. 446, 797-800.

Ten Donkelaar, H.J., 1982. Organization of descending pathways to the spinal cord in amphibians and reptiles. Prog Brain Res. 57, 25-67.

Terriente, J., Gerety, S.S., Watanabe-Asaka, T., Gonzalez-Quevedo, R. and Wilkinson, D.G., 2012. Signalling from hindbrain boundaries regulates neuronal clustering that patterns neurogenesis. Development. 139, 2978-87.

Tesson, L., Usal, C., Menoret, S., Leung, E., Niles, B.J., Remy, S., Santiago, Y., Vincent, A.I., Meng, X., Zhang, L., Gregory, P.D., Anegon, I. and Cost, G.J., 2011. Knockout rats generated by embryo microinjection of TALENs. Nat Biotechnol. 29, 695-6.

Theil, T., Frain, M., Gilardi-Hebenstreit, P., Flenniken, A., Charnay, P. and Wilkinson, D.G., 1998. Segmental expression of the EphA4 (Sek-1) receptor tyrosine kinase in the hindbrain is under direct transcriptional control of Krox-20. Development. 125, 443-52.

Thisse, B., Heyer, V., Lux, A., Alunni, V., Degrave, A., Seiliez, I., Kirchner, J., Parkhill, J.P. and Thisse, C., 2004. Spatial and temporal expression of the zebrafish genome by large-scale in situ hybridization screening. Methods Cell Biol. 77, 505-19.

Thisse, B. and Thisse, C., 2005. Functions and regulations of fibroblast growth factor signaling during embryonic development. Dev Biol. 287, 390-402.

Thisse, C. and Thisse, B., 2008. High-resolution in situ hybridization to whole-mount zebrafish embryos. Nat Protoc. 3, 59-69.

Thomas, K.A., Rios-Candelore, M., Gimenez-Gallego, G., DiSalvo, J., Bennett, C., Rodkey, J. and Fitzpatrick, S., 1985. Pure brain-derived acidic fibroblast growth factor is a potent angiogenic vascular endothelial cell mitogen with sequence homology to interleukin 1. Proc Natl Acad Sci U S A. 82, 6409-13.

Thomas-Jinu, S., Gordon, P.M., Fielding, T., Taylor, R., Smith, B.N., Snowden, V., Blanc, E., Vance, C., Topp, S., Wong, C.H., Bielen, H., Williams, K.L., McCann, E.P., Nicholson, G.A., Pan-Vazquez, A., Fox, A.H., Bond, C.S., Talbot, W.S., Blair, I.P., Shaw, C.E. and Houart, C., 2017. Non-nuclear Pool of Splicing Factor SFPQ Regulates Axonal Transcripts Required for Normal Motor Development. Neuron. 94, 322-336 e5.

Thuringer, F., Cohen, S.M. and Bienz, M., 1993. Dissection of an indirect autoregulatory response of a homeotic Drosophila gene. EMBO J. 12, 2419-30.

Tian, Y., Kolb, R., Hong, J.H., Carroll, J., Li, D., You, J., Bronson, R., Yaffe, M.B., Zhou, J. and Benjamin, T., 2007. TAZ promotes PC2 degradation through a SCFbeta-Trcp E3 ligase complex. Mol Cell Biol. 27, 6383-95.

Tomita, T., Tanaka, S., Morohashi, Y. and Iwatsubo, T., 2006. Presenilin-dependent intramembrane cleavage of ephrin-B1. Mol Neurodegener. 1, 2.

Totaro, A., Castellan, M., Battilana, G., Zanconato, F., Azzolin, L., Giulitti, S., Cordenonsi, M. and Piccolo, S., 2017. YAP/TAZ link cell mechanics to Notch signalling to control epidermal stem cell fate. Nat Commun. 8, 15206.

Townsend, J.A., Wright, D.A., Winfrey, R.J., Fu, F., Maeder, M.L., Joung, J.K. and Voytas, D.F., 2009. High-frequency modification of plant genes using engineered zinc-finger nucleases. Nature. 459, 442-5.

Trainor, P. and Krumlauf, R., 2000. Plasticity in mouse neural crest cells reveals a new patterning role for cranial mesoderm. Nat Cell Biol. 2, 96-102.

Trevarrow, B., Marks, D.L. and Kimmel, C.B., 1990. Organization of hindbrain segments in the zebrafish embryo. Neuron. 4, 669-79.

Tsang, M. and Dawid, I.B., 2004. Promotion and attenuation of FGF signaling through the Ras-MAPK pathway. Sci STKE. 2004, pe17.

Tschaharganeh, D.F., Chen, X., Latzko, P., Malz, M., Gaida, M.M., Felix, K., Ladu, S., Singer, S., Pinna, F., Gretz, N., Sticht, C., Tomasi, M.L., Delogu, S., Evert, M., Fan, B., Ribback, S., Jiang, L., Brozzetti, S., Bergmann, F., Dombrowski, F., Schirmacher, P., Calvisi, D.F. and Breuhahn, K., 2013. Yes-associated protein up-regulates Jagged-1 and activates the Notch pathway in human hepatocellular carcinoma. Gastroenterology. 144, 1530-1542 e12.

Tuckett, F. and Morriss-Kay, G.M., 1989. Heparitinase treatment of rat embryos during cranial neurulation. Anat Embryol (Berl). 180, 393-400.

Tumpel, S., Cambronero, F., Ferretti, E., Blasi, F., Wiedemann, L.M. and Krumlauf, R., 2007. Expression of Hoxa2 in rhombomere 4 is regulated by a conserved cross-regulatory mechanism dependent upon Hoxb1. Dev Biol. 302, 646-60.

Uchikawa, M., Kamachi, Y. and Kondoh, H., 1999. Two distinct subgroups of Group B Sox genes for transcriptional activators and repressors: their expression during embryonic organogenesis of the chicken. Mech Dev. 84, 103-20.

Udan, R.S., Kango-Singh, M., Nolo, R., Tao, C. and Halder, G., 2003. Hippo promotes proliferation arrest and apoptosis in the Salvador/Warts pathway. Nat Cell Biol. 5, 914-20.

Uehara, M., Yashiro, K., Mamiya, S., Nishino, J., Chambon, P., Dolle, P. and Sakai, Y., 2007. CYP26A1 and CYP26C1 cooperatively regulate anterior-posterior patterning of the developing brain and the production of migratory cranial neural crest cells in the mouse. Dev Biol. 302, 399-411.

Urnov, F.D., Miller, J.C., Lee, Y.L., Beausejour, C.M., Rock, J.M., Augustus, S., Jamieson, A.C., Porteus, M.H., Gregory, P.D. and Holmes, M.C., 2005. Highly efficient endogenous human gene correction using designed zinc-finger nucleases. Nature. 435, 646-51.

van de Wetering, M., Cavallo, R., Dooijes, D., van Beest, M., van Es, J., Loureiro, J., Ypma, A., Hursh, D., Jones, T., Bejsovec, A., Peifer, M., Mortin, M. and Clevers, H., 1997. Armadillo coactivates transcription driven by the product of the Drosophila segment polarity gene dTCF. Cell. 88, 789-99.

van der Wees, J., Schilthuis, J.G., Koster, C.H., Diesveld-Schipper, H., Folkers, G.E., van der Saag, P.T., Dawson, M.I., Shudo, K., van der Burg, B. and Durston, A.J., 1998. Inhibition of retinoic acid receptor-mediated signalling alters positional identity in the developing hindbrain. Development. 125, 545-56.

van Eeden, F.J., Granato, M., Schach, U., Brand, M., Furutani-Seiki, M., Haffter, P., Hammerschmidt, M., Heisenberg, C.P., Jiang, Y.J., Kane, D.A., Kelsh, R.N., Mullins, M.C., Odenthal, J., Warga, R.M., Allende, M.L., Weinberg, E.S. and Nusslein-Volhard, C., 1996. Mutations affecting somite formation and patterning in the zebrafish, Danio rerio. Development. 123, 153-64.

Van Hateren, N.J., Das, R.M., Hautbergue, G.M., Borycki, A.G., Placzek, M. and Wilson, S.A., 2011. FatJ acts via the Hippo mediator Yap1 to restrict the size of neural progenitor cell pools. Development. 138, 1893-902.

Varelas, X., Sakuma, R., Samavarchi-Tehrani, P., Peerani, R., Rao, B.M., Dembowy, J., Yaffe, M.B., Zandstra, P.W. and Wrana, J.L., 2008. TAZ controls Smad nucleocytoplasmic shuttling and regulates human embryonic stem-cell self-renewal. Nat Cell Biol. 10, 837-48.

Varelas, X., Samavarchi-Tehrani, P., Narimatsu, M., Weiss, A., Cockburn, K., Larsen, B.G., Rossant, J. and Wrana, J.L., 2010. The Crumbs complex couples cell density sensing to Hippo-dependent control of the TGF-beta-SMAD pathway. Dev Cell. 19, 831-44.

Varshney, G.K., Pei, W., LaFave, M.C., Idol, J., Xu, L., Gallardo, V., Carrington, B., Bishop, K., Jones, M., Li, M., Harper, U., Huang, S.C., Prakash, A., Chen, W., Sood, R., Ledin, J. and Burgess, S.M., 2015. High-throughput gene targeting and phenotyping in zebrafish using CRISPR/Cas9. Genome Res. 25, 1030-42.

Vassilev, A., Kaneko, K.J., Shu, H., Zhao, Y. and DePamphilis, M.L., 2001. TEAD/TEF transcription factors utilize the activation domain of YAP65, a Src/Yes-associated protein localized in the cytoplasm. Genes Dev. 15, 1229-41.

Vassin, H., Bremer, K.A., Knust, E. and Campos-Ortega, J.A., 1987. The neurogenic gene Delta of Drosophila melanogaster is expressed in neurogenic territories and encodes a putative transmembrane protein with EGF-like repeats. EMBO J. 6, 3431-40.

Vigh, B. and Vigh-Teichmann, I., 1998. Actual problems of the cerebrospinal fluid-contacting neurons. Microsc Res Tech. 41, 57-83.

Vitobello, A., Ferretti, E., Lampe, X., Vilain, N., Ducret, S., Ori, M., Spetz, J.F., Selleri, L. and Rijli, F.M., 2011. Hox and Pbx factors control retinoic acid synthesis during hindbrain segmentation. Dev Cell. 20, 469-82.

Vlachakis, N., Choe, S.K. and Sagerstrom, C.G., 2001. Meis3 synergizes with Pbx4 and Hoxb1b in promoting hindbrain fates in the zebrafish. Development. 128, 1299-312.

Vlachakis, N., Ellstrom, D.R. and Sagerstrom, C.G., 2000. A novel pbx family member expressed during early zebrafish embryogenesis forms trimeric complexes with Meis3 and Hoxb1b. Dev Dyn. 217, 109-19.

Voiculescu, O., Taillebourg, E., Pujades, C., Kress, C., Buart, S., Charnay, P. and Schneider-Maunoury, S., 2001. Hindbrain patterning: Krox20 couples segmentation and specification of regional identity. Development. 128, 4967-78.

Wada, K., Itoga, K., Okano, T., Yonemura, S. and Sasaki, H., 2011. Hippo pathway regulation by cell morphology and stress fibers. Development. 138, 3907-14.

Walshe, J., Maroon, H., McGonnell, I.M., Dickson, C. and Mason, I., 2002. Establishment of hindbrain segmental identity requires signaling by FGF3 and FGF8. Curr Biol. 12, 1117-23.

Wang, K., Degerny, C., Xu, M. and Yang, X.J., 2009. YAP, TAZ, and Yorkie: a conserved family of signal-responsive transcriptional coregulators in animal development and human disease. Biochem Cell Biol. 87, 77-91.

Wang, Q. and Margolis, B., 2007. Apical junctional complexes and cell polarity. Kidney Int. 72, 1448-58.

Wang, W., Huang, J., Wang, X., Yuan, J., Li, X., Feng, L., Park, J.I. and Chen, J., 2012. PTPN14 is required for the density-dependent control of YAP1. Genes Dev. 26, 1959-71.

Wang, W., Xiao, Z.D., Li, X., Aziz, K.E., Gan, B., Johnson, R.L. and Chen, J., 2015. AMPK modulates Hippo pathway activity to regulate energy homeostasis. Nat Cell Biol. 17, 490-9.

Wang, X., Yang, N., Uno, E., Roeder, R.G. and Guo, S., 2006. A subunit of the mediator complex regulates vertebrate neuronal development. Proc Natl Acad Sci U S A. 103, 17284-9.

Waskiewicz, A.J., Rikhof, H.A., Hernandez, R.E. and Moens, C.B., 2001. Zebrafish Meis functions to stabilize Pbx proteins and regulate hindbrain patterning. Development. 128, 4139-51.

Waskiewicz, A.J., Rikhof, H.A. and Moens, C.B., 2002. Eliminating zebrafish pbx proteins reveals a hindbrain ground state. Dev Cell. 3, 723-33.

Wassef, M.A., Chomette, D., Pouilhe, M., Stedman, A., Havis, E., Desmarquet-Trin Dinh, C., Schneider-Maunoury, S., Gilardi-Hebenstreit, P., Charnay, P. and Ghislain, J., 2008. Rostral hindbrain patterning involves the direct activation of a Krox20 transcriptional enhancer by Hox/Pbx and Meis factors. Development. 135, 3369-78.

Watt, K.I., Harvey, K.F. and Gregorevic, P., 2017. Regulation of Tissue Growth by the Mammalian Hippo Signaling Pathway. Front Physiol. 8, 942.

Wefers, B., Meyer, M., Ortiz, O., Hrabe de Angelis, M., Hansen, J., Wurst, W. and Kuhn, R., 2013. Direct production of mouse disease models by embryo microinjection of TALENs and oligodeoxynucleotides. Proc Natl Acad Sci U S A. 110, 3782-7.

Wehr, M.C., Holder, M.V., Gailite, I., Saunders, R.E., Maile, T.M., Ciirdaeva, E., Instrell, R., Jiang, M., Howell, M., Rossner, M.J. and Tapon, N., 2013. Salt-inducible kinases regulate growth through the Hippo signalling pathway in Drosophila. Nat Cell Biol. 15, 61-71.

Wei, X. and Malicki, J., 2002. nagie oko, encoding a MAGUK-family protein, is essential for cellular patterning of the retina. Nat Genet. 31, 150-7.

Weicksel, S.E., Gupta, A., Zannino, D.A., Wolfe, S.A. and Sagerstrom, C.G., 2014. Targeted germ line disruptions reveal general and species-specific roles for paralog group 1 hox genes in zebrafish. BMC Dev Biol. 14, 25.
Weinmaster, G., Roberts, V.J. and Lemke, G., 1991. A homolog of Drosophila Notch expressed during mammalian development. Development. 113, 199-205.
Weinmaster, G., Roberts, V.J. and Lemke, G., 1992. Notch2: a second mammalian Notch gene. Development. 116, 931-41.
Weisinger, K., Kohl, A., Kayam, G., Monsonego-Ornan, E. and Sela-Donenfeld, D., 2012. Expression of hindbrain boundary markers is regulated by FGF3. Biol Open. 1, 67-74.
Weisinger, K., Wilkinson, D.G. and Sela-Donenfeld, D., 2008. Inhibition of BMPs by follistatin is required for FGF3 expression and segmental patterning of the hindbrain. Dev Biol. 324, 213-25.
Wendling, O., Ghyselinck, N.B., Chambon, P. and Mark, M., 2001. Roles of retinoic acid receptors in early embryonic morphogenesis and hindbrain patterning. Development. 128, 2031-8.
Wennmann, D.O., Vollenbroker, B., Eckart, A.K., Bonse, J., Erdmann, F., Wolters, D.A., Schenk, L.K., Schulze, U., Kremerskothen, J., Weide, T. and Pavenstadt, H., 2014. The Hippo pathway is controlled by Angiotensin II signaling and its reactivation induces apoptosis in podocytes. Cell Death Dis. 5, e1519.
Westerfield, M., 2007. The zebrafish book : a guide for the laboratory use of zebrafish (Danio rerio), Ed. 5. ed. Printed by the University of Oregon Press ; distributed by the Zebrafish International Resource Center, Eugene, OR.
Wharton, K.A., Johansen, K.M., Xu, T. and Artavanis-Tsakonas, S., 1985. Nucleotide sequence from the neurogenic locus notch implies a gene product that shares homology with proteins containing EGF-like repeats. Cell. 43, 567-81.
White, J.C., Highland, M., Kaiser, M. and Clagett-Dame, M., 2000. Vitamin A deficiency results in the dose-dependent acquisition of anterior character and shortening of the caudal hindbrain of the rat embryo. Dev Biol. 220, 263-84.
White, R.J., Nie, Q., Lander, A.D. and Schilling, T.F., 2007. Complex regulation of cyp26a1 creates a robust retinoic acid gradient in the zebrafish embryo. PLoS Biol. 5, e304.
White, R.J. and Schilling, T.F., 2008. How degrading: Cyp26s in hindbrain development. Dev Dyn. 237, 2775-90.
Whyte, J.J. and Prather, R.S., 2012. CELL BIOLOGY SYMPOSIUM: Zinc finger nucleases to create custom-designed modifications in the swine (Sus scrofa) genome. J Anim Sci. 90, 1111-7.
Wiellette, E.L. and Sive, H., 2004. Early requirement for fgf8 function during hindbrain pattern formation in zebrafish. Dev Dyn. 229, 393-9.
Wilkinson, D.G., Bhatt, S., Cook, M., Boncinelli, E. and Krumlauf, R., 1989. Segmental expression of Hox-2 homoeobox-containing genes in the developing mouse hindbrain. Nature. 341, 405-9.
Wilson, S.I., Rydstrom, A., Trimborn, T., Willert, K., Nusse, R., Jessell, T.M. and Edlund, T., 2001. The status of Wnt signalling regulates neural and epidermal fates in the chick embryo. Nature. 411, 325-30.
Wincent, E., Stegeman, J.J. and Jonsson, M.E., 2015. Combination effects of AHR agonists and Wnt/beta-catenin modulators in zebrafish embryos: Implications for

physiological and toxicological AHR functions. Toxicol Appl Pharmacol. 284, 163-79.
Wingate, R.J. and Hatten, M.E., 1999. The role of the rhombic lip in avian cerebellum development. Development. 126, 4395-404.
Wingate, R.J. and Lumsden, A., 1996. Persistence of rhombomeric organisation in the postsegmental hindbrain. Development. 122, 2143-52.
Wodarz, A., Hinz, U., Engelbert, M. and Knust, E., 1995. Expression of crumbs confers apical character on plasma membrane domains of ectodermal epithelia of Drosophila. Cell. 82, 67-76.
Woo, K. and Fraser, S.E., 1995. Order and coherence in the fate map of the zebrafish nervous system. Development. 121, 2595-609.
Woo, K. and Fraser, S.E., 1997. Specification of the zebrafish nervous system by nonaxial signals. Science. 277, 254-7.
Wood, A.J., Lo, T.W., Zeitler, B., Pickle, C.S., Ralston, E.J., Lee, A.H., Amora, R., Miller, J.C., Leung, E., Meng, X., Zhang, L., Rebar, E.J., Gregory, P.D., Urnov, F.D. and Meyer, B.J., 2011. Targeted genome editing across species using ZFNs and TALENs. Science. 333, 307.
Wright, D.A., Townsend, J.A., Winfrey, R.J., Jr., Irwin, P.A., Rajagopal, J., Lonosky, P.M., Hall, B.D., Jondle, M.D. and Voytas, D.F., 2005. High-frequency homologous recombination in plants mediated by zinc-finger nucleases. Plant J. 44, 693-705.
Wright, I.C., Rabe-Hesketh, S., Woodruff, P.W., David, A.S., Murray, R.M. and Bullmore, E.T., 2000. Meta-analysis of regional brain volumes in schizophrenia. Am J Psychiatry. 157, 16-25.
Wu, C., Qiu, R., Wang, J., Zhang, H., Murai, K. and Lu, Q., 2009. ZHX2 Interacts with Ephrin-B and regulates neural progenitor maintenance in the developing cerebral cortex. J Neurosci. 29, 7404-12.
Wu, L., Aster, J.C., Blacklow, S.C., Lake, R., Artavanis-Tsakonas, S. and Griffin, J.D., 2000. MAML1, a human homologue of Drosophila mastermind, is a transcriptional co-activator for NOTCH receptors. Nat Genet. 26, 484-9.
Wu, S., Huang, J., Dong, J. and Pan, D., 2003. hippo encodes a Ste-20 family protein kinase that restricts cell proliferation and promotes apoptosis in conjunction with salvador and warts. Cell. 114, 445-56.
Wu, S., Liu, Y., Zheng, Y., Dong, J. and Pan, D., 2008. The TEAD/TEF family protein Scalloped mediates transcriptional output of the Hippo growth-regulatory pathway. Dev Cell. 14, 388-98.
Wullimann, M.F., Rink, E., Vernier, P. and Schlosser, G., 2005. Secondary neurogenesis in the brain of the African clawed frog, Xenopus laevis, as revealed by PCNA, Delta-1, Neurogenin-related-1, and NeuroD expression. J Comp Neurol. 489, 387-402.
Wurst, W. and Bally-Cuif, L., 2001. Neural plate patterning: upstream and downstream of the isthmic organizer. Nat Rev Neurosci. 2, 99-108.
Xia, D., Stull, J.T. and Kamm, K.E., 2005. Myosin phosphatase targeting subunit 1 affects cell migration by regulating myosin phosphorylation and actin assembly. Exp Cell Res. 304, 506-17.
Xiao, L., Chen, Y., Ji, M. and Dong, J., 2011. KIBRA regulates Hippo signaling activity via interactions with large tumor suppressor kinases. J Biol Chem. 286, 7788-96.

Xin, M., Kim, Y., Sutherland, L.B., Qi, X., McAnally, J., Schwartz, R.J., Richardson, J.A., Bassel-Duby, R. and Olson, E.N., 2011. Regulation of insulin-like growth factor signaling by Yap governs cardiomyocyte proliferation and embryonic heart size. Sci Signal. 4, ra70.

Xing, W., Kim, J., Wergedal, J., Chen, S.T. and Mohan, S., 2010. Ephrin B1 regulates bone marrow stromal cell differentiation and bone formation by influencing TAZ transactivation via complex formation with NHERF1. Mol Cell Biol. 30, 711-21.

Xu, H.M. and Gutmann, D.H., 1998. Merlin differentially associates with the microtubule and actin cytoskeleton. J Neurosci Res. 51, 403-15.

Xu, P., Tong, Y., Liu, X.Z., Wang, T.T., Cheng, L., Wang, B.Y., Lv, X., Huang, Y. and Liu, D.P., 2015. Both TALENs and CRISPR/Cas9 directly target the HBB IVS2-654 (C > T) mutation in beta-thalassemia-derived iPSCs. Sci Rep. 5, 12065.

Xu, Q., Alldus, G., Holder, N. and Wilkinson, D.G., 1995a. Expression of truncated Sek-1 receptor tyrosine kinase disrupts the segmental restriction of gene expression in the Xenopus and zebrafish hindbrain. Development. 121, 4005-16.

Xu, Q., Mellitzer, G., Robinson, V. and Wilkinson, D.G., 1999. In vivo cell sorting in complementary segmental domains mediated by Eph receptors and ephrins. Nature. 399, 267-71.

Xu, T., Wang, W., Zhang, S., Stewart, R.A. and Yu, W., 1995b. Identifying tumor suppressors in genetic mosaics: the Drosophila lats gene encodes a putative protein kinase. Development. 121, 1053-63.

Xuan, S., Baptista, C.A., Balas, G., Tao, W., Soares, V.C. and Lai, E., 1995. Winged helix transcription factor BF-1 is essential for the development of the cerebral hemispheres. Neuron. 14, 1141-52.

Yagi, R., Chen, L.F., Shigesada, K., Murakami, Y. and Ito, Y., 1999. A WW domain-containing yes-associated protein (YAP) is a novel transcriptional co-activator. EMBO J. 18, 2551-62.

Yan, Y.L., Jowett, T. and Postlethwait, J.H., 1998. Ectopic expression of hoxb2 after retinoic acid treatment or mRNA injection: disruption of hindbrain and craniofacial morphogenesis in zebrafish embryos. Dev Dyn. 213, 370-85.

Yang, D., Yang, H., Li, W., Zhao, B., Ouyang, Z., Liu, Z., Zhao, Y., Fan, N., Song, J., Tian, J., Li, F., Zhang, J., Chang, L., Pei, D., Chen, Y.E. and Lai, L., 2011. Generation of PPARgamma mono-allelic knockout pigs via zinc-finger nucleases and nuclear transfer cloning. Cell Res. 21, 979-82.

Yang, T., Arslanova, D., Gu, Y., Augelli-Szafran, C. and Xia, W., 2008. Quantification of gamma-secretase modulation differentiates inhibitor compound selectivity between two substrates Notch and amyloid precursor protein. Mol Brain. 1, 15.

Yang, X., Zou, J., Hyde, D.R., Davidson, L.A. and Wei, X., 2009. Stepwise maturation of apicobasal polarity of the neuroepithelium is essential for vertebrate neurulation. J Neurosci. 29, 11426-40.

Yayon, A., Klagsbrun, M., Esko, J.D., Leder, P. and Ornitz, D.M., 1991. Cell surface, heparin-like molecules are required for binding of basic fibroblast growth factor to its high affinity receptor. Cell. 64, 841-8.

Yi, C., Shen, Z., Stemmer-Rachamimov, A., Dawany, N., Troutman, S., Showe, L.C., Liu, Q., Shimono, A., Sudol, M., Holmgren, L., Stanger, B.Z. and Kissil, J.L., 2013. The p130 isoform of angiomotin is required for Yap-mediated hepatic epithelial cell proliferation and tumorigenesis. Sci Signal. 6, ra77.

Yi, C., Troutman, S., Fera, D., Stemmer-Rachamimov, A., Avila, J.L., Christian, N., Persson, N.L., Shimono, A., Speicher, D.W., Marmorstein, R., Holmgren, L. and Kissil, J.L., 2011. A tight junction-associated Merlin-angiomotin complex mediates Merlin's regulation of mitogenic signaling and tumor suppressive functions. Cancer Cell. 19, 527-40.

Yin, F., Yu, J., Zheng, Y., Chen, Q., Zhang, N. and Pan, D., 2013. Spatial organization of Hippo signaling at the plasma membrane mediated by the tumor suppressor Merlin/NF2. Cell. 154, 1342-55.

Yip, G.W., Ferretti, P. and Copp, A.J., 2002. Heparan sulphate proteoglycans and spinal neurulation in the mouse embryo. Development. 129, 2109-19.

Yoshida, M. and Colman, D.R., 2000. Glial-defined rhombomere boundaries in developing Xenopus hindbrain. J Comp Neurol. 424, 47-57.

Yu, F.X., Zhang, Y., Park, H.W., Jewell, J.L., Chen, Q., Deng, Y., Pan, D., Taylor, S.S., Lai, Z.C. and Guan, K.L., 2013. Protein kinase A activates the Hippo pathway to modulate cell proliferation and differentiation. Genes Dev. 27, 1223-32.

Yu, F.X., Zhao, B., Panupinthu, N., Jewell, J.L., Lian, I., Wang, L.H., Zhao, J., Yuan, H., Tumaneng, K., Li, H., Fu, X.D., Mills, G.B. and Guan, K.L., 2012. Regulation of the Hippo-YAP pathway by G-protein-coupled receptor signaling. Cell. 150, 780-91.

Yu, J., Zheng, Y., Dong, J., Klusza, S., Deng, W.M. and Pan, D., 2010. Kibra functions as a tumor suppressor protein that regulates Hippo signaling in conjunction with Merlin and Expanded. Dev Cell. 18, 288-99.

Yuen, H.F., McCrudden, C.M., Huang, Y.H., Tham, J.M., Zhang, X., Zeng, Q., Zhang, S.D. and Hong, W., 2013. TAZ expression as a prognostic indicator in colorectal cancer. PLoS One. 8, e54211.

Zecchin, E., Filippi, A., Biemar, F., Tiso, N., Pauls, S., Ellertsdottir, E., Gnugge, L., Bortolussi, M., Driever, W. and Argenton, F., 2007. Distinct delta and jagged genes control sequential segregation of pancreatic cell types from precursor pools in zebrafish. Dev Biol. 301, 192-204.

Zerucha, T. and Prince, V.E., 2001. Cloning and developmental expression of a zebrafish meis2 homeobox gene. Mech Dev. 102, 247-50.

Zhang, F., Maeder, M.L., Unger-Wallace, E., Hoshaw, J.P., Reyon, D., Christian, M., Li, X., Pierick, C.J., Dobbs, D., Peterson, T., Joung, J.K. and Voytas, D.F., 2010a. High frequency targeted mutagenesis in Arabidopsis thaliana using zinc finger nucleases. Proc Natl Acad Sci U S A. 107, 12028-33.

Zhang, H., Deo, M., Thompson, R.C., Uhler, M.D. and Turner, D.L., 2012. Negative regulation of Yap during neuronal differentiation. Dev Biol. 361, 103-15.

Zhang, H., Pasolli, H.A. and Fuchs, E., 2011a. Yes-associated protein (YAP) transcriptional coactivator functions in balancing growth and differentiation in skin. Proc Natl Acad Sci U S A. 108, 2270-5.

Zhang, J., Ji, J.Y., Yu, M., Overholtzer, M., Smolen, G.A., Wang, R., Brugge, J.S., Dyson, N.J. and Haber, D.A., 2009. YAP-dependent induction of amphiregulin identifies a non-cell-autonomous component of the Hippo pathway. Nat Cell Biol. 11, 1444-50.

Zhang, J., Williams, M.A. and Rigamonti, D., 2006. Genetics of human hydrocephalus. J Neurol. 253, 1255-66.

Zhang, L., Ren, F., Zhang, Q., Chen, Y., Wang, B. and Jiang, J., 2008. The TEAD/TEF family of transcription factor Scalloped mediates Hippo signaling in organ size control. Dev Cell. 14, 377-87.

Zhang, N., Bai, H., David, K.K., Dong, J., Zheng, Y., Cai, J., Giovannini, M., Liu, P., Anders, R.A. and Pan, D., 2010b. The Merlin/NF2 tumor suppressor functions through the YAP oncoprotein to regulate tissue homeostasis in mammals. Dev Cell. 19, 27-38.

Zhang, X., Milton, C.C., Poon, C.L., Hong, W. and Harvey, K.F., 2011b. Wbp2 cooperates with Yorkie to drive tissue growth downstream of the Salvador-Warts-Hippo pathway. Cell Death Differ. 18, 1346-55.

Zhang, Y., Zhang, F., Li, X., Baller, J.A., Qi, Y., Starker, C.G., Bogdanove, A.J. and Voytas, D.F., 2013. Transcription activator-like effector nucleases enable efficient plant genome engineering. Plant Physiol. 161, 20-7.

Zhao, B., Li, L., Lu, Q., Wang, L.H., Liu, C.Y., Lei, Q. and Guan, K.L., 2011. Angiomotin is a novel Hippo pathway component that inhibits YAP oncoprotein. Genes Dev. 25, 51-63.

Zhao, B., Li, L., Tumaneng, K., Wang, C.Y. and Guan, K.L., 2010. A coordinated phosphorylation by Lats and CK1 regulates YAP stability through SCF(beta-TRCP). Genes Dev. 24, 72-85.

Zhao, B., Li, L., Wang, L., Wang, C.Y., Yu, J. and Guan, K.L., 2012. Cell detachment activates the Hippo pathway via cytoskeleton reorganization to induce anoikis. Genes Dev. 26, 54-68.

Zhao, B., Wei, X., Li, W., Udan, R.S., Yang, Q., Kim, J., Xie, J., Ikenoue, T., Yu, J., Li, L., Zheng, P., Ye, K., Chinnaiyan, A., Halder, G., Lai, Z.C. and Guan, K.L., 2007. Inactivation of YAP oncoprotein by the Hippo pathway is involved in cell contact inhibition and tissue growth control. Genes Dev. 21, 2747-61.

Zhao, B., Ye, X., Yu, J., Li, L., Li, W., Li, S., Yu, J., Lin, J.D., Wang, C.Y., Chinnaiyan, A.M., Lai, Z.C. and Guan, K.L., 2008a. TEAD mediates YAP-dependent gene induction and growth control. Genes Dev. 22, 1962-71.

Zhao, M., Szafranski, P., Hall, C.A. and Goode, S., 2008b. Basolateral junctions utilize warts signaling to control epithelial-mesenchymal transition and proliferation crucial for migration and invasion of Drosophila ovarian epithelial cells. Genetics. 178, 1947-71.

Zhong, H., Zou, H., Semenov, M.V., Moshinsky, D., He, X., Huang, H., Li, S., Quan, J., Yang, Z. and Lin, S., 2009. Characterization and development of novel small-molecules inhibiting GSK3 and activating Wnt signaling. Mol Biosyst. 5, 1356-60.

Zhou, D., Zhang, Y., Wu, H., Barry, E., Yin, Y., Lawrence, E., Dawson, D., Willis, J.E., Markowitz, S.D., Camargo, F.D. and Avruch, J., 2011. Mst1 and Mst2 protein kinases restrain intestinal stem cell proliferation and colonic tumorigenesis by inhibition of Yes-associated protein (Yap) overabundance. Proc Natl Acad Sci U S A. 108, E1312-20.

Zhou, S., Fujimuro, M., Hsieh, J.J., Chen, L., Miyamoto, A., Weinmaster, G. and Hayward, S.D., 2000. SKIP, a CBF1-associated protein, interacts with the ankyrin repeat domain of NotchIC To facilitate NotchIC function. Mol Cell Biol. 20, 2400-10.

Zhou, X., Wang, S., Wang, Z., Feng, X., Liu, P., Lv, X.B., Li, F., Yu, F.X., Sun, Y., Yuan, H., Zhu, H., Xiong, Y., Lei, Q.Y. and Guan, K.L., 2015. Estrogen regulates Hippo signaling via GPER in breast cancer. J Clin Invest. 125, 2123-35.

Zigman, M., Laumann-Lipp, N., Titus, T., Postlethwait, J. and Moens, C.B., 2014. Hoxb1b controls oriented cell division, cell shape and microtubule dynamics in neural tube morphogenesis. Development. 141, 639-49.

Zinyk, D.L., Mercer, E.H., Harris, E., Anderson, D.J. and Joyner, A.L., 1998. Fate mapping of the mouse midbrain-hindbrain constriction using a site-specific recombination system. Curr Biol. 8, 665-8.

Zou, J., Maeder, M.L., Mali, P., Pruett-Miller, S.M., Thibodeau-Beganny, S., Chou, B.K., Chen, G., Ye, Z., Park, I.H., Daley, G.Q., Porteus, M.H., Joung, J.K. and Cheng, L., 2009. Gene targeting of a disease-related gene in human induced pluripotent stem and embryonic stem cells. Cell Stem Cell. 5, 97-110.

Zou, J., Sweeney, C.L., Chou, B.K., Choi, U., Pan, J., Wang, H., Dowey, S.N., Cheng, L. and Malech, H.L., 2011. Oxidase-deficient neutrophils from X-linked chronic granulomatous disease iPS cells: functional correction by zinc finger nuclease-mediated safe harbor targeting. Blood. 117, 5561-72.

Zou, J., Wen, Y., Yang, X. and Wei, X., 2013. Spatial-temporal expressions of Crumbs and Nagie oko and their interdependence in zebrafish central nervous system during early development. Int J Dev Neurosci. 31, 770-82.

Zu, Y., Tong, X., Wang, Z., Liu, D., Pan, R., Li, Z., Hu, Y., Luo, Z., Huang, P., Wu, Q., Zhu, Z., Zhang, B. and Lin, S., 2013. TALEN-mediated precise genome modification by homologous recombination in zebrafish. Nat Methods.

Appendix A: RNA-seq analysis of Taz mutants

Table A.1. List of genes upregulated in *taz* mutants by 2-fold, identified by whole embryo RNA-seq at 24hpf.

Rank	Gene	Locus (Zv9)	Fold Change
1	*zgc:171759*	25:37234367-37514288	9.31
2	*si:ch211-51e12.7*	4:16557-96586	8.82
3	*hist2h3c*	7:7179599-7335433	6.37
4	*sf1*	7:23976995-23987907	5.74
5	*CR354435.1*	25:37234367-37514288	5.53
6	*ahsa1*	20:26996759-27003788	5.52
7	*zgc:171759*	7:6752107-6822388	5.13
8	*zgc:173585*	25:35811834-36197600	4.83
9	*efn2a*	11:14672385-14882992	4.73
10	*mt2*	18:17193778-17195147	4.60
11	*rrm2*	20:29518376-29524206	4.27
12	*wu:fe37d09*	25:37234367-37514288	4.10
13	*snrpb*	6:57428412-57435514	3.92
14	*tgm2b*	6:1929465-1954565	3.79
15	*ybx1*	8:49255132-49308225	3.74
16	*ewsr1b*	5:26542130-26551313	3.73
17	*akap8l*	1:60320184-60332019	3.72
18	*ppp4r3b*	13:63268-184799	3.71
19	*ghitm*	12:50332113-50682239	3.69
20	*myh9*	3:5725972-5826571	3.64
21	*bhmt*	21:205877-409532	3.64
22	*mrpl53*	19:33402873-33409411	3.63
23	*pole4*	11:6231837-6258031	3.63
24	*nt5dc2*	8:24492066-24509673	3.53
25	*mrps12*	21:24875327-24878859	3.50
26	*sart3*	5:22231956-22264717	3.47
27	*irx1a*	16:820640-824806	3.47
28	*sox19b*	7:27452376-27657933	3.46
29	*nap1l1*	4:2154966-2241467	3.43
30	*khdrbs1a*	13:45629553-45641972	3.34
31	*snx10a*	19:20137179-20287222	3.34
32	*zgc:163061*	7:76848664-76849492	3.31
33	*actn3b*	7:7866375-7964197	3.30
34	*g3bp2*	23:44158983-44180552	3.26
35	*parp1*	20:43680065-43721706	3.17
36	*zgc:174938*	16:49646802-49651286	3.17
37	*C5H8orf4*	5:29511197-29512206	3.17
38	*col9a3*	23:511454-541005	3.08

39	*C20H6orf162*	20:207047-209443	3.05
40	*lamc1*	2:35601426-35700011	3.03
41	*snu13a*	3:59026289-59034874	3.00
42	*si:ch73-265d7.2*	23:44750135-44758090	2.97
43	*rfxap*	10:35982020-36004657	2.96
44	*col8a1a*	9:31123963-31137545	2.93
45	*tp53inp2*	23:2503319-2563684	2.88
46	*si:dkey-261m9.9*	7:7179599-7335433	2.84
47	*kansl2,mlh3,snora2*	23:24876533-24897024	2.84
48	*si:dkey-261m9.9*	25:37234367-37514288	2.84
49	*pbxip1a*	19:8076531-8258524	2.77
50	*scaf4a*	10:26335140-26351292	2.76
51	*zgc:171759*	7:7179599-7335433	2.74
52	*hnrnpa0b*	14:40046936-40347389	2.72
53	*foxa1*	17:10280425-10283287	2.71
54	*hpn*	16:47923071-48161918	2.70
55	*cpamd8*	22:21568319-21626021	2.70
56	*utp18*	19:49796245-50216235	2.69
57	*hnrnpa0l*	14:40046936-40347389	2.69
58	*srsf10b*	17:53940076-53946422	2.68
59	*plekhf1*	7:47585059-47586479	2.64
60	*aamp*	6:59640312-59648623	2.63
61	*tpp2*	1:101923-337150	2.63
62	*srsf9*	10:1601417-1921801	2.61
63	*CT956064.3*	20:55774137-55775909	2.57
64	*serpinb14*	16:54847384-54904454	2.56
65	*si:dkey-286j15.1*	22:32699556-32962075	2.56
66	*alyref*	3:60271346-60353645	2.55
67	*fkbp1b*	20:44670112-44702001	2.55
68	*tns3*	2:23915-34815	2.54
69	*hrsp12*	19:34197698-34214418	2.54
70	*mettl14*	1:18807187-18811863	2.54
71	*znf622*	2:41536203-41544585	2.54
72	*otud5b*	11:26614890-26623498	2.53
73	*cbln10*	2:37658832-37659476	2.53
74	*ryr1b*	18:33833795-34076691	2.53
75	*irf2bp1*	18:44769996-44777969	2.53
76	*ewsr1a*	10:7004084-7016917	2.53
77	*fam53c*	21:28798828-29091653	2.51
78	*taf15*	15:1814483-1833117	2.50
79	*U3*	1:15200419-15200634	2.50
80	*rps10*	6:54129853-54135857	2.49
81	*ric3*	25:36366302-36431549	2.49

82	*snord12*	11:7378561-7385649	2.48
83	*si:ch211-51h9.7*	8:2494155-2766810	2.47
84	*ssr3*	18:32802231-32809465	2.46
85	*dnajc12*	13:51344383-51348551	2.45
86	*hmcn2*	8:33461669-33633934	2.45
87	*erbb2ip*	10:15483429-15627857	2.44
88	*ddx54*	5:75308841-75341152	2.43
89	*slc43a2a*	15:27717706-27886928	2.43
90	*gpc4*	14:31959831-32021524	2.42
91	*prrc2b,abl1*	5:74986817-75285543	2.40
92	*tcf7l1a*	10:43409344-43663060	2.39
93	*twf1a*	25:872079-887831	2.39
94	*mlxip*	5:70310776-70495795	2.37
95	*tmem123*	18:35612292-35620973	2.37
96	*fcho1*	8:20556563-20676269	2.37
97	*rngtt*	20:739034-1143381	2.36
98	*tjp2b*	8:11975936-12060379	2.35
99	*chmp1a,slc10a3*	25:38442718-38453017	2.35
100	*serbp1*	6:34817916-34893386	2.34
101	*khdrbs1b*	19:31403392-31649529	2.34
102	*prp*	13:39679468-39719858	2.33
103	*ict1*	12:174499-326691	2.32
104	*taf4*	11:21263491-21266548	2.32
105	*dusp8*	25:23444041-23775968	2.32
106	*apobb.2*	20:31243402-31334713	2.31
107	*irf2bp2a*	13:50420358-50422920	2.29
108	*hist2h2ab*	25:35811834-36197600	2.28
109	*tab1*	6:129498-133994	2.28
110	*nfkbiaa*	20:16922346-16924995	2.27
111	*hnrnpa0a*	14:25267555-25279621	2.27
112	*cdk12*	19:5480216-5529545	2.27
113	*rab5c*	3:17259273-17295765	2.27
114	*tmem88a*	10:22972284-22979870	2.25
115	*cask,ddx3b*	6:59348537-59576610	2.25
116	*ywhae2*	7:75462952-75489311	2.25
117	*fam98b*	17:53159828-53165070	2.25
118	*ctsba*	17:32828688-32841875	2.24
119	*wnk1*	25:21785802-21827111	2.23
120	*sat2b*	5:63582312-63622810	2.22
121	*polm*	10:46127810-46384541	2.22
122	*aqp11*	18:47169562-47260292	2.22
123	*asb5,spata4*	14:37614211-37632865	2.21
124	*stt3b*	16:42051636-42144309	2.21

125	*fam192a*	18:17366855-17383492	2.20
126	*ywhae2*	7:75462952-75489311	2.20
127	*si:dkeyp-1h4.6*	18:7054755-7056958	2.19
128	*bloc1s4*	19:26165194-26179444	2.19
129	*zgc:162396*	9:29721865-29725302	2.19
130	*ikzf2*	9:41029563-41041566	2.19
131	*cox15*	13:585679-596107	2.17
132	*smarce1*	3:35071190-35080284	2.17
133	*tnrc6b*	12:20161960-20442982	2.16
134	*scaf11*	4:1478638-1499411	2.15
135	*khdc4*	16:58309746-58324684	2.15
136	*tcerg1*	21:40470525-40507406	2.15
137	*si:dkey-202p8.1*	16:32341424-32375366	2.15
138	*sox21b*	9:55101926-55104239	2.15
139	*ccdc82*	21:39333973-39358051	2.15
140	*mitfa*	6:43321686-43364600	2.15
141	*map7d1a*	16:39984863-40096287	2.15
142	*si:ch73-334e23.1,sox2*	22:40262172-40512173	2.14
143	*si:dkey-227h16.2*	20:30057391-30126147	2.14
144	*ponzr5*	7:23824656-23831062	2.14
145	*si:ch211-165l15.1*	8:6740395-6743635	2.14
146	*camlg*	21:44326403-44372933	2.13
147	*pds5b*	15:32066845-32129981	2.13
148	*lgals2b*	6:456974-463584	2.13
149	*inppl1a*	15:46337695-46607672	2.12
150	*si:ch211-142h2.1*	2:29427286-29476797	2.12
151	*slc30a6*	13:223546-226088	2.12
152	*col23a1*	21:30858751-31045466	2.12
153	*csnk1a1*	14:40046936-40347389	2.11
154	*adarb1b,si:dkey-222l20.1*	9:46294453-46611462	2.11
155	*cat*	25:7801936-7811828	2.10
156	*rnf25*	3:32808121-32817144	2.10
157	*cby1*	12:20161960-20442982	2.10
158	*virma*	16:28797730-28968381	2.10
159	*vwa5a*	25:210563-417262	2.09
160	*col11a2*	19:7796148-7847933	2.09
161	*aebp2*	4:2794208-2816337	2.09
162	*ttc9b*	18:35122765-35459616	2.08
163	*hist2h2ab*	25:35811834-36197600	2.08
164	*qser1*	18:44091261-44112584	2.07
165	*agps*	9:1576648-1629334	2.07
166	*smyd1*	8:1105968-1120160	2.07
167	*anxa1b*	5:67531648-67546887	2.07

168	*atp1a3b,si:ch73-22o12.1*	16:12166970-12425846	2.07
169	*dennd5b*	4:15717725-15775199	2.06
170	*tsc2*	1:54750008-54822856	2.05
171	*ptch2*	2:33685223-33711408	2.04
172	*lima1*	11:1991814-2366683	2.04
173	*khsrp*	1:55499472-55511646	2.04
174	*pan3*	24:22328251-22356651	2.04
175	*wdr32*	13:8924817-8937561	2.03
176	*sox21a*	6:7331079-7332155	2.03
177	*tp53bp2*	13:241908-536569	2.03
178	*itpa*	20:14856045-14864220	2.03
179	*bysl*	22:525996-539400	2.03
180	*mss51*	24:40671513-40690017	2.03
181	*zgc:172014*	12:2934033-3096082	2.02
182	*msrb3*	4:11956991-11978717	2.02
183	*si:ch211-210c8.5*	23:33972477-33988926	2.01
184	*hnrnpa1a*	11:1991814-2366683	2.01
185	*nf1*	15:30159316-30282109	2.01
186	*cpeb4*	21:40224197-40230696	2.00
187	*cherp*	22:4589133-4631130	2.00
188	*prrc2a*	19:27226174-27255583	2.00

Table A.2. Gene Ontology (GO) terms associated with genes upregulated in *taz* mutants.

GO Term	Number of genes within cluster	P-value
nucleus	30	2.40E-03
nucleic acid binding	23	2.60E-04
nucleotide binding	23	3.60E-03
Metal-binding	18	5.50E-02
RNA binding	16	8.00E-07
DNA binding	16	7.10E-02
Nucleotide-binding, alpha-beta plait	15	8.20E-09
RRM	14	1.30E-08
RNA recognition motif domain	14	1.40E-08
Zinc	13	5.60E-02
Zinc-finger	10	6.40E-02
Spliceosome	8	1.90E-04
HMG	6	1.00E-04
High mobility group (HMG) box domain	6	1.00E-04
Repressor	6	9.90E-04
intracellular ribonucleoprotein complex	6	6.70E-03
DNA-binding region:HMG box	5	8.60E-07
mRNA splicing, via spliceosome	5	2.80E-03
proteinaceous extracellular matrix	5	2.20E-02
RNA-binding	5	3.60E-02
Herpes simplex infection	5	8.30E-02
Transcription factor SOX	4	2.50E-05
K Homology domain	4	3.10E-03
KH	4	3.90E-03
K Homology domain, type 1	4	4.70E-03
Collagen triple helix repeat	4	2.70E-02
dorsal/ventral pattern formation	4	4.40E-02
Zinc finger, RanBP2-type	3	1.20E-02
ZnF_RBZ	3	1.20E-02
notochord development	3	3.70E-02
compositionally biased region:Poly-Ser	3	6.00E-02
collagen trimer	3	6.10E-02
Collagen	3	7.20E-02
NOD-like receptor signaling pathway	3	7.40E-02
Extracellular matrix	3	8.00E-02
compositionally biased region:Pro-rich	3	8.00E-02
fin regeneration	3	8.00E-02
RNA processing	3	8.20E-02

mRNA processing	3	9.20E-02
region of interest:Cys-rich	2	2.30E-02
Domain of unknown function DUF4211	2	2.70E-02
BAT2, N-terminal	2	2.70E-02
Protein of unknown function DUF1042	2	2.70E-02
Interferon regulatory factor 2-binding protein 1 & 2, zinc finger	2	2.70E-02
negative regulation of protein kinase B signaling	2	4.20E-02
RNA polymerase II-binding domain	2	5.30E-02
nuclear matrix	2	5.80E-02
RNA processing and modification	2	6.10E-02
central nervous system neuron development	2	6.20E-02
CID domain	2	6.60E-02
positive regulation of sequence-specific DNA binding transcription factor activity	2	8.90E-02
response to copper ion	2	9.50E-02
notochord morphogenesis	2	9.50E-02

Table A.3. List of genes downregulated in *taz* mutants by 2-fold, identified by whole embryo RNA-seq at 24hpf.

Rank	Gene	Locus (Zv9)	Fold Change
1	*mrpl53*	19:33510984-33517695	10.51
2	*scarna6*	15:44796642-44844611	9.48
3	*diaph1*	23:2575942-2686460	6.69
4	*fam49bb*	24:10593705-10669643	5.73
5	*vti1a*	12:32845791-33163215	5.58
6	*emc4*	7:1648459-1649128	5.15
7	*U3*	12:2848500-2848712	4.81
8	*rnaset2l*	15:19200548-19421864	4.29
9	*aga*	14:37648801-37657608	4.26
10	*zan,senp3b*	7:27452376-27657933	3.78
11	*slc22a7a*	11:31605157-31618427	3.57
12	*trit1*	19:31968163-32045480	3.56
13	*arpc5b*	20:34176293-34180204	3.54
14	*zgc:195170*	22:4339289-4459490	3.50
15	*prss23*	14:31672126-31677943	3.49
16	*ralbb*	11:44690880-44697041	3.47
17	*krt1-19d*	19:5948855-5957044	3.40
18	*becn1*	12:15513877-15583053	3.36
19	*fibinb*	7:35632832-35636148	3.32
20	*mustn1a*	6:40772133-40773355	3.22
21	*chchd5*	3:53533515-53536919	3.17
22	*cldnf*	15:2630160-2681586	3.13
23	*si:ch211-207l22.2*	16:37961592-38005407	3.10
24	*capn2b*	22:27058701-27091581	3.03
25	*snf8*	12:21993646-22010870	3.02
26	*crp4*	24:39601013-39634395	2.89
27	*CABZ01117575.1*	25:38215960-38219959	2.89
28	*ENSDARG00000090305*	7:72818894-72885791	2.88
29	*actc1c*	25:14370302-14386180	2.78
30	*zgc:153921,zgc:172253*	3:1768526-2046655	2.78
31	*CU855890.3*	9:48944314-49269546	2.77
32	*cldn23,si:dkey-88l16.3*	10:14836098-15077423	2.76
33	*rrm2*	19:49363392-49368575	2.75
34	*si:ch211-117m20.5*	5:32253548-32254918	2.75
35	*si:ch211-217g15.3*	13:24807851-24811634	2.75
36	*nell2a*	25:1011062-1036782	2.65
37	*dscr3*	10:143057-294579	2.64
38	*CABZ01049025.1*	5:69208227-69263250	2.63

39	*si:dkeyp-52c3.1*	3:2303333-2305285	2.63
40	*tk1*	11:45704913-46264009	2.60
41	*mb*	1:55620124-55751826	2.59
42	*cryba2a*	6:13690805-13694235	2.57
43	*ptgdsb*	24:17576414-17578562	2.54
44	*csnk1a1*	14:40046936-40347389	2.53
45	*rnasel3*	14:40044380-40046544	2.52
46	*mfap4*	1:59886129-59887907	2.51
47	*s100v2*	19:24749217-24753488	2.51
48	*rab11fip1b*	10:42675289-42717230	2.51
49	*CABZ01071911.1*	4:59281147-59288933	2.50
50	*crygm2d10*	9:23343182-23344647	2.48
51	*megf6a*	23:21413541-21757933	2.47
52	*si:dkey-261m9.9*	7:7179599-7335433	2.47
53	*crygm2d12*	9:23238021-23239027	2.44
54	*lin28a*	19:14873055-14904755	2.43
55	*hmbsa*	5:32157457-32173443	2.43
56	*apoa1bp*	19:7864652-8053457	2.42
57	*lhfpl2b*	5:53817145-53834085	2.42
58	*aip*	1:40343978-40401983	2.42
59	*nrbf2b*	12:9323886-9333929	2.42
60	*anxa1c*	5:67519125-67531098	2.40
61	*grb10a*	19:23619652-23736134	2.40
62	*pdlim3a*	1:16463747-16477756	2.40
63	*si:ch211-197e7.1,si:dkey-156k2.3,zgc:173709*	4:52794388-52983004	2.40
64	*homer2*	18:2-3535	2.40
65	*fam234a*	24:41187780-41210397	2.39
66	*ankrd49*	15:2842745-2849115	2.38
67	*mpzl3*	15:46725846-46906096	2.36
68	*CR407594.2*	4:33167582-33177462	2.36
69	*si:dkey-57k17.1*	4:29987294-29999214	2.35
70	*dcps*	10:40647871-40658612	2.34
71	*creb3l2*	4:4585555-4625417	2.34
72	*aqp4*	20:18209214-18235347	2.34
73	*pdik1l*	19:14917589-14949425	2.33
74	*mgst3a*	20:49279845-49295820	2.33
75	*myo9b*	22:5036110-5063333	2.33
76	*fkbp1ab*	23:16855981-16863043	2.33
77	*si:ch211-39i22.1*	9:57815818-57861001	2.32
78	*mblac1*	7:27452376-27657933	2.32
79	*aldh4a1*	11:42964410-43266081	2.31
80	*gcnt4b*	21:14036217-14052102	2.31

81	*myt1*	23:7846396-7915851	2.31
82	*bud13*	21:21812040-21820329	2.31
83	*hmox2b*	3:12980162-13000159	2.31
84	*si:ch211-162i8.5*	4:51078368-51097810	2.30
85	*arl4ca*	22:14121841-14125333	2.30
86	*nhlrc3*	10:31511-35379	2.30
87	*dolpp1*	21:4260252-4276931	2.29
88	*sc5d*	21:23806972-23813231	2.29
89	*ttyh2*	12:40082637-40236089	2.29
90	*si:dkey-29j8.2*	4:39602791-39696345	2.29
91	*asah1b*	1:15253618-15406897	2.28
92	*pkp3b*	7:34262623-34314532	2.28
93	*slc25a44a*	25:6619164-6629524	2.28
94	*elavl3*	3:46836266-47038021	2.26
95	*uqcrfs1*	7:46459041-46585553	2.26
96	*atad1a*	5:18496508-18511731	2.26
97	*mgaa*	17:10011286-10034877	2.25
98	*pdgfrl*	14:31118641-31259780	2.25
99	*rdh12*	13:33279149-33289529	2.24
100	*pklr*	16:57790202-57955740	2.24
101	*trim105*	14:19873586-19890362	2.23
102	*si:ch211-133l5.8*	8:21397949-21400497	2.23
103	*dbnla*	10:43723550-43737936	2.23
104	*cep63*	6:27604866-27633698	2.23
105	*slc35a2*	8:9492404-9515619	2.22
106	*C19H6orf228*	19:4288701-4295324	2.21
107	*zgc:92380*	9:48848807-48881961	2.21
108	*chl1a*	23:11453540-11554975	2.20
109	*dclk1a*	10:35765474-35895175	2.20
110	*sema3d*	18:8636380-8703586	2.20
111	*sft2d2*	6:36788141-36792403	2.19
112	*krt23*	19:5974114-5976185	2.19
113	*crygm2d19*	9:23220375-23221462	2.19
114	*fam20a*	12:3498119-3532003	2.19
115	*il10rb*	9:390551-398350	2.19
116	*dync1li1*	19:18571690-18607846	2.19
117	*prdm2b*	11:27122901-27151137	2.19
118	*cryba1b*	21:38020623-38029817	2.19
119	*stard3*	19:5593149-5610199	2.19
120	*bcl2a*	24:29060030-29152131	2.18
121	*zgc:171775*	23:10253421-10271922	2.18
122	*ftcd*	22:12910169-12925826	2.18
123	*bada*	21:26583367-26584522	2.17

124	*ccdc160*	14:32343765-32345545	2.17
125	*akr7a3*	11:42944034-42959301	2.17
126	*myadm*	2:37470875-37477927	2.16
127	*nrip1b*	10:39622826-39682405	2.16
128	*hbae1*	3:55965768-55983723	2.16
129	*mmp30*	10:40051609-40071834	2.16
130	*zdhhc4*	12:19597419-19604397	2.16
131	*cryba4*	10:45544673-45552554	2.15
132	*epdl2*	21:27907450-27917942	2.15
133	*cryba1l*	14:49248445-49256727	2.15
134	*prelid1b*	23:46022486-46033550	2.15
135	*mmp17b*	14:52549874-52585077	2.15
136	*fam136a*	10:6248116-6271082	2.14
137	*hbae1.3*	3:55965768-55983723	2.13
138	*marveld1*	13:40047913-40051366	2.12
139	*nccrp1*	5:38450812-38454718	2.10
140	*pdia6*	20:31243402-31334713	2.10
141	*CU041386.1*	25:20230695-20237940	2.10
142	*exosc4*	2:1709544-1713596	2.10
143	*crygm2d21*	9:23331590-23332757	2.09
144	*dmxl2*	18:38106501-38148812	2.09
145	*plpp2b*	22:21871192-21906444	2.09
146	*zgc:110366*	2:6837102-6853273	2.08
147	*zgc:113442*	6:1407152-1416138	2.08
148	*abhd17c*	7:11729399-11823924	2.08
149	*pip4p1b*	1:9494180-9502818	2.07
150	*and1*	24:27076156-27079975	2.07
151	*he2*	22:14196008-14259496	2.07
152	*panx1a*	15:2466934-2481000	2.07
153	*cdk6*	19:41209038-41293131	2.07
154	*ndrg3b*	23:14944532-15101965	2.07
155	*cyp2x7*	25:17601340-17752074	2.06
156	*napepld*	4:19416084-19421695	2.06
157	*cart4*	19:43762290-43765119	2.06
158	*crybb1l1*	14:49239149-49245598	2.06
159	*pacsin1a*	23:3473662-3773434	2.05
160	*tmem176l.1*	16:49582368-49589405	2.05
161	*tusc3*	1:14899826-14908864	2.05
162	*spata5*	14:579993-591942	2.05
163	*dct*	9:55311303-55336342	2.05
164	*dhrs7ca*	3:59497987-59514357	2.05
165	*foxi3b*	14:35644822-35646509	2.04
166	*clybl*	9:32201018-32292626	2.04

167	*slc25a1b*	10:23319645-23359125	2.04
168	*zdhhc23b*	24:21700607-21887995	2.03
169	*mettl24*	20:53757869-53785338	2.03
170	*jak2a*	21:205877-409532	2.03
171	*hdac5*	3:23145908-23267719	2.03
172	*syce3,si:ch211-232m8.3*	14:35641108-35643512	2.02
173	*BX640584.4,si:dkeyp-44b5.5*	4:42891082-43154243	2.02
174	*usp46*	20:23071312-23099512	2.02
175	*rab11al*	16:49892215-49910320	2.02
176	*si:dkey-48n15.2*	13:16310124-16327580	2.02
177	*gpx1b*	6:42269718-42272629	2.02
178	*si:ch211-202f3.3*	17:45744867-45766708	2.02
179	*rhoq*	12:26624130-26677931	2.01
180	*pigp*	10:143057-294579	2.01
181	*scinla*	6:20198782-20261782	2.01
182	*nog1*	3:10693518-10695681	2.01
183	*rspo2*	16:41119537-41219580	2.01
184	*malt1*	5:69300318-69330394	2.01
185	*slc27a3*	10:16426304-16446317	2.01
186	*zmat5*	5:33713718-33717859	2.00
187	*si:ch211-105c13.3*	16:24875504-24893486	2.00

Table A.4. Gene Ontology (GO) terms associated with genes downregulated in *taz* mutants.

GO Term	Number of genes within cluster	P-value
Metal-binding	18	3.60E-02
Metabolic pathways	16	4.50E-02
hydrolase activity	13	2.00E-02
extracellular region	11	1.10E-02
Hydrolase	11	6.70E-02
XTALbg	9	7.70E-10
Beta/gamma crystallin	9	6.60E-09
Gamma-crystallin-related	9	6.60E-09
Secreted	8	2.30E-02
oxidoreductase activity	8	5.40E-02
oxidation-reduction process	8	7.80E-02
signal peptide	7	1.70E-02
Oxidoreductase	6	8.10E-02
Iron	5	6.70E-02
cartilage development	4	1.30E-02
Thioredoxin-like fold	4	5.80E-02
heme binding	4	6.90E-02
ZnMc	3	1.70E-02
Peptidase, metallopeptidase	3	2.60E-02
Metalloprotease	3	6.50E-02
Metallopeptidase, catalytic domain	3	9.40E-02
neural crest cell migration	3	9.70E-02
Pyruvate/Phosphoenolpyruvate kinase-like domain	2	2.50E-02
chondrocyte differentiation	2	5.90E-02
glutathione peroxidase activity	2	8.30E-02
response to endoplasmic reticulum stress	2	9.20E-02
regulation of endocytosis	2	9.80E-02